Transcriptomic and Glycobiological Profiling of Synovial Fibroblasts in Rheumatoid Arthritis: The Role of Sialylation in Fibroblast-Macrophage Crosstalk

CAGLAR CIL

BSc, MSc

A thesis submitted in fulfilment of requirements for the degree of Doctor of Philosophy

School of Infection and Immunity,

College of Medical, Veterinary & Life Sciences,

University of Glasgow.

September 2025

Abstract

Rheumatoid arthritis (RA) is a chronic autoimmune disease in which synovial fibroblasts (SFs) and macrophages perpetuate inflammation and tissue destruction. While immune cell directed therapies are effective, treatment resistance underscores the importance of stromal contributions. Glycosylation, particularly sialylation, has emerged as a key regulatory mechanism in stromal-immune crosstalk.

Here, we investigated the role of sialylation in shaping SF function and macrophage responses. Bulk RNA sequencing of human RA synovia revealed TNF-α driven remodelling of glycosylation pathways, with upregulation of ST3GAL family members, indicating a pro–α2-3 bias in inflamed fibroblasts. Single-cell RNA-seq mapped these alterations to discrete fibroblast subsets and linked them to lectin receptor expression in tissue-resident macrophages, including Siglecs and Galectins.

Using an in vitro desialylation model, we demonstrated that selective removal of α2-3 sialic acids reprogrammed SFs toward a pro-inflammatory phenotype, enhancing cytokine secretion. Conditioned media from these fibroblasts induced M1-like polarisation of bone marrow derived macrophages, with increased Il1b, Nos2, CD80/CD86, and pathway enrichment for TNF and NF-κB signalling, In contrast, broad α2-3/α2-6 cleavage elicited mixed macrophage responses, while less α2-3 linked sialic acid removal had minimal effects. Protein-level analyses confirmed increased PD-L1 in macrophages exposed to desialylated fibroblast supernatants.

These findings identify stromal sialylation as a molecular checkpoint regulating joint inflammation. Loss of α2-3 sialylation above certain thresholds functions as a pro-inflammatory switch in SFs, amplifying macrophage activation and sustaining chronic inflammation. Targeting stromal glycosylation offers a potential therapeutic avenue and biomarker strategy in RA.

Table of Contents

List of Tables

List of Figures

Acknowledgement

I would like to express my deepest gratitude to my supervisors, Dr. Miguel Pineda, Professor Mariola Kurowska-Stolarska, and Professor Thomas Otto, for their invaluable guidance, support, and encouragement throughout my PhD journey. Their expertise, constructive feedback, and dedication have been instrumental in shaping both my research and my development as a scientist.

I am also sincerely grateful to Professor Margaret Harnett and Dr. Megan Macleod for their insightful discussions and for broadening my scientific perspective. Their input has greatly enriched the direction and depth of my work.

I wish to thank Diane Vaughan and Alana Hamilton for their outstanding assistance with flow cytometry experiments. Their technical expertise and patience were essential to the success of many aspects of this project.

I also acknowledge Dr. Piaopiao Pan and Dr. Yilin Wang for being an exceptional lab mate and colleague.

I would like to extend my gratitude to the Turkish Ministry of National Education for supporting my academic journey through the YLSY Abroad Scholarship Program, which made this opportunity possible.

I am especially thankful to Atakan Doğan, who has always encouraged me in science and made every moment of this journey more meaningful and valuable.

Most of all, I owe my deepest gratitude to my mother, Hamiyet Cil, whose unwavering love, sacrifice, and endless belief in me have been the greatest source of strength in my life; this thesis is as much hers as it is mine.

Author’s Declaration

“I hereby declare that, except where due acknowledgment is made to the contributions of others, this dissertation is entirely the result of my own work and has not been submitted, either in whole or in part, for any other degree or qualification at the University of Glasgow or any other institution.”

Printed Name: CAGLAR CIL

Signature:

Abbreviations

ACPA	ANTI-CITRULLINATED PROTEIN ANTIBODIES
ACR	AMERICAN COLLEGE OF RHEUMATOLOGY
ANTI-CARP	ANTI-CARBAMYLATED PROTEIN ANTIBODIES
ARG-1	ARGINASE-1
AU	*ARTHROBACTER UREAFACIENS*
BMDMS	*BONE MARROW DERIVED MACROPHAGES*
CCA	CANONICAL CORRELATION ANALYSIS
CMP-NEU5AC	CYTIDINE 5′-MONOPHOSPHATE-SIALIC ACID
CP	*CLOSTRIDIUM PERFINGENS*
CTLA-4	CYTOTOXIC T-LYMPHOCYTE ASSOCIATED PROTEIN 4
DEG	*DIFFERENTIALLY EXPRESSED GENES*
DMARDS	DISEASE-MODIFYING ANTIRHEUMATIC DRUGS
DNMT1	DNA METHYLTRANSFERASE-1
ECM	EXTRACELLULAR MATRIX
EGFR	EPIDERMAL GROWTH FACTOR RECEPTOR
ELLA	ENZYME-LINKED LECTIN ASSAY
EMT	*EPITHELIAL-MESENCHYMAL TRANSITION*
EULAR	EUROPEAN LEAGUE AGAINST RHEUMATISM
FAPA	FIBROBLAST ACTIVATION PROTEIN ALPHA
FLS	*FIBROBLAST-LIKE SYNOVIAL CELLS*
G0	AGALACTOSYLATION
GAL	GALACTOSE
GALNAC	N-ACETYLGALACTOSAMINE
GLCNAC	N-ACETYLGLUCOSAMINE
GNE	UDP-N-ACETYLGLUCOSAMINE 2-EPIMERASE/N-ACETYLMANNOSAMINE KINASE
GSVA	GENE SET VARIATION ANALYSIS
GWAS	GENOME-WIDE ASSOCIATION STUDIES
HAPLN1	HYALURONAN AND PROTEOGLYCAN LINK PROTEIN 1
HN	HEMAGGLUTININ-NEURAMINIDASE
IL	INTERLEUKIN

JAK	JANUS KINASE
L	*LECTENZ*
LPS	*LIPOPOLYSACCHARIDE*
MANNAC	N-ACETYLMANNOSAMINE
MBP	MANNOSE-BINDING PROTEIN
MGATS	N-ACETYLGLUCOSAMINYLTRANSFERASES
MIRNAS	MICRORNAS
MMP	MATRIX METALLOPROTEINASE PROTEIN
MRC1 OR CD206	MANNOSE RECEPTOR C TYPE 1
MTX	METHOTREXATE
NES	NORMALISED ENRICHMENT SCORES
NSAIDS	NON-STEROIDAL ANTI-INFLAMMATORY DRUGS
OPCML	OPIOID BINDING PROTEIN/CELL ADHESION MOLECULE-LIKE
PADI	PEPTIDYLARGININE DEIMINASES
PADI-2	PEPTIDYL ARGININE DEIMINASE TYPE 2
PCA	PRINCIPAL COMPONENT ANALYSIS
PCDH10	PROTOCADHERIN 10
PDPN	PODOPLANIN
PTPN22	TYROSINE PHOSPHATASE NON-RECEPTOR TYPE 22
RA	RHEUMATOID ARTHRITIS
RANKL	RECEPTOR ACTIVATOR OF NUCLEAR FACTOR-KB LIGAND
RF	RHEUMATOID FACTOR
RNA-SEQ	BULK AND SINGLE-CELL RNA SEQUENCING
RPK	READS PER KILOBASE
SCRNA-SEQ	*SINGLE-CELL RNA SEQUENCING*
SFS	SYNOVIAL FIBROBLASTS
SIGLECS	SIALIC ACID-BINDING IMMUNOGLOBULIN-LIKE LECTINS
TLR	TOLL-LIKE RECEPTOR
TNF	TUMOUR NECROSIS FACTOR
TPM	TRANSCRIPTS PER MILLION
TRSMS	TISSUE-RESIDENT SYNOVIAL MACROPHAGES

UPA	*EARLY UNDIFFERENTIATED ARTHRITIS*
VC	*VIBRIO CHOLERAE*
A2,3-SIALYLTRANSFERASES	ST3GALTS
A2,6-SIALYLTRANSFERASES	ST6GALTS
A2,8-SIALYLTRANSFERASES	ST8SIA

1. Chapter 1 General Introduction

1.1 Rheumatoid Arthritis

Rheumatoid arthritis (RA) is a persistent autoimmune condition characterised by systemic inflammation that primarily leads to destructive processes in the joints, which may result in deformity if left untreated. The initial presentation of RA frequently accompanied by symptoms including morning stiffness, fatigue, and joint pain, which may result in considerable functional disability and diminished quality of life (Santos-Moreno et al., 2022). Epidemiological research suggests that RA affects an estimated 1% of the worldwide population, exhibiting a higher prevalence among women and reaching peak onset between the ages of 35 and 50 (Godha et al., 2023). RA is correlated with several comorbidities, most notably cardiovascular diseases, as both conditions are aggravated by shared inflammatory pathways (England et al., 2018).

RA pathogenesis is believed to occur with a multifactorial origin, involving both genetics, and environmental factors such as the genetic predisposition and environmental triggers (i.e., smoking) that result in inappropriate activation of immune system leading to the perpetuation of inflammation and joint damage (Guo et al., 2018). Although aetiology of RA remains unknown, current therapies mainly target immune cells and their inflammatory pathways, and still some patients develop resistance to these therapies, indicating the importance of finding other targets that impact the stromal components of RA (Németh et al., 2022). Therefore, an enhanced comprehension of the disease's nature is imperative to develop more efficacious treatments and innovative preventive strategies.

1.2 Factors affecting RA development and disease treatments.

1.2.1 Genetic, epigenetic and environmental factors

Genetic factors are critically implicated in the pathogenesis of RA, with research demonstrating that carrying specific alleles, especially those within the HLA-DRB1 gene, are correlated with an elevated risk of developing this condition (Cvjetićanin et al., 2019; Hamshere et al., 2007). In addition, patients with RA demonstrated different autoantibodies including rheumatoid factor (RF), anti-carbamylated protein antibodies (anti-CarP) and anti-citrullinated protein antibodies (ACPA) of

which involved in inflammatory processes that result in bone destruction (van Delft & Huizinga, 2020).

Genome-wide association studies (GWAS) have identified polymorphic variants of the tyrosine phosphatase non-receptor type 22 (PTPN22) gene, the Cytotoxic T-Lymphocyte Associated Protein 4 (CTLA4), the signal Transducer and Activator of Transcription 4 (STAT4), and variants of the genes encoding the enzymes peptidylarginine deiminases (PADI)-2 and PADI-4, which are associated with an elevated risk for the development of RA (Abbasifard et al., 2020; X. Chang et al., 2013; Zhou et al., 2021).

In addition to contribution of genetics factors, epigenetics also plays important role in the development of RA. Previous studies showed aberrant DNA methylation in stromal RA SFs and many other immune cells. For instance, expression of the DNA methyltransferase-1 (DNMT1) is reduced in RA synovial fibroblasts (SFs) compared to osteoarthritis, in response to interleukin 1 (IL-1) stimulation (Nakano et al., 2013). Other studies also found similar results in immune cells, where DNA hypomethylation observed in T-cells, B-cells and monocytes of patients with RA with a lower expression DNMT1 (de Andres et al., 2015). Histone modifications are also playing important role in shaping gene expressions by changing accessibility of histone proteins to transcription factors through mechanisms including acetylation, ubiquitinylation, citrunillation and methylation. In RA synovial tissues, in addition to the overall increase of acetylation, histone deacetylase activity was significantly lower than OA synovial tissues, with reduced expression of HDA-1 and HDA-2 proteins (Huber et al., 2007). This suggest that there is a shift toward hyperacetylation in RA compared to OA synovial tissues. In another study investigating the role of histone deactylases in regulating inflammation in RA SFs, authors found that HDAC3, but not HDAC1/2, HDAC6, or HDAC8, played a crucial role in driving the inflammatory gene program. Using selective HDAC3/6 inhibitors and siRNA knockdown, they showed that blocking HDAC3 reduced IL-1β-induced inflammatory gene expression by preventing STAT1 phosphorylation and activation, mainly through suppression of type I interferon production. (Angiolilli et al., 2017). This indicates that HDAC3 is essential for sustaining the pro-inflammatory signaling in RA SFs.

Abnormal expression of microRNAs (miRNAs) was also observed in RA synovial tissues. miRNA-155 expression in RA SFs is upregulated, and this decreased matrix metalloproteinase protein-3 (MMP-3) levels and reduced proliferation and invasion of RA SFs, indicating that its upregulation may be protective (Long et al., 2013). miRNA-221 expression is also upregulated in serum and synovial tissues of RA patients, where its inhibition reduced the production of LPS-induced pro-inflammatory cytokines in RA SFs (S. Yang & Yang, 2015).

Apart from those genetic and epigenetic influencers, RA development is also affected by environmental triggers. Previous meta-analysis study suggested that viral exposures may be a risk factor for RA (Kudaeva et al., 2019). The odd ratios for the risk of RA development were found to be significantly higher for Parvo B19 and hepatitis C infection compared to controls. However, cytomegalovirus and hepatitis B infections did not show significant correlation with RA. On the other hand, Chikungunya virus is associated with persistent arthritis (Kudaeva et al., 2019). Regarding SARS-coV-2, there are reports demonstrating inflammatory reactive arthritis phenotypes in post-Covid patients (Ciaffi et al., 2023; Slouma et al., 2022). Apart from those, changes in the microbiome were also associated to the etiopathogenesis of RA, where the presence of *P. gingivalis,* and mycoplasma DNAs have been correlated with the development of autoimmunity and RA (S. Li et al., 2013).

Other environmental factors that might play some role in RA development are pollution and tobacco smoking. Air pollutants increase the likelihood of RA development especially when exposed to PM2.5 and NO2 (K.H. Chang et al., 2016). Specifically, PM2.5 exposure predicted ACPA positivity. This situation was also observed in the smoking where multivariate regression models predicted increased ACPA and RF positivity involved in RA autoantibody status (Alex et al., 2020). The impact of cigarette smoking on immune responses, oxidative stress and epigenetic changes in RA is discussed in a previous review (K. Chang et al., 2014). Smoking is the clearest environmental risk factor for RA development. It was reported to lead genome-wide changes in DNA methylation where authors identified 187 differentially methylated CpG sites through array-based methods (Zeilinger et al., 2013). Apart from those, hormone replacement therapies applied greater than 5 years resulted in significantly higher risk for RA development (Eun et al., 2020). Causes involved in RA development illustrated in Figure 1-1.

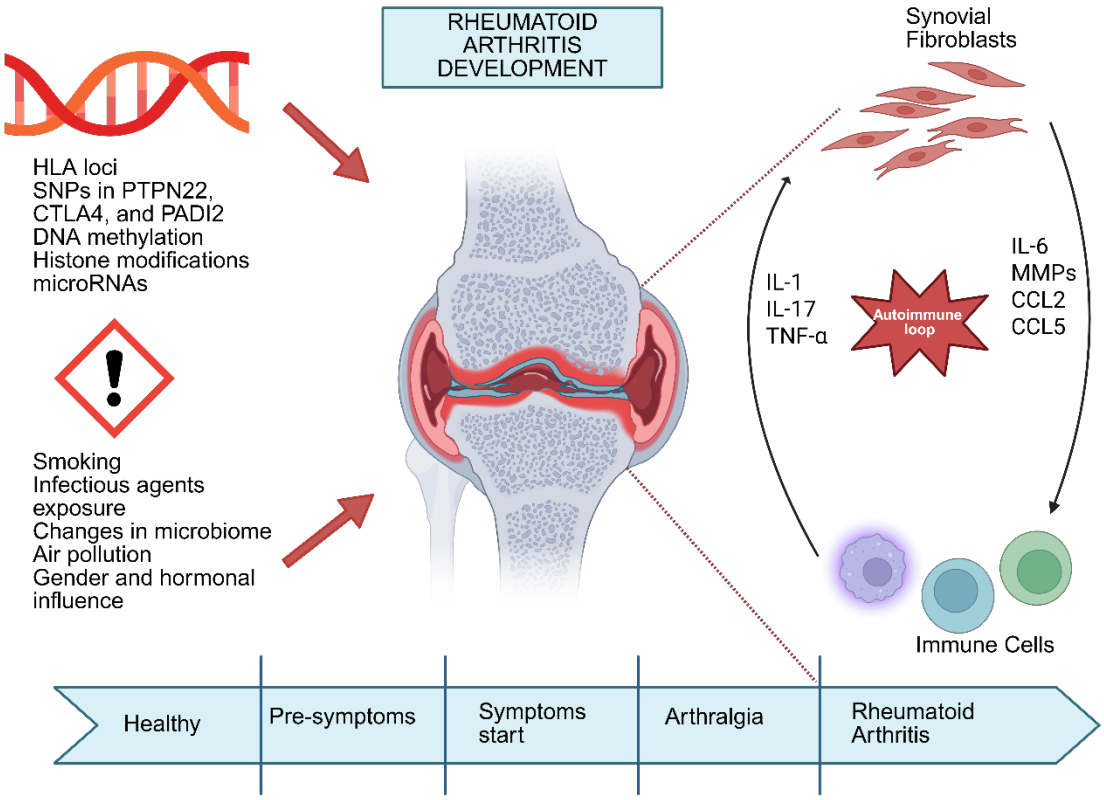

Figure 1-1 Development of Rheumatoid Arthritis

Genetics and environmental factors affecting RA development. In brief, carrying specific alleles in HLA loci, SNPs in some genes, epigenetic modifications, and environmental exposures such as viral exposures, air pollution and tobacco smoking promotes risk for RA development. These changes affect both stromal and immune cells, changing their behaviours to promote inflammatory mediators and finally healthy individuals develop RA. Illustration is created by Biorender.

1.2.2 Medications and Treatment in RA

RA is a chronic inflammatory disorder characterised by synovitis and systemic manifestations, which requires a multifaceted treatment approach. Management strategies primarily focus on pharmacological therapies, including disease-modifying antirheumatic drugs (DMARDs), both synthetic (csDMARDs) and biological (bDMARDs), alongside non-steroidal anti-inflammatory drugs (NSAIDs) and glucocorticoids. The European League Against Rheumatism (EULAR) and the American College of Rheumatology (ACR) guidelines emphasise early intervention with DMARDs like methotrexate (MTX), particularly in patients with early-stage RA, to mitigate the risk of joint damage and improve long-term outcomes (Al-Ani et al., 2021; Kerschbaumer et al., 2020).

Conventional synthetic DMARDs, such as MTX, are considered the first-line treatment, known for their efficacy in reducing disease activity and preventing structural damage. For patients who cannot tolerate MTX or whose disease does not respond adequately to it, alternative DMARDs such as leflunomide and sulfasalazine are recommended (Hazlewood et al., 2016). bDMARDs, including tumour necrosis factor (TNF) inhibitors like etanercept, certolizumab pegol and adalimumab, represent another crucial aspect of RA management. These biologics have been shown to improve clinical outcomes significantly, including achieving remission and reducing disease activity, despite their higher costs and potential adverse effects (Ma & Xu, 2013; Witoszyńska-Sobkowiak et al., 2024). Emerging therapy options, such as Janus kinase (JAK) inhibitors, also provide additional treatment avenues, especially for patients with inadequate responses to traditional therapies (Singh & Singh, 2020).

The use of biologics in the treatment of RA has largely focused on immune cells due to their pivotal role in the inflammatory processes underpinning the disease. Biologics primarily target specific inflammatory mediators and immune pathways rather than direct stromal elements such as synovial fibroblasts, which play a different yet interconnected role in RA pathogenesis. Firstly, immune cells, particularly T cells and macrophages, are key contributors to the inflammatory environment in RA. These cells secrete pro-inflammatory cytokines such as TNF-α, IL-1β, and IL-6, which are crucial in driving the inflammatory response that characterises RA (F. Zhang et al., 2019). Biologics such as TNF inhibitors and IL-6 receptor antagonists specifically target these cytokines to reduce inflammation and alleviate symptoms of RA. The rationale behind targeting immune cells is to disrupt the primary cytokine-driven cascade that perpetuates inflammation, whereas fibroblasts may be more downstream effectors in this pathway. Although SFs contribute to RA through their production of matrix-degrading enzymes and cytokines that enhance inflammation and tissue destruction (Lefevre et al., 2015), the activation of these fibroblasts is largely a secondary effect of the cytokines released by immune cells (Noss & Brenner, 2008). Furthermore, while there is therapeutic interest in targeting RA SFs due to their role in joint destruction, current biologic therapies are specifically designed to ameliorate the immune-driven processes of RA rather than directly targeting fibroblasts. As a result, more research is needed to functionally reveal the markers associated with RA SFs and finding therapeutics to reduce SF-mediated inflammation.

1.3 Understanding of Synovial Pathophysiology

1.3.1 Healthy vs Rheumatoid Arthritis Synovium

The healthy synovium is a specialised connective tissue that lines the joints, critical for maintaining joint homeostasis and function. It comprises two primary layers: the intima, primarily composed of SFs and the sub-lining layer, which contains various immune cells, endothelial cells, and extracellular matrix components providing structural support (Smith, 2011). In healthy individuals, the intima is typically 1-2 cells thick, with SFs accounting for majority of this layer. Sublining layer on the other hand comprises blood vessels, fat cells, SFs and relatively less lymphocytes and macrophages (Smith, 2011). In a healthy state, SFs perform essential functions, including contributing to the synthesis of synovial fluid, a viscous substance that lubricates the joint and reduces friction during movement. This fluid also contains nutrients and waste products vital for the maintenance of articular cartilage (Gul et al., 2024). Healthy SFs exhibit a balanced proliferation and apoptosis rate, ensuring a stable environment in the joint (Bartok & Firestein, 2010). However, they retain the capacity to become activated in response to inflammatory or mechanical stimuli and healthy SFs contribute to RA by responding to inflammatory cues and undergoing stable epigenetic and functional reprogramming, transforming from tissue-maintaining cells into autonomous drivers of chronic inflammation and joint destruction(Bartok & Firestein, 2010; Frank-Bertoncelj et al., 2017; Karouzakis et al., 2018). Healthy synovium also maintains a homeostatic balance of immune cells. Macrophages and other immune cells contribute to a protective homeostatic environment, participating in immune surveillance while avoiding excessive inflammatory responses (Kurowska-Stolarska & Alivernini, 2022). Furthermore, the healthy synovium supports inflammation and immune challenges without transition to chronic inflammatory states. These functions are however impaired during the progression of RA (Alivernini et al., 2020).

The rheumatoid synovium exhibits distinctive characteristics that are different from normal synovial tissue, reflecting the pathological processes underlying RA. One key pathological feature is the hyperplasia of the synovial lining layer, which is exacerbated by the infiltration of various immune cells including macrophages, T and B lymphocytes, and plasma cells (Hitchon & El-Gabalawy, 2011). The presence of these immune cells perpetuates inflammation and joint damage. The synovial lining in RA can reach a thickness of several cell layers, contributing to

the pathological formation of a pannus, a pathological tissue that invades and destroys underlying cartilage and bone. This pannus tissue comprises of macrophages, and fibroblasts which express high levels of proteases (Hitchon & El-Gabalawy, 2011). SFs here are not only proliferating excessively but they also express pro-inflammatory cytokines and matrix-modulating enzymes that consolidate inflammation and tissue degradation (Bottini & Firestein, 2013). Angiogenesis is another hallmark of the rheumatoid synovium, driven by factors such as angiopoietin-like protein 2 (Angptl2) and vascular endothelial growth factor (VEGF) (Okada et al., 2010). This neo-vascularisation supports the hyperplastic synovium and enhances the infiltration of inflammatory cells, thereby further perpetuating the inflammatory cycle (Okada et al., 2010). Moreover, the inflammatory microenvironment within the rheumatoid synovium is rich in cytokines, including TNF-α, IL-1, and IL-6, which collectively contribute to synovitis and joint destruction (Fang et al., 2020). Recent studies also highlighting the roles of stromal cells such as telocytes which indicate a dynamic interplay between resident and infiltrating cells within the synovium during disease progression (Rosa et al., 2021). General outlook into healthy vs arthritic synovium is illustrated in Figure 1-2.

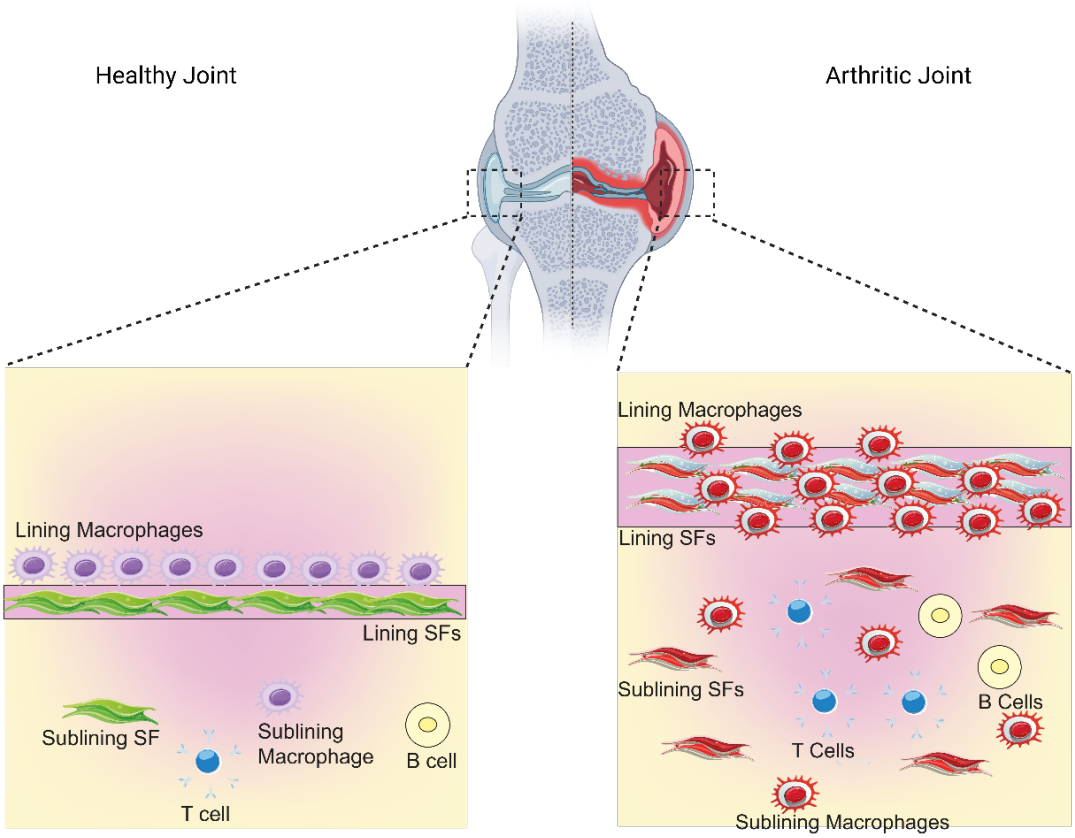

Figure 1-2 Comparison of Healthy vs Arthritic Joint Synovium

In healthy joints, the intimal lining layer is typically 1-2 cells thick, with SFs and macrophages accounting majority of this layer through proper cellular composition, balanced cell dynamics, and regulated immune responses. In RA, on the other hand, cellular dynamics are disrupted, causing abnormal expansion and remodelling of both the synovial lining and sublining layers, which results in synovial hyperplasia. Sublining layer of synovium is thicker and consisted of proinflammatory SFs and infiltration of immune cells. Illustration is created by Biorender and Adobe Illustrator.

1.4 Synovial Fibroblasts in Health vs Rheumatoid Arthritis

SFs are mesenchymal origin cells that contribute to both the maintenance of healthy joint function and the pathological changes seen in chronic inflammation associated with RA. The expression of specific surface markers by these fibroblasts helps understanding their functionality and roles during health and disease. In healthy synovial tissue, SFs primarily play a supportive role, assisting with the maintenance of joint homeostasis. They contribute to synovial fluid production, maintain the integrity of the extracellular matrix, and limit the inflammatory response through regulated cytokine and chemokine secretion (Noss & Brenner, 2008). Some of the markers on healthy synovial fibroblasts include expressions of CD90 (Thy-1), CD34, low levels podoplanin (PDPN), vimentin, CDH-11 and CD55. These markers help describe their identity as fibroblasts and reflect their healthy states (Bartok & Firestein, 2010; Mizoguchi et al., 2018).

As RA progresses, SFs undergo significant phenotypic changes. These activated synovial fibroblasts lose their regulatory balance, proliferate uncontrollably, and contribute to the destruction of the joint structure. They express elevated levels of various pro-inflammatory cytokines, such as IL-6, and matrix-degrading enzymes like MMPs that facilitate cartilage and bone destruction (Matsuda et al., 2023). Proinflammatory environment is maintained by the fibroblasts' increased secretion of matrix metalloproteinases, notably MMP-9, which facilitates tissue remodelling and degradation (Xue et al., 2014). RA SFs also exhibits a unique array of markers that distinguish them from their healthy counterparts. Critical to their function in RA are cellular signalling pathways activated by pro-inflammatory cytokines such as TNF-α. For instance, RA SFs have been shown to express IRF1, which is critical for the TNF-driven interferon response and contributes to the inflammatory microenvironment characteristic of RA (Bonelli et al., 2019). Distinct markers,

particularly HLA-DR and CD90, are prominently expressed in RA fibroblast subsets, underscoring their activated state and responsiveness to cytokines such as interferon-gamma (S. Zhao et al., 2022). Additionally, RA SFs produce Receptor Activator of Nuclear Factor-κB ligand (RANKL), a key factor promoting osteoclastogenesis and bone erosion in RA (Matsuda et al., 2023). Furthermore, SFs in RA have been found to form invadopodia-like structures that enhance their invasive properties into cartilage, facilitated by proteins such as cortactin and Src kinase (Lauzier et al., 2011). Diverse signalling pathways, including TLR, Notch, and various cytokine-mediated signalling routes, modulate the function of RA SFs. Dysregulation of these pathways leads to their persistent activation and supports the chronic inflammatory state observed in the disease (Brentano et al., 2005; K. Wei et al., 2020; Woods et al., 2006), summarised in Table 1-1.

Table 1-1 Characteristics of Synovial Fibroblasts in Rheumatoid Arthritis.

Characteristics	Examples	References
Proinflammatory Markers	The presence of HLA-DR$^+$CD90$^+$ SFs characterises a proinflammatory phenotype, with a significant response to IFN-γ, indicating their involvement in synovial inflammation.	(Zhao et al., 2022)
Matrix Metalloproteinases (MMPs) and Joint Destruction	Increased expression of MMP-9 is found in RA SFs, playing a crucial role in promoting inflammation, fibroblast survival, and matrix degradation. Evidence suggests that MMP-2 does not exhibit the same effects, which are distinct to RA fibroblasts. SFs form a destructive hyperplastic pannus that invades cartilage and bone, contributing significantly to disease pathology. Their activation leads to	(Lefèvre et al., 2009; Müller-Ladner et al., 2007; Xue et al., 2014)

	the secretion of cytokines and chemokines that exacerbate inflammation and joint damage. Other MMPs relevant in joint destruction are MMP-1 and MMP-3.	
Hyperproliferation and Migration	RA SFs show enhanced proliferation and migration capabilities. Studies indicate that increased fibroblast density correlates with joint inflammation and erosion in RA, with local proliferation being the main contributor to synovial hyperplasia.	(Matsuo et al., 2016)
Cytokine Secretion	RA fibroblasts are notable for their constitutive production of several cytokines, including IL-6. This cytokine release is a key factor in the inflammatory environment of the joint, causing further recruitment of immune cells and perpetuating inflammation.	(Bucala et al., 1991; Fang et al., 2020)
Signalling Pathways	Various signalling mechanisms including TLR, Notch, and p21-related pathways, NFκβ and MAPK have been implicated in the activation and function of synovial fibroblasts in RA. Aberrant signalling through these pathways leads to sustained fibroblast activation and contributes to RA pathology.	(Brentano et al., 2005; Choi et al., 2014; K. Wei et al., 2020; Woods et al., 2006; X. Zhang et al., 2021)

Cell-Cell Communication and Adhesion	Fibroblast interactions through cadherin-11 enhance cytokine expression and promote angiogenesis, thereby supporting the inflammatory milieu in RA. Fucosyltransferases also modulate angiogenesis, leukocyte-SF adhesion, and SF proliferation.	(Isozaki et al., 2014; Valencia et al., 2004)

1.4.1 Functional Subsets of Rheumatoid Arthritis Synovial Fibroblasts

In the context of RA, SFs encompass distinct subsets with unique functional characteristics that impact disease pathogenesis. Mizoguchi et al. investigated the functional and transcriptional differences among fibroblast subsets derived from human synovial tissues in RA. Utilising advanced techniques including microarray, bulk transcriptomics and single-cell transcriptomics, the authors identified a total of seven distinct fibroblast subsets, each characterised by specific surface protein phenotypes. They further categorised these seven subsets into three primary groups, highlighting their functional and anatomical specificity: $CD34^{-}THY1^{-}$, $CD34^{-}THY1^{+}$, and $CD34^{+}$ SFs. $CD34^{-}THY1^{+}$ population expanded in deep sublining of RA synovium, increasing the expression of genes involved in migratory responses such as TWIST1, CTHRC1, POSTN, PDGFRB, LOXL2, and MMP14. $CD34^{-}THY1^{-}$ SFs increased the expression MMP1 and MMP3 and found to be more abundant in osteoarthritis (OA) compared to RA. On the other hand, $CD34^{+}$ SFs demonstrated increased expression of genes such as IL6, CXCL12, and CCL2 and they are located both lining and sublining layers of RA synovium (Mizoguchi et al., 2018).

Micheroli et al utilised a deconvolution analysis to dissect the composition and functional implications of SF clusters across various synovial pathotypes, namely fibroid, lymphoid, and myeloid. The study identified four distinct clusters of SFs, each characterised by specific marker genes. The first cluster was lining $PRG4^{+}$ SFs which are characterised by the expression of CD55 and MMP3, indicating their role in maintaining joint homeostasis and cartilage integrity. $CXCL12^{+}$ sublining subsets expressed CXCL12, CCL2, and ADAMTS1, indicating their

involvement in chemokine-mediated recruitment of immune cells, thus potentially contributing to inflammatory responses within the synovial environment. $POSTN^+$ sublining SFs expressed POSTN alongside various collagen genes, suggesting their active role in extracellular matrix remodelling and tissue repair. $CXCL14^+$ sublining SFs on the other hand demonstrated high levels of CXCL14 and CD34, indicating a distinct functional capacity in modulating inflammation and possibly influencing immune cell migration and retention within the synovium. Analysis of these subsets across the various synovial pathotypes revealed differential expression patterns tied to disease activity, suggesting that specific fibroblast clusters may dominate certain inflammatory or repair contexts within RA. Furthermore, the relationship between SF composition and clinical parameters of disease activity emphasises the significance of fibroblast heterogeneity in the progression of RA. This work provided the importance of understanding the specific contributions and characteristics of these fibroblast subsets, which may provide insights into targeted therapeutic strategies aimed at modifying disease outcomes in RA patients. The distinct functions of these subsets suggest that they could serve as biomarkers for different disease scenarios or provide targets for more personalised interventions (Micheroli et al., 2022).

The research conducted by Zhang et al. explores the cellular compositions and states within the synovial tissues of patients with RA. This study employs a multimodal approach combining scRNA-seq and mass cytometry to achieve a comprehensive understanding of the various immune and fibroblast cell populations contributing to joint inflammation. The study involved 51 individuals, including those with RA and OA, to delineate the specific inflammatory cell states present. Utilizing canonical correlation analysis (CCA) of 5,265 single-cell transcriptomic profiles, the researchers annotated 18 populations of cells within the synovial tissue. Authors identified different subsets of T-cells, B-cells, monocytes and SFs. Among those, THY^+CD34^+ sublining fibroblasts are demonstrated to be high in leukocyte poor RA compared to OA. THY^+CD34^-HLA-DR^+ sublining FLS demonstrated higher levels of IL6, CXCL12, and HLA-DRA gene expressions, indicating their role on active cytokine production. These specific cell subtype also expressed genes related to MHC class II presentation and the interferon γ-mediated signalling pathway, indicating their pathogenic roles in RA. $DKK3^+THY^+CD34^-$ $HLA\text{-}DR^{low}$ RA and OA sublining SFs upregulated DKK3, CADM1, and COL8A2 genes. $CD55^+$ lining RA SFs however expressed lubricin

and demonstrated to be higher in OA and leukocyte poor RA (F. Zhang et al., 2019).

Croft et al. investigated the role of different SF subsets in the pathogenesis of RA. The authors employed advanced single-cell transcriptomic analysis to identify and characterise discrete fibroblast subsets present in the synovial tissue. Specifically, they focused on distinct populations defined by the expression of key surface markers, including fibroblast activation protein alpha (FAPα) and THY1. Authors found that $FAP\alpha^{+}THY1^{+}$ sublining SFs a pro-inflammatory group that contributes to the inflammatory milieu by secreting various cytokines, including IL-6 and chemokines such as CXCL12 and CCL2. These fibroblasts are crucial in promoting inflammation and leukocyte recruitment, which exacerbates synovitis. $FAP\alpha^{+}THY1^{-}$ lining SFs on the other hand exhibited destructive properties associated with joint damage. They were associated with bone and cartilage erosion, providing a link between fibroblast activation and structural damage in the joints. They expressed higher levels of MMPs and RANKL (Croft et al., 2019).

1.5 Macrophages in Rheumatoid Arthritis

1.5.1 Circulating Monocytes and Macrophage Polarisation

Circulating monocytes are a crucial component of the innate immune system, acting as precursors to various cell types involved in inflammation and tissue repair. They originate from bone marrow progenitors and populate the bloodstream, where they play multiple roles, including phagocytosis, antigen presentation, and the regulation of adaptive immune responses (Seta & Kuwana, 2007). Depending on their maturation, human circulating monocytes can differentiate into various subsets, primarily categorised into classical, intermediate, and non-classical monocytes based on surface markers like CD14 and CD16 (Kapellos et al., 2019). In inflammatory diseases, circulating monocytes play a significant role in the inflammatory process and disease pathology. The functional characteristics of circulating monocytes are tightly related to their phenotypic expression. Classical monocytes express $CD14^{++}CD16^{-}$, intermediate monocytes express $CD14^{++}CD16^{+}$, and non-classical monocytes express $CD14^{dim}CD16^{++}$. For instance, the $CD14^{++}CD16^{+}$ subset, identified as intermediate monocytes, has been implicated in inflammatory processes and presents increased frequencies in conditions such as RA and atherosclerosis (Krychtiuk et al., 2015; Rong et al., 2014). Intermediate monocytes from synovial fluid in RA patients expressed

increased levels of HLA-DR and promoted Th1 and Th17 responses (Yoon et al., 2014), increasing levels of proinflammatory cytokines such as TNF-α, IL-1β and IL-6, and differentiating into M1 macrophages that are involved in synovial inflammation (J. Yang et al., 2014). Classical $CD14^{++}CD16^{-}$ monocytes on the other hand produce high levels of TNF-α, IL-1β, IL-10 and IL-6, and when they stimulated with G-MCSF and IL-4, classical monocytes but not intermediate and non-classical monocytes differentiate into monocyte-derived dendritic cells (mo-DCs) (Boyette et al., 2017). Komano et al. identified osteoclasts that are differentiated from classical monocytes by the RANKL and MCSF treatment. In their paper, they demonstrated that precursors of osteoclasts are $CD16^{-}$ classical monocytes but not $CD16^{+}$ monocytes in human RA synovial joints (Komano et al., 2006). Non-classical monocytes also known as patrolling monocytes are involved in early inflammatory responses. They have capability of differentiating into M2 macrophages which is involved in resolution of inflammation (Cros et al., 2010; Thomas et al., 2015). Circulating monocytes are also important in mediating inflammatory responses and are rapidly recruited to sites of tissue injury or infection. This recruitment is largely influenced by chemokines, such as CCL2, which guide monocytes to areas of inflammation where they can differentiate into macrophages or dendritic cells (Ingersoll et al., 2011). The circulating monocytes during RA development were illustrated in Figure 1-3. Monocyte to macrophage polarisation is important process where imbalance between M1 and M2 macrophages have shown one of the drivers in RA (Kinne et al., 2007). Classically activated macrophages, referred to as M1-polarised macrophages, become activated by the cytokine interferon-Ɣ (IFN-Ɣ) and play a role in Th1 responses. M1 macrophages generate pro-inflammatory cytokines, such as TNF-α, IL-1, IL-6, IL-12, and IL-23. They are essential for defending the host against virus and intracellular bacteria during acute infections or tumour development. IFN-Ɣ, LPS, and G-MCSF drive macrophages to polarise into the M1 type (Lee, 2019). Conversely, alternatively activated macrophages, referred to as M2 polarised macrophages, are involved in tissue repair and resolution of inflammation characterised by the production of anti-inflammatory cytokines such as IL-10 and TGF-β (Mia et al., 2014). M2 macrophages have four different subtypes which named M2a, M2b, M2c and M2d. M2a macrophages are activated by IL-4 and IL-13 and play a crucial role in tissue repair and wound healing. They exhibit elevated expression of the mannose receptor (CD206), which enables them to engulf apoptotic cells and debris, facilitating healing processes (Anders & Ryu, 2011).

M2b macrophages play regulatory roles in health vs disease and are activated by exposure to immune complexes and toll-like receptor (TLR) agonists, also express high levels of CCL1 and TNFSF14. They secrete both pro-inflammatory and anti-inflammatory cytokines (L. Wang et al., 2019). The differentiation of M2c macrophages occurs through the IL-10 and glucocorticoids and they express CD163 scavenger surface receptor and Mer receptor tyrosine kinase (MerTK). M2c macrophages involved in resolution of inflammation during the late phage of infection (Anders & Ryu, 2011; L. Wang et al., 2019). M2d macrophages, also referred to as Tumour Associated Macrophages (TAMs) are activated by adenosine receptor agonists stimulation and secrete high levels of IL-10, iNOS and VEGF and low levels of TNF-α and IL-1β, IL-12 (Ferrante et al., 2013; L. Wang et al., 2019). They function in tissue repair, and cancel cell invasion (L. Wang et al., 2019).

Palacios et al. in their research highlighted the role of activin A, a member of the TGF-β family, in mediating the pro-inflammatory polarisation of macrophages within the synovial fluid of RA patients. The study suggests that activin A is a key player in driving macrophage polarisation towards an M1 phenotype, correlating with elevated inflammation levels seen in RA. This finding provides the important connection between specific cytokines in the synovial environment and macrophage behaviour, proposing a potential target for therapeutic intervention (Soler Palacios et al., 2015).

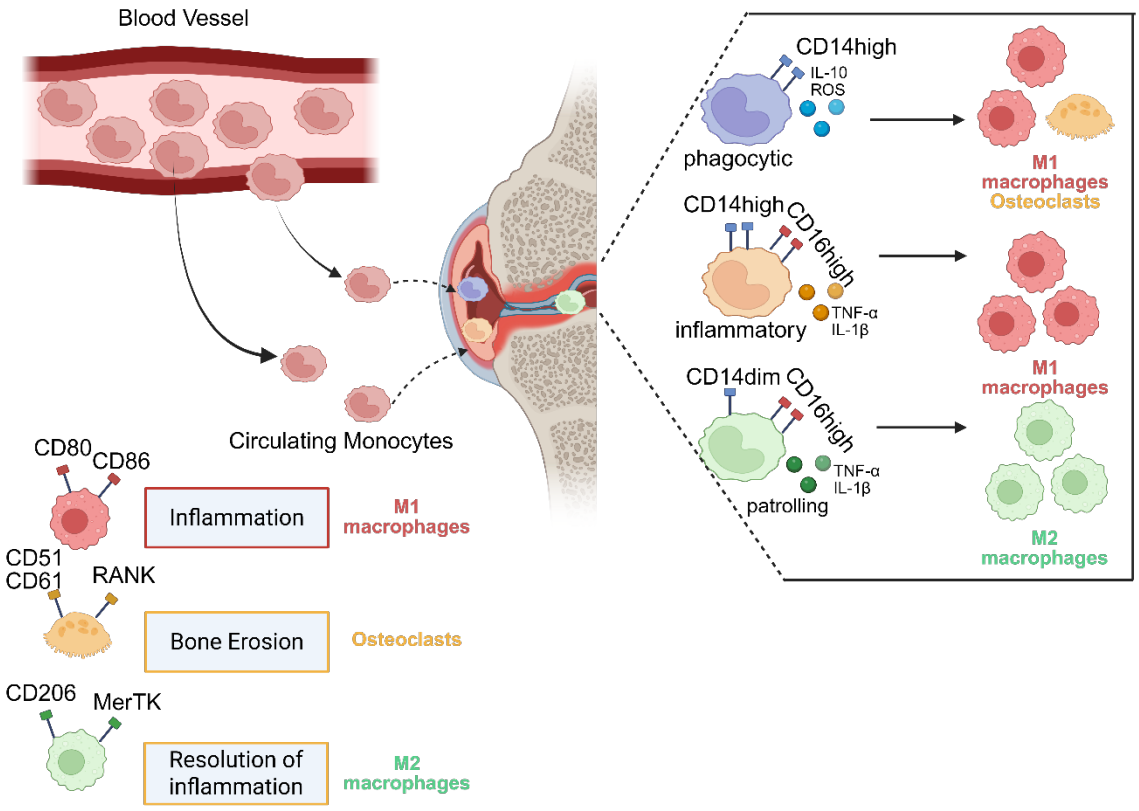

Figure 1-3 Human Circulating Monocytes Differentiate into Macrophages in Rheumatoid Arthritis Development

Circulating monocytes can be classified into three distinct subsets: classical monocytes ($CD14^{high}$), intermediate monocytes ($CD14^{high}CD16^{high}$), and non-classical monocytes ($CD14^{dim}CD16^{high}$). Circulating monocytes moves into the RA joint and polarise into osteoclasts, M1 or M2-like macrophages. Depending on their function, while proinflammatory osteoclasts and M1 macrophages involved in bone erosion, and inflammation, anti-inflammatory M2 macrophages function in resolution of inflammation. Illustration is created by Biorender.

Murine circulating monocytes play crucial roles in various immune responses, serving as precursors to macrophages and dendritic cells. These monocytes exhibit distinct functional capacities that are critical for understanding both homeostatic and pathological conditions. In mice, circulating monocytes can typically be classified into three main subsets based on the differential expression of surface markers Ly6C and CCR2. The $Ly6C^{high}$ group is often associated with inflammatory responses and is considered the inflammatory monocyte subset, while $Ly6C^{low}$ cells are regarded as non-inflammatory. These subsets are linked to distinct migration patterns and functional capabilities (J. Yang et al., 2014). The polarisation of murine monocytes is influenced by the local microenvironment,

characterised by the presence of cytokines and other signalling molecules. When activated by pro-inflammatory stimuli, such as LPS, murine monocytes tend to polarise towards the M1 phenotype associated with enhanced expression of TNF-α and IL-6, and increased phagocytic activity (Orecchioni et al., 2019). Conversely, exposure to cytokines like IL-4 promotes M2 polarisation, which is characterised by a tissue-repair phenotype and a more potent role in resolving inflammation (Orecchioni et al., 2019). Understanding this polarisation process is important to leveraging therapeutic approaches aimed at rebalancing inflammatory responses. In summary, murine circulating monocytes are diverse and highly adaptive cells that play critical roles in both homeostasis and inflammation. Their classification into distinct subsets, their dynamic polarisation in response to environmental cues, and their functional implications in disease highlight their potential as targets for therapeutic interventions aimed at modulating immune responses.

Considering RA, M1 macrophages seems to largely affect disease progression as they consisted of pro-inflammatory characteristics. Jeganathan et al. determined how different M1/M2 inflammatory stimuli affect the differentiation of murine macrophages into osteoclasts following exposure to RANKL. The researchers used bone marrow-derived monocytes from mice, which were subjected to various polarisation conditions before being cultured with RANKL and M-CSF. The stimuli used for macrophage polarisation included pro-inflammatory factors such as IFN-γ to induce M1 polarisation and IL-4 to induce M2 polarisation. Subsequent analysis involved assessing the formation of multinucleated giant cells and their osteoclastogenic properties. Exposure to M1-inducing factors led to an enhanced formation of osteoclasts compared to controls. This effect was likely mediated by the pro-inflammatory cytokines produced during M1 polarisation. Conversely, M2 polarisation, induced by IL-4, resulted in reduced osteoclast formation, indicating that M2-type macrophages are less prone to differentiate into osteoclasts. The results suggest a significant modulation effect of macrophage polarisation on osteoclastogenesis, with M1 macrophages promoting bone resorption processes (Jeganathan et al., 2014).

IL-26 cytokine is previously reported to be highly upregulated in RA. However, their roles in terms of macrophage polarisation are unknown. IL-26, as reported by Lin et al., skewed macrophages towards an M1 polarisation in both human and mice by activating the cJUN and NF-κB pathways. Authors' findings provide

knowledge on important roles of pro-inflammatory cytokines in shaping macrophage behaviour and the potential therapeutic implications of targeting these pathways to alter the disease course in RA (Lin et al., 2020).

The expressions of F4/80 and CD11b are critical for identifying and understanding the roles of murine macrophages in various physiological and pathological processes, including inflammation and tissue homeostasis. F4/80 is a well-known cell surface glycoprotein widely regarded as a pan-macrophage marker in mice and is primarily expressed in tissue-resident macrophages. F4/80 expression is crucial for differentiating between macrophage subsets (dos Anjos Cassado, 2017). Studies have shown that F4/80^{+} macrophages can be categorised based on their expression of other markers. For instance, CD11b^{+} F4/80^{low} CD206^{-} cells are typically categorised as M1-type macrophages, which are associated with pro-inflammatory functions. In contrast, CD11b^{+} F4/80^{high} CD206^{+} macrophages exhibit an M2-like phenotype, which is associated with anti-inflammatory responses and tissue repair (Y. Li et al., 2014). The balance between these phenotypes influences the severity of inflammation and joint damage, with M1 macrophages contributing to disease exacerbation and M2 macrophages potentially mitigating damage.

M1 macrophages are identified by elevated levels of markers such as inducible nitric oxide synthase (iNOS), TNF-α, IL-6, IL-12, and IL-1β. For instance, Kuninaka et al. observed that markers like Il12a and Nos2 were significantly upregulated following skin injury in mice, indicating robust M1 activation during the initial phases of wound healing (Kuninaka et al., 2022). In contrast, M2 macrophages exhibit markers such as arginase-1 (Arg1) and mannose receptor C type 1 (Mrc1 or CD206). Studies such as those by Jablonski et al. have elucidated the expression profiles of M1 and M2 markers in BMDMs and highlighted the distinct gene expression patterns between different macrophage states (Jablonski et al., 2015). For instance, M1 markers included Il-6, Il1a, Serpinb2, Cxcl9 and Cxcl3, while M2 markers were Arg1, Retnla, Tmem26 and Socs2 (Jablonski et al., 2015).

It is also important to note the role of macrophage polarisation in osteolytic disease such as periodontitis which is similar to RA. In both conditions, pro-inflammatory M1 macrophages are major sources of cytokines such as TNF-α, IL-1β, and IL-6, which drive chronic inflammation and stimulate osteoclastogenesis, ultimately leading to progressive bone resorption and tissue damage. Conversely,

M2 macrophages promote resolution and repair by producing anti-inflammatory mediators and supporting tissue regeneration. A key pathogenic feature of both RA and periodontitis is the impaired transition from M1- to M2-like phenotypes, resulting in a persistent inflammatory environment that sustains osteolysis. This shared immunopathology highlights the importance of macrophage polarisation not only as a biomarker of disease activity but also as a potential therapeutic target. We have previously demonstrated that macrophages play a central role in both bone loss and regeneration in inflammatory osteolytic diseases like periodontitis. Using a mouse ligature-induced periodontitis model, our group at University of Toronto showed that proinflammatory M1 macrophages dominate during active inflammation, producing TNF-α and driving osteoclast-mediated bone resorption, whereas resolving M2 macrophages expressing CD206, IL-10, and TGF-β become prevalent during healing and correlate with bone regeneration. Depleting macrophages with clodronate liposomes prevented bone loss but impaired subsequent healing, while inducing M2-like macrophages with rosiglitazone reduced bone resorption and enhanced regeneration. In vitro, IL-4 activated M2 macrophages exhibited anti-inflammatory and pro-resolving functions, promoted osteoblast mineralisation, and inhibited osteoclast activity, partly through the secretion of cystatin C. Depleting cystatin C abolished these anabolic effects, highlighting its key role in linking inflammation resolution to bone formation. In conclusion, the findings presented in our research emphasise the dual functionality of macrophages in bone dynamics, specifically demonstrating that resolving macrophages not only alleviate inflammation but also play a significant role in anabolic bone processes. By promoting bone formation and reducing bone resorption, these macrophages hold therapeutic potential for treating conditions characterised by chronic inflammation and osteolysis, such as periodontal disease and RA. This opens avenues for future research to explore targeted macrophage-based strategies in bone disease management (Viniegra et al., 2018).

Tissue-resident synovial macrophages (TRSMs) are important in the pathogenesis of RA, playing a key role in both the maintenance of joint homeostasis and the progression of inflammation. Their characteristics, functions, and the dynamics of their polarisation directly influence the inflammatory landscape of the synovium in RA. TRSMs are primarily found in the synovial lining layer and the sublining layer of the joint. They are derived from a distinct lineage during embryonic

development, unlike monocyte-derived macrophages that infiltrate during inflammation (Culemann et al., 2019). Studies indicate that these macrophages play a protective role under steady-state conditions by maintaining tissue homeostasis and responding to local signals (Alivernini et al., 2020; Culemann et al., 2019). For instance, synovial lining macrophages expressing CX3CR1 have been demonstrated to create an internal immunological barrier at the synovial lining. These macrophages mitigate inflammation by forming a tight-junction-based barrier to protect intra-articular structures (Culemann et al., 2019). Alivernini et al. identified different tissue-resident SMs in patients with early/active RA, treatment-refractory/active RA, and RA in sustained remission (Alivernini et al., 2020). They showed that two subpopulations were involved in sustained remission, $MerTK^{pos}TREM2^{high}$ and $MerTK^{pos}LYVE1^{pos}$. On the other hand, early arthritis and treatment-refractory active RA patients demonstrated a reduced number of MerTK clusters and an increased number of $MerTK^{neg}CD48^{neg}SPP1^{pos}$ and $MerTK^{neg}CD48^{neg}S100A12^{pos}$ clusters. Furthermore, while $MerTK^{-}CD206^{-}$ TRSM produced inflammatory mediators, $MerTK^{+}CD206^{+}$ TRSM released lipid mediators that resolve inflammation and activate the repair phenotype in SFs. These data indicate that SMs demonstrate complex heterogeneity and dynamic changes occurring in tissue resident and circulating-derived SMs. However, further research is required to fully understand the role of macrophage networks in the pathogenesis of RA.

1.6 Crosstalk Between Synovial Fibroblasts and Macrophages in Rheumatoid Arthritis

The crosstalk between synovial fibroblasts and macrophages is a critical area of study in understanding the pathophysiology of RA. This interaction significantly influences the inflammatory environment within the synovial tissue, contributing to both joint inflammation and tissue destruction. The proliferation of SFs in RA correlates with increased macrophage infiltration, indicating mutual reinforcement of their inflammatory roles. The role of SFs extends to direct interactions with macrophages, promoting their activation and modulating inflammatory responses (Knab et al., 2022; Zheng et al., 2024). For instance, macrophages can secrete factors that influence the SF phenotype, leading to enhanced invasiveness and secretion of matrix-degrading enzymes, a hallmark of joint erosion in RA. Macrophages also secrete various pro-inflammatory cytokines, and chemokines which result in increased IL-6 and MMPs production in SFs. This creates an

autoimmune loop that perpetuates inflammation (Cheng et al., 2021; Matsuda et al., 2023).

Early studies by Scott et al. investigated RA SF and macrophage interactions in a coculture system. They found that there is a cartilage degradation caused by SF and macrophage interactions (Scott et al., 1997). CCR2 expressed in RA SFs and involved in SF-mediated inflammation. Li et al. investigated the impact of CCR2 antagonists on SF and macrophage crosstalk in RA. CCR2 inhibition reduced cytokines and MMPs released by SFs, but it did not change their proliferative and migrative behaviours (R. Li et al., 2023). Further coculture experiments with macrophages demonstrated that macrophage-mediated inflammation was also indirectly repressed with a reduced expression of IL-1, IL-6, and TNF-α in macrophages.

As mentioned previously, macrophages in RA can be categorised into distinct subsets that are critical for inflammatory processes and joint pathology. Recent findings have highlighted a subset of $MERTK^{+}$ macrophages, associated with disease remission, that can induce repair responses in fibroblasts (Alivernini et al., 2020).Conversely, the presence of $HBEGF^{+}$ macrophages in RA tissues has been implicated in promoting fibroblast invasiveness through epidermal growth factor receptor (EGFR) signalling pathways, indicating a significant intercellular communication that perpetuates joint damage (Kuo et al., 2019). The crosstalk between these SFs and macrophages thus creates a self-sustaining inflammatory loop that is marked by reciprocal positive feedback mechanisms, enhancing disease severity and persistence (Zheng et al., 2024). Single-cell RNA sequencing studies have further deepened our understanding of the heterogeneity within both synovial macrophages and fibroblasts, revealing distinct polarisation states and activation profiles that are influenced by their microenvironment (Cheng et al., 2021).

1.7 Cell Sialylation and Rheumatoid Arthritis

N-glycans and O-glycans are critical components of glycoproteins found ubiquitously across living organisms, possessing distinct structural characteristics and biological functions. N-glycans are covalently bonded to the nitrogen of asparagine residues (Asn) within the amino acid sequence of proteins, typically following the consensus sequence Asn-X-Ser/Thr, where X can be any amino acid

except proline (Imperiali & O'Connor, 1999). All N-glycans share a conserved core structure composed of two N-acetylglucosamine (GlcNAc) residues linked to three mannose (Man) residues, which can be further elaborated through the addition of fucose, sialic acid or extended chains. This structural diversity underlies the wide range of biological functions mediated by N-glycans, including their roles in protein folding, stability, and recognition events central to cellular signalling (Moremen et al., 2012). In contrast, O-glycans are attached to the hydroxyl group of serine or threonine residues in proteins. The most common initiating sugar for O-glycans is N-acetylgalactosamine (GalNAc), which forms a core structure that can be further extended with additional sugars such as galactose (Gal) and sialic acid (Kudelka et al., 2015). Sialic acids are family of sugars notably includes N-acetylneuraminic acid (Neu5Ac) and serves significant biological functions, such as influencing cellular interactions, mediating immune responses, and providing a protective role against pathogens. Sialic acids can link to glycans via two distinct configurations: α2,3 and α2,6, which can dramatically alter their functional properties and interaction dynamics (Pongracz et al., 2019, 2021). The structural characterisation of these linkages is essential in various fields, particularly in oncology. For instance, differential analysis of serum glycome sialic acid linkages have been shown to refine the diagnosis of ovarian cancer, highlighting how linkage-specific sialic acid profiles can serve as biomarkers for disease states. In this study, increased α-2,3/α-2,6-sialylation ratio for both afucosylated and fucosylated N-glycans was found in early and late-stage ovarian cancer patients (Dědová et al., 2019).

Cell sialylation is a critical post-translational modification that plays a significant role in modulating various cellular functions. Sialic acids, found at the terminal ends of glycan chains, impact cell signalling, immune responses, and cellular interactions, including those between SFs and macrophages. The dysregulation of sialylation patterns can contribute to the pathophysiology of RA, influencing fibroblast activation and inflammatory processes within the synovial joint. Recent studies have highlighted how loss of α2-6 sialylation can lead to a pro-inflammatory phenotype in synovial fibroblasts. Specifically, Wang et al. demonstrated that decreased α2-6 sialylation in SFs correlates with increased expression of inflammatory cytokines and chemokines, suggesting that sialic acids may act as regulatory mechanisms to maintain cellular homeostasis in the synovium (Y. Wang et al., 2021). This change may affect fibroblasts directly and

their interactions with other immune cells, including macrophages, indicating a crucial role for sialylation in maintaining SF integrity and function. In the immune context, sialylation could alter the activity of arthritogenic IgG, since they are hyposialylated in experimental collagen-induced arthritis, which could potentially modulate the inflammatory response in RA (Ohmi et al., 2016).

1.7.1 Sialic Acid Biosynthesis and Desialylation

Sialic acid biosynthesis in humans is primarily mediated by a critical enzyme known as UDP-N-acetylglucosamine 2-epimerase/N-acetylmannosamine kinase (GNE), which facilitates the conversion of UDP-N-acetylglucosamine to N-acetylmannosamine (ManNAc) and subsequently to N-acetylneuraminic acid (Neu5Ac) (Zieger et al., 2022). GNE thus plays a pivotal role in the synthesis and regulation of sialic acids. The activity of this enzyme is crucial, as disturbances in the GNE gene can lead to severe congenital defects, including thrombocytopenia (Zieger et al., 2022). The incorporation of sialic acids into glycoproteins and glycolipids is performed by a group of enzymes called sialyltransferases, which utilise cytidine 5′-monophosphate-sialic acid (CMP-Neu5Ac) as a donor substrate (L. Wang et al., 2016). This transfer typically occurs at the non-reducing ends of carbohydrate chains and is crucial for the biological functions of glycoconjugates in cellular recognition, immune modulation, and signal transduction (Y. Li & Chen, 2012). Sialyltransferases can be categorised based on the type of linkage they create when adding sialic acid to sugar residues. Two primary linkage types include α2,3-Sialyltransferases (ST3GalTS) and α2,6-Sialyltransferases (ST6GalTS). ST3Gal enzymes transfer sialic acid to the hydroxyl group of galactose or galactosamine residues, forming α2,3 linkages. Examples include ST3Gal1, ST3Gal2, and ST3Gal3, each with slightly different substrate specificities. ST6Gal enzymes add sialic acid to the 6-hydroxyl position of galactose in a variety of glycoproteins and glycolipids. Prominent members include ST6Gal1 and ST6Gal2 (Harduin-Lepers et al., 2001; Y. Li & Chen, 2012). The ST6GALNAC family, which includes ST6GalNAc-1, ST6GalNAc-2, ST6GalNAc-4, and ST6GalNAc-5, is known for modifying glycoproteins and glycolipids by adding sialic acids in an α2,6 linkage (Harduin-Lepers et al., 2012). Additionally, there are α2,8-sialyltransferases (ST8Sia) that add sialic acid in chains, primarily involved in synthesising polysialic acid, an important structural component in neural and embryonic tissues (L.-Y. Chang et al., 2009; Harduin-Lepers et al., 2001). The overall sialic acid biosynthesis pathway is illustrated at Figure 1-4.

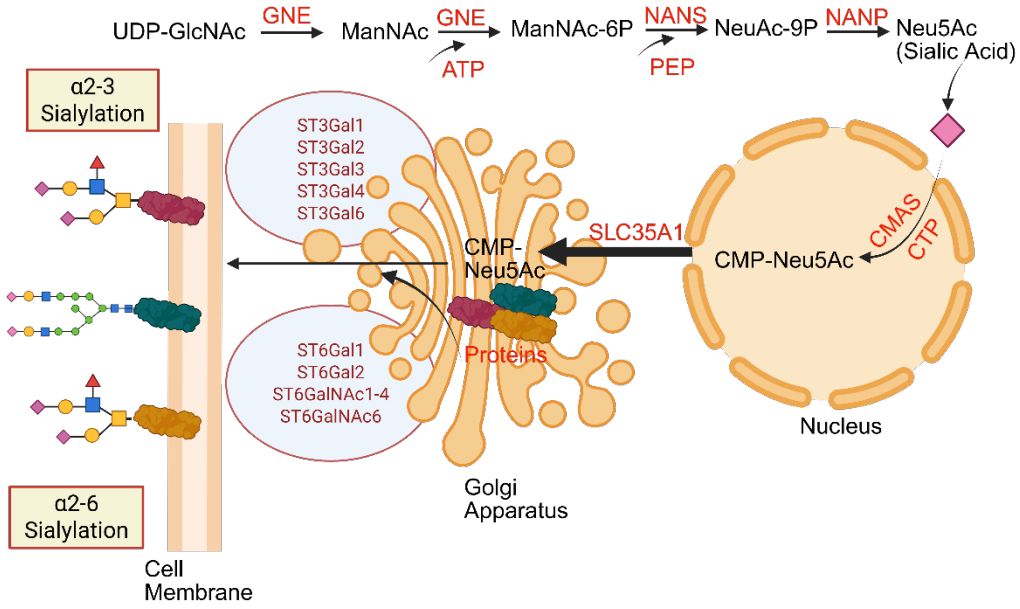

Figure 1-4 Biosynthesis of Sialic Acid

The production of sialic acid (Neu5Ac) occurs within cells, involving enzymes highlighted in red. The initial processes in this pathway take place in the cytoplasm beginning with the substrate UDP-GlcNAc, derived from glucose. The pathway's rate-limiting step is catalysed by GNE, which transforms UDP-GlcNAc into ManNAc. Following this, ManNAc kinase (originating from the kinase domain of GNE) or other cytoplasmic kinase enzymes phosphorylate ManNAc, forming ManNAc-6-phosphate. NANS catalyses the condensation of ManNAc-6-P with phosphoenolpyruvate (PEP) to form N-acetylneuraminic acid-9-phosphate (Neu5Ac-9-P), marking a key committed step in the pathway. NANP then dephosphorylates Neu5Ac-9-P to yield free Neu5Ac. Meanwhile, in the cell nucleus, Neu5Ac is converted to CMP-sialic acid, which then travels to the Golgi apparatus, where it provides Neu5Ac for the sialylation of newly formed glycoproteins. Mature sialylated glycoproteins may be either secreted or integrated into the plasma membrane. Illustration is created by Biorender.

Sialidases, also referred to as neuraminidases, are enzymes that hydrolyse sialic acid residues from glycoproteins, glycolipids, and oligosaccharides, playing a pivotal role in desialylation processes. This enzymatic action is crucial for various biological functions and impacts several physiological and pathological processes, including cell signalling, immune response modulation, and pathogen-host interactions. Desialylation is an important biological event because it is involved in the catabolism of glycoconjugates which regulate their lifespan and involved in their recycling (M. Wei & Wang, 2019). Sialidases can be classified based on their specificities and cellular localizations into four known types in mammals: NEU1,

NEU2, NEU3, and NEU4. Each type exhibits distinct substrate preferences and biological roles. NEU1, for instance, is primarily located in the lysosome but is also present on the plasma membrane, where it contributes to the desialylation of membrane glycoproteins. Its activity can regulate signalling pathways by modulating the presence of sialic acids on cell surfaces, thereby influencing cellular interactions and immune responses (Kawecki et al., 2019). NEU2 has been identified as having cytosolic localisation and is involved in various physiological processes, including the degradation of glycoproteins and the modulation of inflammatory responses. On the other hand, NEU3 is predominantly associated with the plasma membrane and is known to facilitate desialylation in response to extracellular stimuli, which can significantly alter cell behaviour and signalling mechanisms (Kawecki et al., 2019; M. Wei & Wang, 2019). In addition, pathogens exploit host sialidases to facilitate their invasion and colonization. For example, the sialidases secreted by certain bacteria, such as *Tannerella forsythia* and *Escherichia coli*, can desialylate host cell glycans, enhancing adherence and invasion of epithelial cells by altering the local glycan environment (Honma et al., 2011) In the realm of infectious diseases, bacterial sialidases can exploit the host's sialic acid content. For example, desialylation of glycoproteins on host cells can enhance bacterial adherence and invasion, as seen with *Pseudomonas aeruginosa* where the enzyme NEU1 facilitates pathogen adhesion by modifying the host's mucosal barriers (Lillehoj et al., 2015). Beyond fibrosis, sialidases are instrumental in modulating immune responses. For instance, the desialylation of TLR4 by NEU1 enhances microglial activation in response to lipopolysaccharides, leading to increased release of pro-inflammatory cytokines such as IL-6 (Allendorf et al., 2020).

Considering desialylation in SFs, our group have previously examined how alterations in sialylation affect naïve synovial fibroblast functions pivotal in arthritogenesis. Using a recombinant sialidase from *Clostridium perfringens,* which significantly cleaves both α2-6 and α2-3 linked sialic acids, our previous work showed that naïve fibroblasts with reduced sialylation exhibit altered migratory capabilities and display an activated state, marked by the production of inflammatory mediators like cytokines and chemokines, as well as mechanisms associated with anti-viral responses (Y. Wang et al., 2022).

1.8 Hyposialylation vs Hypersialylation in Health vs Disease

Hyposialylation and hypersialylation are two critical glycosylation states involving the addition and removal of sialic acid residues from glycoproteins and glycolipids, playing significant roles in both health and disease. The balance between these two states is central to immune regulation, cellular signalling, and disease progression. Hyposialylation refers to a reduced presence of sialic acid on the surface of glycoproteins and glycolipids. This state can lead to several pathophysiological consequences, particularly in autoimmune diseases, and neurodegenerative disorders. In autoimmune conditions, hyposialylated glycoproteins can trigger chronic inflammation and uncontrolled immune responses (Bordron et al., 2021). Scherer et al. investigated the Fc glycosylation profiles of ACPA in RA, comparing them with total IgG1 from serum and synovial fluid. They demonstrated that ACPA IgG1 from serum have markedly reduced terminal sialic acid residues and a trend toward increased agalactosylation (G0) compared with total serum IgG1, changes associated with heightened proinflammatory potential. In synovial fluid, ACPA were even more agalactosylated and asialylated, a pattern not observed in total synovial fluid IgG1, suggesting local antibody production within inflamed joints. Rheumatoid factor positive patients showed higher G0 and lower sialylation levels on ACPA than RF negative patients, implying a possible link between glycosylation state and RF binding. Core fucosylation remained high in all groups. These findings demonstrate that ACPA possess a distinct, compartment and RF dependent glycosylation profile that may enhance their pathogenic role in RA (Scherer et al., 2010). Malhotra et al. in their study showed that in RA, IgG antibodies undergo a shift in glycosylation, specifically, an increase in Fc glycoforms lacking galactose (G0) and terminating in GlcNAc. Using NMR, X-ray crystallography, and molecular modelling, the authors demonstrate that the loss of terminal galactose increases Fc oligosaccharide mobility and exposes GlcNAc residues, enabling binding to mannose-binding protein (MBP), a lectin of the innate immune system. When multiple IgG-G0 molecules are presented to MBP, complement activation occurs through the lectin pathway, independently of C1q. Experiments confirmed that MBP binding and complement activation are driven by Fc-associated G0 structures, are inhibited by mannose, and that MBP is present in RA synovial fluid at similar levels to serum. These findings suggest that in RA, autoantibodies carrying G0 glycans in inflamed joints could trigger complement activation via MBP, contributing to chronic synovial

inflammation and linking adaptive and innate immunity through altered IgG glycosylation (Malhotra et al., 1995). Specifically, the expression of ACPA is decreased by sialylation through an enzyme ST6GAL1 in both sera and B cells of RA patients and this is influenced by the transcription factor CTCF (H. Zhao et al., 2024), also indicating the prominent role of glycosylation in the development of RA autoantibodies.

Similar to the hyposylation process observed in autoantibodies, a study investigating SFs glycobiology done by our group, combined transcriptomic and mass spectrometry based glycomic analyses in human samples and a collagen-induced arthritis (CIA) mouse model, found that pro-inflammatory SFs, particularly $CD90^{+}$ sublining fibroblasts, lose α2-6 linked sialic acid due to TNF-mediated downregulation of the sialyltransferase ST6Gal1. This hyposialylation exposes terminal galactose residues, enhancing susceptibility to galectin-3 driven inflammatory signalling and potentially altering interactions with immune regulatory lectins such as siglecs which are sialic acid binding proteins involved in recognition of sialic acids. Experimentally, enzymatic or siRNA-induced removal of sialic acid was sufficient to trigger pro-inflammatory cytokine production in resting SFs. In both mice and humans, higher α2-6 sialylation correlated with remission, suggesting a protective, anti-inflammatory role. We propose that loss of α2-6 sialylation is a molecular switch converting SFs into a pathogenic phenotype, offering new biomarker and therapeutic opportunities in RA by targeting stromal glycosylation (Y. Wang et al., 2021).

By contrast, conditions that included heavily immunosuppression like cancer have an opposite sialylation affect compared to autoimmune conditions like RA. Hypersialylation in cancer is a critical focus of research, highlighting its significant role in tumour progression, immune evasion, and therapeutic resistance. The phenomenon is characterised by the overexpression of sialic acid residues on the surface of cancer cells, which can alter cell interactions, promote metastasis, and contribute to a suppressive tumour microenvironment. One of the primary mechanisms by which hypersialylation aids tumour cells is through immune evasion. Cancer-derived sialylated glycoproteins can bind to sialic acid-binding immunoglobulin-like lectins (Siglecs) on immune cells, effectively suppressing their activating signals (Adams et al., 2018; Z. Wang et al., 2020). Consequently, tumours with high sialic acid content often experience reduced anti-tumour

immune responses, leading to advanced malignancy and poorer prognoses (Pietrobono & Stecca, 2021). Moreover, hypersialylation is linked to increased tumour cell motility and invasiveness. Sialylated molecules can enhance cancer cell adhesion and migration through altered interactions with the extracellular matrix and other cell types, promoting metastatic capabilities (Pietrobono & Stecca, 2021). The role of hypersialylation extends to chemoresistance as well. Tumours with high levels of sialylation often exhibit resistance to conventional chemotherapeutic agents, complicating treatment regimens (Liu et al., 2018; Ou et al., 2020).

1.9 Sialic Acid Recognising Proteins

The recognition of sialic acids by specific proteins is crucial for numerous physiological processes including cell-cell communication, immune regulation, and pathogen interactions. Among the most prominent sialic acid-recognising proteins are the Siglecs, which are integral to the modulation of immune responses. Siglecs represent a specialised class of proteins that bind sialic acids, playing important roles in cellular signalling and interactions (Crocker & Varki, 2001; Pillai et al., 2012) In addition to Siglecs, various viruses exploit sialic acid for attachment and entry into host cells, indicating another critical aspect of sialic acid biology. For instance, the hemagglutinin-neuraminidase (HN) protein of parainfluenza viruses and the spike proteins of coronaviruses demonstrate varying selectivity for different sialic acid linkages, thus influencing their tissue tropism and infectivity (Fukushima et al., 2015; Schwegmann-Weßels & Herrler, 2006).

The study by Büll et al. (2021) developed an expanded cell-based human sialome array using genetically engineered HEK293 cells to map the fine binding specificities of human Siglecs in the natural context of cell-surface glycoconjugates. By systematically knocking out and reintroducing specific sialyltransferases and selected sulfotransferases, as well as engineering O-glycan presentation on mucin-like protein domains, the authors dissected the biosynthetic and structural requirements for Siglec recognition. They found that Siglec-4, -7, and -15 preferentially recognise distinct GalNAc-type O-glycans but with strong selectivity for how these glycans are patterned on particular protein backbones (e.g., MUC1 for Siglec-4, GP1bα for Siglec-7, clustered STn for Siglec-15). Sulfation via CHST1 markedly enhanced binding of Siglec-3, -7, -8, and -15, and the 6′-sulfo-sialyl-LacNAc epitope was identified as a key ligand for Siglec-3

(CD33) and Siglec-8. The work demonstrates that Siglec recognition depends not just on glycan structure but also on glycoprotein context and post-synthetic modifications like sulfation, providing a platform for identifying natural Siglec ligands and informing therapeutic targeting in immunity, cancer, and neurodegeneration. In the Büll et al. study, Siglec-1 (sialoadhesin/CD169) was found to have a broad binding profile across many α2-3-linked sialosides presented on both N- and O-glycans. Unlike several other Siglecs, its binding was not strongly enhanced by sulfation but was highly dependent on the presence of α2-3 sialic acids on underlying Galβ1-4GlcNAc motifs. The engineered cell-based array showed that Siglec-1 robustly recognised these motifs in multiple glycoprotein contexts, consistent with its known role as a macrophage receptor that captures sialylated pathogens and apoptotic cells.

Galectins are a family of soluble β-galactoside-binding proteins that play pivotal roles in various biological processes, including cell adhesion, proliferation, apoptosis, and immune modulation (Reesink et al., 2016; Zhuo & Bellis, 2011). Among this family, galectin-1 and galectin-3 are particularly significant due to their ability to interact with glycoproteins and affect cellular responses. The importance of these interactions is heavily influenced by sialylation, a post-translational modification that involves the addition of sialic acid residues to glycans on cell surfaces. Sialylation modifies the binding capacities of galectins. For instance, galectin-3 has been shown to bind effectively to glycoproteins with non-sialylated glycans, while sialylation can inhibit this interaction (Reesink et al., 2016). Specifically, α2,6-sialylation directly impacts galectin-1 binding to cell surface glycans. The binding of galectin-1 is largely inhibited by terminal α2,6-sialylation, as this modification prevents galectin-1 from effectively accessing its binding partners, thereby modulating cell adhesion and migration (Suila et al., 2014; Zhuo & Bellis, 2011).

The galectin lattice is a dynamic network formed when galectins that crosslink glycosylated receptors and lipids at the cell surface. Among the mammalian galectins, galectin-3 is unique in its ability to form pentamers, enabling multivalent binding that organizes transmembrane proteins into functional microdomains. This lattice regulates receptor diffusion, compartmentalization, endocytosis, and signalling, influencing key processes such as T cell activation, receptor tyrosine kinase signalling, and adhesion via integrins and cadherins. The strength of

glycoprotein incorporation into the lattice depends on the number and branching of N-glycans, which are shaped by Golgi N-acetylglucosaminyltransferases (MGATs) and the availability of UDP-GlcNAc from the hexosamine biosynthesis pathway, linking the lattice directly to cellular metabolic status. By integrating glycan structure with spatial receptor organization, the galectin lattice emerges as a crucial regulator of cell communication, signalling, and immune responses (Nabi et al., 2015). Sialylation plays a key modulatory role because terminal sialic acids on glycans can mask the galactose residues required for galectin binding, thereby weakening or preventing lattice formation; conversely, desialylation can expose galactose moieties and enhance galectin and ligand interactions. In this way, the galectin lattice integrates glycan branching, sialylation status, and metabolic cues to fine-tune receptor organization and cell signalling in immunity, adhesion, and tissue homeostasis (Troncoso et al., 2023).

1.10 Thesis Aims

The overall aim of this thesis is to elucidate the role of sialylation in regulating SF function and its immunomodulatory interplay with macrophages in the context of RA. By integrating transcriptomic analyses, targeted glycan remodelling, and functional co-culture assays, this work seeks to uncover how sialic acid structures influence fibroblast activation states, cytokine secretion, and downstream immune responses.

Specifically, the thesis will:

1. Characterise transcriptional alterations in glycosylation-related pathways in SFs in RA
    - Define how inflammatory conditions in vivo (across early arthritis, active disease, and remission) and in vitro (via TNF-α stimulation) reshape the expression of genes involved in glycan biosynthesis, with a particular focus on sialic acid metabolism and capping.
2. Experimentally determine the functional consequences of sialic acid removal in naïve SFs

- Use an in vitro desialylation model with linkage-specific sialidases to dissect how different sialylation patterns (e.g., α2,3- vs. α2,6-linkages) regulate SF activation, cytokine production, and potential acquisition of inflammatory phenotypes in the absence of cytokine stimulation.

3. Investigate the impact of fibroblast-derived secretomes on macrophage polarisation

    - Assess whether conditioned media from differently desialylated SFs can influence macrophage polarisation towards pro-inflammatory (M1) or anti-inflammatory (M2) states, thereby elucidating glycan-mediated mechanisms of stromal-myeloid crosstalk.

4. Map glycan-lectin interactions in RA tissue macrophages

    - Profile the expression of Siglecs and Galectins in human tissue-resident macrophages across distinct RA disease stages to identify potential receptors mediating SF-macrophage interactions and their modulation by sialylation status.

Through this integrated approach, the thesis aims to bridge molecular glyco-biology with immunopathology, providing mechanistic insight into how sialylation acts as a regulatory checkpoint in stromal and immune communication, and identifying potential glycan-targeted strategies for modulating inflammation in RA.

2. Chapter 2 Materials and Methods

2.1 Mice

Male C57B/6 mice, aged 8 weeks, were acquired from Envigo (UK) and housed at the Biological Services Unit of the University of Glasgow in compliance with Home Office guidelines.

2.2 Mouse SF isolation and culture

The process for isolating and culturing SFs was previously outlined (Armaka et al., 2009). In preparing mouse synovial tissue for digestion, the skin and soft tissue were stripped from the mouse limbs. The bones maintaining intact joints were then dissected and placed into DMEM supplemented with 10% FCS, 1% l-Glutamine, 1% Penicillin-Steptomycin, nystatin, and 1 mg/ml type IV collagenase from Sigma. The samples were incubated in a shaking oven at 37 °C for 1 hour and 20 minutes. Vortexing was performed to release the cells. Subsequently, the cells underwent centrifugation and were washed twice with DMEM containing 10% FCS. For culturing, the cells were plated and grown until adherent fibroblast colonies filled the plate. Non-adherent cells along with tissue fragments were removed once adherent cells were visible, usually after 48 hours. Fibroblasts grew until confluent and were then replated into culture flasks following trypsinisation. The SFs were expanded and utilised at passage 3 to 5 only, where culture purity was confirmed via flow cytometry, examining PDPN expression (Biolegend, catalogue number 156203) and CD11b expression (Invitrogen, catalogue number 11-0112-85), the latter showing less than 1% positivity. All antibodies were used at a dilution of 1:200.

2.3 Cd11b$^+$ Cell Depletion

In primary SF cultures, contamination by CD11b+ cells was eliminated using bead technology from Miltenyi Biotec. The cells were tagged with biotinylated anti-CD11b antibodies (Biolegend catalogue number 101204) at a concentration of 2 µg/ml, incubated on ice for 15 minutes in PBS mixed with a labelling buffer (0.5% BSA and 2 mM EDTA), and then washed twice using 3 ml of the labelling buffer to remove any unbound antibodies. The cell suspension, consisting of 10^7 cells, was further mixed in 90 µl of labelling buffer and 10 µl of Anti-Biotin MicroBeads (MACS Miltenyi Biotec catalogue number 130-090-485), thoroughly mixed, and incubated at 4°C for another 15 minutes. Post-incubation, the cells were washed by adding 3

ml of labelling buffer followed by centrifugation at 300 g for 10 minutes, and the supernatant was completely removed. For separation, cells were suspended in 500 µl of labelling buffer. A magnetic separation was performed by placing the magnetic separation columns within MACS® Separators equipped with strong magnets and pre-rinsed with the labelling buffer. The prepared cell suspension was added to the columns, where $CD11b^+$ cells were immobilized magnetically, allowing the SFs to be eluted. Pure SFs were retrieved by washing the columns thrice with the labelling buffer. The purity of the collected SFs was confirmed by Flow cytometry analysis assessing PDPN expression and absence of CD11b.

2.4 Mouse BMDMs isolation and culture

To isolate mouse BMDMs, we used same C57B/6 mouse during SFs isolation. In brief, femurs were dissected, and marrow was flushed with cold RPMI (10% FBS, 1% l-Glutamine, 1% Penicillin-Steptomycin and Fungin, Invivogen catalogue number anti-fn-1) using a 25G needle; gently triturated. Approximately $3\text{-}5\times10^6$ total marrow cells per 10 cm tissue-culture treated dish are seeded in complete RPMI medium supplemented with M-CSF (PeproTech. catalog number 315-02) at 20ng/ml. Cultures are incubated at 37 °C, 5% CO_2, and on day 3 and day 5 if desired half to two-thirds of the medium is gently replaced with fresh M-CSF containing medium, with floating debris removed and disturbance minimised. By days 6–7, mature, adherent, and spread macrophages are obtained; cells are washed with warm PBS and detached using Gibco accutase (catalogue number 11599686) or gentle scraping. Purity is verified by $F4/80^+$ (Biolegend, catalog number 123110) and $CD11b^+$ (Invitrogen, catalogue number 11-0112-85) staining.

To polarise BMDMs, mature cells differentiated for 6–7 days in M-CSF containing medium are gently washed with warm PBS and re-plated in tissue-culture–treated plates at the desired density in complete RPMI 10% heat-inactivated FBS. For M1-like (classical) activation, macrophages are stimulated with lipopolysaccharide (LPS; 10 ng/mL, Sigma Aldrich, catalogue number L4391) and interferon-γ (IFN-γ; 10 ng/mL, PepProTech, catalogue number 315-05) for 24 h. For M2-like (alternative) activation, macrophages are treated with interleukin-4 (IL-4; 10 ng/mL, PepProTech, catalogue number 214-14) for 24 h. Control (M0) macrophages are maintained in complete RPMI medium supplemented with

MCSF without polarising cytokines for the same duration. After stimulation, cells were harvested for flow cytometry analysis, with phenotypic validation performed using canonical markers such as Cd86 for M1 or CD206 for M2.

2.5 Desialylation of SFs in vitro

Cells seeded in 12-well plates underwent three washes with cold PBS and were then exposed for 1 hour to growth conditions with neuraminidases sourced from Clostridium perfringens (CP, Roche, catalogue number 11585886001), Arthrobacter ureafaciens (AU, Roche, catalogue number 10269611001), Vibrio cholerae (VC, Sigma Aldrich, catalogue number N6514-1UN), and Lectenz (L, 2B Scientific, GE0302-5KU), all diluted in a sialidase buffer (PBS: RPMI 1640 = 1:1, pH=6.8), or just the sialidase buffer for negative control (NT). Cells kept in culture for 6 more hours in complete medium for RNA extraction.

2.6 Collection of Supernatants Following Desialylation and Coculture with BMDMs

After treating SFs with the aforementioned neuraminidases for 1h on 12-well plates, SFs were thoroughly washed with cold PBS three times, and then 1ml of fresh DMEM complete medium was added onto the wells. Wells were incubated with complete DMEM medium for 24h. Then, supernatants including released molecules from SFs following desialylation were collected, labelled and put into freezer for further use.

For coculture experiments, SFs supernatants were used to incubate resting state BMDMs for 24h. Then, cells were deattached with Gibco accutase (catalogue number 11599686) to identify the changes in macrophage polarisation markers. In brief, 1ml of NT, AU, VC, and L- treated SFs supernatants were added onto the resting state BMDMs 7 days after MSCF treatment from bone marrow state. For controlling M1 and M2 macrophage polarisation, 10ng/ml LPS and IFN-γ, and 10ng/ml IL-4 stimulation used in complete DMEM medium. For RNA isolation, cells were kept in supernatant cultures for 6 hours in complete medium. Then, RNA isolation was performed.

2.7 ELISAs

IL-6 secretions were measured using ELISA kits (R&D, Duo set) according to the manufacturer's guidelines. The supernatants collected after 24 hours (refer to Step 2.6) were placed in 96-well plates following desialylation, utilising recombinant sialidases from *Clostridium perfringens* (CP, Roche, catalogue number 11585886001), *Arthrobacter ureafaciens* (AU, Roche, catalogue number 10269611001), *Vibrio cholerae* (VC, Sigma Aldrich, catalogue number N6514-1UN), and Lectenz (L, 2B Scientific, GE0302-5KU).

2.8 SFs Migration Assay

Naïve SFs were cultured in 2-well u-dishes (ibidi, catalogue number IB-81176) following the instructions provided by the manufacturer. Inserts were removed to create gaps. Subsequent to this, supernatants from NT, AU, VC, and L-treated SFs (as outlined in Step 2.6) were introduced and allowed to incubate for a period of 5 days. The reduction in percent wound area between Day 0 and Day 5 was measured using the Image J wound healing tool, as detailed by Suarez-Arnedo et al., 2020.

2.9 Enzyme Linked Lectin Assay (ELLA)

SFs seeded in 96-well plates were subjected to three wash cycles with cold PBS. Subsequently, the cells were preserved with Fixation buffer (Biolegend, catalogue number 420801) for 20 minutes at room temperature under dark conditions. The fixed cells underwent washing with PBS containing 0.05% Tween20 (Sigma, #P1379) and were then incubated with carbo-free blocking buffer for 20 minutes to prevent nonspecific interactions. Thereafter, cells were exposed to biotinylated lectins for 30 minutes in PBS with 5% carbo-free blocking buffer (Vector Labs, catalogue number SP-5040-125). Sambucus Nigra Lectin (SNA, 2B Scientific, catalogue number B-1305), Maackia Amurensis Lectin (MALI, 2B Scientific, catalogue number B-1315), Peanut Agglutinin Lectin (PNA, 2B Scientific, catalogue number B-1075-5), and Aleuria Aurantia Lectin (AAL, 2B Scientific, catalogue number B-1395-1), staining were identified using HRP-conjugated streptavidin for 20 minutes, followed by three wash cycles with the wash buffer. The visualisation reaction was induced using an HRP substrate, and the measurements were taken at 405 nm using a Tecan Sunrise plate reader.

Cell number was quantified using crystal violet (0.04 mg/ml, Sigma, catalogue number C0775). Briefly, cells were stained with 100 µl of crystal violet for 30 min at room temperature, then washed at least three times to remove any residual dye, followed by adding 100 µl of 1% SDS solution (Sigma, catalogue number 05030) and incubation for 1 hour in a shaker. Absorbance was read at 595 nm using a Tecan Sunrise plate reader.

2.10 Immunofluorescent Staining

Cells (~2,000/well) were seeded in ibidi 12 well chambers and, after adherence, treated with buffer only or with CP, AU, VC or L sialidase prepared in RPMI:PBS (1:1, pH 6.8). Cells were fixed in 4% paraformaldehyde at room temperature (RT) for 30 min and washed with PBS, then permeabilized in PBS containing 0.05% Triton X-100 for 2 times at room temperature, followed by PBS washes. Endogenous biotin was blocked using an avidin/biotin blocking kit per manufacturer's instructions (Vector Labs, catalogue number SP-2001-1). Non-specific binding was blocked with 5% carbo-free blocking buffer in PBS for 30–60 min, after which samples were incubated with biotinylated lectin, SNA, MAL, AAL or PNA (typically 1:500, ~2–20 µg/mL) overnight at 4C. Following PBS washes three times, cells were incubated with Alexa Fluor® 647-conjugated streptavidin for 45–60 min at RT protected from light, washed in PBS in three times, and mounted using a DAPI-containing mounting medium (ThermoFisher Scientific, catalogue number S36968) prior to imaging. Controls included buffer-only streptavidin only conditions, and imaging parameters were kept constant across treatments. The staining was observed through an EVOS FL Auto 2 microscopes.

2.11 Flow Cytometry Analysis Across Different Conditions

2.11.1 SFs Purity Check

SFs purity was assessed by flow cytometry using PDPN as a fibroblast marker and CD11b as a myeloid/macrophage exclusion marker. Cells were detached at 70–90% confluence with trypsin (3 min, 37 °C) and neutralised with complete medium, passed through a 40 µm strainer, and washed twice in ice-cold FACS buffer (PBS, 2% heat-inactivated FBS, 2 mM EDTA). After Fc-receptor blockade (30 min, 4 °C), cells were stained with fluorochrome-conjugated anti-PDPN and anti-CD11b antibodies (non-overlapping emission spectra) for 30 min at 4 °C in the dark, followed by two washes. Unstained, and fluorescence-minus-one (FMO)

controls for PDPN and CD11b were included in every run. Where fixation was required, samples were resuspended in 1% PFA in PBS and acquired within 24 h on a digital flow cytometer. Analysis (FlowJo) proceeded by sequential gating: debris exclusion (FSC/SSC), doublet discrimination (FSC-A vs FSC-H and SSC-A vs SSC-H), and final bivariate PDPN vs CD11b gating using FMO-informed thresholds. SF purity was defined a priori as the percentage of $PDPN^{+}CD11b^{-}$ events within singlets; experiments were accepted when purity was with ≤5% $CD11b^{+}$ contaminants.

2.11.2 BMDM Polarisation Through Desialylated Synovial Fibroblasts

Macrophage phenotyping in response to desialylated SF-conditioned media was performed by multiparameter flow cytometry. Briefly, primary macrophages (BMDMs) were cultured with SF supernatants generated from enzymatically desialylated SFs (see SF desialylation/conditioned media methods) alongside matched control supernatants. After incubation, cells were collected, washed in ice-cold FACS buffer (PBS, 2% heat-inactivated FBS, 2 mM EDTA), and stained on ice in the dark without permeabilisation using a fixable amine-reactive viability dye (eFluor 780) followed by fluorochrome-conjugated antibodies to F4/80 and CD11b for macrophage identification, and the following activation/phenotype markers: CD80, CD86, CD40, MerTK, LYVE-1, TREM2, CD206, and PD-L1 (CD274).We used single-stain compensation controls (capture beads) and fluorescence-minus-one (FMO) controls for each analytical marker were included in every run to define positivity thresholds. Data were acquired on a flow cytometer BD LSRFortessa). Analysis was conducted in FlowJo using the following sequential gates: debris exclusion (FSC/SSC), doublet discrimination (FSC-A vs. FSC-H and SSC-A vs. SSC-H), live cells ($eFluor\ 780^{-}$), macrophages ($F4/80^{+}CD11b^{+}$), and within this parent gate, quantification of CD80, CD86, CD40, MerTK, LYVE-1, TREM2, CD206, and PD-L1 expression using FMO-informed thresholds. Outcomes were summarised as the percentage of positive cells and median fluorescence intensity (MFI) for each marker within live $F4/80^{+}CD11b^{+}$ macrophages; sample MFIs were background-corrected using the relevant FMOs prior to statistical analysis. Characteristics of antibodies for flow cytometry experiments are provided in Table 2-1.

Table 2-1 List of antibodies used for Flow Cytometry.

Antigen	Flurophore	Clone	Supplier	Catalogue number	Concentration used
F4/80	PE	BM8	Biolegend	123110	2 µg
CD11B	FITC	M1/70	Thermofischer Scientific	11-0112-85	2 µg
CD80	PE-Dazzle	16-10A1	Biolegend	104738	2 µg
CD86	PerCP Cy5.5	GL-1	Biolegend	105027	2 µg
CD206	BV421	C068C2	Biolegend	141717	2 µg
MerTK	BV711	2B10C42	Biolegend	151515	2 µg
LYVE-1	APC	223322	R&D	FAB2125A	2 µg
PDL-1	BUV395	MIH5	BD Biosciences	745616	2 µg
CD40	PE-Cy7	3/23	Biolegend	124622	2 µg
VSIG4	BV650	17C9	BD Biosciences	749503	2 µg
TREM2	AF700	237920	R&D	FAB17291N	2 µg
PDPN	AF647	PMab-1	Biolegend	156203	2 µg
Viability Dye	efluor-780	N/A	Thermofischer Scientific	65-0865-14	1 µg

2.12 RNA Isolation, Sequencing and Data Analysis

2.12.1 RNA Isolation and Sequencing in Desialylated SFs

Total RNA was isolated from SFs following desialylation (with matched buffer controls) using the Qiagen RNeasy (Plus) Mini Kit with on-column DNase I digestion (RNase-Free DNase Set; Qiagen). Briefly, SFs at ~70–85% confluence were rinsed with ice-cold PBS and lysed directly in the culture vessel with Buffer RLT supplemented with β-mercaptoethanol. Lysates were mechanically homogenized by repeated passage (10–15 strokes) through a sterile syringe fitted with a 21G needle on ice to shear genomic material and ensure uniform viscosity. The cleared lysate was then processed according to the manufacturer's instructions; on-column DNase I treatment was performed to eliminate residual genomic DNA, followed by the standard wash steps and elution in RNase-free water. RNA yield and purity were assessed by spectrophotometry (A260/280 ~1.9–2.1; A260/230 >2.0), and integrity was confirmed by capillary electrophoresis (RIN ≥9). High-quality RNA was advanced to stranded poly(A) mRNA library preparation and Illumina paired-end sequencing with 2x100, 30 M paired-end reads was done by BMKGENE company. FASTQ files obtained were subjected to initial quality control prior to alignment and expression quantification as detailed in the RNA-seq analysis section.

2.12.2 RNA Isolation and Sequencing in BMDMs Cocultured with Desialylated SFs Conditioned Media

BMDMs were exposed to SF-conditioned media generated after enzymatic desialylation of SFs (with matched buffer-only controls) for 6 hours, after which total RNA was extracted. The same RNA isolation protocol mentioned at section 2.12.1 was used to isolate RNAs from BMDMs. RNA was eluted in RNase-free water, quantified by spectrophotometry (A260/280 ≈ 1.9–2.1; A260/230 > 2.0), and integrity assessed by capillary electrophoresis (RIN ≥ 8). Library preparation and sequencing were performed by the Polyomics Facility (University of Glasgow) using a stranded poly(A)-selected mRNA workflow where libraries were pooled and sequenced on an Illumina platform to obtain 2x100, 30 M paired-end reads. FASTQ files obtained were subjected to initial quality control prior to alignment and expression quantification as detailed in the RNA-seq analysis section. This work was supported by Wellcome [204820/Z/16/Z]. Experimental overview of the study was illustrated at Figure 2-1.

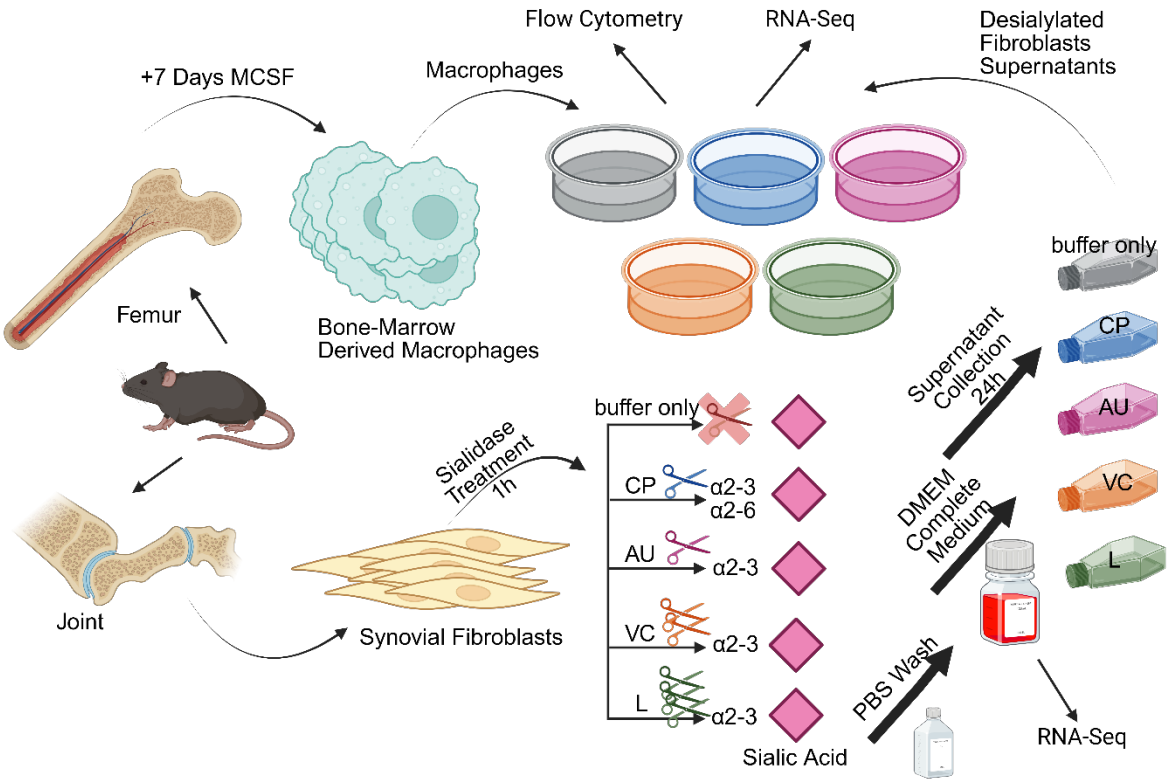

Figure 2-1 Experimental Overview of the Wet Lab Work

2.12.3 RNA-Seq Data Analysis in Desialylated SFs and BMDMs Data

Raw paired-end reads were processed against the mouse reference genome (mm10). Adapters and low-quality bases were assessed with FastQC/MultiQC and trimmed where necessary, after which reads were aligned to mm10 using HISAT2. Gene-level quantification was performed with featureCounts on the UseGalaxy servers, in paired-end, applying basal thresholds. Gene identifiers were converted to official gene symbols using BioMart. The resulting count matrix was imported into DESeq2 (R), where low-count genes were filtered, and differential expression was tested with the DeSeq2 package. Genes meeting Padj < 0.05 and $|\log_2$ fold change| > 1 were considered differentially expressed. For sample-level QC and data structure, rlog-transformed counts were used to compute PCA in R. Heatmaps of normalised expression for top DE genes and selected gene sets were generated with the pheatmap package (R), using row scaling (scale = "row") and hierarchical clustering with sample/condition annotations. We implemented an R pipeline to perform condition-wise pathway analysis for four contrasts (CP, AU, VC, and L versus nontreated). Raw count matrices and sample metadata are loaded, the treatment factor is releveled to use nontreated as the reference, and a DESeq2 model (~ treatment) is fitted after removing genes with zero total counts.

Results are Benjamini–Hochberg–adjusted, and genes meeting the user-set thresholds (default in the script: padj < 0.05 and $|\log_2 FC| \geq 1$) are retained as differentially expressed. Gene symbols are then converted to Entrez IDs using org.Mm.eg.db via clusterProfiler::bitr, and, for each contrast, KEGG over-representation analysis is run for Mus musculus (mmu) (Wu et al., 2021). The top enriched pathways per condition are collated and visualised with ggplot2 as bubble plots, where point size encodes −log10(adjusted p) and colour encodes the adjusted p-value, enabling side-by-side comparison of the leading KEGG terms across conditions. Similar approach is used for GO BP and MF enrichments.

The pipeline to obtain DEGs for all conditions takes a raw count matrix spanning all conditions (NT, CP, AU, VC, L for desialylated SFs and NT, CP, AU, VC, L, M1 and M2 for BMDMs cocultured with desialylated SFs conditioned media), harmonises gene identifiers, performs differential expression, and visualizes the results. First, it reads the counts, renames the first column as entrezgene_id, and uses Ensembl BioMart for mouse (mmusculus_gene_ensembl) to map Entrez IDs to gene symbols (external_gene_name). After merging and removing duplicated symbols, the table is reindexed by gene symbol and written out. The script then builds a DESeq2 object (design = ~ treatment), filters genes with zero counts, estimates size factors, generates normalised counts, and writes log2-transformed values. A helper function runs four pairwise analyses (CP, AU, VC, L vs the nontreated reference), extracting DEGs per contrast with padj < 0.05 and |log2FC| ≥ 1, and tags each set by condition before concatenation. The union of all DEG symbols is used to subset the log-normalised matrix, which is z-scored by gene and plotted as a clustered heatmap with sample annotations by treatment, providing a global view of how enzyme treatments shift gene expression relative to control.

To evaluate how different treatments are similar to M1 or M2 like macrophage polarisation, raw count data were imported into R and integrated with sample metadata specifying treatment groups. A DESeq2 dataset was constructed (design: ~ treatment), genes with zero counts across all samples were removed, and normalisation was performed by estimating size factors. Normalised counts were $\log_2$-transformed with a pseudocount to stabilize variance. Curated M1 and M2 macrophage marker gene sets in GMT format were loaded with GSEABase

and used as input for single-sample gene set variation analysis (GSVA). Enrichment scores for each signature were extracted per sample and combined with metadata for statistical analysis. Differences across treatments were assessed using one-way ANOVA, while a polarisation index (M1 – M2 GSVA score) was calculated and tested similarly. Pairwise comparisons against the untreated control were evaluated with t-tests and visualized on boxplots generated with ggplot2 and ggpubr. GSVA scores and polarization indices were exported as CSV files to support reproducibility. All analyses were performed in R (packages: DESeq2, GSVA, GSEABase, ggplot2, ggpubr).

2.13 RNA Seq Analysis of Publicly Available Bulk RNA Seq and Single Cell RNA-Seq Data

2.13.1 Analysis of Bulk-RNA Seq Datasets

Raw sequencing reads obtained from ENA database with an accession number PRJEB14422 were quality-trimmed using Trimmomatic. The resulting high-quality reads were aligned to the human reference genome and transcriptome (hg38) and subsequently assigned to genomic features with featureCounts. Raw counts matrix for TNF-stimulated vs unstimulated RA SF data was obtained from NCBI GEO with an accession number GSE163548. Gene expression quantification was performed within the R/Bioconductor framework. Differential expression analysis between RA and healthy samples was carried out using DESeq2. Genes were considered differentially expressed if they exhibited an absolute log2 fold change greater than 1 and a P-value below 0.05. For sample-level QC and data structure, rlog-transformed counts were used to compute PCA in R. Heatmaps of normalised expression for top DE genes and selected gene sets were generated with the pheatmap package (R), using row scaling (scale = "row") and hierarchical clustering with sample/condition annotations.

Bulk RNA-seq count matrices from the Ge et al. (2021) synovial fibroblast dataset (GSE163548) were processed in R. After removing non-expression columns and setting GeneIDs as row names, sample metadata were aligned to the count matrix. Gene identifiers were harmonised by mapping Entrez IDs to HGNC symbols via biomaRt (Ensembl), then duplicated or unmapped genes were dropped and the matrix was re-indexed by HGNC symbol. Counts were converted to a numeric matrix, missing values (if any) set to zero, genes with zero variance

removed, and lowly expressed genes filtered (expression >1 count in ≥3 samples). To account for unwanted variation, surrogate variables (SVs) were estimated with sva using a model including the biological group, and the SVs were incorporated into the design formula. A DESeq2 dataset was constructed (design ~ SVs + group), and variance-stabilized (VST) log counts were obtained (blind = FALSE) for visualization. Sample structure was assessed by principal component analysis (PCA) on VST counts and by heatmaps scaled by gene (row). Differential expression was performed with DESeq2; differentially expressed genes were defined as those with FDR-adjusted p-value < 0.05 and |log2 fold-change| > 1, and their VST expression profiles were exported and visualized with sample-level annotations (group and anatomical location). For pathway-focused exploration, a curated list of glycosyltransferases (GTs) was intersected with the normalized matrix to generate GT-only expression tables and PCA plots for comparison with whole-transcriptome structure.

Glycosyltransferase (GT) genes were isolated from a log-normalized synovial RNA-seq matrix by intersecting gene symbols with a curated GT list. Briefly, the count table and GT list were read into R, gene symbols were added as an explicit column, and overlapping entries were identified with plyr::match_df, merged, and deduplicated by symbol. The resulting GT-only expression matrix was reformatted to use gene symbols as row names and subjected to principal component analysis (PCA) with prcomp on the transposed matrix (samples as observations), using unit-variance scaling (scale.=TRUE). Percent variance explained for each principal component was computed from the singular values, and a biplot-ready data frame containing PC1, PC2, and sample identifiers was generated. PCA results were visualized with ggplot2, using geom_point and ggrepel for non-overlapping sample labels, a viridis discrete palette for colorblind-friendly aesthetics, and a centered, bold title referencing the Frank-Bertoncelj et al. (2017) dataset.

To evaluate pathway enrichment, raw SFs RNA-seq counts and sample metadata were imported into R. A DESeq2 object was created with design ~ group, size factors were estimated for library-size normalisation, and normalised counts as well as log2-transformed values [log2(counts + 1)] were computed for downstream visualization. Differential expression was performed using DESeq2 with independent filtering and a false discovery rate (FDR) threshold of 0.05; results

were sorted, nonessential columns (baseMean, lfcSE, stat, pvalue) were dropped, and differentially expressed genes (DEGs) were defined as those with adjusted P < 0.05 and |log2 fold-change| > 1. The DEG table was exported and reformatted with gene symbols, log2 fold-changes, and adjusted P-values for enrichment analysis. Pathway enrichment was then conducted using pathfindR against KEGG and Gene Ontology collections (Biological Process and Molecular Function) to identify significantly overrepresented pathways among DEGs (Ulgen et al., 2019).

Raw RNA-seq read counts from SF samples were analysed in R using the DESeq2 pipeline. Genes with zero counts across all samples were removed, and size factors were estimated for normalization. Normalised counts were $\log_2$-transformed and exported for downstream analyses. Differential gene expression between RA vs healthy fibroblasts and TNF-stimulated vs unstimulated RA SFs were performed using a negative binomial generalised linear model with DESeq2, applying independent filtering and an adjusted significance threshold of FDR < 0.05. Test statistics from the DESeq2 results were used to rank all genes for gene set enrichment analysis (GSEA). Pathway analysis was carried out using the fgsea package with the GlycoEnzOnto gene sets, which represent curated glycosylation and glycoenzyme pathways. Genes were ranked according to DESeq2 test statistics, and enrichment was assessed with 10,000 permutations, considering gene sets with a minimum of 2 and maximum of 500 genes. Significant pathways were defined based on nominal p < 0.05, and both positively and negatively enriched pathways were identified. Top pathways were visualized using enrichment plots and GSEA summary tables.

Raw SF RNA-seq counts from PRJEB14422 and GSE163548 were preprocessed in R by removing duplicate entries based on HGNC symbols and discarding genes with missing values. Gene lengths were obtained from Ensembl by calculating the genomic span between annotated start and end coordinates for each gene. The resulting gene-length table was merged with the count matrix, and expression values were normalised to transcripts per million (TPM) by first computing reads per kilobase (RPK) for each gene, followed by scaling against the total RPKs per library. The TPM matrix was saved with HGNC symbols as identifiers, and condition-level summaries were generated by averaging TPM values across replicates of unstimulated RA vs TNF-stimulated RA SFs or healthy vs RA SFs

yielding per-gene mean TPMs for comparative analyses. These average TPM values were further used to predict glycosylation pathways related to sialic acid at https://glycosmos.org/glycomaple/Human.

2.13.2 Analysis of Single Cell RNA-Seq Dataset

Single-cell RNA-seq data were obtained from Mariola-Kurowska group, provided as a pre-processed Seurat object. The object had already undergone standard preprocessing steps, including quality control, normalization, and clustering as described in the original study (Alivernini et al., 2020). For the purposes of this thesis, analyses were conducted directly on this prepared Seurat object. Subsequent work focused on characterising cell-type specific expression of sialyltransferases, galectins, and Siglecs across disease states (UPA, Active, Remission).

For the present analysis, lining FLS, sublining FLS or macrophages were subset according to the CellType annotation, and samples were grouped into UPA, active RA, and remission states. Expression of a curated panel of genes, including sialytransferases for lining and sublining FLS and Siglecs and galectins for macrophages was assessed within the relevant cell type subset. Dot plots were generated using Seurat's DotPlot function and visualised with ggplot2, with percentage of cells expressing each gene represented by dot size and average scaled expression by color gradient. Differential expression testing was conducted with Seurat's FindMarkers using the MAST hurdle model on log-normalised RNA counts, comparing Active versus UPA and Active versus Remission. There were no prior thresholds (logfc.threshold=0, min.pct=0) to avoid bias against lowly expressed lectins. Multiple testing correction used the Benjamini–Hochberg procedure as implemented in Seurat, and adjusted $P < 0.05$ was considered significant. A curated list of sialylation- and lectin-related genes was applied post hoc to filter DE results for pathway-focused interpretation. Effect sizes are reported as average log2 fold change (avg_log2FC) computed on log-normalised expression. Bar plots of avg_log2FC, with significance status indicated, were generated in ggplot2.

2.14 Statistical Analysis

Statistical analysis was performed using GraphPad Prism version 10. For normalised values, we tested whether distributions differed significantly from zero. Data normality was assessed with the Shapiro–Wilk test. If normality was confirmed ($p > 0.05$), a one-sample t-test was applied. If normality was not met, the non-parametric Wilcoxon signed-rank test was used instead. Statistical significance was reported as: $p < 0.05$ (), $p < 0.01$ (), $p < 0.001$ (), $p < 0.0001$ (****); “ns” indicates not significant.

3. Chapter 3 Transcriptomic and Glycobiological Profiling of Synovial Fibroblasts in Rheumatoid Arthritis

3.1 Introduction

As mentioned in the general introduction, RA is a chronic, systemic autoimmune disorder primarily affecting synovial joints, characterised by persistent inflammation, synovial hyperplasia, cartilage destruction, and bone erosion. This progressive joint damage leads to pain, loss of function, and decreased quality of life for millions worldwide. Despite advances in therapeutics, the complex molecular mechanisms driving RA pathogenesis remain incompletely understood, hindering the development of targeted and curative treatments (Bartok & Firestein, 2010; Firestein & McInnes, 2017).

SFs are resident stromal cells within the synovium that normally maintain joint homeostasis by producing extracellular matrix components and regulating immune cell recruitment. However, in RA, SFs undergo a pathological transformation acquiring an aggressive, activated phenotype. These RA SFs contribute directly to inflammation and joint damage through secretion of pro-inflammatory cytokines, matrix-degrading enzymes, and by invading cartilage and bone (Y. Zhang et al., 2025). Elucidating the transcriptional changes underpinning SF activation is therefore critical to understanding RA pathogenesis and identifying novel therapeutic targets.

Transcriptomic profiling, through bulk and single-cell RNA sequencing (RNA-seq), has become an invaluable tool for characterising global gene expression changes in RA-affected tissues and cells (Frank-Bertoncelj et al., 2017; Ge et al., 2021). RNA-seq offers high sensitivity and dynamic range, allowing for quantification of known and novel transcripts with single-base resolution. This enables comprehensive analyses of differential gene expression between disease and healthy states, as well as pathway enrichment to reveal dysregulated biological processes.

Among the diverse pathways implicated in RA, glycosylation, which is the covalent attachment of carbohydrates to proteins and lipids, has gained increasing attention for its role in modulating immune responses and cell signalling. Glycans influence

protein folding, but also receptor binding, and cell-cell interactions, thus playing vital roles in both normal physiology and disease states (Reily et al., 2019). Alterations in glycosylation patterns, particularly in immune-related cells and SFs, can exacerbate inflammation and autoimmunity. For instance, aberrant expression of glycosyltransferases, enzymes that mediate sugar addition and modification, have been observed in the synovial fluids and SFs from RA patients (Hafkenscheid et al., 2017; Y. Wang et al., 2021).

The emerging data in the field of glycobiology related to RA underscores the importance of integrating transcriptomic data with detailed analyses of glycosylation-related genes and pathways. Understanding how glycosylation machinery is transcriptionally regulated in SFs can shed light on mechanisms driving their pathological phenotype and perhaps identify potential biomarkers or therapeutic targets.

In this chapter, we aimed to characterise the transcriptomic alterations in SFs associated with RA, focusing on the genes involved in glycan biosynthesis. Our aim will be to identify how inflammatory conditions, both in patients and in vitro through TNF-α stimulation, reshape the gene expression landscape of SFs and influence glycosylation-related pathways, especially those involving sialylation. Sialic acids are acidic sugars found at the outermost end of the glycan chains with a negative charge and hydrophilicity (A. Varki, 2008). As they are expressed in the outer cell membranes, they play important roles in modulating interactions with the environment (A. Varki & Schauer, 2009). The dysregulation of cell sialylation is often associated with several diseases including cancer and autoimmunity (Dobie & Skropeta, 2021; Mahajan & Pillai, 2016). Sialyltransferases facilitate the attachment of sialic acid to complex glycans within the endoplasmic reticulum and Golgi. These enzymes catalyse the reaction that transfers sialic acid residues from their CMP-activated sugar donors to various receptor molecules (X. Chen & Varki, 2010). Sialyltransferases attaches sialic acids to the oligosaccharides with specific locations such as α2-3, α2-6 and α2-8 linkages. The type of linkages and relative are key to determine the cellular function of the sialylome. For example, increased expression of α2-3 sialic acids contributes to tumour progression and immune responses through interactions with lectins and immune cells (Hugonnet et al., 2021). There is also increased α2-6 sialylation pattern being observed in human colonic malignancies (Sata et al., 1991). Although the biological consequences of

different sialylation patterns frequently documented in cancer research, recent research indicated that in rheumatoid arthritis, a deficiency in α2,6-sialylation promotes a pro-inflammatory phenotype in SFs, contributing to disease perpetuation through an autocrine loop involving inflammatory cytokines like IL-6 and TNF-α (Y. Wang et al., 2021). However, current research is needed to further understand the role of sialylation patterns in autoimmune diseases, specifically in RA disease.

To address this, we applied a systematic analytical framework to bulk RNA-seq datasets obtained from publicly available sources. We performed comparative analyses between RA and healthy donor-derived SFs, as well as between TNF-α-stimulated and unstimulated RA SFs, in order to model both disease-driven and cytokine-induced transcriptional changes. Our workflow included a classical pipeline, including differential gene expression analysis, followed by Gene Ontology (GO), and KEGG enrichment analyses to uncover key biological processes and molecular pathways dysregulated in RA. Additionally, we developed a glycobiological perspective into our analysis by mapping differentially expressed genes associated to glycosylation. To systematically identify dysregulated glycobiological processes, we utilised the GlycoEnzOnto framework, which enabled pathway-level interpretation of glycosylation-networks. In addition, we employed the GlycoMaple tool to predict potential alterations in glycan structures based on gene expression data. Particular emphasis was placed on genes involved in sialic acid biosynthesis and sialyltransferases. This integrated approach allowed us to uncover how RA and TNF-α stimulation alter glycosylation programs, potentially contributing to the pro-inflammatory phenotype of SFs.

3.2 Results

3.2.1 Transcriptomic Characterisation and Functional Enrichment of Synovial Fibroblasts in Rheumatoid Arthritis

In work published in 2017, Frank-Bertoncelj investigated the epigenetic underpinnings of SFs and their transcriptional responses in a joint-specific context (Frank-Bertoncelj et al., 2017). This paper focused on the regulation of HOX gene expression, which is crucial for the anatomical and functional diversity observed in the synovium across different joints. The research highlights the differential transcriptional profiles of SFs sourced from diverse anatomical locations, indicating that these profiles may have impact on the susceptibility of specific joints

to diseases such as RA. We used the RNA-Seq dataset from Frank-Bertoncelj et al. paper provided with an accession number PRJEB14422 at European Nucleotide Archive database. This dataset included SFs from different anatomical locations obtained from RA patients and SFs from non-arthritic subjects with arthralgia. Although original paper included osteoarthritic subjects as well, we excluded samples from osteoarthritic patients, as we focused our study on inflammatory RA. Using this dataset, we investigated transcriptomics changes from RA compared to healthy SFs. Since earlier studies didn't fully explore glycosylation in the context of human RA, this new targeted analysis will help us to identify changes in glycosylation more relevant to the clinic and translational approaches, especially in sialylation that might contribute to the pro-inflammatory behaviour of SFs in RA. Remarkably, this approach allows us to predict pathway-level dysregulations that are otherwise masked in standard transcriptome-wide comparisons.

Transcriptomic data analysis includes data preprocessing steps such as quality control and trimming, alignment of reads to reference genomes, gene quantification, differential expression analysis using DESeq2, and downstream functional enrichment including gene ontology and KEGG pathway analyses (Figure 3-1). We applied these pipelines to characterise RA vs healthy SFs.

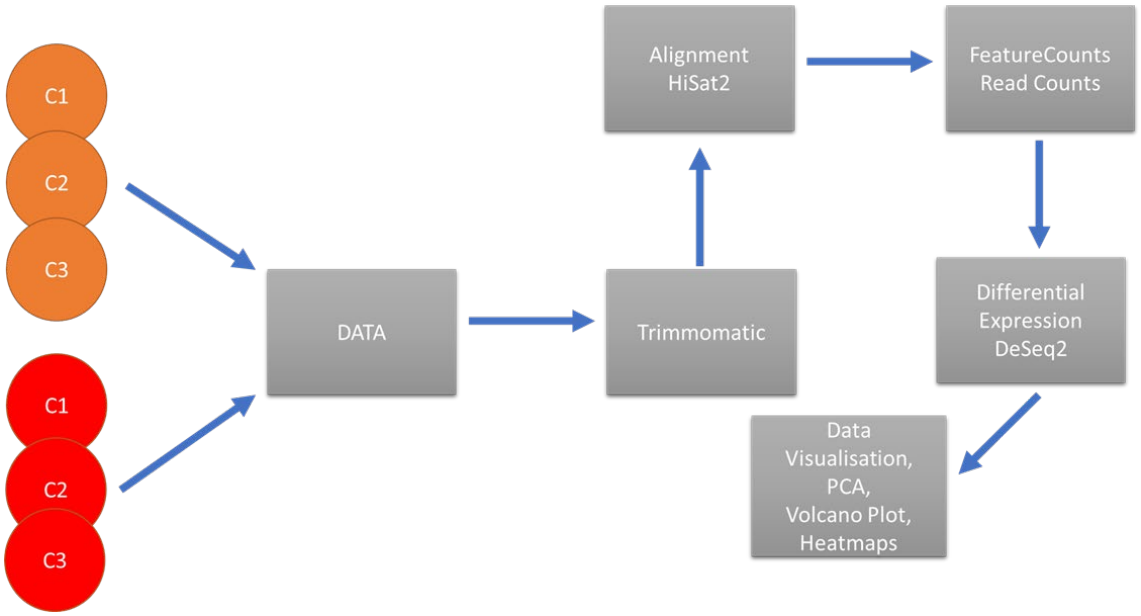

Figure 3-1 Overview of RNA-seq data analysis pipeline.

Workflow represents the steps taken for bulk RNA-seq data analysis, from raw readings to differential gene expression analysis and visualisation. Samples from distinct conditions (represented by orange and red circles, e.g control and arthritic) will be considered. Reads are trimmed using Trimmomatic to remove adapters and low-quality bases. High-quality reads are then aligned to reference genome using HiSat2. FeatureCounts is used to quantify read counts per gene. Differential expression analysis is performed using DESeq2. The results are visualised using principal component analysis (PCA), volcano plots, and heatmaps.

Characteristics of SFs samples are provided in Table 3-1. Briefly, the dataset comprises SFs samples isolated from joints of both RA patients and healthy controls with arthralgia. Arthralgia refers to joint pain that may arise without any apparent inflammation or damage in the joints (Van Steenbergen et al., 2018). Samples were obtained from knee, shoulder, and metacarpophalangeal (MCP) joints, with fibroblasts expanded in culture to passages 5 through 7. Donors ranged in age from 42 to 78 years, predominantly female, with RA patients exhibiting disease durations between 7 and 51 months. RA patients were receiving various treatments including DMARDs, biologics, corticosteroids, and NSAIDs. This clinical and experimental information provides essential context for interpreting the transcriptomic profiles analysed in the study and in our targeted analysis in this chapter.

Table 3-1 Samples obtained from Frank-Bertoncelj et al. (2017) bulk-RNA Seq data (n=12).

Patient Group	Location obtained	Cell Type	Sex	Age	Disease Duration	Treatment
RA	knee	SFs (P6)	Female	54	16	DMARD, biologic, NSAID, corticosteroid
RA	knee	SFs (P5)	Female	64	7	DMARD, biologic
RA	knee	SFs (P6)	Female	71	51	DMARD, NSAID, corticosteroid
RA	shoulder	SFs (P6)	Female	68	38	Biologic, corticosteroid
RA	shoulder	SFs (P6)	Female	78	32	Biologic
RA	shoulder	SFs (P6)	Female	68	27	DMARD
RA	MCP (hand)	SFs (P6)	Female	52	21	DMARD
RA	MCP (hand)	SFs (P5)	Female	69	50	DMARD, NSAID
RA	MCP (hand)	SFs (P6)	Female	78	23	DMARD, corticosteroid
Healthy (arthralgia)	knee	SFs (P7)	Female	59		
Healthy (arthralgia)	knee	SFs (P7)	Female	49		
Healthy (arthralgia)	knee	SFs (P7)	Male	42		

Clinical information of synovial fibroblasts used in Frank-Bertoncelj et al. (2017) paper. Synovial fibroblasts were isolated from synovial tissue following joint replacement surgery, expanded ex vivo, and RNA extracted at the indicated passage (P5-P7). RA= Rheumatoid arthritis, MCP=metacarpophalangeal joint, SFs=Synovial fibroblasts, DMARD=Disease modifying anti-rheumatic drug, NSAID=Non-steroid anti-inflammatory drug.

In order to investigate how SF samples group based on their global gene expression profiles, we conducted PCA to observe transcriptomic differences

between disease vs healthy states. Samples from RA patients cluster separately from healthy controls, indicating distinct transcriptomic differences between disease and healthy states (Figure 3-2A). This separation confirms that RA SFs have a unique gene expression signature compared to healthy ones. This is further confirmed by the global heatmap of significantly differentially expressed genes in RA vs healthy SFs (Figure 3-2B).

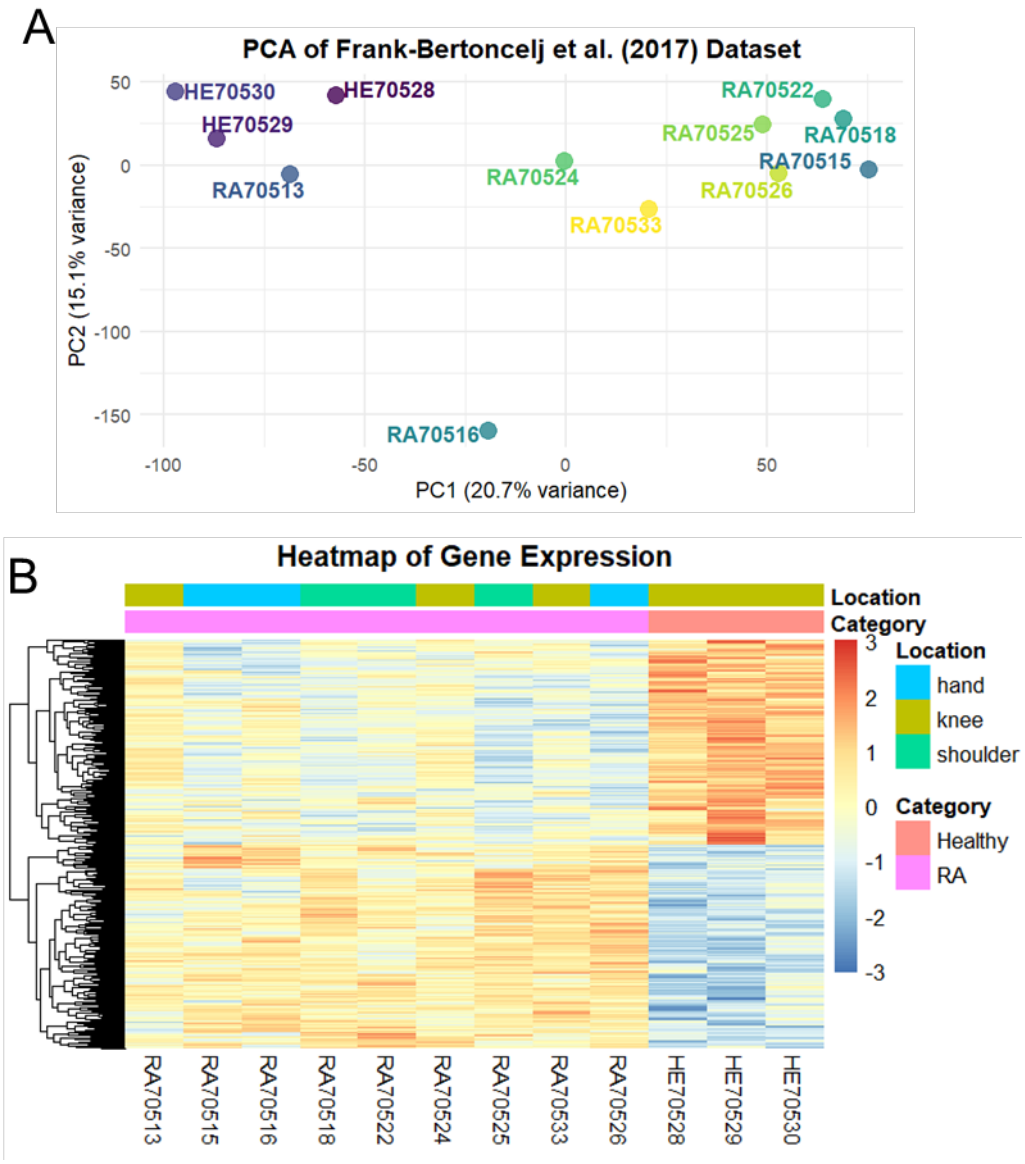

Figure 3-2 Principal Component Analysis (PCA) and Heatmap of Gene Expression from Frank-Bertoncelj et al. (2017) Dataset.

RNA-Seq was used to analysed gene expression in expanded synovial fibroblasts from healthy (HE) and Rheumatoid Arthritis (RA) joints. **A)** PCA plot shows the distribution of samples based on gene expression profiles, x-axis shows the first principal component (PC1) accounting for 20.7% of the variance, y-axis represents the second principal

component (PC2) accounting for 15.1%. Each dot represents individual patients, with colours distinguishing between groups; Healthy (blue/purple), RA (green/yellow) (RA). **B)** Heatmap of significantly differentially expressed genes in synovial fibroblasts from healthy and rheumatoid arthritis (RA) patients, clustered by expression levels. Rows represent genes, and columns represent samples. The colour scale indicates relative gene expression levels (blue = low expression, yellow = high expression) using Z scores. The top annotation bars indicate sample metadata, "Category" (pink: Healthy, yellow: RA) and "Location" (blue: hand, green: knee, orange: shoulder).

Next, differential gene expression analysis revealed significant transcriptional alterations associated with disease pathology. The volcano plot (Figure 3-3A-B) illustrates the distribution of differentially expressed genes (DEGs) by their fold change and statistical significance (|fold change| > 2, adjp<0.05), highlighting a 296 significantly upregulated and 298 downregulated in RA samples. This widespread gene regulation indicates extensive remodelling of the SF transcriptome in RA. Supporting this, the heatmap of the top 20 most significantly altered genes demonstrates clear segregation between RA and healthy samples based on gene expression profiles. Sample clustering also reflects variation related to joint location (hand, knee, shoulder), suggesting spatial heterogeneity in SF gene expression corroborating the main finding shown in the original paper (Frank-Bertoncelj et al., 2017). Together, these data underscore the complex molecular changes driving SF activation in RA and provide candidate genes for further functional investigation. Among those differentially expressed genes in RA vs healthy SFs, PADI2 and HAPLN1 emerged as particularly relevant to RA pathogenesis, given their roles in promoting citrullination and extracellular matrix remodelling, respectively (Chang et al., 2013; Chen et al., 2022).

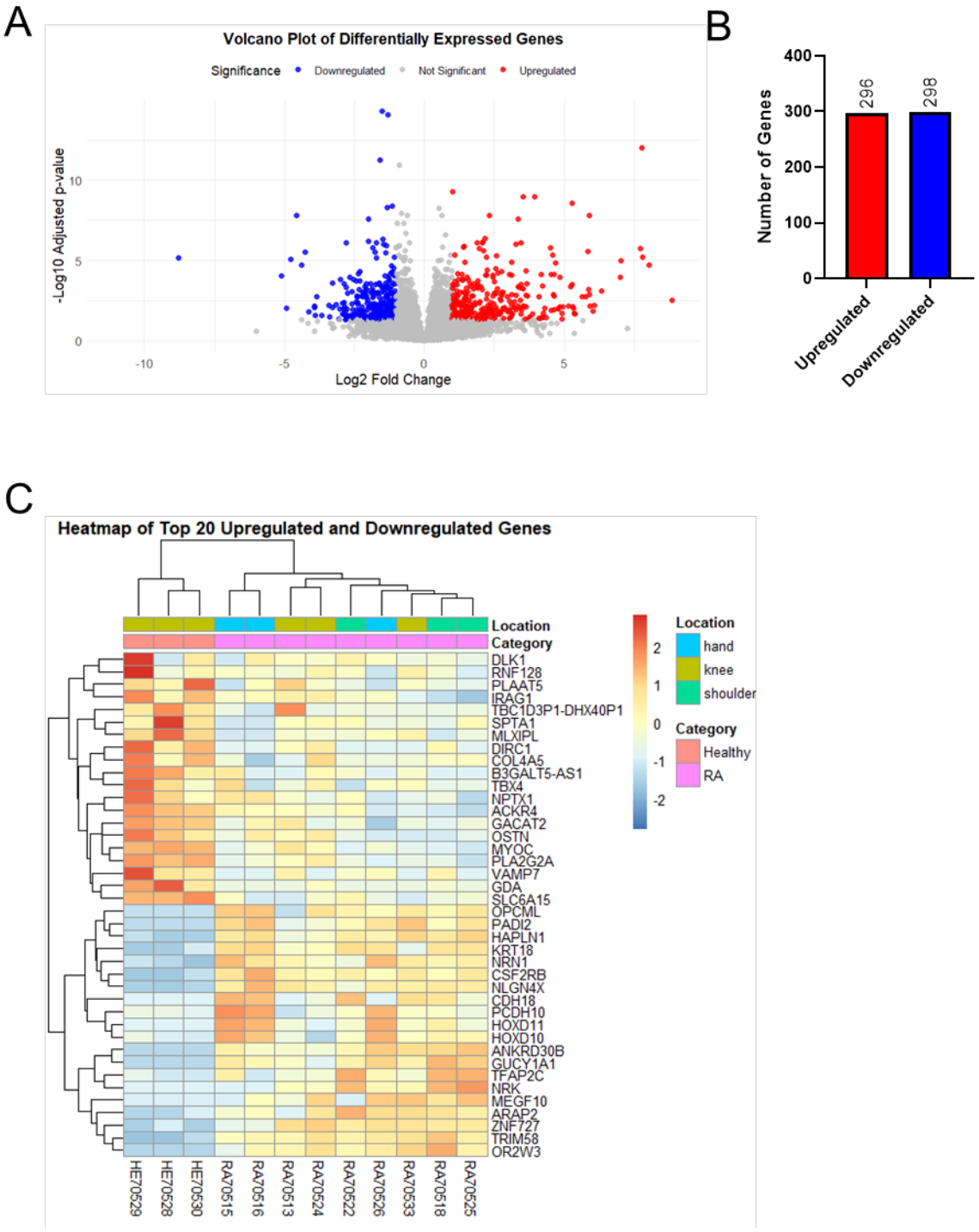

Figure 3-3 Arthritic synovial fibroblasts show a distinct inflammatory transcriptomic signature.

SFs from clinical samples were expanded in vitro for RNA-Seq analysis, as explained in Frank Bertocelj et al. (2017) paper to evaluate gene expression. Differential gene expression was analysed using DESeq2, with significance defined as $|\log_2 FC| > 1$ and padj < 0.05.

A) Volcano Plot displays differentially expressed genes (DEGs) in RA vs. healthy SFs. Upregulated (red) and downregulated (blue) genes met the significance threshold, while non-significant genes are not met the significance shown in grey.
B) Bar Graph shows the numbers of significantly up- and downregulated genes.
C) Heatmap highlights the top 20 DEGs, with red indicating high and blue low expression. Clustering groups samples by similarity, annotated by sample location and condition. Gene expression values are log_2-transformed and Z-score normalised (row-scaled).

Differential gene expression analysis of SFs from RA patients revealed significant enrichment of key signalling pathways associated with disease pathogenesis. Notably, the JAK-STAT signalling pathway emerged as highly enriched, reflecting its central role in mediating inflammatory cytokine signalling and immune responses in RA. The enrichment of the Notch signalling pathway suggests involvement in fibroblast activation and cellular differentiation processes. Furthermore, alterations in the extracellular matrix (ECM)-receptor interaction pathway highlight the remodelling of the joint microenvironment that supports synovial hyperplasia and tissue invasion. Dysregulation of cytokine-cytokine receptor interactions further points to a complex network of inflammatory signalling that drives the disease. These findings corroborate a molecular framework associated to aberrant behaviour of RA SFs (Figure 3-4A).

Functional enrichment of biological processes among differentially expressed genes revealed that peptidyl-tyrosine phosphorylation was the most significantly enriched term, indicating elevated kinase-mediated signal transduction in RA SFs. This enhancement in phosphorylation events is consistent with activation of multiple signalling cascades regulating inflammation and cell proliferation. Enrichment of cell-cell adhesion processes reflects changes in the interactions between fibroblasts and their surrounding extracellular matrix, contributing to the invasive and aggressive phenotype of RA fibroblasts. The Notch signalling pathway and protein autophosphorylation processes were also enriched, supporting their roles in cell fate determination and intracellular signalling modulation within the inflamed synovium. Additional enriched processes, such as protein localisation to the plasma membrane, suggest complex regulation of protein trafficking and membrane receptor dynamics that influence SF function (Figure 3-4B).

Molecular function enrichment analysis further elucidated the key activities underlying RA SF pathology. The most significantly enriched function was protein tyrosine kinase activity, highlighting the importance of tyrosine kinases as regulators of intracellular signalling pathways driving inflammation and cellular activation. Enrichment of structural components of the cytoskeleton indicates remodelling of cellular architecture necessary for increased fibroblast motility and tissue invasion. Several transcription-related functions were enriched, including RNA polymerase II-specific DNA-binding transcription factor binding and histone deacetylase binding, pointing to epigenetic and transcriptional regulatory mechanisms that modulate gene expression in RA fibroblasts. Moreover, enrichment of adhesion-related molecular functions, such as integrin binding, cadherin binding, and cell adhesion molecule binding, underscores the altered cell adhesion properties that facilitate SF interaction with the extracellular matrix and contribute to joint destruction (Figure 3-4C).

A

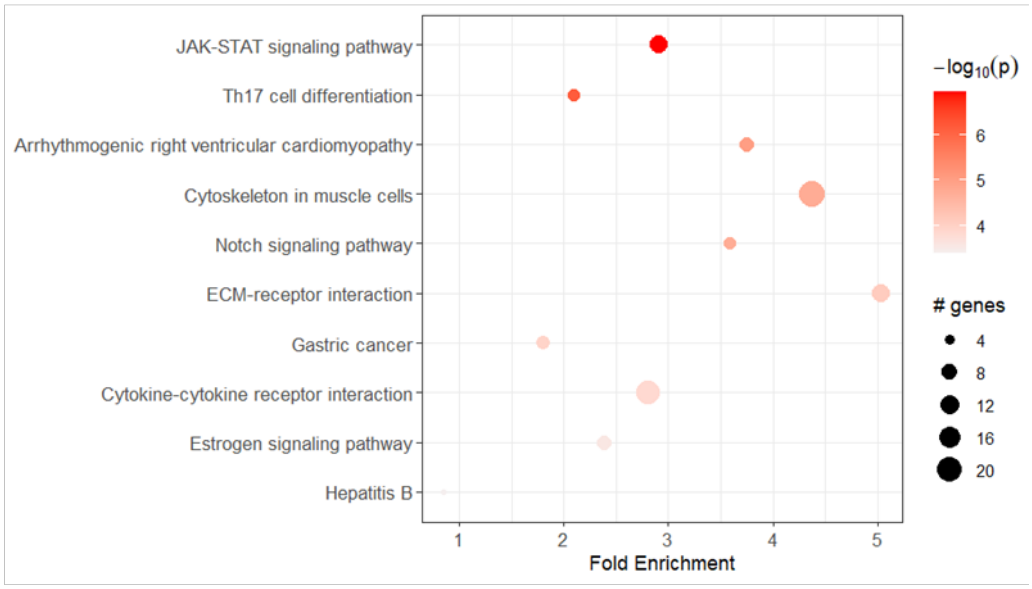
KEGG
JAK-STAT signaling pathway
Th17 cell differentiation
Arrhythmogenic right ventricular cardiomyopathy
Cytoskeleton in muscle cells
Notch signaling pathway
ECM-receptor interaction
Gastric cancer
Cytokine-cytokine receptor interaction
Estrogen signaling pathway
Hepatitis B
1
2
3
4
5
Fold Enrichment
−log10(p)
6
5
4
genes
4
8
12
16
20

B

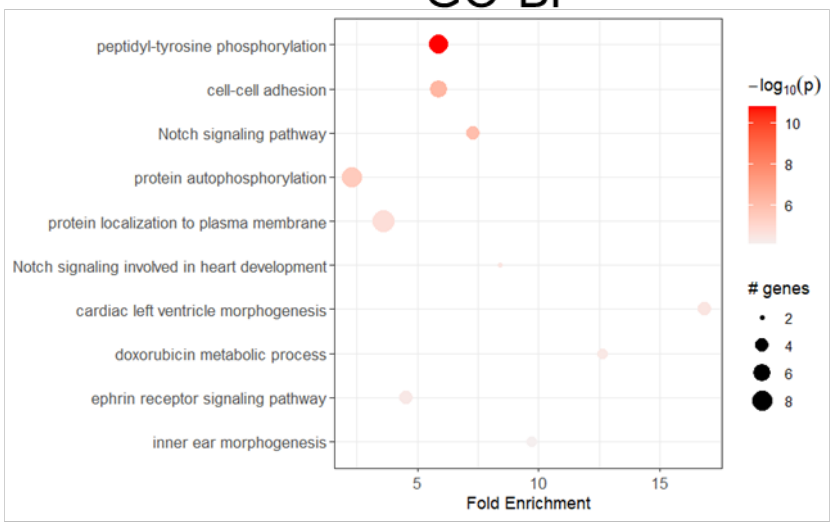
GO-BP
peptidyl-tyrosine phosphorylation
cell-cell adhesion
Notch signaling pathway
protein autophosphorylation
protein localization to plasma membrane
Notch signaling involved in heart development
cardiac left ventricle morphogenesis
doxorubicin metabolic process
ephrin receptor signaling pathway
inner ear morphogenesis
5
10
15
Fold Enrichment
−log10(p)
10
8
6
genes
2
4
6
8

C

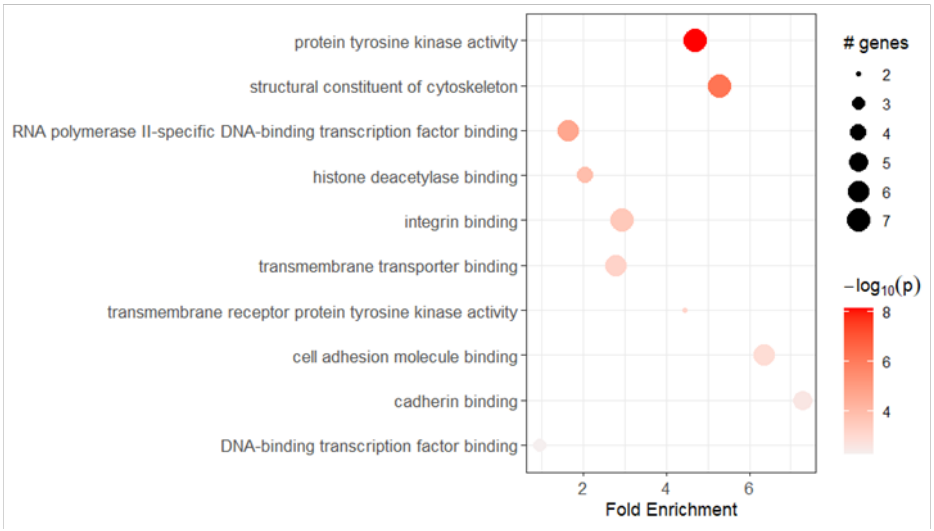
GO-MF
protein tyrosine kinase activity
structural constituent of cytoskeleton
RNA polymerase II-specific DNA-binding transcription factor binding
histone deacetylase binding
integrin binding
transmembrane transporter binding
transmembrane receptor protein tyrosine kinase activity
cell adhesion molecule binding
cadherin binding
DNA-binding transcription factor binding
2
4
6
Fold Enrichment
genes
2
3
4
5
6
7
−log10(p)
8
6
4

Figure 3-4 Enrichment Analysis Reveals Key Biological Processes, Molecular Functions, and Pathways in Differentially Expressed Genes.

Functional enrichment analysis was performed using the PathfindR package to identify significantly enriched (A) KEGG pathways, (B) biological process, and (C) molecular function among differentially expressed genes (DEGs). Differential gene expression was analysed using DESeq2, with significance defined as $|\log_2 FC| > 1$ and padj < 0.05. Enrichment analysis results are plotted as −log10(p) values against fold enrichment, with gene counts per pathway indicated. Dot size represents the number of genes associated with each term, while colour intensity reflects significance ($-\log_{10}$(p-value)).

3.2.2 Glycosylation Pathway Dynamics and Sialyltransferase Dysregulation in Rheumatoid Arthritis Synovial Fibroblasts

Standard RNA-seq pipelines, while powerful for capturing global transcriptional changes, are inherently limited in their ability to uncover meaningful differences in glycobiology due to the complex glycan-protein interactions that are not always collated in predefined biological pathways. Furthermore, glycan biosynthesis is not solely determined by the transcriptional levels of glycosylation-related genes, it is instead orchestrated by a tightly regulated interplay of enzyme localisation, substrate availability, nucleotide sugar transporters, and post-translational modifications (Hou et al., 2016; Kouka et al., 2022). Moreover, standard pipelines tend to focus on well-characterised biological pathways such as inflammation or metabolism and often exclude glycoenzymes due to low expression, poor annotation, or the absence of glycosylation-specific categories in conventional pathway databases like KEGG, GO, or Reactome. As a result, differential expression analyses frequently miss subtle but biologically significant shifts in glycosylation, such as changes in sialylation patterns. Furthermore, because glycan structures are not directly encoded in the genome and cannot be inferred from RNA levels alone, RNA-seq provides relatively less insight into glycan isomerism, linkage types, or branching patterns. Without the integration of specialised tools such as GlycoMaple (Y.-F. Huang et al., 2021), which predicts glycan structures based on gene expression, or GlycoEnzOnto (Groth et al., 2022), which maps glycosylation reactions using an ontology-based approach, standard pipelines cannot translate transcriptional data into functional glycomic predictions. Therefore, to extract glycobiological insight from transcriptomic data, researchers must augment traditional RNA-seq analysis with custom glycobiology

focused gene sets, dedicated databases, and complementary experimental techniques such as lectin arrays or mass spectrometry to validate predicted changes at the glycan level.

Considering these limitations in the RNA-seq pipelines, we next investigated the changes in the glycosylation signatures by performing a PCA using only genes related to glycosyltransferase enzymes. This approach allowed us to observe transcriptomic differences based only on the changes in the glycosyltransferase genes. Similar to the overall PCA, RA and healthy samples separate clearly, meaning differences in glycosylation-related gene expression of 152 glycosyltransferase enzymes also distinguish RA from healthy SFs (Figure 3-5). PC1 here explains even more variance (25.8%) than the overall PCA (20.7%), emphasising the importance of glycosylation gene changes in RA pathology. In summary, the PCA plots demonstrate that not only the global transcriptome can differentiate between healthy and RA cells, but also specific glycosylation pathways are specific in RA patients and healthy controls. This supports the hypothesis that altered glycosylation plays a role in progression of disease outcome.

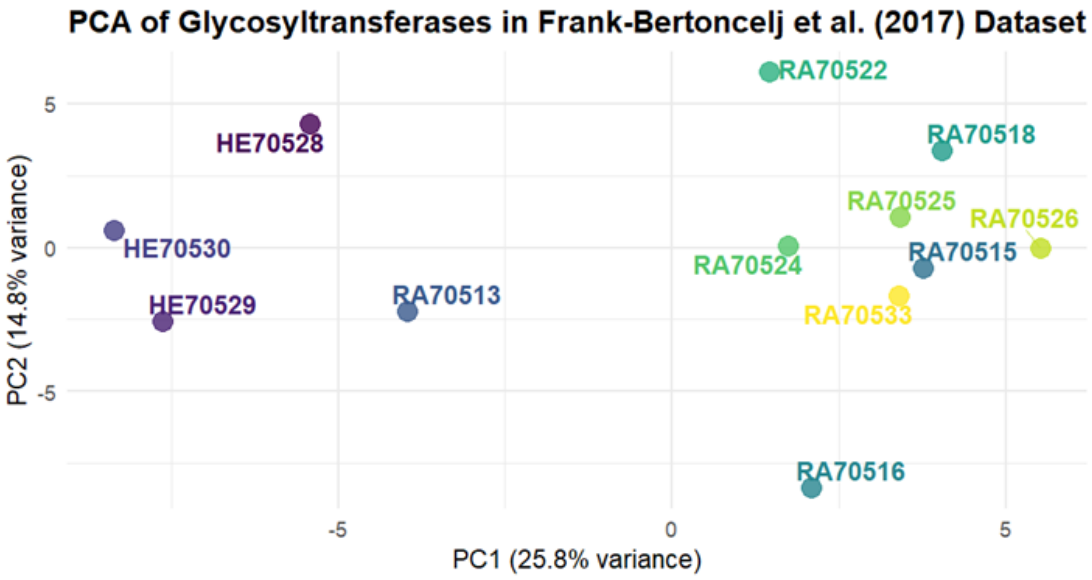

Figure 3-5 Principal Component Analysis of Glycosyltransferase Genes in Frank-Bertoncelj Bulk-RNA Seq Dataset.

PCA analysis was conducting using glycosyltransferase genes only, where first principal component (PC1) accounts for 25.8% the variance, while the second principal component (PC2) accounts for 14.8%.

A recent paper presented a new bioinformatic tool named GlycoEnzOnto, that is designed for pathway and molecular function enrichment analysis specifically focused on glycan biosynthetic pathways. It enables identification and visualisation of overrepresented biological pathways and molecular functions associated with glycoenzymes, thereby providing deeper insights into their roles in various cellular processes and enhancing the understanding of glycosylation's functional impact in biology (Groth et al., 2022).

GlycoEnzOnto pathway enrichment analysis which performed on all dataset demonstrated that several glycosylation-related biosynthetic pathways, including glycosylation-related, glycan biosynthetic, and dolichol precursor biosynthetic pathways, showed positive normalised enrichment scores (NES) between 1.46 and 1.75. Although their adjusted p-values (padj) ranged from 0.023 to 0.19, only the glycosylation-related pathway reached a statistically significant threshold (padj = 0.023), indicating a trend toward upregulation of glycan biosynthesis genes. In contrast, glycan degradation pathways exhibited negative NES values (approximately -1.56 to -1.67) but did not reach statistical significance after adjustment (padj ~0.15), suggesting a potential but not definitive downregulation of catabolic processes. Overall, these results suggest an enrichment of glycosylation related pathways, providing further evidence that genes involved in glycosylation are dysregulated in chronic RA (Figure 3-6).

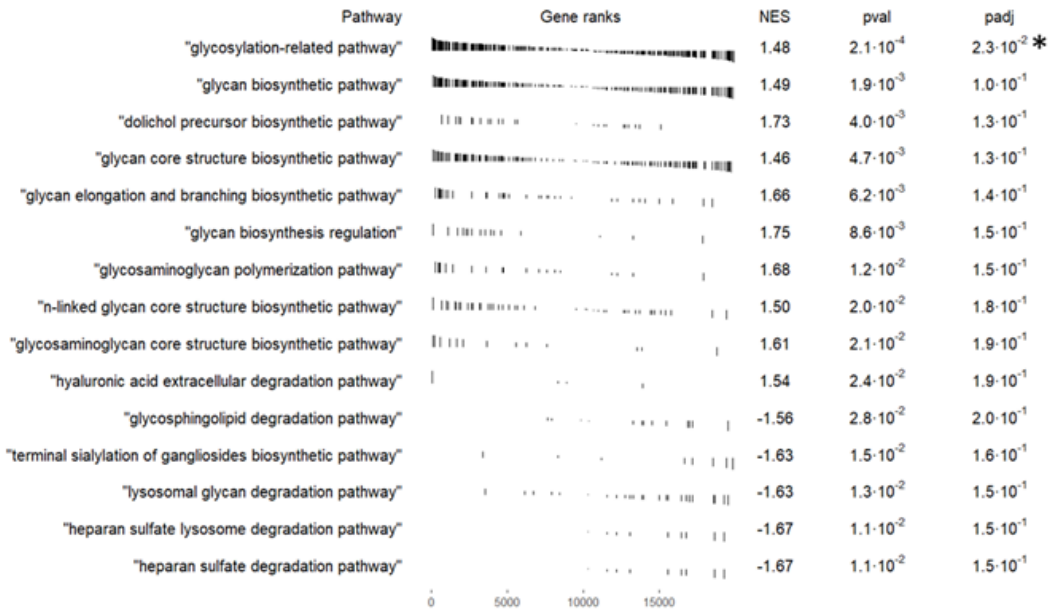

Figure 3-6 Glycosylation-Related Pathway Significantly Changed in RA SFs expanded ex vivo.

RA SFs show distinct glycosylation profiles predicted by GlycoEnzonto Enrichment Analysis. Gene set enrichment analysis (GSEA) was performed to identify glycosylation-related pathways with significant enrichment. Each pathway is shown with its normalised enrichment score (NES), p-value, and adjusted p-value (padj). The NES represents the degree of pathway enrichment after normalising for gene set size. Positive NES values indicate pathways enriched in upregulated genes while negative NES values indicate pathways enriched in downregulated genes. Higher absolute NES values suggest stronger enrichment. The x-axis represents the position in the ranked list of genes. Each black tick mark corresponds to a gene associated with the given pathway, showing where it appears in the ranked list of genes. Longer lines highlight genes with stronger contributions to enrichment, such as those with high differential expression or statistical significance. A dense cluster of marks near the top or bottom leads to a higher NES, indicating strong pathway enrichment. Significantly enriched pathways are marked with (*).

Next, we aimed to predict would be synthesised by the cells given their current glycan-related transcriptome. To do this, we used GlycoMaple, a computational tool that integrates glycosylation biosynthesis pathways with gene expression data to analyse and visualise the activity of glycosylation-related enzymes. By mapping transcriptomic data onto curated glycan synthesis pathways, GlycoMaple enables researchers to predict changes in glycan structures and identify alterations in

glycosylation patterns across biological conditions (Y.-F. Huang et al., 2021). The glycan structural complexity arises from the various monosaccharides involved, their branching structures, and the distinct linkages between these sugars. Glycan structures attached to proteins can mostly be classified into N-glycans and O-glycans, each exhibiting unique configurations and functional implications in cellular interactions and signalling. While N-glycans attached to the proteins at asparagine residues, O-glycans are linked to serine or threonine residues (Gao et al., 2019; Wilkinson & Saldova, 2020). To understand changes predicted in glycosylation dynamics, we next utilised GlycoMaple prediction tool to predict different pathways in both N- and O-glycans. The diagram in Figure 3-7 illustrated biosynthetic pathways of various complex glycans, highlighting the enzymatic steps involved in synthesizing ABO blood group antigens, Lewis antigens, polysialic acids (Poly-Sia), LacdiNAc structures, HNK-1, and polylactosamine chains. The pathway demonstrates the branching and interplay between different glycan structures, showing how enzymes may modify core glycan backbones to create diverse cell surface carbohydrate structures. Among the reactions, galactosylation is increased in RA through the enzymes B3GALT5, B3GALT1, B3GALT2, indicating that there may be an increased synthesis of galactose (and extension of glycan chains containing LacNAc groups) between RA vs healthy SFs.

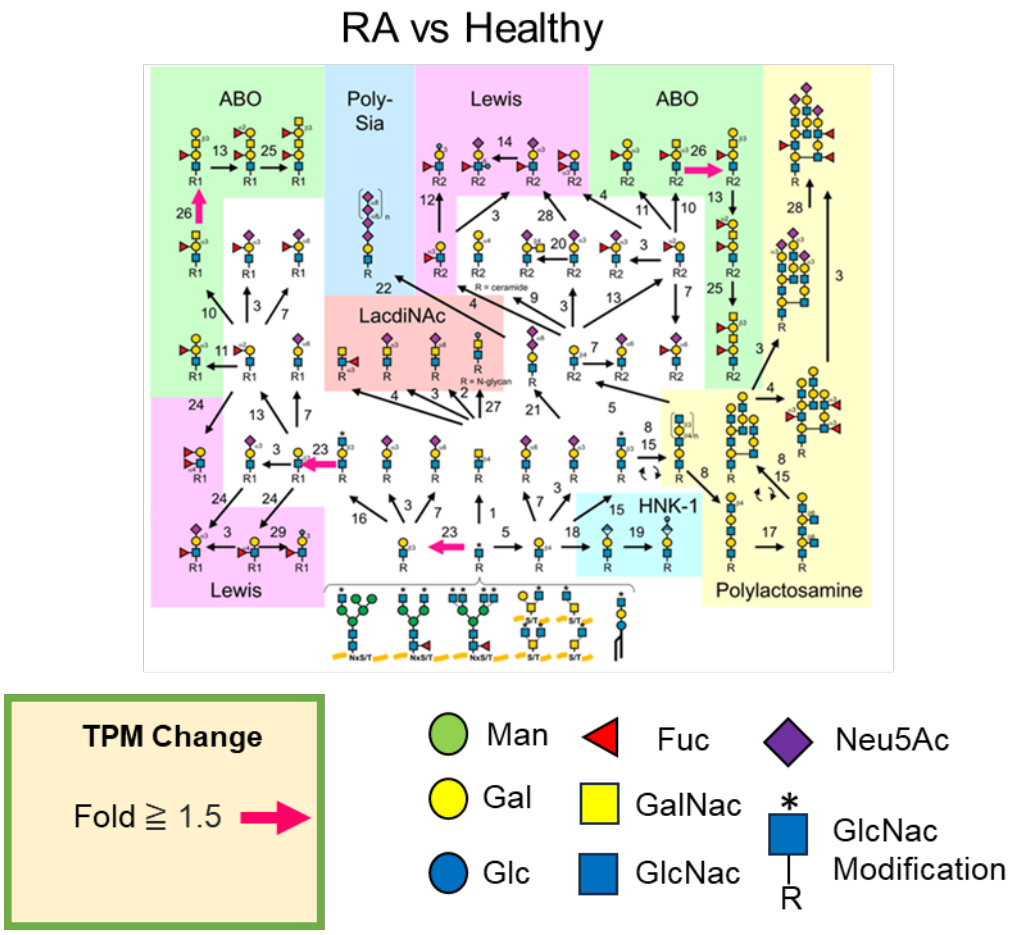

Figure 3-7 Comparison of N- and O-Glycan Capping Pathways Between RA and Healthy SFs expanded ex vivo.

Pathways related to complex capping of glycans between RA vs Healthy SFs mapped using GlycoMaple based on the TPM gene expression values and then mean TPM values compared between RA (n=9) vs Healthy SFs (n=3) in Frank-Bertoncelj et al. (2017) dataset. Significant fold changes were annotated with pink arrows. Reaction numbers 23 and 26 have shown to demonstrate changes in the galactose modifications through the enzymes named B3GALT5, B3GALT1, B3GALT2, indicating the galactose modification occurs in glycans.

Since RA SFs alters glycosylation pathways, next we investigated how the enzymes directly responsible for sialylation are affected in RA compared to healthy SFs. This interest was driven by previous worked published by our group, where it was observed that in mouse models of RA, SFs had a reduced expression of α2,6-sialosides (Y. Wang et al., 2021). Furthermore, the levels of sialic acid in human cells could be dysregulated, given our findings using GlycoMaple to predict glycan structures. These indicated that RA SFs displays increased expression of β1,3-

galactosyltransferases (B3GALTs), which catalyse the addition of galactose to N-acetylglucosamine, forming type I or type II lactosamine (LacNAc) structures. This upregulation of B3GALTs may lead to an expanded pool of LacNAc units, which serve as critical acceptor substrates for sialyltransferases. Sialyltransferases transfer sialic acids in α2,3-, α2,6-, or α2,8-linkages onto terminal galactose or N-acetylgalactosamine residues, thereby determining the capping structure of glycans. An increased abundance of LacNAc chains could shift the balance of sialylation by providing more substrates for α2,3-sialyltransferases, which preferentially sialylate terminal galactose residues. At the same time, the structural context of these glycans may change, potentially affecting the accessibility or activity of competing α2,6-sialyltransferases. As a result, the overall pattern and type of terminal sialic acid capping may change. We also included genes for enzymes involved in sialic acid biosynthesis genes, in addition to sialytransferases. These enzymes produce sialic acid molecules and metabolomic precursors inside the cell, generating CMP-sialic acid through a multi-step pathway primarily in the cytoplasm and nucleus (Table 3-3). Sialic acid capping genes encode sialyltransferases, enzymes located mainly in the Golgi apparatus that transfer these activated sialic acids onto the terminal positions of glycan chains on glycoproteins and glycolipids, thereby modifying the cell surface (Table 3-2). While biosynthesis genes supply the building blocks, capping genes execute the final attachment of sialic acid residues to glycans, determining the structure and function of cell surface glycoconjugates (Y. Li & Chen, 2012).

Table 3-2 The characteristics of sialyltransferase enzymes involved in sialic acid capping.

Sialyltransferase (ST)	Function (Catalysed Sialic Acid Linkage)	Preferred substrate
ST3GAL1	Adds α2,3-linked sialic acid	O-glycans on glycoproteins
ST3GAL2	Transfers α2,3-linked sialic acid	Gangliosides (e.g., GM1)
ST3GAL3	Catalyses α2,3 sialylation	N-glycans, O-glycans
ST3GAL4	Involved in α2,3 sialylation	Glycolipids, glycoproteins
ST3GAL5	Adds α2,3-linked sialic acid	Lactosylceramide (forming GM3)
ST3GAL6	Adds α2,3-linked sialic acid	Core 1 O-glycans, lactosylceramide
ST6GAL1	Adds α2,6-linked sialic acid	N-glycans (on glycoproteins)
ST6GAL2	Adds α2,6-linked sialic acid	N-glycans (brain-specific)
ST6GALNAC1	Catalyses α2,6 sialylation	O-glycans, glycosphingolipids
ST6GALNAC2	Adds α2,6-linked sialic acid	O-glycans (immune cell signalling)
ST6GALNAC3	Adds α2,6-linked sialic acid	Glycolipids
ST6GALNAC4	Adds α2,6-linked sialic acid	O-glycans in mucins
ST6GALNAC5	Transfers α2,6-linked sialic	Gangliosides
ST6GALNAC6	Adds α2,6-linked sialic acid	O-glycans (cancer-associated markers)
ST8SIA1	Catalyses α2,8-linked sialylation	Gangliosides (e.g., GD3, GT3)
ST8SIA2	Adds α2,8-linked sialic acid	N-glycans, polysialic acid chains
ST8SIA3	Adds α2,8-linked sialic acid	Glycoproteins
ST8SIA4	Involved in polysialylation	Neural cell adhesion molecules (NCAM)
ST8SIA5	Adds α2,8-linked sialic acid	Glycolipids

Table 3-3 The characteristics of key genes involved in sialic acid biosynthesis.

Gene	Function (Role in Sialic Acid Pathway)	Modified/Produced Structure
GNE	Initiates sialic acid synthesis via epimerase and kinase activity on UDP-GlcNAc	ManNAc-6-P (precursor to Neu5Ac)
NANS	Synthesises Neu5Ac-9-P from ManNAc-6-P and phosphoenolpyruvate	Neu5Ac-9-P (sialic acid precursor)
NANP	Converts Neu5Ac-9-P to free Neu5Ac through dephosphorylation	Neu5Ac (sialic acid)
CMAS	Activates Neu5Ac by adding CMP, forming CMP-Neu5Ac for sialyltransferases	CMP-Neu5Ac (activated sialic acid donor)
SLC35A1	Transports CMP-Neu5Ac into the Golgi lumen for glycan sialylation	CMP-Neu5Ac (Golgi-localised)
CASD1	O-acetylates CMP-Neu5Ac at C7/C9 positions (regulates diversity of sialic acid forms)	O-acetylated CMP-sialic acids
GCNT2	Modifies glycan core structures (e.g. I-branching); may influence sialylation by altering acceptor sites	Branched poly-N-acetyllactosamine chains
SIAE	Removes O-acetyl groups from sialic acids (sialic acid esterase)	De-O-acetylated sialic acids

To understand how sialic acid biosynthesis and capping genes significantly differ between RA vs healthy SFs, we analysed the expression of sialic acid related genes to identify which ones were differentially regulated. The results (Figure 3-8) illustrate the differential expression patterns of key sialic acid biosynthesis (NANS) and capping (ST6GAL1, ST3GAL5, ST3GAL6, ST8SIA1) genes across synovial tissue samples from RA patients and healthy controls, collected from different joint locations. NANS expression is generally higher in RA samples compared to healthy controls, with some variation based on joint location. Notably, sialyltransferase genes such as ST3GAL6 and ST3GAL5 are significantly downregulated in RA samples. Violin plots further explain these trends, showing

statistically significant decreased expression of ST3GAL6, ST3GAL5, and ST8SIA1 in RA samples compared to healthy controls (adj p-values < 0.05), while ST6GAL1 expression significantly upregulated in RA samples compared to healthy SFs (Figure 3-8). These results suggest that while sialic acid biosynthesis is active in RA synovium, the capping of glycans with sialic acid via specific sialyltransferases is dysregulated, potentially contributing to altered glycosylation patterns in the disease state, indicating that overall sialylation pattern may be altered in SFs between RA vs health state.

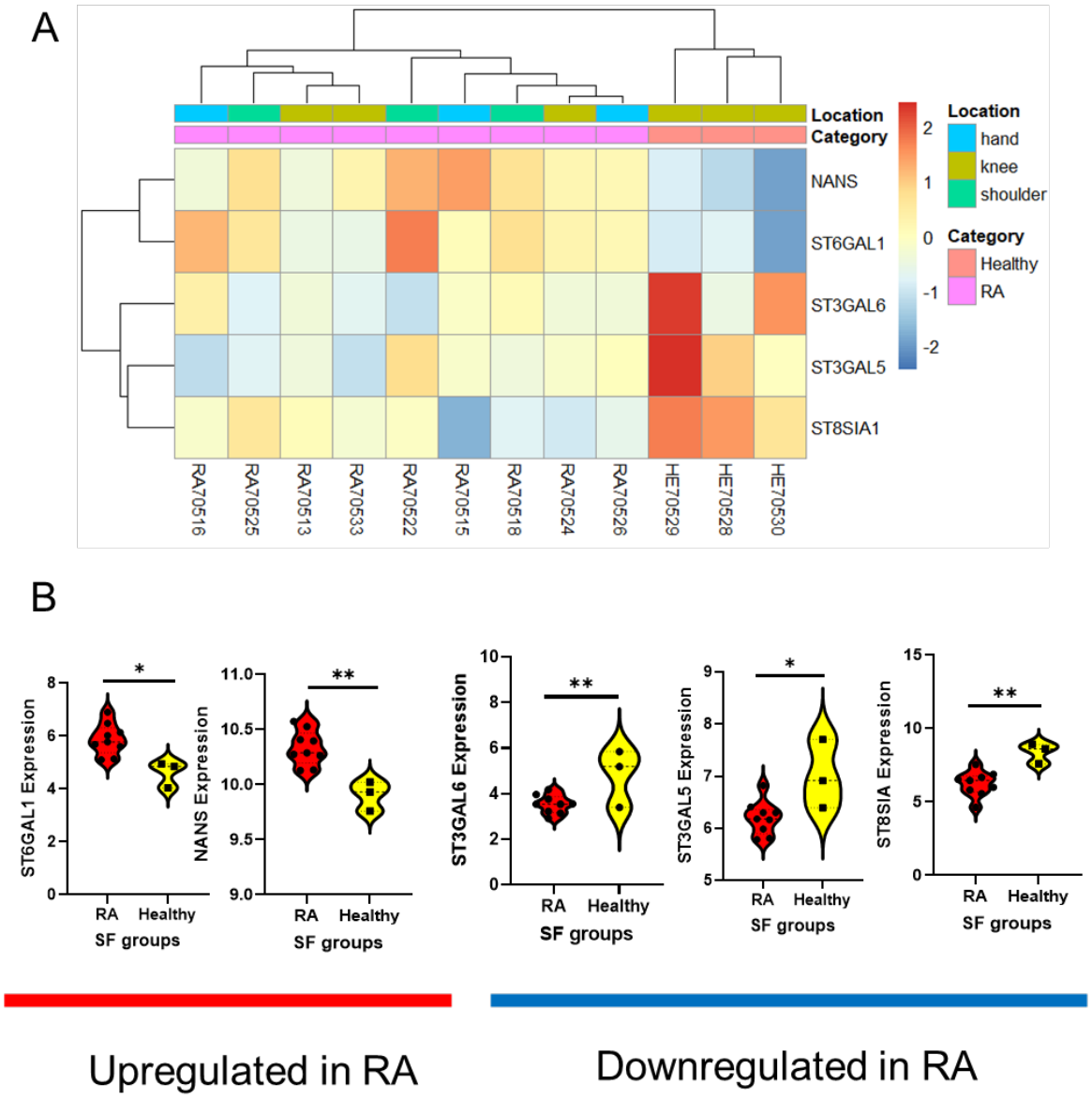

Figure 3-8 Differentially Expressed Genes Involved in Sialylation in Rheumatoid Arthritis (RA) vs. Healthy Synovial Fibroblasts.

Figure A illustrates the differentially expressed genes involved in sialylation identified through RNA-seq analysis using DESeq2. The analysis compared gene expression profiles between rheumatoid arthritis (RA) and healthy SFs samples, with a significance threshold set at an adjusted p-value (adjp) < 0.05. Gene expression is Z-score normalised, with upregulated genes shown in red and downregulated genes in blue. The locations (hand, knee, shoulder) and categories (Healthy, RA) are indicated to provide context for the tissue sources and disease states analysed. Figure B in violin plots show gene expressions of significantly differentially expressed sialyltransferases obtained from normalised logarithmic gene counts. *adjp <0.05 and **adjp<0.01 obtained from DESeq2.

3.2.3 Transcriptomic Changes in Rheumatoid Arthritis Synovial Fibroblasts in Response to TNF Stimulation

In the joint microenvironment of RA, SFs are key effectors that respond dynamically to inflammatory cues, particularly TNF-α. Produced by macrophages, T cells, and SFs themselves, TNF-α activates signalling pathways such as NF-κB, MAPK, and JAK/STAT within SFs, leading to the upregulation of adhesion molecules, pro-inflammatory cytokines (e.g., IL-6, CCL2), and matrix-degrading enzymes (e.g., MMPs). This drives SFs toward an aggressive, hyperplastic phenotype resistant to apoptosis and capable of invading cartilage and bone. TNF-α also shapes the inflammatory microenvironment by enhancing SF interactions with immune cells, endothelial cells, and osteoclasts, thereby promoting immune cell infiltration, sustained inflammation, and joint destruction (Pap et al., 2000).

To investigate the impact of inflammatory cytokines on the SF glycome, we used a publicly available bulk RNA-Seq dataset from the study by Ge et al. (2021). Bulk RNA-Seq data from in vitro TNF-α-stimulated and unstimulated RA SFs, derived from patients with varying age and sex backgrounds, were initially used to validate cytokine-induced activation of RA SFs. While our previous ex vivo analyses revealed glycosylation-related alterations in RA SFs, more mechanistic insights are needed to determine the direct influence of individual cytokines. Therefore, to dissect the specific role of TNF-α, a central pro-inflammatory mediator in RA pathogenesis, we focused on its direct effect on SF glycosylation. TNF-α is known to regulate glycosylation during inflammation, making it a critical factor in understanding glycan remodeling in chronic inflammatory diseases such as RA. Specifically, TNF-α can modulate the expression of key glycosylation enzymes, including sialyltransferases, fucosyltransferases, and galactosyltransferases (Y. Wang et al., 2021; Xu et al., 2011; Yu et al., 2022). These changes can alter the

structure and composition of cell surface and secreted glycans, ultimately influencing how immune cells recognise and respond to their environment. This targeted approach allows us to explore whether there is a direct link between TNF-α signaling and glycosylation remodeling in RA SFs.

The RA patient cohort consisted of 16 individuals (10 females, 6 males) ranging in age from 44 to 77 years, with synovial samples collected from various joints including the shoulder, knee, wrist, and finger. Most patients were seropositive for rheumatoid factor, although a few were seronegative. Inflammatory status, as measured by CRP levels, varied widely across patients from as low as 0.7 mg/L to as high as 60.8 mg/L, indicating a broad range of systemic inflammation. Disease activity, assessed by DAS28 scores, ranged from 1.25 to 2.89, suggesting that most patients were in the low to moderate disease activity range. VAS scores, reflecting patient-reported pain, also varied, with some reporting no pain and others scoring as high as 9. Patients were undergoing various treatment regimens, including conventional DMARDs like methotrexate, biologics such as infliximab (TNF-α inhibitors), tocilizumab (IL-6 inhibitors), and rituximab (B-cell inhibitors), and in some cases, JAK inhibitors or NSAIDs, indicating heterogeneous therapeutic backgrounds (Table 3-4).

Table 3-4 Clinical information of Rheumatoid Arthritis synovial fibroblasts used in Ge et al. (2021) paper.

Sample	Group	Location	Sex	Age	Rheumatoid Factor	CRP (mg/l)	VAS	DAS 28	Medication	Diagnosis
US_FLS292	control	finger	f	44	seropositive		1.9		Methotrexate	RA
TNF_FLS292	TNF	finger								RA
US_FLS336	control	knee	m	73	seronegative	2.2		1.38	.	RA
TNF_FLS336	TNF	knee								RA
US_FLS346	control	knee	m	61	seropositive	3.4	9	2.19	Methotrexate, Infliximab, Steroids	RA

TNF_FLS346	TNF	knee								RA
US_FLS407	control	shoulder	f	70	seropositive	2	8	2.89	Methotrexate	RA
TNF_FLS407	TNF	shoulder								RA
US_FLS415B	control	finger	f	55	seropositive	24.4			Steroids, Tociluzimab	RA
TNF_FLS415B	TNF	finger								RA
US_FLS435	control	shoulder	f	66	seropositive	4			Rituximab	RA
TNF_FLS435	TNF	shoulder								RA
US_FLS230	control	wrist	f	65	seronegative				Methotrexate, Steroids	RA
TNF_FLS230	TNF	wrist								RA
US_FLS387	control	wrist	m	75	seronegative	6.2	6	1.87	Tocilizumab	RA
TNF_FLS387	TNF	wrist								RA
US_FLS285	control	wrist	m	70	seropositive				Abatacept	RA
TNF_FLS285	TNF	wrist								RA
US_FLS379	control	finger	f	77	seropositive	26	0		Methotrexate, Steroids	RA
TNF_FLS379	TNF	finger								RA
US_FLS331	control	shoulder	m	61	seropositive	0.7	6	1.25	Methotrexate, Etancercept	RA
TNF_FLS331	TNF	shoulder								RA
US_FLS430	control	shoulder	f	69	seropositive	3.8				RA
TNF_FLS430	TNF	shoulder								RA

US_FLS466	control	shoulder	f	76	seropositive	7.8		2		RA
TNF_FLS466	TNF	shoulder								RA
US_FLS438	control	shoulder	f	53	seropositive	60.8			Tofacitinib, NSAR	RA
TNF_FLS438	TNF	shoulder								RA
US_FLS427	control	knee	m	60		6.4			Infliximab	RA
TNF_FLS427	TNF	knee								RA
US_FLS217	control	knee	f	73		10.2				RA
TNF_FLS217	TNF	knee								RA

Clinical information of RA SFs used in Ge et al. (2021) paper. Unstimulated RA SFs obtained from different joint locations stimulated with 10ng/ml TNF-α for 24 hours. CRP= C-Reactive Protein, VAS=Visual analogue scale, DAS= Disease Activity Score, RA= Rheumatoid arthritis, SFs=Synovial fibroblasts, DMARD=Disease modifying anti-rheumatic drug, NSAR=Non-steroid anti-inflammatory drug.

The PCA provide a clear separation between control (US) and TNF-stimulated (TNF) RA SFs based on transcriptomic profiles. The first PCA plot, encompassing the full gene expression dataset from Ge et al. (2021), shows that control and TNF-treated samples cluster distinctly along the second principal component (PC2), which accounts for 14.8% of the variance. This separation highlights the substantial transcriptional shift induced by TNF stimulation across multiple donors and joint locations (Figure 3-9A). The accompanying heatmap further supports these findings, illustrating global gene expression patterns of DEGs across samples (Figure 3-9B). Hierarchical clustering of both genes and samples shows a strong division between TNF-treated and control groups. Control samples tend to cluster together and exhibit more uniform gene expression, while TNF-treated samples display broader transcriptional variation, consistent with an activated inflammatory phenotype.

A

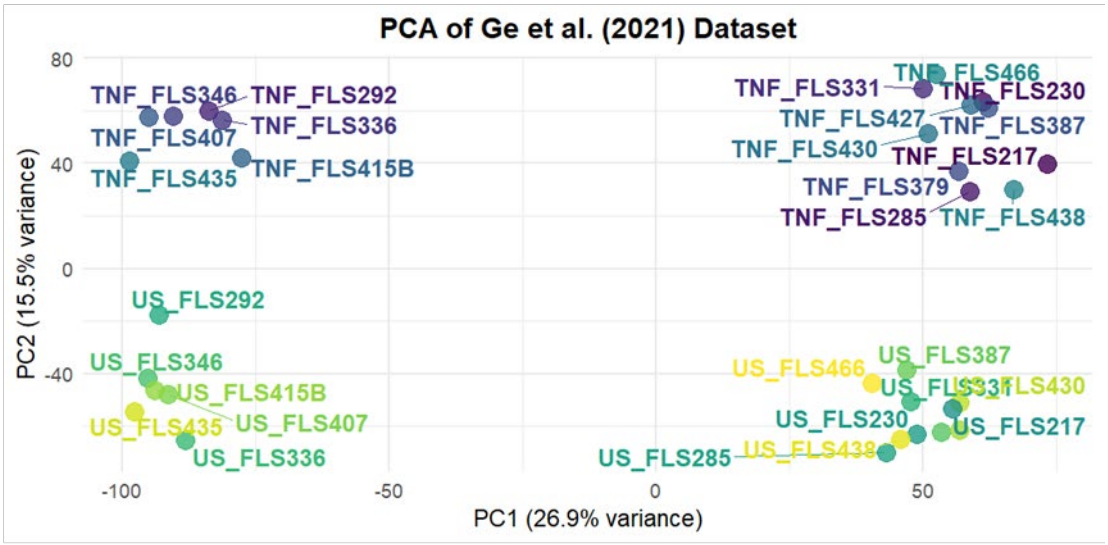

B

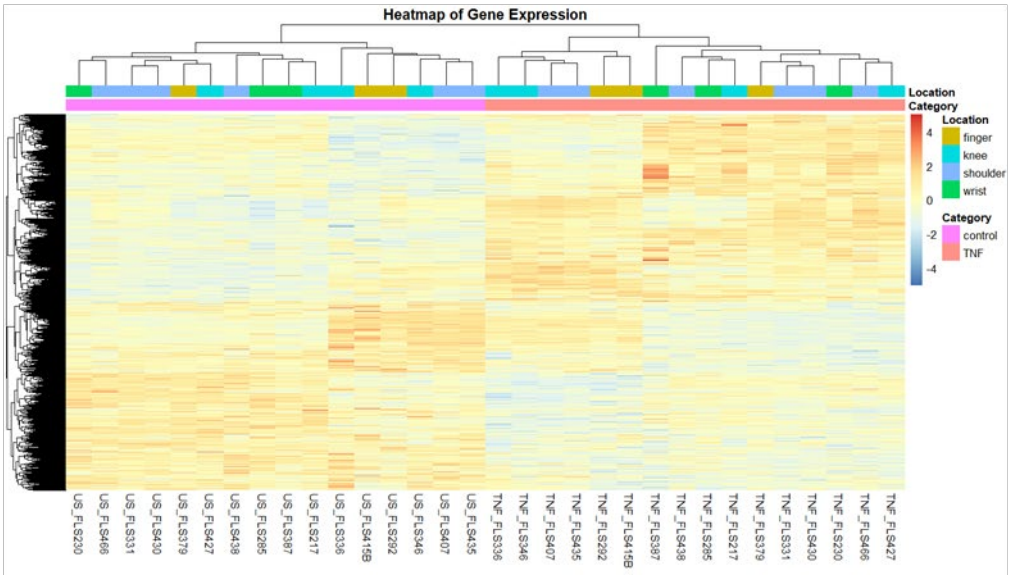

Figure 3-9 Principal Component Analysis (PCA) and Heatmap of Gene Expression from Ge et al. (2021) Dataset.

RNA-Seq was used to analysed gene expression in expanded RASFs with or without 10 ng/ml 24h TNF stimulation. Sva package is used to remove batch effects among experimental variables. A) PCA plot shows the distribution of samples based on gene expression profiles, x-axis shows the first principal component (PC1) accounting for 26.9% of the variance, y-axis represents the second principal component (PC2) accounting for 15.5%. Each dot represents individual RA SFs, with colours distinguishing between groups; TNF stimulated SFs (blue/purple), RA SFs (green/yellow). B) Heatmap of significantly differentially expressed genes in synovial fibroblasts from rheumatoid arthritis (RA) patients with TNF stimulation or unstimulation, clustered by expression levels. Rows

represent genes, and columns represent samples. The color scale indicates relative gene expression levels (blue = low expression, yellow = high expression) using Z scores. The annotation bars above the heatmap indicate sample locations (color-coded) and treatment categories (control vs. TNF). Clustering patterns suggest potential location- and treatment-specific differences in gene expression.

The presented volcano plot illustrates the differential gene expression profile of RA SFs following TNF stimulation compared to unstimulated control conditions. A large number of genes are significantly altered, with a predominant shift toward upregulation, as shown by the 1337 genes upregulated with log2 fold change >1 and adjusted p-value < 0.05. In contrast, 816 genes are significantly downregulated, indicating that TNF induces a broad transcriptional activation response in SFs (Figure 3-10A). We next quantified the number of differentially expressed genes, where the number of upregulated genes greatly exceeds the number of downregulated ones, highlighting TNF's strong pro-inflammatory effect on fibroblasts (Figure 3-10B). The accompanying heatmap further visualises the expression patterns of the top 20 most significantly upregulated and downregulated genes. TNF-stimulated RA SFs samples cluster distinctly from unstimulated RA SFs, indicating consistent transcriptional changes across donors and joint locations. Prominently upregulated genes include CXCL9, CXCL10, CXCL11, CXCL1, CXCL3, CXCL6, CCL5, CCL20, IDO1, and IL1B, many of which are associated with inflammation, interferon signalling, and immune cell recruitment. This gene expression profile suggests that TNF stimulation reprograms RA SFs toward a highly activated inflammatory phenotype, characterised by chemokine production and immune activation (Figure 3-10C).

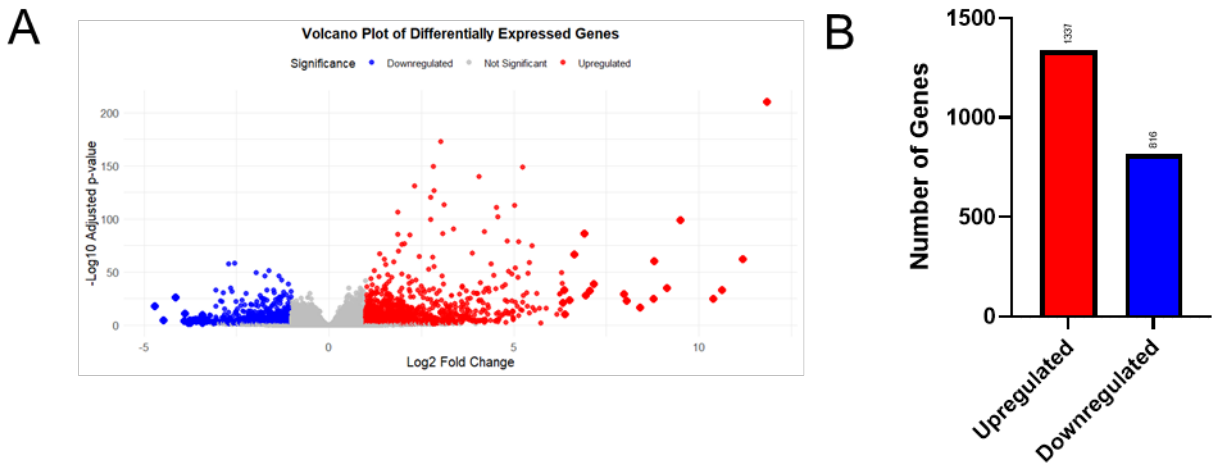

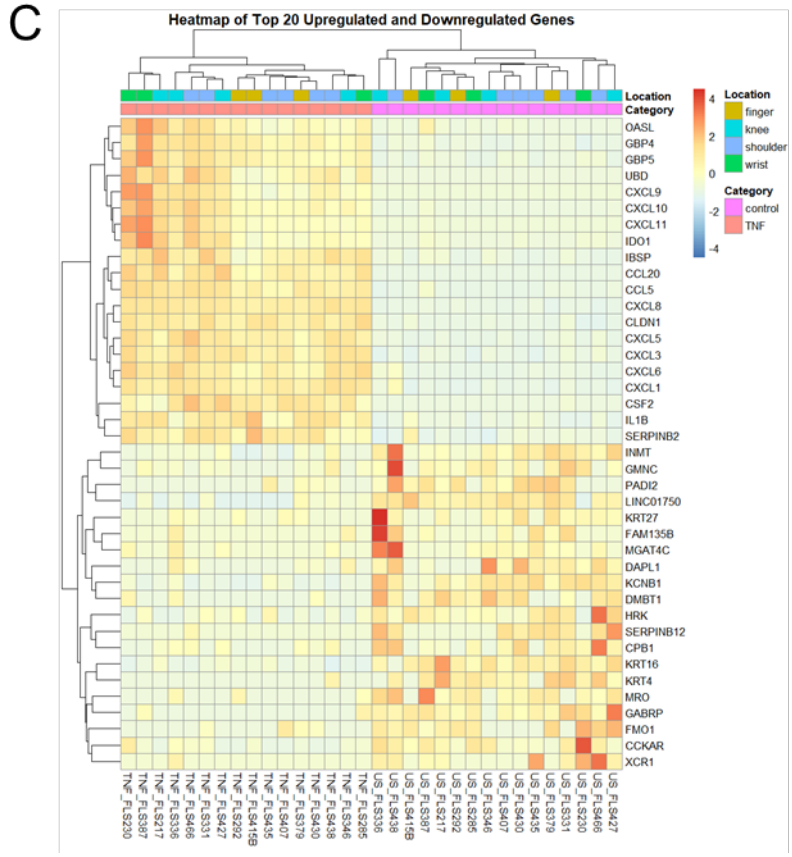

Figure 3-10 TNF stimulated RA synovial fibroblasts show a distinct inflammatory transcriptomic signature.

SFs from clinical samples were expanded ex vivo for RNA-Seq analysis and stimulated with 10 ng/ml TNF for 24h, as explained in Ge et al. (2021) to evaluate gene expression. Batch effects were removed with sva package. Differential gene expression was analysed using DESeq2, with significance defined as $|\log_2 FC| > 1$ and padj < 0.05.

A) Volcano Plot: Displays differentially expressed genes (DEGs) in RA TNF stimulated (TNF) vs. unstimulated RA SFs (control. Upregulated (red) and downregulated (blue) genes met the significance threshold, while non-significant genes are not met the significance shown in grey.
B) Bar Graph: Shows the number of significantly up- and downregulated genes, revealing a distinct distribution.
C) Heatmap: Highlights the top 20 DEGs, with red indicating high and blue low expression. Clustering groups samples by similarity, annotated by sample location and condition. Gene expression values are $\log_2$-transformed and Z-score normalised (row-scaled).

In order to understand how transcriptomic changes in response to TNF stimulation are leading to the activation of different pathways, we conducted a KEGG pathway enrichment (Figure 3-11A). The KEGG pathway enrichment analysis reveals that the genes of interest are predominantly involved in pathways regulating the cell cycle and inflammatory signalling. The most significantly enriched pathway is the cell cycle, indicating strong involvement in cellular proliferation. Other highly enriched pathways include NF-kappa B signalling, TNF signalling, cellular senescence, and antigen processing and presentation, which together suggest an active immune or stress-related response. Overall, these results confirm that the gene set is enriched in regulatory pathways essential for both immune activation and cell division.

In the GO Biological Process analysis (Figure 3-11B), the top enriched processes include positive regulation of canonical NF-kappa B signalling, protein phosphorylation, and various cell cycle-related events such as G2/M transition and mitotic cytokinesis. These terms highlight a dual focus on immune signalling which occurs particularly on the NF-κB, as a central inflammatory pathway, and mitotic regulation, reinforcing the theme observed in the KEGG analysis. Additionally, terms like response to virus and mitotic spindle assembly checkpoint signalling suggest that the cells are simultaneously responding to external stress signals and maintaining precise control over cell division.

The GO Molecular Function enrichment points to genes involved in signal transduction, protein degradation, and transcriptional regulation. The most significantly enriched function is ubiquitin-protein transferase activity, a key mechanism for controlling protein turnover and regulating various signalling

pathways (Qu et al., 2021). Functions such as DNA-binding transcription factor activity, protein kinase activities (tyrosine and serine/threonine), and peptide antigen binding indicate that the gene set encodes molecules central to transcriptional control, immune recognition, and cellular signalling. Together, these findings suggest that the system under study is undergoing dynamic changes in both proliferative and immune-regulatory states (Figure 3-11C).

A

KEGG

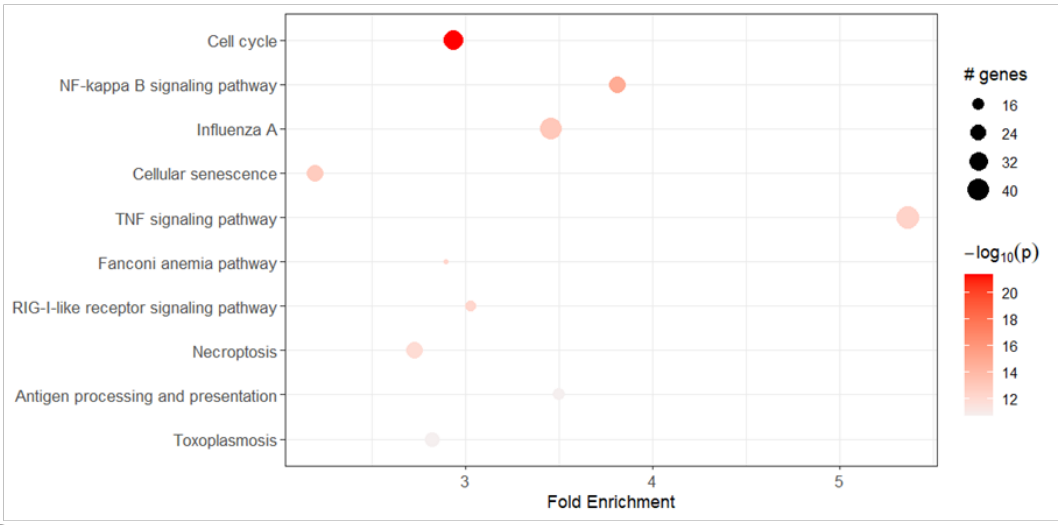

B

GO-BP

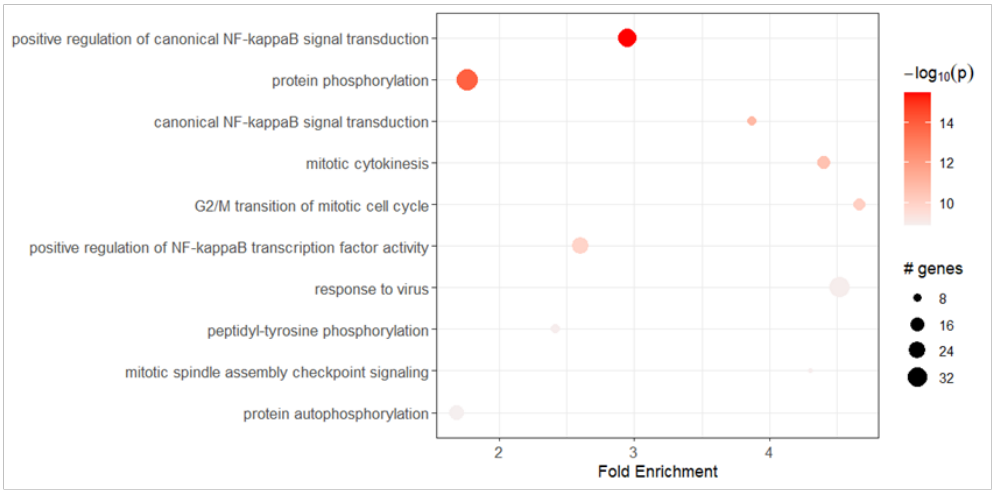

C

GO-MF

Figure 3-11 Enrichment Analysis Reveals Key Biological Processes, Molecular Functions, and Pathways in Differentially Expressed Genes.

Functional enrichment analysis was performed using the PathfindR package to identify significantly enriched (A) KEGG pathways, (B) biological processes, and (C) molecular functions among differentially expressed genes (DEGs) Differential gene expression was analysed using DESeq2, with significance defined as $|\log_2 FC| > 1$ and padj < 0.05. Enrichment analysis results are plotted as −log10(p) values against fold enrichment, with gene counts per pathway indicated. Dot size represents the number of genes associated with each term, while colour intensity reflects significance ($-\log_{10}$(p-value)).

3.2.4 TNF-Mediated Remodelling of Glycosylation Pathways in Rheumatoid Arthritis Synovial Fibroblasts

After demonstrating significant differences in global gene signatures between TNF stimulated vs unstimulated RA SFs, we investigated the changes in the glycosyltransferase enzymes. The PCA plot, focusing specifically on glycosyltransferase genes, similarly reveals a clear distinction between control and TNF-treated samples, though with slightly less variance explained by the first component. These data suggest that TNF stimulation not only alters global gene expression but also induces glycan remodelling (Figure 3-12). Collectively, these results expand the conclusion that TNF drives a robust and coordinated transcriptional program in RA SFs regardless of anatomical joint origin.

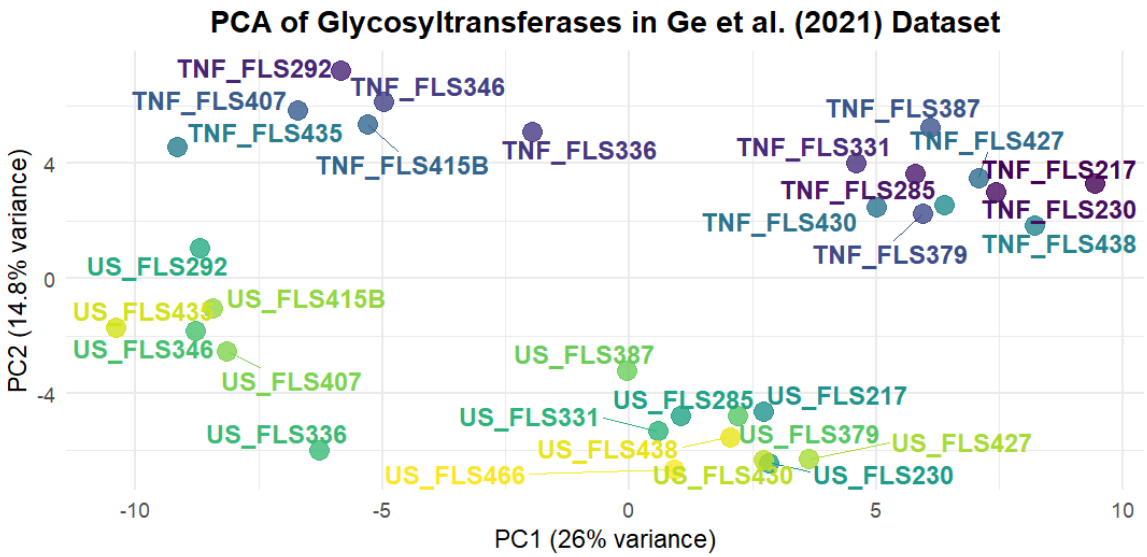

Figure 3-12 Principal Component Analysis (PCA) of Glycosyltransferase Genes Expression from Ge et al. (2021) Dataset.

PCA analysis was conducting using glycosyltransferase genes only, where first principal component (PC1) accounts for 26.0% the variance, while the second principal component (PC2) accounts for 14.8%.

Next, we investigated changes in the glycosylation gene signatures through GlycoEnzOnto pathway enrichment analysis. Gene set enrichment analysis of TNF-stimulated RA SFs revealed a selective activation of glycosylation-associated pathways. Among the pathways analysed, only the "glycosylation-related pathway" (NES = 1.62, padj = 1.3×10^{-2}) and the "glycan biosynthetic pathway" (NES = 1.56, padj = 2.2×10^{-2}) were significantly enriched, indicating a transcriptional upregulation of genes involved in general glycosylation and glycan assembly. This suggests that TNF stimulation induces glycosylation remodelling in RA SFs by enhancing core biosynthetic processes required for glycan production, potentially contributing to altered glycan-mediated signalling in the inflamed synovial microenvironment (Figure 3-13).

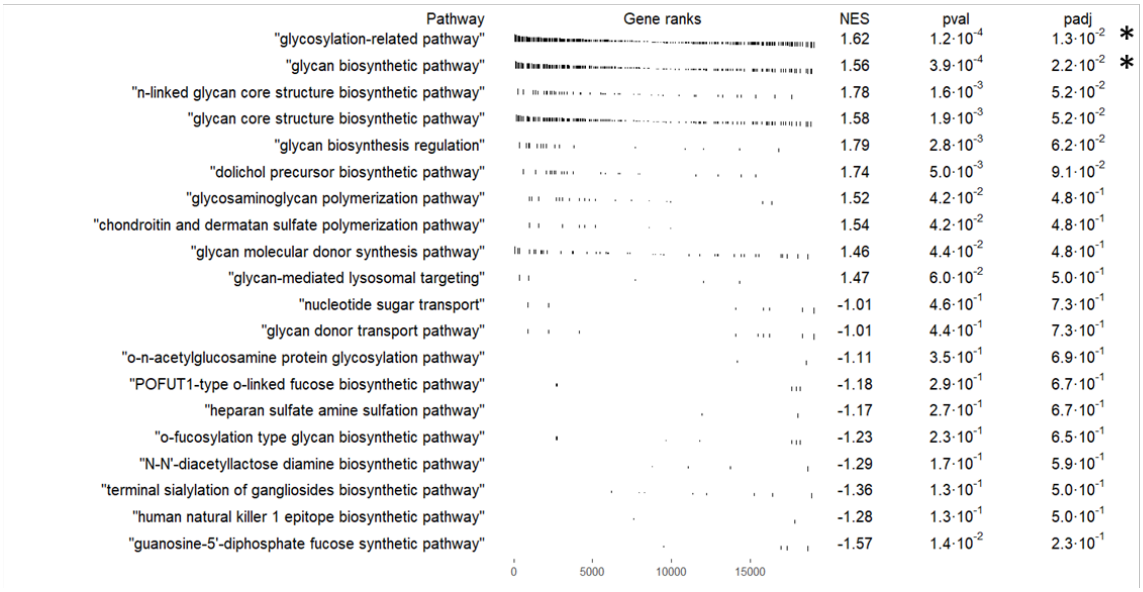

Figure 3-13 Glycosylation-Related Pathway Significantly Changed in TNF stimulated RA SFs expanded ex vivo.

TNF stimulated RA SFs show distinct glycosylation profiles predicted by GlycoEnzonto Enrichment Analysis. Gene set enrichment analysis (GSEA) was performed to identify glycosylation-related pathways with significant enrichment. Each pathway is shown with its normalised enrichment score (NES), p-value, and adjusted p-value (padj). The NES represents the degree of pathway enrichment after normalising for gene set size. Positive NES values indicate pathways enriched in upregulated genes while negative NES values indicate pathways enriched in downregulated genes. Higher absolute NES values suggest stronger enrichment. The x-axis represents the position in the ranked list of genes. Each black tick mark corresponds to a gene associated with the given pathway, showing where it appears in the ranked list of genes. Longer lines highlight genes with stronger contributions to enrichment, such as those with high differential expression or statistical significance. A dense cluster of marks near the top or bottom leads to a higher NES, indicating strong pathway enrichment. Significantly enriched pathways are marked with (*).

GlycoMaple analysis suggested TNF-induced transcriptional remodelling of glycosylation pathways in RA SFs. Comparison of TNF-stimulated vs unstimulated RA SFs revealed that reaction steps 9, 23, and 26 demonstrated significant transcriptional changes associated with galactose modification of glycans (Figure 3-14). These steps involve the enzymes A4GALT, B3GALT5, B3GALT1, and B3GALT2, which contribute to the extension and branching of galactose-

containing structures. Upregulation at these nodes suggests that galactosyltransferase activity is enhanced under TNF stimulation, potentially leading to altered glycan composition and downstream functional consequences such as modified ligand binding, immune recognition, or glycan-dependent signalling. GlycoMaple tool also predicted changes in O-glycan biosynthesis. Comparison of O-glycan biosynthesis pathways between healthy and RA SFs revealed inflammation-driven remodelling in the glycosylation landscape. Specifically, pathway mapping based on the Ge et al. (2021) dataset indicated that reaction 5, catalysed by ST3GAL1, showed increased expression in TNF-stimulated RA SFs compared to their unstimulated counterparts. This step is critical for the sialylation of core 1 O-glycans, suggesting an upregulation of terminal sialic acid modifications in the inflammatory setting. Arrows representing TPM values and fold changes highlighted multiple enzymes with moderate to high expression levels, reflecting a dynamic modulation of O-glycan biosynthesis under TNF stimulation (Figure 3-15). These findings support the hypothesis that RA-associated inflammation alters O-glycan profiles in SFs, potentially impacting barrier properties, cell-cell interactions, and immune modulation within the joint microenvironment.

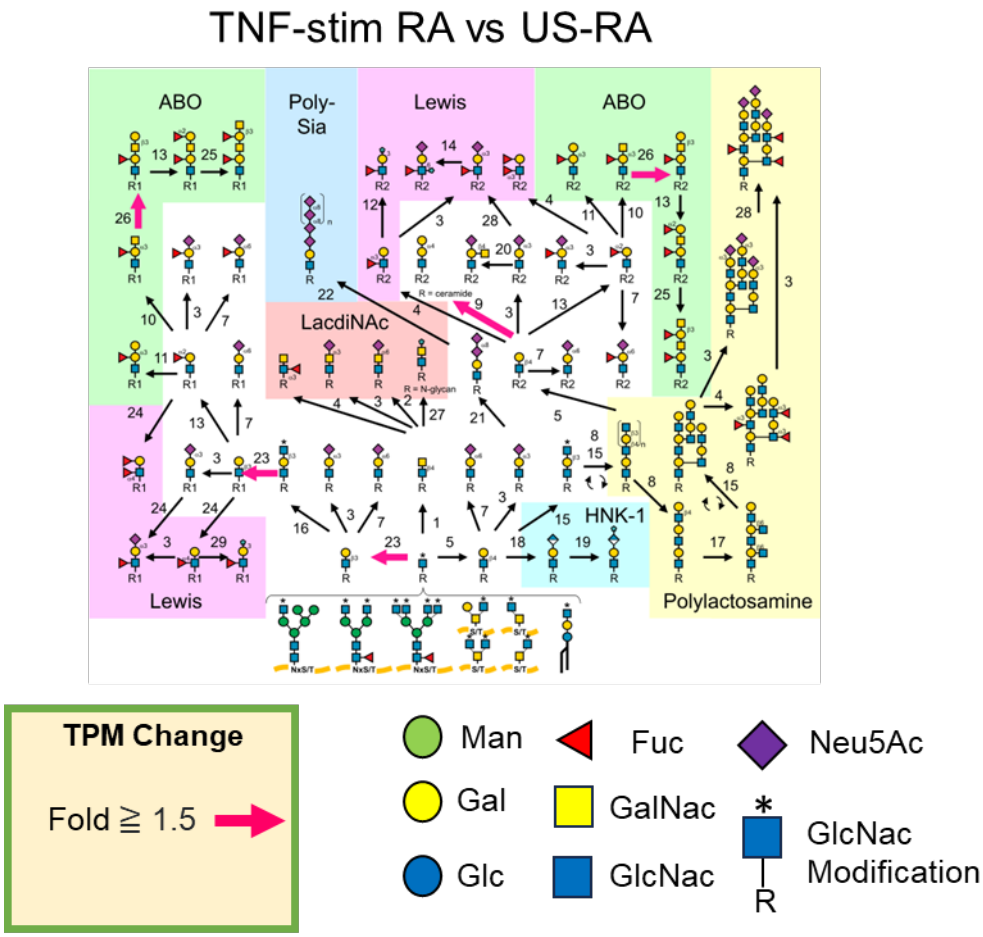

Figure 3-14 Comparison of N- and O-Glycan Capping Pathways Between RA and Healthy SFs expanded ex vivo.

Pathways related to complex capping of glycans between Healthy and RA SFs mapped using GlycoMaple based on the TPM gene expression values and then mean TPM values compared between unstimulated RA (n=16) vs TNF-stimulated RA SFs (n=16) in Ge et al. (2021) dataset. Significant fold changes were annotated with pink arrows. Reaction numbers 9, 23 and 26 have shown to demonstrate changes in the galactose modifications through the enzymes named A4GALT, B3GALT5, B3GALT1, B3GALT2, indicating the galactose modification occurs in glycans.

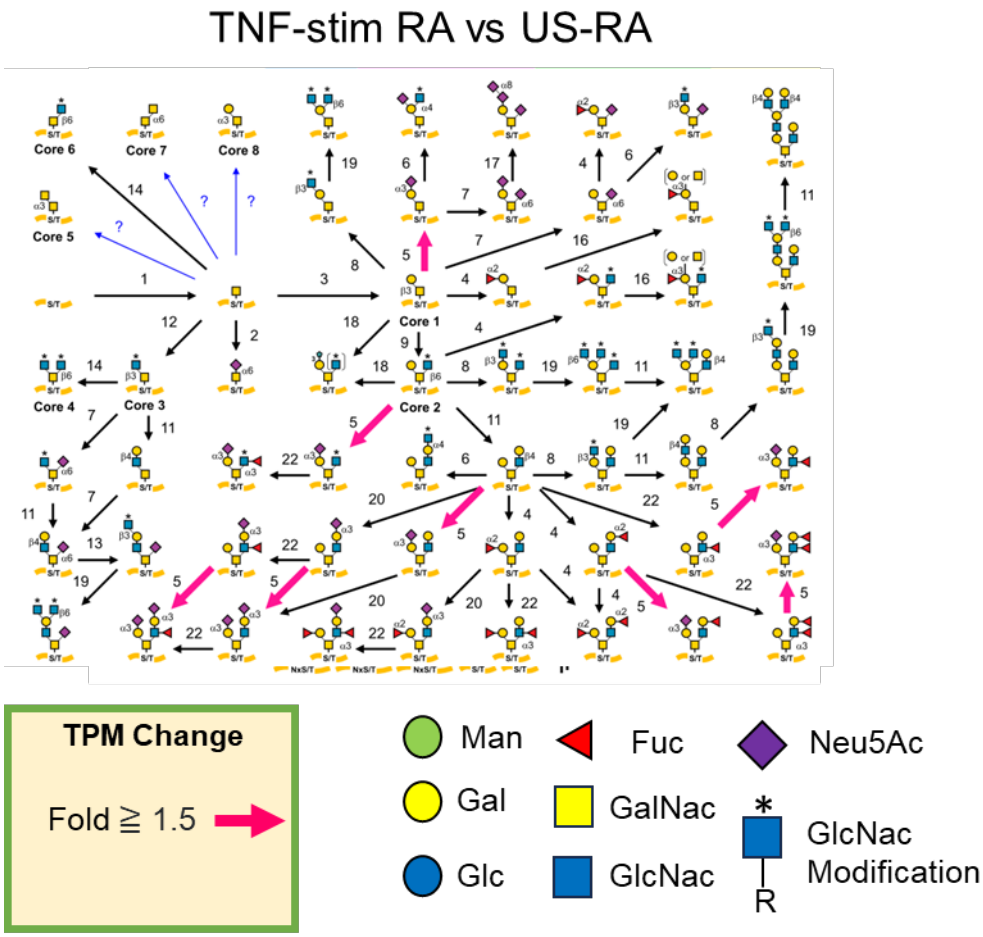

Figure 3-15 Comparison of Mucin Type O-Glycan Biosynthesis Pathways Between RA and Healthy SFs expanded ex vivo.

Pathways related to mucin type O-glycan biosynthesis between Healthy and RA SFs mapped using GlycoMaple based on the TPM gene expression values and then mean TPM values compared between unstimulated RA (n=16) vs TNF-stimulated RA SFs (n=16) in Ge et al. (2021) dataset. Significant fold changes were annotated with pink arrows. Reaction number 5 indicates changes ST3GAL1.

To understand how sialic acid biosynthesis and capping genes significantly differ between TNF-stimulated vs unstimulated RA SFs, we generated heatmaps of significantly DEGs directly involved in sialylation. The heatmap analysis revealed distinct clustering between unstimulated control and TNF-stimulated RA SFs, indicating a global shift in sialylation gene expression upon inflammatory stimulation. Among the sialyltransferase genes analysed, ST3GAL1, ST3GAL3 and ST3GAL4 were notably upregulated in TNF-treated cells (Figure 3-16A).

These findings were further supported by violin plot analysis, which confirmed the upregulation of ST3GAL1, ST3GAL3, and ST3GAL4 in TNF-treated cells compared to controls. These enzymes play key roles in terminal sialylation, pointing toward inflammation-induced remodelling of the glycan capping landscape. In our analysis of RA SFs stimulated with TNF-α, we observed significant upregulation of GNE and CASD1, two key genes involved in sialic acid metabolism and modification. GNE, the rate-limiting enzyme for de novo sialic acid biosynthesis, was transcriptionally induced by TNF-α, suggesting that inflammatory signalling enhances the internal pool of Neu5Ac sialic acid precursors. Concurrently, CASD1, responsible for 9-O-acetylation of sialic acids, was also upregulated, indicating a shift toward structurally modified sialylation. Conversely, ST6GALNAC6 and ST3GAL5 were downregulated in TNF-stimulated SFs, indicating a selective suppression of certain sialylation pathways. Notably, SLC35A1, a CMP-sialic acid transporter essential for transferring sialic acid into the Golgi, and SIAE, an enzyme responsible for deacetylating sialic acid derivatives, were both downregulated in TNF-stimulated RA SFs. These findings point to a complex regulatory network in which TNF simultaneously enhances specific α2,3-sialylation processes while limiting sialic acid transport and alternative modifications, ultimately reshaping the sialylation landscape in the inflamed synovial microenvironment. Together, these results suggests that TNF stimulation modulates both the biosynthesis and terminal incorporation of sialic acids in RA SFs, potentially altering glycan-mediated interactions in the synovial microenvironment (Figure 3-16B).

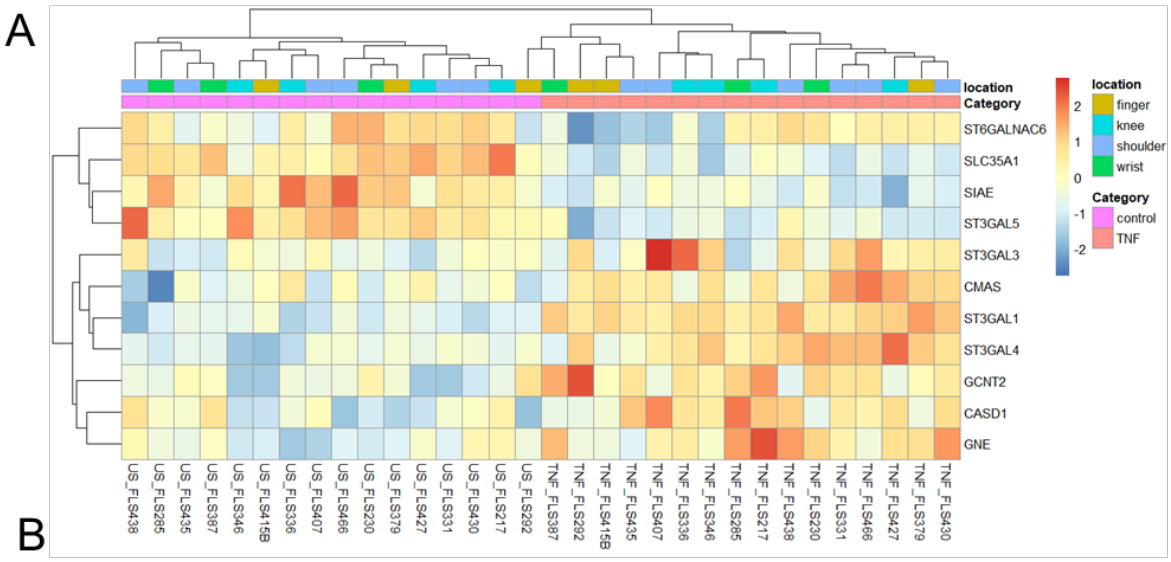

B

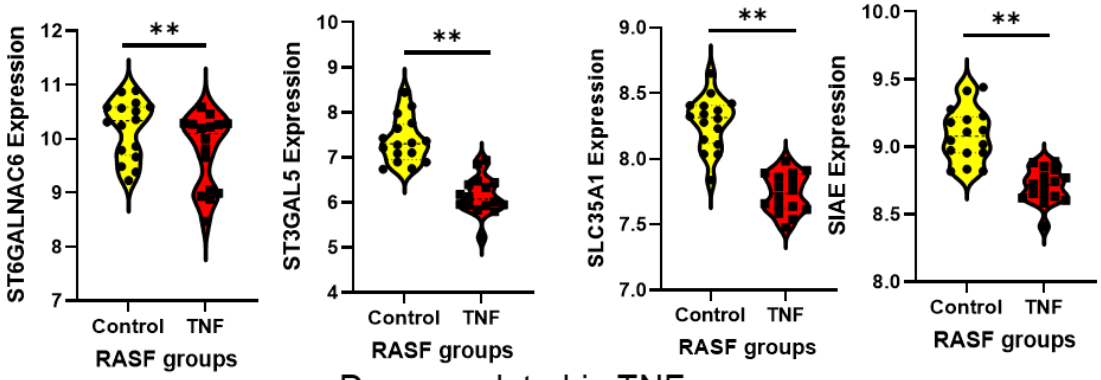

Downregulated in TNF

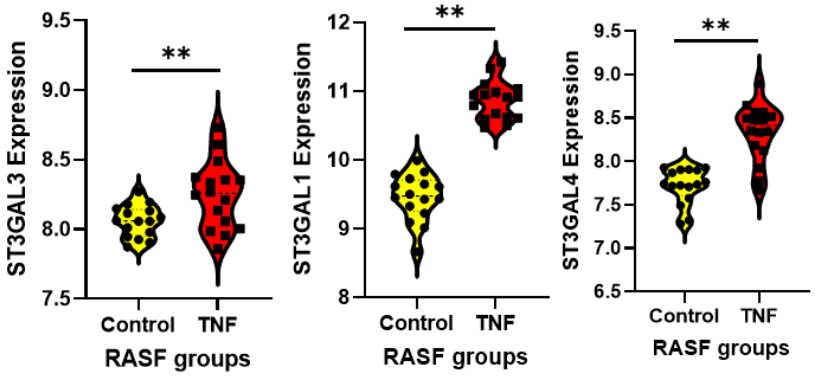

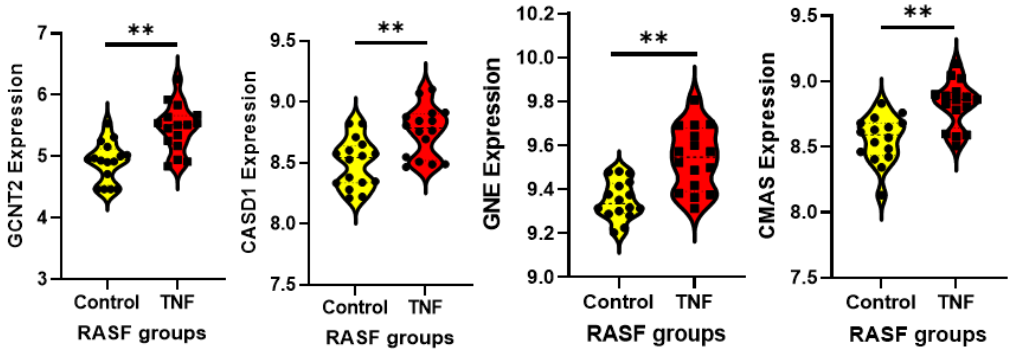

Upregulated in TNF

Figure 3-16 Differentially Expressed Genes Involved in Sialylation Between TNF stimulated vs Unstimulated Rheumatoid Arthritis Synovial Fibroblasts.

Figure A illustrates the differentially expressed genes involved in sialylation identified through RNA-seq analysis using DESeq2. The analysis compared gene expression profiles between TNF stimulated vs unstimulated RA SFs samples, with a significance threshold set at an adjusted p-value (adjp) < 0.05. Gene expression is Z-score normalised, with upregulated genes shown in red and downregulated genes in blue. The locations (finger, wrist, knee, shoulder) and categories (TNF, control) are indicated to provide context for the tissue sources and disease states analysed. Figure B in violin plots show gene expressions of significantly differentially expressed sialyltransferases obtained from normalised logarithmic gene counts. *adjp <0.05 and **adjp<0.01 obtained from DESeq2.

3.3 Discussion

This chapter presents a comprehensive transcriptomic analysis of SFs in RA, focusing on gene differential expression, and glycosylation. The findings build on the current understanding of RA pathogenesis by highlighting the transcriptional reprogramming of RA SFs both in the disease state ex vivo and in response to TNF-α stimulation in vitro, particularly considering the modulation of glycosylation in general, and sialic-acid related pathways in particular.

The pro-inflammatory role of SFs in RA has been extensively demonstrated in recent years, and our first general analysis of activated cells both ex vivo, and in vitro, confirmed this observation. Initial principal component analysis (PCA) demonstrated clear transcriptomic separation between RA and healthy SFs, confirming that RA SFs acquire a distinct gene expression profile. This is furthermore confirmed by the PCA demonstrating transcriptomic separation between TNF-stimulated and unstimulated RA-SFs, indicating that TNF drives additional gene expression changes which makes RA SFs transcriptionally more different phenotypes. In the presence of TNF-α, RA SFs demonstrated upregulation of genes associated with inflammation (e.g., IL1B, prior studies (Huber et al., 2006; Lefevre et al., 2015). These results also validate subsequent glycome-related data, since we confirmed that cells had been activated and are highly inflammatory.

Among the differentially expressed genes identified in RA SFs, PADI2 (Peptidyl Arginine Deiminase Type 2) was significantly upregulated compared to healthy controls. PADI2 plays a critical role in citrullination, a post-translational modification converting arginine residues into citrulline, which alters protein structure and antigenicity. A previous study found an association between the PADI2-encoding gene and RA where increased PADI2 expression have been observed in RA SFs (X. Chang et al., 2013). The upregulation of PADI2 in SFs highlights its contribution to local citrullination processes within the inflamed joint microenvironment, reinforcing its potential as a therapeutic target to mitigate pathogenic citrullination and subsequent autoimmune responses in RA. HAPLN1 (Hyaluronan and Proteoglycan Link Protein 1) also identified as differentially expressed in RA SFs compared to healthy controls. HAPLN1 is a critical extracellular matrix glycoprotein that stabilises the assembly of hyaluronan and proteoglycans, maintaining the structural integrity of connective tissues. Indeed, in a previous report, HAPLN1 contributed RA pathogenesis by promoting the proliferation and pro-inflammatory phenotype of RA SFs (Y. Chen et al., 2022).

Although other genes significantly upregulated in RA are not very well studied in the context of joint inflammation, their potential in understanding SFs pathophysiology is still of interest. For instance, OPCML (Opioid Binding Protein/Cell Adhesion Molecule-Like) and PCDH10 (Protocadherin 10) are two tumour suppressor genes involved in cell adhesion (Dobre et al., 2021). Altered expression of OPCML may affect fibroblast adhesion, migration, or interaction with the extracellular matrix, contributing to the aggressive, invasive phenotype of RA SFs. Likely, changes in the expressions of PCDH10 may also influence SF behaviour, affecting their interactions with neighbouring cells and extracellular matrix components. OPCML and PCDH10, though less characterised in RA, may represent novel contributors to fibroblast adhesion, migration, and interaction with the extracellular matrix.

Pathway enrichment analyses underscored the centrality of immune and cell cycle signalling in RA SF biology. Notably, the JAK-STAT, NF-κB, and TNF signalling pathways were enriched in both RA vs healthy and TNF-stimulated vs control SF comparisons, highlighting their essential roles in sustaining chronic inflammation and fibroblast activation. Additionally, Th17 differentiation, Notch signalling, and

cytokine-receptor interaction pathways were implicated, emphasizing the crosstalk between immune cells and stromal cells in the synovial niche.

A key novel aspect of this chapter is the detailed examination of glycosylation-related transcriptional programs. Using GlycoEnzOnto and GlycoMaple tools, we demonstrated that RA SFs display significant alterations in glycosylation gene expression. In RA vs healthy comparisons, both global and glycosylation-specific PCA plots revealed that changes in glycoenzyme transcription are sufficient to distinguish disease from health. GlycoEnzOnto analysis showed enrichment of glycan biosynthesis pathways, particularly the glycosylation-related pathways. These findings align with prior literature suggesting that aberrant glycosylation contributes to immune dysregulation in RA (Axford, 1999; Hafkenscheid et al., 2017, 2019; Reily et al., 2019; Y. Wang et al., 2021).

GlycoMaple-based data provided further support to the hypothesis that glycan structural remodelling is associated with RA SFs. Specifically, galactosyltransferase enzymes such as B3GALT1, B3GALT2, and B3GALT5 were transcriptionally upregulated at key nodes (e.g., reactions 23 and 26), suggesting increased galactose capping on glycans. Previous reports also align with the role of aberrant galactosylation patterns in the inflammatory responses (Manwar Hussain et al., 2012). Moreover, alterations in LacdiNAc, Lewis, and polylactosamine branches indicate the emergence of complex glycan structures that may influence immune cell recognition and synovial inflammation.

A key limitation of the RA vs healthy SFs dataset is that the healthy control samples are younger than the RA samples. Age is a strong modifier of transcriptional programs and has well-described effects on glycosylation, including reductions in galactosylation and α2-6 sialylation with advancing age (Paton et al., 2021). As such, some of the differences observed in glycosyltransferase and glycosidase expression between RA and healthy samples may partly reflect age-related changes rather than disease-specific mechanisms. As we cannot have the corresponding age matched patient sample identifiers, we were not able to run DeSEq2 for modelling age in differential expression. Results should therefore be interpreted with caution.

In TNF-stimulated RA SFs, a similar glycosylation remodelling was observed. GlycoEnzOnto enrichment revealed that TNF specifically upregulated genes within the "glycosylation-related" and "glycan biosynthetic" pathways. GlycoMaple analysis highlighted increased activity at enzymatic steps involved in LacdiNAc formation and galactose extension (A4GALT, B3GALT family), further supporting TNF's role in modulating glycan complexity. Interestingly, mucin-type O-glycan biosynthesis also showed TNF-induced changes, particularly through increased expression of ST3GAL1, which catalyses α2-3 sialylation of core 1 O-glycans.

While GlycoMaple provides a valuable predictive framework to infer glycosylation pathway activity based on transcriptomic data, it does not account for post-transcriptional regulation, enzyme localisation, or substrate availability (Hou et al., 2016; Kouka et al., 2022). Furthermore, it lacks integration of dynamic biochemical constraints and does not reflect actual glycan structures. Therefore, GlycoMaple predictions should be interpreted with caution and ideally validated by direct experimental approaches such as lectin profiling or mass spectrometry based glycomics.

A particularly insightful finding of this chapter is the regulation of sialylation in TNF stimulated RA SFs. While certain α2,3-sialyltransferases such as ST3GAL1, ST3GAL3, ST3GAL4 and biosynthesis enzymes GNE and CASD1 were upregulated upon TNF stimulation, key transport enzymes SLC35A1 and deacetylation enzymes SIAE were downregulated. This suggests a complex regulatory landscape where TNF enhances specific terminal modifications but simultaneously restricts sialic acid flux and processing. Moreover, enzymes like ST6GALNAC6 and ST3GAL5 were downregulated, indicating selective inhibition of alternative sialylation. The transcriptomic and glycobiological analyses presented in this chapter provide clear evidence that sialylation pathways are dynamically regulated in RA SFs, particularly in response to TNF stimulation. Taken together, these results indicate that TNF reshapes the sialylation profile of SFs in a targeted manner, likely altering glycan-mediated signalling, immune evasion, and cell-cell communication in the inflamed synovium. However, the functional consequences of these changes in glycan-receptor interactions are beyond the capabilities of RNA-Seq based experiments and must be confirmed experimentally in the laboratory.

Sample location (knee, shoulder, wrist, or finger) did not appear to be the major driver of gene expression variability, as clustering was predominantly defined by TNF-α treatment. These transcriptional changes were largely independent of joint location, underscoring the consistency of TNF's effect across different anatomical sites. This finding reinforces the utility of TNF-α as a driver of pathogenic transformation in RA SFs and supports the generalisability of these molecular signatures.

Comparing RA vs healthy SFs vs TNF-stimulated, a few important results should be considered as well. First of all, some expected matrix metalloproteinases and chemokines did not differentially and significantly express in RA vs healthy SFs datasets. This results maybe because of the nature of 2D cultures in which prolonged cultures in 2D leads to loss of disease associated phenotypes (Zimmermann et al., 2000). This should be overcome by using 3D cultures, specifically Alvetex Scaffolds where a previous result confirmed that putting arthritic SFs from 2D to 3D scaffolds restored key genetic signatures related to arthritic pathways (Khan et al., 2022).

In previous study published by our group, murine data demonstrated that TNF-α stimulation downregulates St6gal1 expression and reduces α2,6-sialylation in SFs (Y. Wang et al., 2021). However, analysis of human RA SFs revealed an upregulation of ST6GAL1. This apparent inconsistency may be attributed to several factors. First, species-specific regulatory mechanisms likely contribute to divergent responses in glycosylation pathways. Second, unlike the controlled in vitro TNF-α stimulation used in mice, human samples represent complex, chronic disease states where cells are exposed to multiple inflammatory signals and therapeutic interventions. Notably, many of the human samples were derived from patients receiving biologic treatments, including TNF-α inhibitors, which may alter the inflammatory milieu and potentially lead to compensatory or rebound upregulation of ST6GAL1. Since α2,6-sialylation can dampen immune responses, increased ST6GAL1 expression in treated patients might reflect an attempt to restore immune homeostasis under anti-TNF therapy. These findings highlight the importance of contextual factors, such as treatment status and chronicity, when translating insights from murine models to human disease. Interestingly, GlycoMaple predictions based on transcriptomic data also indicated an increase in α2,3-sialylation in O-glycan capping. This shift could alter the α2,3/α2,6-sialylation

ratio, a feature that may align more closely with our murine findings, where α2,6-sialylation was selectively reduced. Thus, despite elevated ST6GAL1 expression, the net sialylation profile might still be skewed toward α2,3, suggesting a potential imbalance in sialic acid linkage types that could influence immune recognition and cell-cell interactions in RA synovium.

RA is increasingly recognised not as a single disease, but as a heterogeneous syndrome with multiple molecular and immunological subtypes. This heterogeneity is reflected in differences in serological status, disease progression, and response to therapy. As a result, patient stratification has become essential for personalised treatment strategies. Sialic acid, particularly the balance between α2,6- and α2,3-sialylation, has emerged as a promising biomarker candidate to capture this heterogeneity. Altered sialylation patterns in RA, such as the loss of α2,6-sialylation on SFs have been associated with increased inflammatory potential in SFs and immune dysregulation. Glycan-based profiling could therefore help identify patient subgroups with distinct pathological mechanisms. However, sialic acid expression is highly dynamic and influenced by environmental factors including cytokine exposure, nutrient availability, microbiota composition, infections, and therapeutic interventions such as biologics or corticosteroids. These variables must be carefully considered when evaluating sialylation as a biomarker. Overall, integrating glycomic signatures into clinical and transcriptomic data may improve our ability to classify RA into biologically meaningful subtypes and tailor treatment accordingly.

In summary, this chapter highlights the integrated role of inflammation and glycosylation in shaping RA SF function. TNF stimulation not only induces widespread transcriptional reprogramming of inflammatory genes but also drives a coordinated alteration in glycosylation-related pathways, particularly those involved in galactosylation and sialylation. These changes may collectively promote immune activation, alter glycan-mediated receptor interactions, and reinforce the pathogenic phenotype of SFs. Future work is needed to functionally validate these glycoenzymatic changes and explore their potential as biomarkers or therapeutic targets in RA.

These findings raise important questions about the functional role of sialic acids in SF biology, particularly how the presence or absence of terminal sialylation

influences SF behaviour. To directly address this, the next chapter investigates the consequences of enzymatic desialylation in naïve, unstimulated SFs. Rather than studying SFs already shaped by inflammatory cytokines, this approach allows us to uncover the baseline regulatory role of sialic acids in modulating fibroblast phenotype, cytokine responsiveness, and cell-cell communication.

Altogether, this next chapter builds upon the transcriptional findings by functionally dissecting the biological significance of sialic acid removal in SFs, offering further insight into the role of glycan remodelling in rheumatoid arthritis pathogenesis.

4. Chapter 4 Exploring the Role of Surface Sialic Acid in Synovial Fibroblast Function Through Enzymatic Desialylation

4.1 Introduction

Our previous transcriptomic analysis in Chapter 3 showed that SFs from RA patients display marked alterations in glycosylation-associated gene expression. Among these, genes involved in sialic acid metabolism and capping, such as ST3GAL1, ST3GAL3, ST3GAL4, GNE, and CASD1, were significantly upregulated upon TNF stimulation, whereas others like ST6GALNAC6, ST3GAL5, and SLC35A1 were downregulated. These findings pointed toward a selective remodelling of sialylation processes in inflamed SFs, potentially impacting their inflammatory phenotype, surface glycan composition, and downstream immunological interactions.

Sialic acids, terminal negatively charged sugars on glycoproteins and glycolipids, are essential modulators of immune cell recognition, and cell-cell signalling (N. M. Varki & Varki, 2007). They regulate ligand interactions through sialic acid-binding immunoglobulin-type lectins (Siglecs), galectins, and selectins, impacting cell adhesion, motility, and cytokine responses (Pearson et al., 2018; A. Varki & Angata, 2006; Zhuo et al., 2008). In RA, loss of specific sialic acid residues or altered sialyltransferase expression has been implicated in promoting synovial inflammation (Y. Wang et al., 2021). The role of sialic acids in regulating SF function is increasingly recognised, yet the specific consequences of their removal, particularly in the naïve, non-inflammatory setting, remain poorly understood. Sialic acids exhibit significant chemical diversity, including various modifications such as acetylation and different glycosidic linkages (e.g., α2,3-, α2,6-, or α2,8-linkages), each of which may influence cellular interactions and signalling differently. However, the functional implications of this heterogeneity have not been systematically explored in SFs. To address this gap, we aim to selectively remove sialic acids from SFs expanded from healthy mice, enabling a more precise investigation into how different sialylation patterns contribute to SF behaviour and

potentially shape immune responses. This approach will help elucidate the specific roles of sialic acid linkages in modulating fibroblast function independently. To experimentally interrogate this question, we designed an in vitro desialylation model using SFs isolated from naïve C57BL/6 mice. The present chapter investigates the functional consequences of desialylation in unstimulated SFs. Rather than analysing cells already activated by cytokines or in vivo disease signals, this approach allows for the assessment of whether removal of sialic acids is sufficient to trigger fibroblast activation, cytokine production, or altered interaction with immune components. By applying specific sialidases to cultured naïve SFs, we aim to determine whether removal of terminal sialic acids is sufficient to prime or activate fibroblasts, mimicking inflammatory features typically induced by cytokines such as TNF-α. This strategy tests the hypothesis that sialic acids act as a suppressive or stabilizing glycan feature, and that desialylation alone may initiate pro-inflammatory signalling or alter fibroblast-immune interactions. Moreover, these experiments may reveal whether the glycan-dependent changes observed in RA SFs reflect not only transcriptional programming but also functional consequences of sialic acid presence or absence on the cell surface.

In order to cleave cell surface sialic acids, we used *Clostridium perfingens* (CP), *Arthrobacter ureafaciens* (AU)*, Vibrio cholerae* (VC) and Lectenz (L) recombinant sialidases of which are commercially obtained, and that show different substrate specificity, allowing us to have a range of distinct desialylation. CP sialidases cleave sialic acids that are linked to glycoproteins and glycolipids on the surfaces of host cells. The specific linkages targeted by these enzymes include α2-3 and α2-6 sialic acid connections. Research has indicated that the hydrolytic activity of sialidases from CP can vary for different linkages, with higher overall activity observed against α2-6 sialic acid receptors compared to α2-3 receptors, although all three types of linkages can be hydrolysed by these enzymes (Kurnia et al., 2022; J. Li & McClane, 2014). The sialidases from AU demonstrate broad substrate specificity, effectively hydrolysing sialic acid linkages found in glycoproteins and glycolipids. Specifically, research has shown that AU sialidases can cleave both α2-3, α2-6, and α2-8 linked sialic acids (Christensen & Egebjerg, 2005). VC sialidase on the other hand exhibits specificity concerning the sialic acid linkages it can hydrolyse. Specifically, research has shown that sialidase from VC functions primarily to cleave sialic acid linkages, specifically α2-3 and α2-6, while

potentially affecting α2-8 linkages (Kaisar et al., 2021). Lectenz (α2-3 sialidase) is a recombinant sialidase cloned from Streptococcus pneumoniae and expressed in Escherichia coli which selectively remove α2-3 linked sialic acids without touching other linkages.

Cultured SFs were treated with different sialidases (*Clostridium perfringens, Arthrobacter ureafaciens, Vibrio cholerae*, Lectenz), each with distinct linkage specificities toward α2,3- and α2,6-linked sialic acids. However, specific sialic acid cleavage will also depends on the sialylated glycoconjugates found in the cell or tissue of study. Therefore, our first goal was to evaluate the types of sialic acid-containing glycans that these enzymes were able to cleave in the murine SFs. Enzyme-linked lectin assay (ELLA) and immunofluorescent staining confirmed differential sialic acid cleavage patterns across treatments. Subsequent transcriptomic profiling of these desialylated SFs revealed treatment-specific transcriptional reprogramming, with Lectenz sialidase eliciting the most pronounced pro-inflammatory gene signatures. Further functional assays, including wound healing migration experiments were used to assess the biological impact of desialylation on SF phenotype and behaviour. Strikingly, conditioned media from desialylated SFs altered the migratory capacity of naïve SFs, suggesting that sialic acid loss is involved in the increased migratory capacities occurring in the synovial microenvironment, acting in a paracrine way.

This chapter provides experimental evidence that desialylation of naïve SFs is sufficient to induce pro-inflammatory gene expression and functional changes in activated SFs but also it expands the findings that α2-3 desialylation under certain thresholds does not necessarily induce pro-inflammatory activations as observed in sialidase treated naïve SFs. These findings support a model in which sialylation above certain thresholds acts as a gatekeeper of stromal immune tone and offer insight into how glycan alterations may actively contribute to inflammatory joint pathology. Our results highlight glycan editing, by recombinant sialidases, as a potential regulator of SF-mediated inflammation and underscore the relevance of glycosylation in stromal immunobiology. By dissecting the role of sialic acid removal in SF biology, this work expands on the transcriptomic observations of Chapter 3 and offers mechanistic insight into how glycan modifications may functionally reprogram fibroblasts toward a pro-inflammatory phenotype even in the absence of classical inflammatory stimuli. These findings indicate that

sialylation is a critical checkpoint in stromal activation and identify novel intervention points for restoring synovial homeostasis in RA.

4.2 Results

4.2.1 Recombinant Sialidases Differentially Cleave α2-6 and α2-3 Sialic Acid Linkages on Naïve Synovial Fibroblasts

To generate our experimental cell model, mouse synovium was isolated from mouse joints and digested with collagenase to generate single suspensions. Cell were expanded in vitro and used for experiments between passage 3 and 5. To confirm the cellular identity and purity of in vitro cultured SFs, flow cytometric analysis was performed based on the positive expression of podoplanin (PDPN), a fibroblast marker, and the lack of expression of CD11b, a myeloid-lineage marker. Following enzymatic detachment with trypsin, cells were stained with fluorophore-conjugated antibodies and analysed. The histogram overlays show that the majority of the cultured cells expressed high levels of PDPN, confirming their fibroblastic identity. In contrast, minimal to negligible expression of CD11b was detected, indicating the absence of contaminating myeloid cells such as macrophages or monocytes. Quantitatively, 79.4% of cells were $PDPN^+$, while only 1.11% were $CD11b^+$, confirming that the cultures predominantly consisted of pure synovial fibroblasts with minimal immune cell contamination (Figure 4-1).

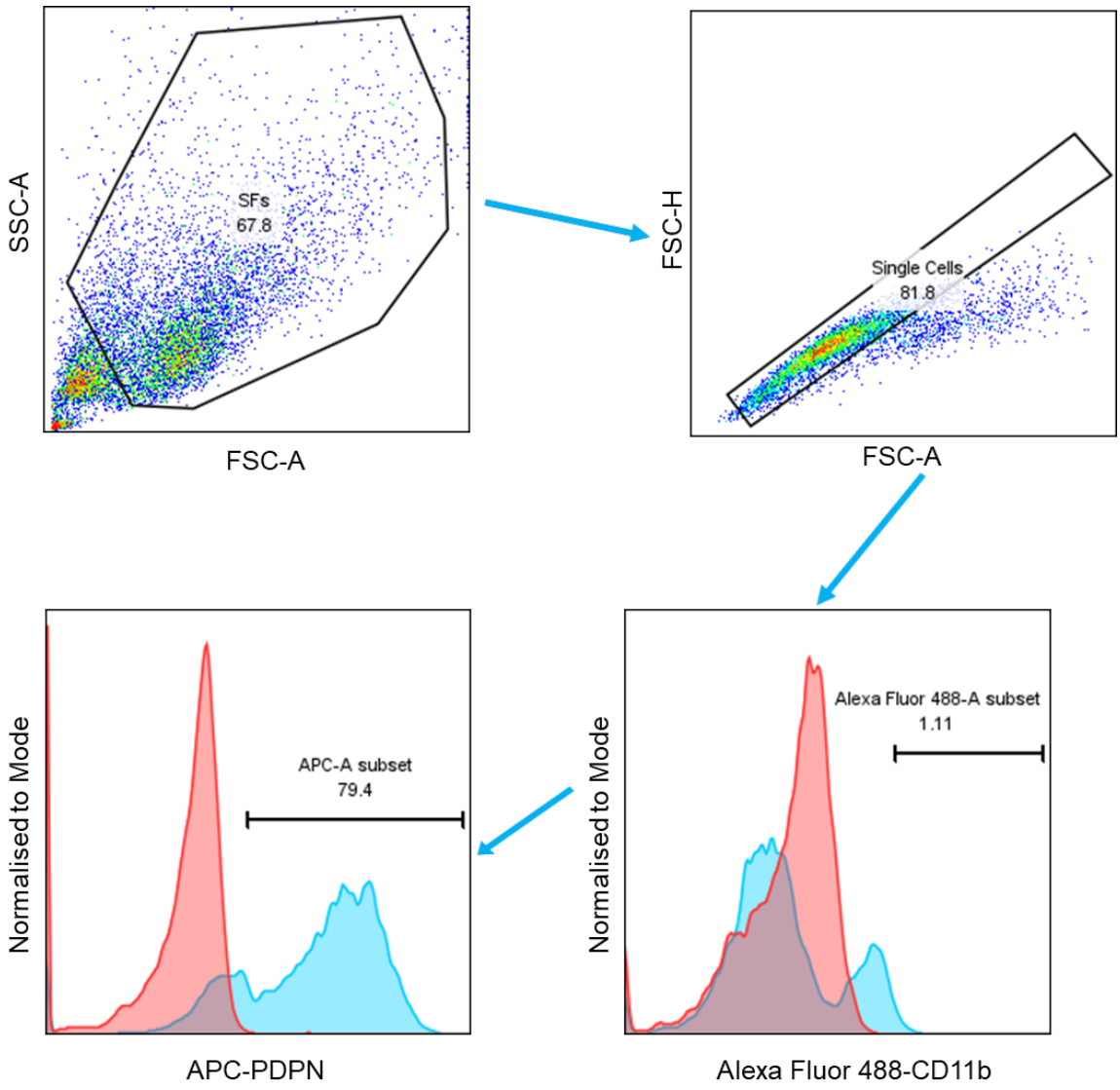

Figure 4-1 Synovial Fibroblasts (SFs) purity check using flow cytometry.

Ex vivo cultured SFs were detached with trypsin and expression of PDPN and CD11b positive cells were evaluated by flow cytometry.

Although the enzymatic activities of CP, AU, VC, and L sialidases are well-characterised in terms of their preference for specific sialic acid linkages (e.g., α2,3-, α2,6-, or α2,8), their functional impact may vary depending on the cellular context. In particular, the glycan landscape of SFs is highly cell-type-specific and influenced by factors such as differentiation state, microenvironment, and activation status. As a result, the same sialidase may cleave distinct sialylated structures in SFs compared to other cell types. Therefore, despite established substrate preferences, CP, AU, VC, and L sialidases may exhibit differential efficiency or specificity in removing sialic acids from the surface of SFs, potentially revealing context-dependent roles for sialylation in fibroblast biology.

Understanding of the efficacy and specificity of this recombinant sialidases are potentially important because they may perform different sialic acid cleavage depending on the different cell types. This situation may further change behaviour of SFs in the inflammatory context.

To assess the efficacy and specificity of various recombinant sialidases on modifying the sialylation landscape of naïve SFs, we treated in vitro cultured SFs with a panel of sialidases and measured cell surface glycan alterations using enzyme-linked lectin assays (ELLA). To evaluate the efficiency of terminal α2,6-sialic acid removal from SFs, we evaluated SNA binding following treatment with four different sialidases. Among the tested enzymes, CP sialidase treatment resulted in a significant reduction in SNA binding compared to untreated controls, indicating potent desialylation of α2,6-linked sialic acids. In contrast, AU, VC, and L sialidases showed no significant reduction in SNA signal, suggesting limited activity against α2,6-sialic acids in this cellular context. Interestingly, L sialidase treatment even resulted in a slight increase in SNA binding, though this was not statistically significant. These results suggest that CP sialidase is the most effective enzyme for removing α2,6-linked sialic acids from the surface of naïve SFs under these conditions (Figure 4-2A). To investigate the removal of α2,3-linked sialic acids from SFs, we measured MAL binding. All four enzymes, CP, AU, VC, and L, significantly reduced MAL binding compared to untreated controls, indicating effective cleavage of α2,3-sialic acid residues. Notably, CP, VC and L sialidases resulted in the most pronounced reduction, while AU showed significant but slightly less potent effects. These results suggest that, unlike α2,6-sialic acid removal (as shown in the SNA data), multiple sialidases are capable of efficiently targeting α2,3-linked sialic acids on the surface of naïve SFs, with CP, VC and L showing the strongest desialylation activity in this context. Importantly, when considered alongside SNA binding data, CP appears to have dual specificity, showing moderate activity toward both α2,6- and α2,3-linked sialic acids. This broader substrate range suggests that CP may be useful in models requiring more comprehensive desialylation of cell surface glycans.

Concomitantly, increased PNA binding following CP, AU, VC, and L treatment confirmed the exposure of underlying Galβ1-3GalNAc structures, consistent with effective desialylation of terminal residues (Figure 4-2C). AAL binding, which detects core fucosylation, remained largely unchanged across all sialidase

treatments (Figure 4-2D). This was expected, since sialidases specifically remove terminal sialic acids and do not affect fucose residues. Therefore, AAL binding served as a useful internal control to confirm that the enzymes were acting selectively on sialic acids. These results demonstrate that distinct sialidases exhibit selective preferences for specific sialic acid linkages on SFs, allowing targeted modulation of glycan presentation.

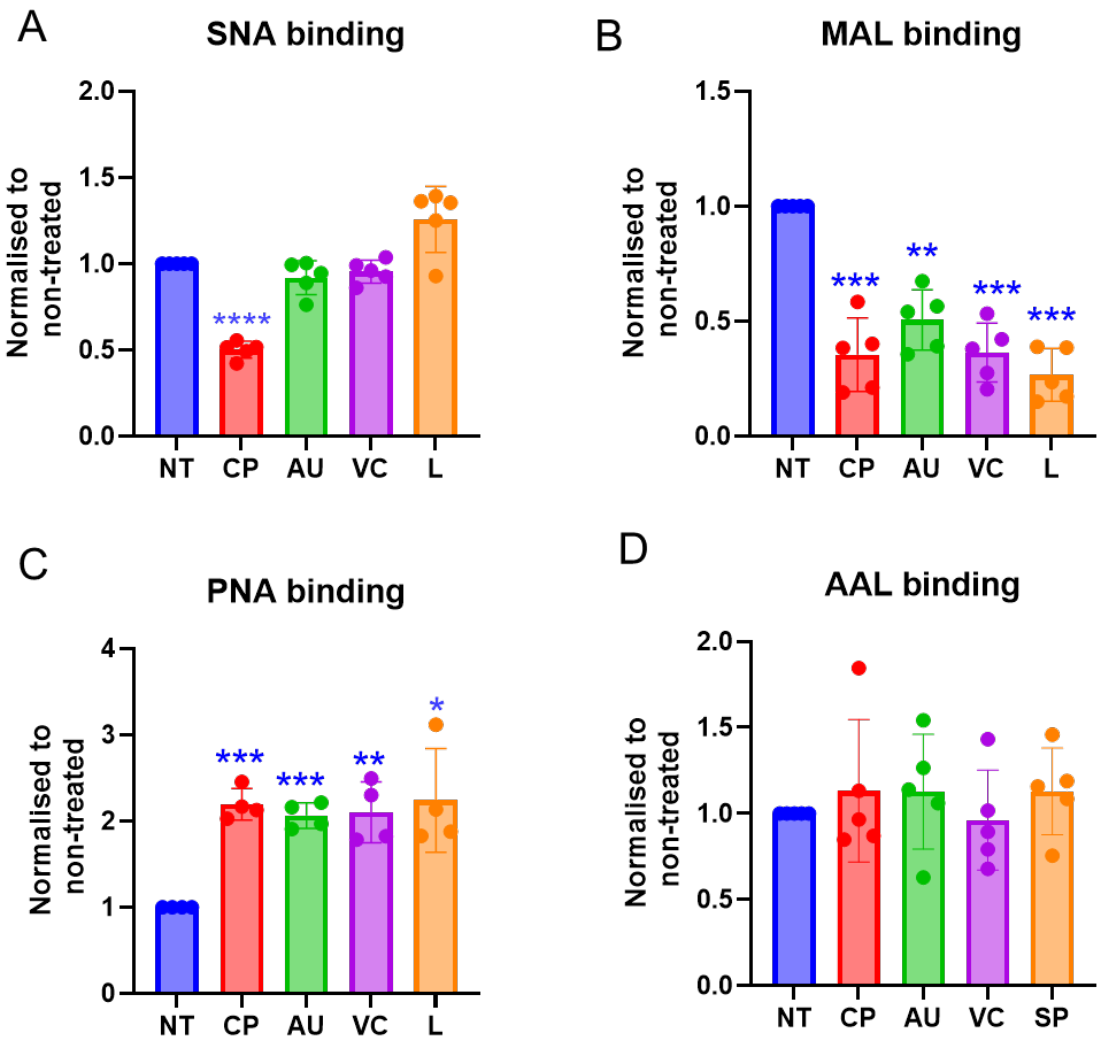

Figure 4-2 Recombinant sialidases have different impact on removing α2-6 or α2-3 sialic acid on naïve SFs.

Synovial fibroblasts (SFs) were treated with different sialidases, and changes in glycan structures were assessed by enzyme-linked lectin assay (ELLA). (A-D) Binding of specific biotinylated lectins was used to detect surface glycan epitopes. Bars represent mean ± SD; dots represent biological replicates. Statistical comparisons were performed using the one-sample Wilcoxon test for SNA and treatment in the L group, and one sample t-tests for all other comparisons. (A) SNA binding, indicating α2,6-linked sialic acid, (B) MAL

binding, indicating α2,3-linked sialic acid, (C) PNA binding, indicating desialylated Galβ1-3GalNAc (exposed after sialic acid removal), (D) AAL binding, indicating core fucose-containing structures.*P < 0.05, **P < 0.01, ***P < 0.001, ****P < 0.0001 versus untreated control.

To confirm these results, naïve synovial fibroblasts were stained with SNA lectin (Alexa Fluor 647, red) following enzymatic treatments, which will also reveal the subcellular location of a2-6-sialic acid in the cells. DAPI counterstaining was used to visualise nuclei (blue). The non-treated control group exhibited strong and widespread binding, consistent with abundant expression of α2-6-linked sialic acid on the SF surface. In contrast, sialidase-treated groups displayed variable reductions in SNA staining intensity. Among the treatments, CP- treated group showed visibly most reduced fluorescence, indicating effective removal of α2-6 sialic acid. However, the reduction was not as profound as complete signal loss, suggesting partial cleavage. AU-, VC- and L-treated groups retained moderate SNA signal, implying less efficient cleavage of α2-6-linked sialic acids by these enzymes under the conditions used (Figure 4-3). Taken together, the SNA staining confirms that sialidase treatment alters α2-6 sialylation patterns, with CP enzymes exhibiting more potent activity in reducing α2-6 sialic acid levels on naïve SFs, while AU, VC and L treatments appear less effective in this context.

To assess the capacity of distinct recombinant sialidases to remove α2-3-linked sialic acids, naïve SFs were stained with MAL lectin. Nuclei were counterstained with DAPI for cellular orientation. In non-treated SFs, a strong signal was observed, indicative of abundant α2-3-linked sialylation. Following sialidase treatment, fluorescence intensity markedly decreased in all conditions, with variable efficiency. Notably, VC- and L-treated SFs showed the most substantial reduction in MAL staining, indicating that these enzymes were highly effective at removing α2-3-linked sialic acids. The strongest α2-3-linked sialic acid reduction occurred at L- treated naïve SFs, confirming the ELLA assay data. AU and CP treatments also led to a visible decline in MAL binding, albeit to a lesser extent compared to VC and L. This gradient in signal intensity suggests that VC and L sialidases exhibit superior α2-3 cleavage activity, while the least removal of α2-3-linked sialic acid is observed at AU-treated naïve SFs (Figure 4-4).

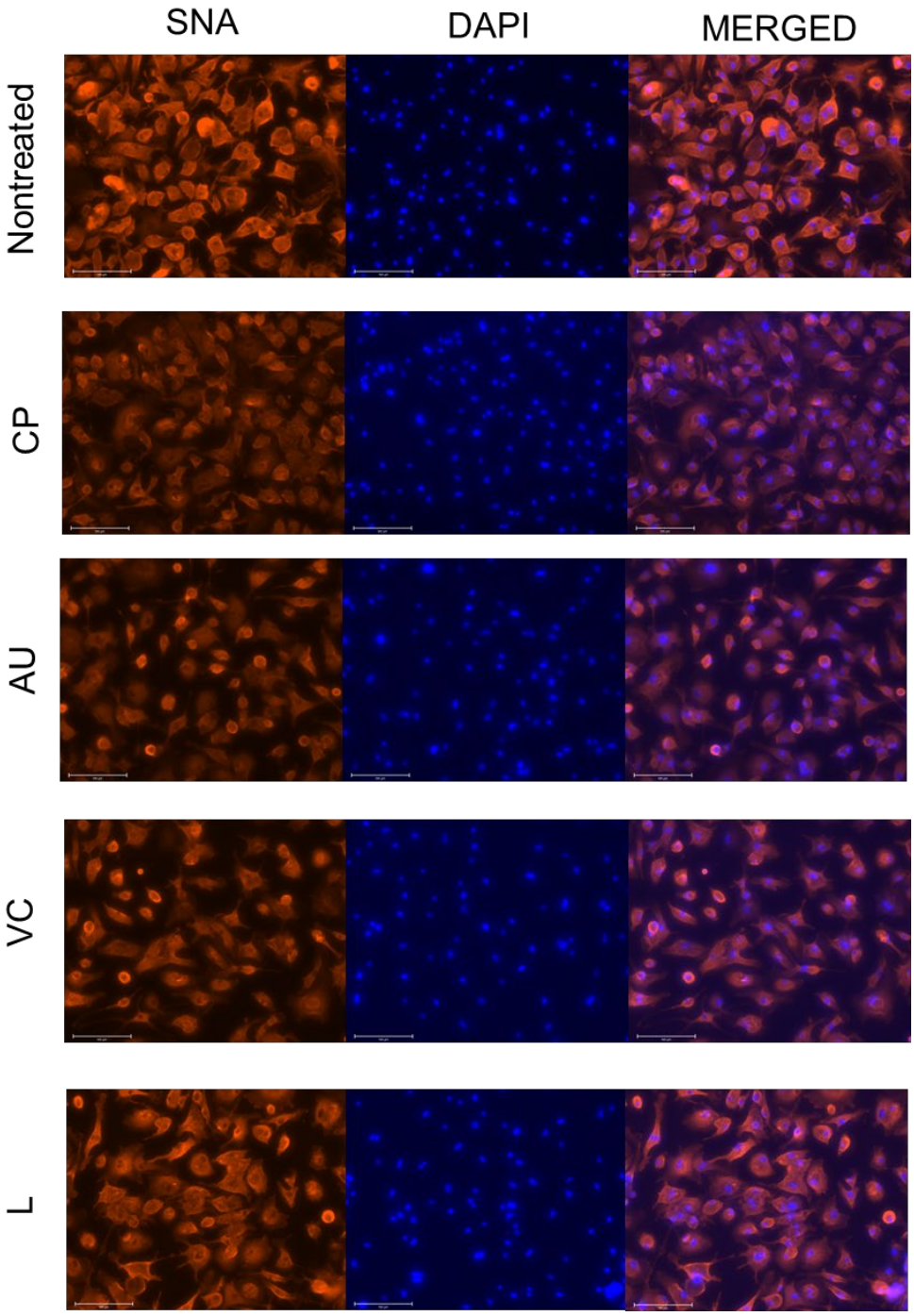

Figure 4-3 Immunofluorescent evaluation of SNA binding in naïve SFs following sialidase treatments.

Ex vivo cultured SFs were stained for SNA expression, visualised using Alexa Fluor 647 (red) and counterstaining with DAPI (blue) under 20X magnification. Scale bar, 100 μm. Images were obtained using an EVOSTM FL Auto 2 microscopes.

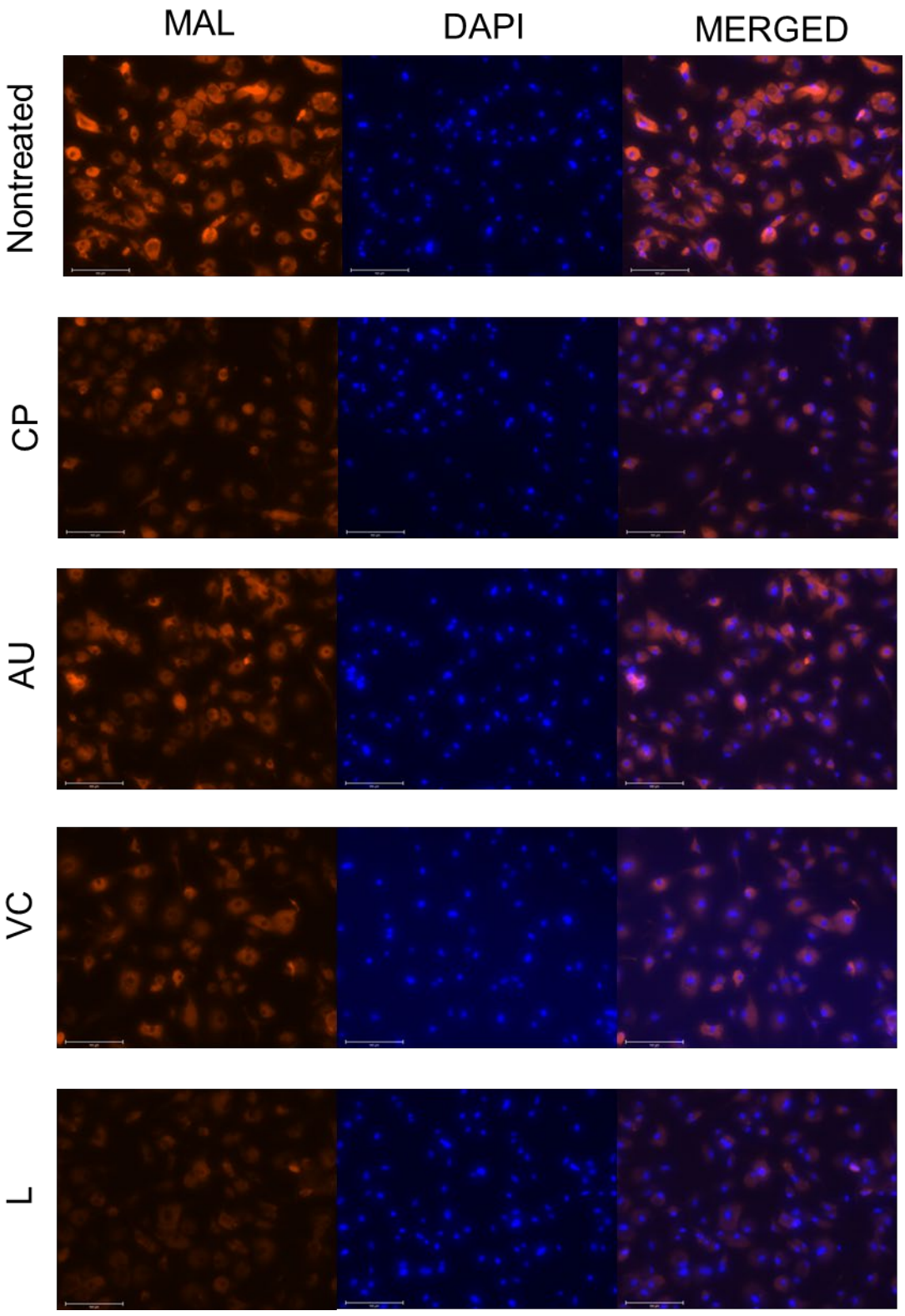

Figure 4-4 Immunofluorescent evaluation of MAL binding in naïve SFs following sialidase treatments.

Ex vivo cultured SFs were stained for MAL expression, visualised using Alexa Fluor 647 (red) and counterstaining with DAPI (blue) under 20X magnification. Scale bar, 100 μm. Images were obtained using an EVOSTM FL Auto 2 microscopes.

To evaluate the extent of desialylation in O-glycans, we employed PNA lectin staining. Under normal physiological conditions, these epitopes are capped by terminal sialic acids and become accessible only after enzymatic removal. In non-treated SFs, PNA binding was relatively weak, suggesting the majority of Galβ1-3GalNAc moieties were masked by terminal sialylation. Upon treatment with various recombinant sialidases, a notable increase in red fluorescence was observed, reflecting successful cleavage of sialic acid residues.

Among all conditions, VC- and L-treated cells showed the most intense PNA staining, both on the cell membrane and throughout the extracellular matrix (ECM), indicating a strong desialylating effect that may not only impact cell surface glycoconjugates but also involved in extracellular secreted or matrix-bound components. The fluorescence pattern in these groups was more widespread and punctate. In contrast, CP- and AU-treated SFs exhibited a moderate increase in PNA signal compared to controls, though still less prominent than VC or L. These differences further support a hierarchy of enzymatic efficacy, with VC and L being more potent in exposing underlying galactose residues (Figure 4-5).

As AAL selectively binds to α1,6-fucosylated N-glycans, which are not substrates for sialidases, making it a reliable control marker for glycan features unaffected by desialylation. Across all treatment conditions including CP, AU, VC, and L, the intensity and distribution of AAL staining (red) remained comparable to non-treated controls. Cells displayed strong membrane and cytoplasmic fucosylation signals with no apparent reduction in staining intensity following sialidase exposure (Figure 4-6). DAPI staining confirmed equivalent cell density across wells. This unaltered AAL signal validates that the observed reductions in SNA and MAL staining are due to specific sialidase activity rather than global glycan degradation or cellular damage. Thus, core fucosylation serves as a robust internal control, demonstrating the specificity and selectivity of the enzymatic desialylation approach used in this study.

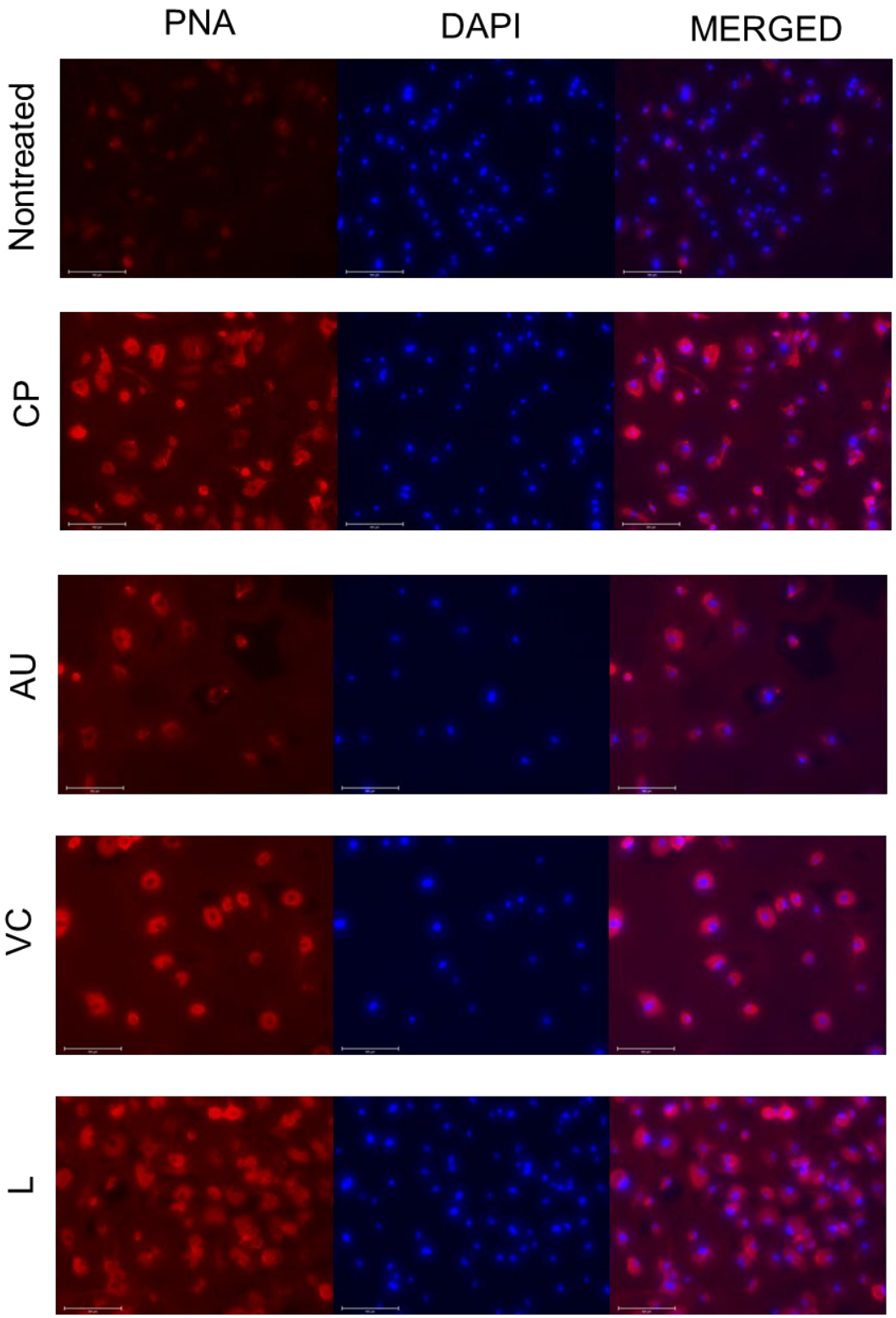

Figure 4-5 Immunofluorescent evaluation of PNA binding in naïve SFs following sialidase treatments.

Ex vivo cultured SFs were stained for PNA expression, visualised using Alexa Fluor 647 (red) and counterstaining with DAPI (blue) under 20X magnification. Scale bar, 100 μm. Images were obtained using an EVOSTM FL Auto 2 microscopes.

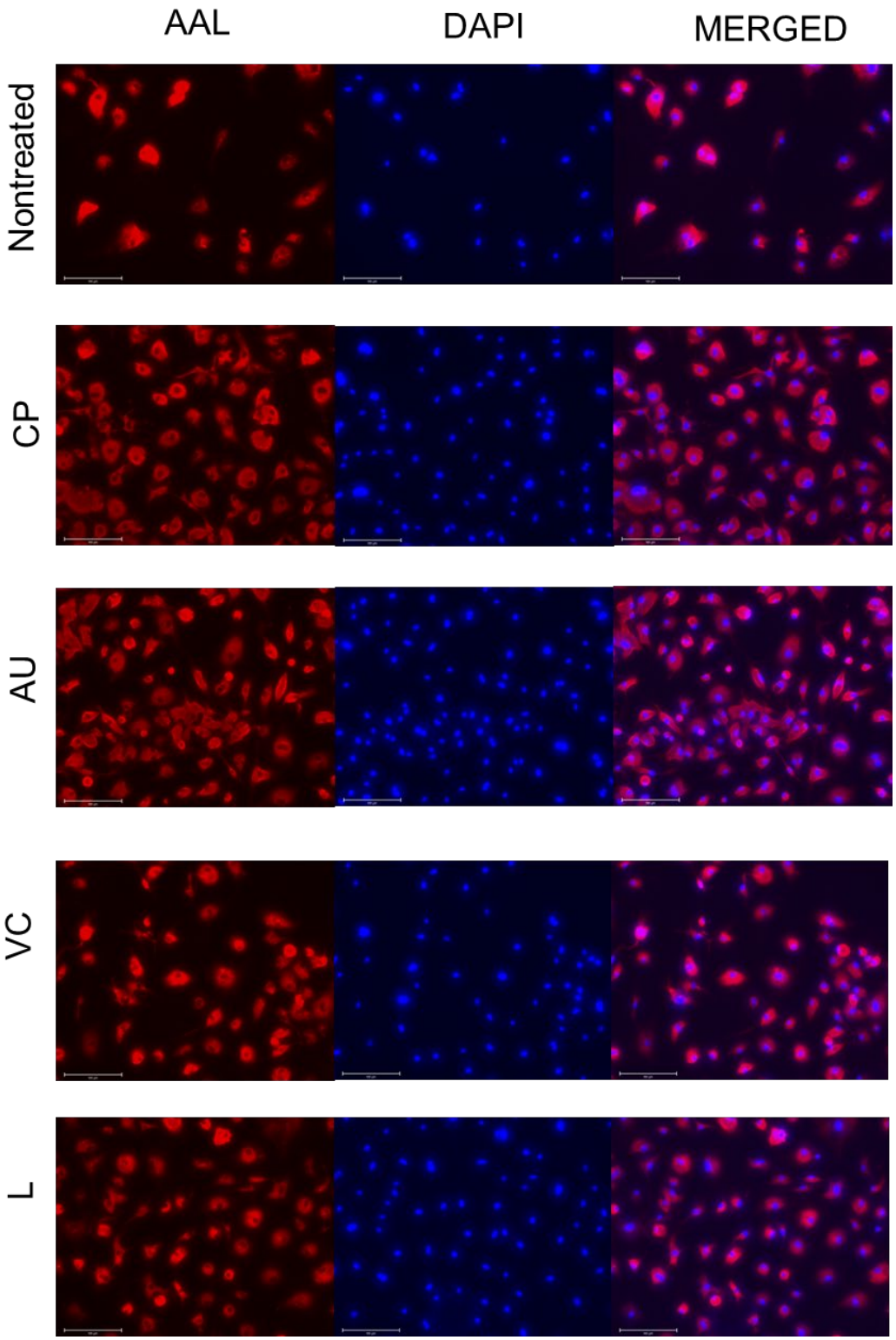

Figure 4-6 Immunofluorescent evaluation of AAL binding in naïve SFs following sialidase treatments.

Ex vivo cultured SFs were stained for AAL expression, visualised using Alexa Fluor 647 (red) and counterstaining with DAPI (blue) under 20X magnification. Scale bar, 100 μm. Images were obtained using an EVOSTM FL Auto 2 microscopes.

In summary, the immunofluorescence data supported the ELLA experiments where CP, VC and L sialidases most potently reduce α2-3 sialylation, while AU retain moderate residual staining, supporting partially retained sialylation or incomplete enzymatic activity under the tested conditions.

Previous work in the group (Y. Wang et al., 2021) showed that CP treatment indiced IL-6 production in SFs, but whether all sialic acid is involved in cell activation was unclear. Therefore, we used our new defined sialidase set to determine whether cell activation is linked to any loss of sialic acid, or whether only specific types lead to inflammatory responses. To evaluate the effect of enzymatic desialylation on basal inflammatory activation in naïve SFs, IL-6 levels were measured in the conditioned media 24 hours after sialidase treatment, in the absence of any cytokine stimulation. The data revealed that desialylation above certain thresholds was sufficient to enhance IL-6 secretion in a manner that closely paralleled the extent of α2-3 sialic acid removal. Specifically, VC- and Lectenz-treated SFs showed the most significant increase in IL-6 production, correlating with their strong α2-3 desialylation activity as confirmed by both ELLA (MAL binding) and immunofluorescence staining. CP-treated SFs exhibited a moderate but statistically significant rise in IL-6 levels, while AU-treated SFs showed no significant change compared to non-treated controls. This lack of IL-6 production in AU-treated cells may reflect a threshold effect, where α2-3 cleavage below certain levels, such as that observed in AU-treated SFs, fails to sufficiently expose pro-inflammatory glycan epitopes or alter receptor accessibility. Collectively, these findings suggest that removal of α2-3-linked sialic acids, particularly beyond a certain threshold, plays a key role in modulating steady-state IL-6 secretion in SFs, linking surface glycan remodelling to innate inflammatory potential (Figure 4-7A).

Importantly, our experimental cells still responded to endogenous inflammatory factors, since exogenous cytokines and Lipopolysaccharide (LPS) led to a marked increase in IL-6 production. LPS induced the highest levels among all tested conditions. IL-17, TNF-α, IL-1β, and Galectin-3 also significantly elevated IL-6 secretion compared to untreated controls, confirming that SFs are highly responsive to both cytokine and lectin-mediated stimulation (Figure 4-7B). These experiments served as essential functional controls for the ELLA and ELISA assays, demonstrating that the cells were viable, responsive, and transcriptionally competent throughout the experimental window. Without this validation,

interpretation of the desialylation experiments would lack context and confidence, as it would remain unclear whether a lack of cytokine production reflected biological effects or compromised cell health.

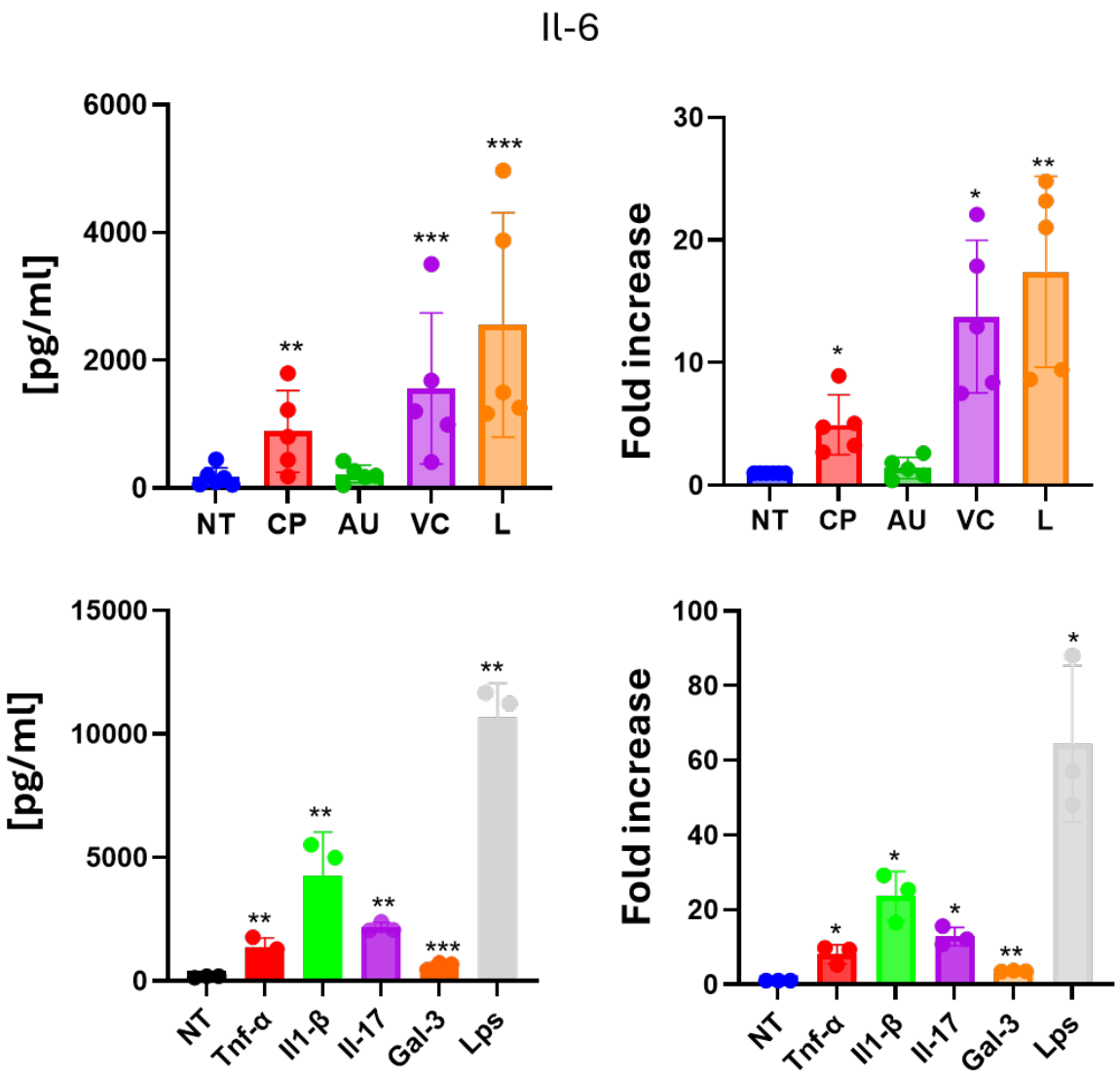

Figure 4-7 IL-6 secretion by synovial fibroblasts following treatment with different sialidases and cytokines.

SFs were treated with (A) buffer only (control, blue), *Clostridium perfringens sialidase* (CP), *Arthrobacter ureafaciens* sialidase (AU), *Vibrio cholerae* sialidase (VC), or Lectenz sialidases (L). SFs were treated with (B) DMEM only (control, blue), 10 ng/ml Tnf-α, Il1-β, Il17, Gal-3 and LPS for 24h. IL-6 levels in the culture supernatants were quantified by ELISA. Bars represent mean ± SD. Individual dots represent independent biological replicates. Statistical analysis were performed using ratio paired t-tests or one sample t tests. *p < 0.05, **p < 0.01 versus nontreated control.

Collectively, these results indicate that both pro-inflammatory stimuli and desialylation converge on a shared outcome: upregulation of IL-6, a key effector of synovial inflammation, although the amount of Il-6 production differs. This reinforces the concept that loss of sialic acid structures on SFs may act as a self-contained pro-inflammatory signal akin to external immune triggers.

Next, we decided to investigate the functional consequences of the observed SF-activation upon distinct enzymatic desialylation. To assess how desialylation-induced changes in SFs affect their surrounding microenvironment, we collected the cell culture used for enzymatic desalylation (conditioned media), and we used that medium to stimulate resting cells and evaluate the paracrine effects on cell migration. This approach allows us to isolate the impact of secreted factors from desialylated SFs on the behaviour of otherwise untreated, naïve SFs. By exposing naïve SFs to the soluble mediators released from SFs treated with different sialidases, we aimed to determine whether alterations in sialylation could drive a more migratory phenotype through indirect signalling. This is particularly relevant in the context of RA, where fibroblast activation and migration contribute to pannus formation and joint destruction. Using this setup, we observed that conditioned media from VC- and L-treated SFs both targeting α2-3-linked sialic acids most strongly promoted wound closure, suggesting a role for specific sialic acid structures in regulating fibroblast-derived pro-migratory cues. CP-treated SFs also promoted migration compared to untreated controls, while AU-treated SFs, which exhibited less α2-3 desialylation, induced only a modest effect (Figure 4-8). These findings underscore the importance of sialylation not only in cell-intrinsic functions but also in shaping the inflammatory and migratory landscape via secreted factors. Taken together, these results support the notion that removal of α2-3 sialic acid on SFs creates a pro-inflammatory secretory phenotype that not only boosts IL-6 but also enhances the migratory potential of neighbouring fibroblasts, an effect reminiscent of activated states seen in RA.

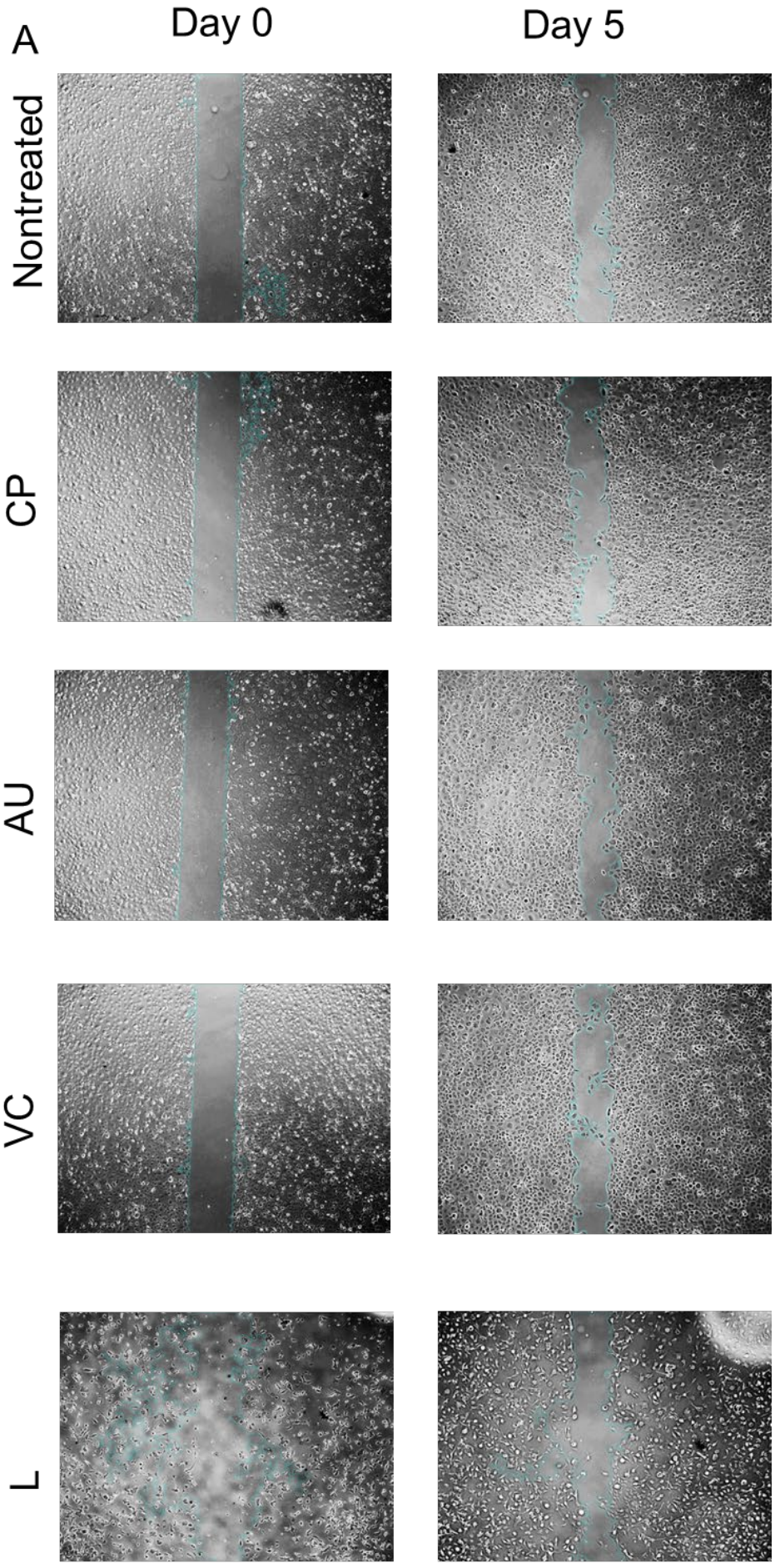
A
Day 0
Day 5
Nontreated
CP
AU
VC
L

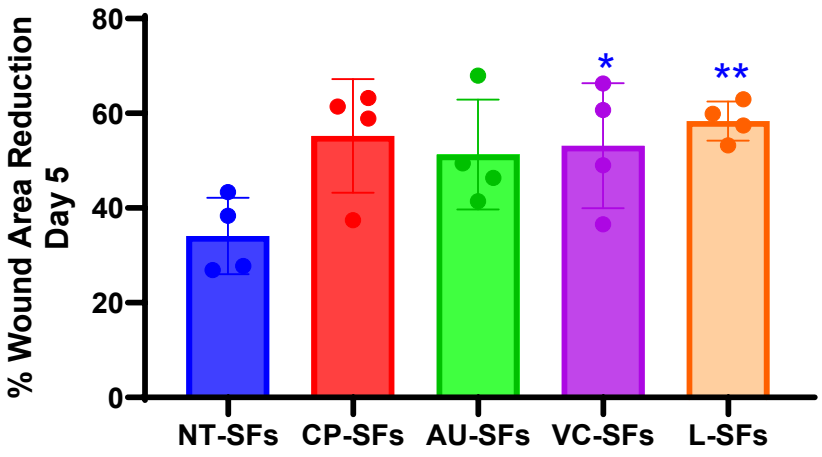

Figure 4-8 The impact of sialidase treated SFs supernatants on SFs migrations.

SFs were extracted from naive C57B/6 mice and expanded *ex vivo*. Cells were seeded in ibidi migration chambers and incubated with desialylated SFs supernatants. Migration assay was performed once the inserts were removed and ended after 5 days of incubation.
Images show one representative experiment. A) Superimposed blue lines delineate the cell-free area. B) Bar charts show the percent wound area reduction from four independent experiments. CP SFs vs NT SFs were compared Mann-Whitney U tests, remaining groups were compared unpaired t-tests. *p < 0.05, **p < 0.01 versus nontreated control.

4.2.2 Desialylation Induces Distinct Transcriptional Reprogramming in Synovial Fibroblasts

Having established that recombinant sialidases differ markedly in their ability to cleave specific sialic acid linkages on naïve SFs, especially with VC and Lectenz demonstrating the most efficient removal of α2-3-linked sialic acids, we next focused on studying how such glycan alterations impact the transcriptional reprogramming in naïve SFs. Given the pivotal role of sialylation in modulating receptor signalling, cell-matrix interactions, and immune recognition, we hypothesised that desialylation above certain thresholds may trigger broader changes in SF identity beyond glycan remodelling. To explore this, we performed bulk RNA sequencing of SFs treated with individual sialidases to assess whether distinct patterns of desialylation are associated with specific transcriptional reprogramming events.

To understand how gene expression varied across different sialidase treatments, we generated a heatmap with DEG for all conditions. The heatmap visualisation demonstrates distinct transcriptional reprogramming in SFs following treatment with various sialidases. Among the groups, L-treated SFs displayed the most pronounced shift in global gene expression, clustering separately and exhibiting substantial upregulation and downregulation of a large set of genes compared to the nontreated controls. CP-treated SFs also exhibited transcriptional changes, forming a discrete cluster indicative of a broad response likely driven by its dual cleavage activity on both α2-6 and α2-3 sialic acid linkages. VC-treated SFs, which predominantly cleave α2-3 sialic acid, shared some transcriptional signatures with CP but exhibited a moderately distinct profile, suggesting a more selective transcriptional response. In contrast, AU-treated SFs clustered closely with nontreated controls and showed minimal transcriptional deviation, consistent with previous ELLA findings indicating limited sialic acid cleavage. Collectively, this pattern supports that the extent and specificity of sialic acid cleavage directly correlate with the magnitude and nature of gene expression changes in SFs (Figure 4-9).

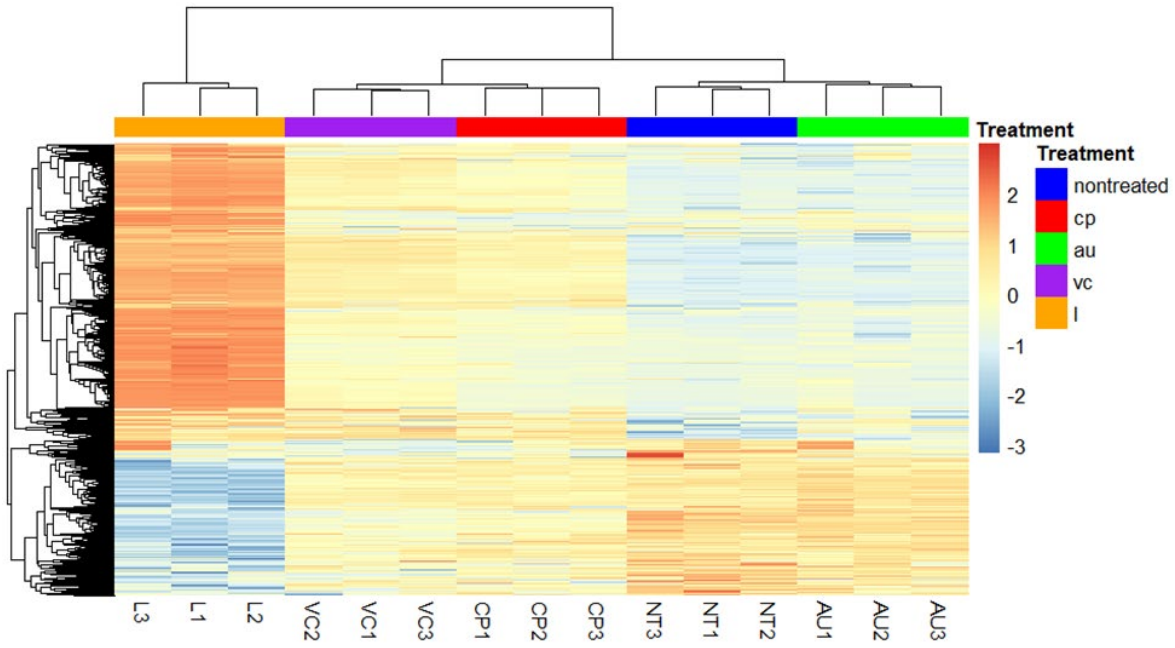

Figure 4-9 Heatmap illustrating the expression patterns of differentially expressed genes across multiple treatment groups in mouse synovial fibroblasts samples.

RNA-seq count data were normalised using DESeq2 size factor normalisation, log2-transformed, and then scaled by gene (row-wise z-score) to highlight relative expression differences. DEGs were identified for each treatment condition compared to the

nontreated control (absolute log2 fold change > 1, adjusted p-value < 0.05) and combined into a comprehensive gene set for visualisation. Samples are annotated by treatment group with a colour key: Nontreated (blue), Cp (red), Au (green), Vc (purple), and L (orange). Both genes (rows) and samples (columns) are hierarchically clustered using Euclidean distance and complete linkage to reveal expression pattern similarities. This heatmap highlights distinct transcriptional signatures associated with each treatment condition.

The principal component analysis (PCA) plot clearly illustrates that sialidase treatments induce distinct transcriptional profiles in SFs, with the degree of separation correlating with the extent of desialylation observed in earlier analyses (Figure 4-10). Lectenz-treated SFs (L1-L3) show the most pronounced shift along PC1, accounting for nearly 30% of the variance, and form a tight cluster distant from all other groups, indicating robust and consistent transcriptional reprogramming. This aligns with the earlier evidence that Lectenz most effectively cleaves α2-3-linked sialic acids and induces the highest IL-6 production and migratory response.VC-treated samples (VC1-VC3), which also efficiently removed α2-3 sialic acid, form a distinct cluster moderately separated from the non-treated (NT) group and lie in a transitional zone on the PCA plot, suggesting a moderate yet reproducible gene expression shift. In contrast, AU-treated SFs (AU1-AU3), which showed less α2-3 desialylation, cluster closely with NT controls, supporting the idea that sialic acid removal under certain thresholds results in limited transcriptional impact.

CP-treated SFs (CP1-CP3), which induced intermediate levels of α2-6 desialylation, show greater divergence from NT controls along PC2, yet do not cluster with either VC or Lectenz, indicating a unique transcriptional signature possibly driven by α2-6 cleavage and its downstream effects (Figure 4-10). Overall, this PCA analysis demonstrates that the magnitude and specificity of desialylation, particularly the targeting of α2-3 linkages, are strongly associated with the scale of transcriptomic reprogramming in SFs.

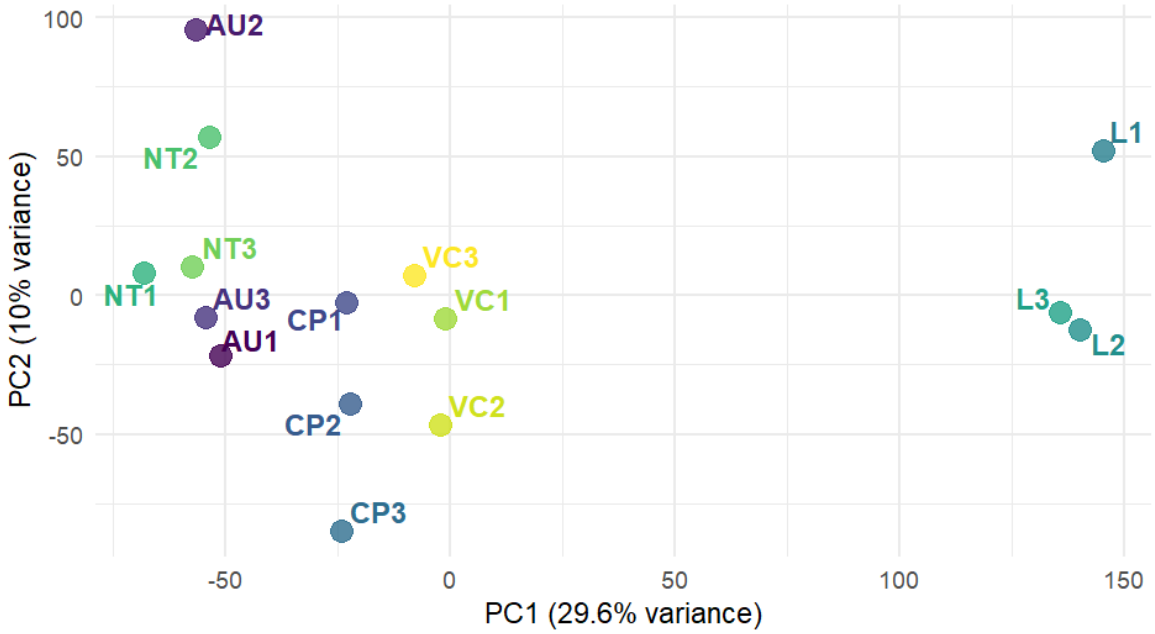

Figure 4-10 Principal Component Analysis of Global Transcriptional Changes in Synovial Fibroblasts Following Sialidase Treatment.

RNA-sequencing was performed on naïve SFs treated with recombinant sialidases (CP, AU, VC, L) or left untreated (NT). Principal component analysis (PCA) was conducted based on the normalised logarithmic counts. PC1 and PC2 account for 29.6% and 10% of the total variance, respectively. Each point represents one biological replicate. L-treated SFs (L1-L3) clustered distinctly along PC1, indicating a strong transcriptional shift. VC-treated cells (VC1-VC3) showed intermediate divergence from NT (NT1-NT3), whereas AU-treated cells (AU1-AU3) remained proximal to the NT cluster, reflecting minimal transcriptional reprogramming. CP-treated SFs (CP1-CP3) formed a separate group, suggesting a unique expression profile. These results highlight that the extent and specificity of desialylation drive distinct transcriptomic responses in SFs.

Given that CP sialidase demonstrated the ability to cleave both α2-6- and α2-3-linked sialic acid residues on the surface of naïve SFs, this dual effect of broad desialylation capacity might significantly influence downstream gene expression. Unlike other enzymes with more selective activity, CP's dual specificity may potentially disrupts a wider array of glycan-mediated regulatory mechanisms. To investigate whether this enzymatic profile translates into functional transcriptional changes, we next performed bulk RNA sequencing on CP-treated SFs and compared their transcriptomic landscape to non-treated controls.

The data presented illustrate the transcriptional changes induced in SFs following treatment with CP sialidase (Figure 4-11A-B). The volcano plot shows a clear skew

toward gene upregulation, with a substantial number of genes significantly upregulated in CP-treated SFs compared to non-treated controls. In contrast, only a small number of genes were significantly downregulated, suggesting that CP treatment predominantly activates gene expression.

The accompanying heatmap highlights the top differentially expressed genes between CP-SFs and NT-SFs. Pro-inflammatory genes such as Il1b, Ccl2, Ccl20, Cxcl2, Mmp9 and Mmp1b were markedly upregulated in CP-treated cells, pointing to an enhanced inflammatory and tissue-remodelling phenotype. This suggests that CP-mediated desialylation may promote a pro-inflammatory and invasive transcriptional program in SFs (Figure 4-11C). Transcriptomic analysis also revealed that CP-treated SFs exhibited a distinct upregulation of key pro-inflammatory genes, including Nos2 and Csf2, which are associated with nitric oxide production and GM-CSF signalling, respectively.

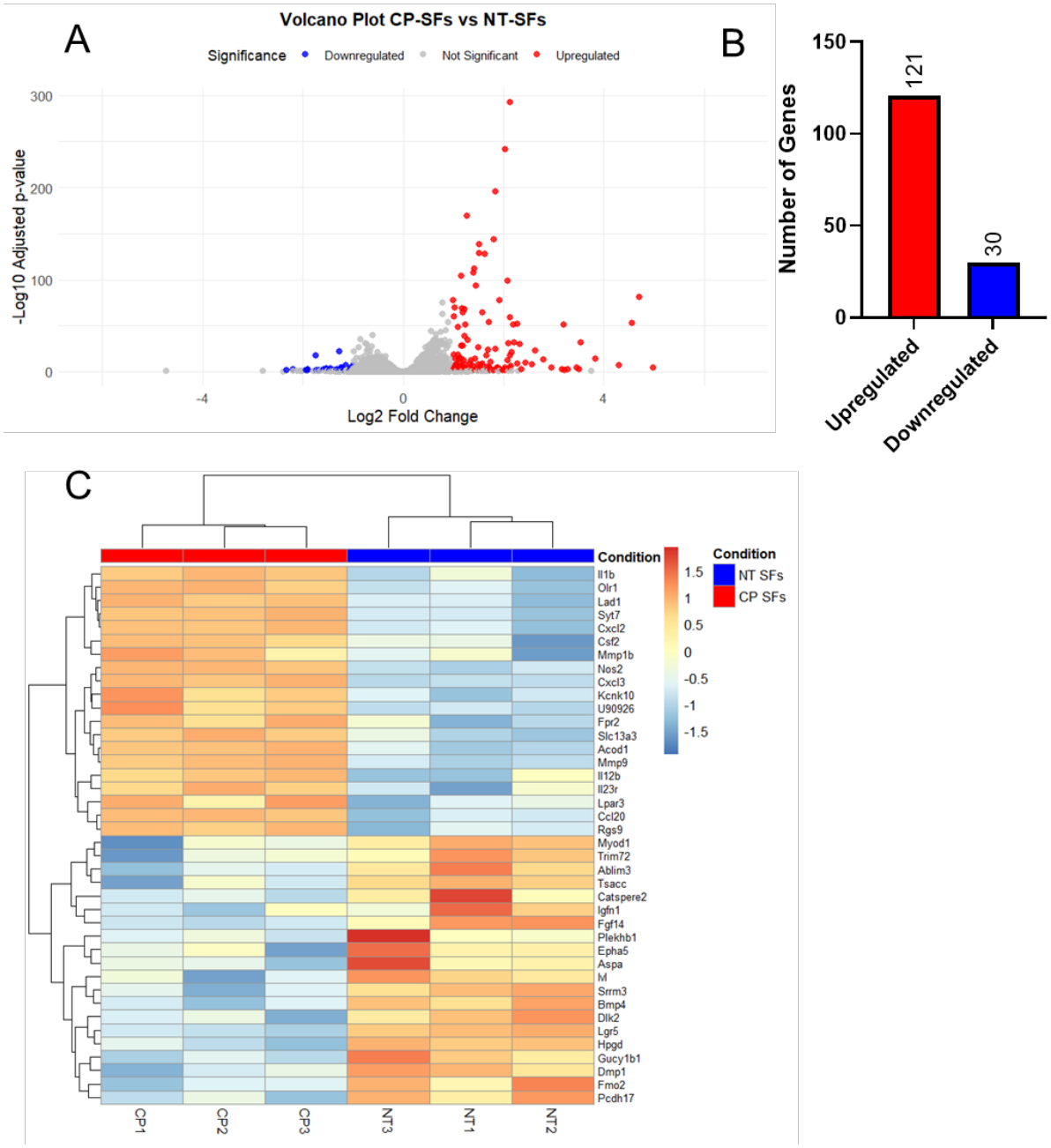

Figure 4-11 CP-treated naïve synovial fibroblasts demonstrate distinct inflammatory transcriptomics profiles.

Naïve SFs from C57b/6 mice stimulated with CP sialidase to evaluate gene expression. Differential gene expression was analysed using DESeq2, with significance defined as $|\log_2 FC| > 1$ and padj < 0.05.

A) Volcano Plot: Displays differentially expressed genes (DEGs) in CP-stimulated (CP-SFs) vs. nontreated naïve SFs (NT-SFs). Upregulated (red) and downregulated (blue) genes met the significance threshold, while non-significant genes are not met the significance shown in grey.

B) Bar Graph: Shows the number of significantly up- and downregulated genes, revealing

a distinct distribution.
C) Heatmap: Highlights the top 20 DEGs, with red indicating high and blue low expression. Clustering groups samples by similarity, annotated by sample location and condition. Gene expression values are $\log_2$-transformed and Z-score normalised (row-scaled).

Overall, these results indicate that CP sialidase treatment induces a strong pro-inflammatory and matrix-remodelling gene signature in SFs, likely through removal of sialic acid structures that normally suppress activation. This supports the notion that altered glycosylation can function as a potent modulator of fibroblast pathogenicity.

When differential expression analysis was performed using the same thresholds ($\log_2$ fold change > 1 and adjusted $p < 0.05$), no genes met these criteria in AU-treated SFs compared to non-treated controls. This lack of differentially expressed genes suggests that AU treatment, consistent with its less α2-3 sialic acid cleavage observed in lectin binding assays, does not induce a robust transcriptional response. Furthermore, IL-6 secretion measured by ELISA also remained low in AU-treated SFs, reinforcing the idea that desialylation under certain thresholds fails to initiate a strong inflammatory or transcriptional response. Together, these findings suggest that a critical threshold of sialic acid removal is necessary to drive the glyco-inflammatory reprogramming observed with more potent sialidase treatments.

Enzymatic cleavage of α2-3-linked sialic acids by VC treatment leads to a profound pro-inflammatory transcriptional shift in SFs. The volcano plot shows a substantial number of significantly upregulated genes in VC-treated SFs compared to untreated controls (Figure 4-12A-B), while the heatmap (Figure 4-12C) reveals marked induction of inflammatory mediators including Nos2, Il1b, Cxcl3, Cxcl10, Ccl20, Ccl22 and Mmp1a. These genes are characteristic of the activated, arthritis-associated SF phenotype. This response aligns with prior ELLA results showing that VC is among the effective sialidases in removing α2-3-linked sialic acid residues from the SF surface. The robust induction of Nos2 is particularly notable, as iNOS is known to be enriched in RA SFs and contributes to nitric oxide mediated joint inflammation. Additionally, previous ELISA data demonstrated that VC-treated SFs secreted significantly elevated levels of IL-6 even in the absence

of exogenous cytokine stimulation, further confirming that α2-3 desialylation alone is sufficient to trigger SF activation. Altogether, these findings suggest that targeted removal of α2-3 sialic acid structures such as achieved with VC treatment can reprogram naïve SFs into a transcriptionally and functionally pro-inflammatory state, mirroring key features observed in the rheumatoid joint.

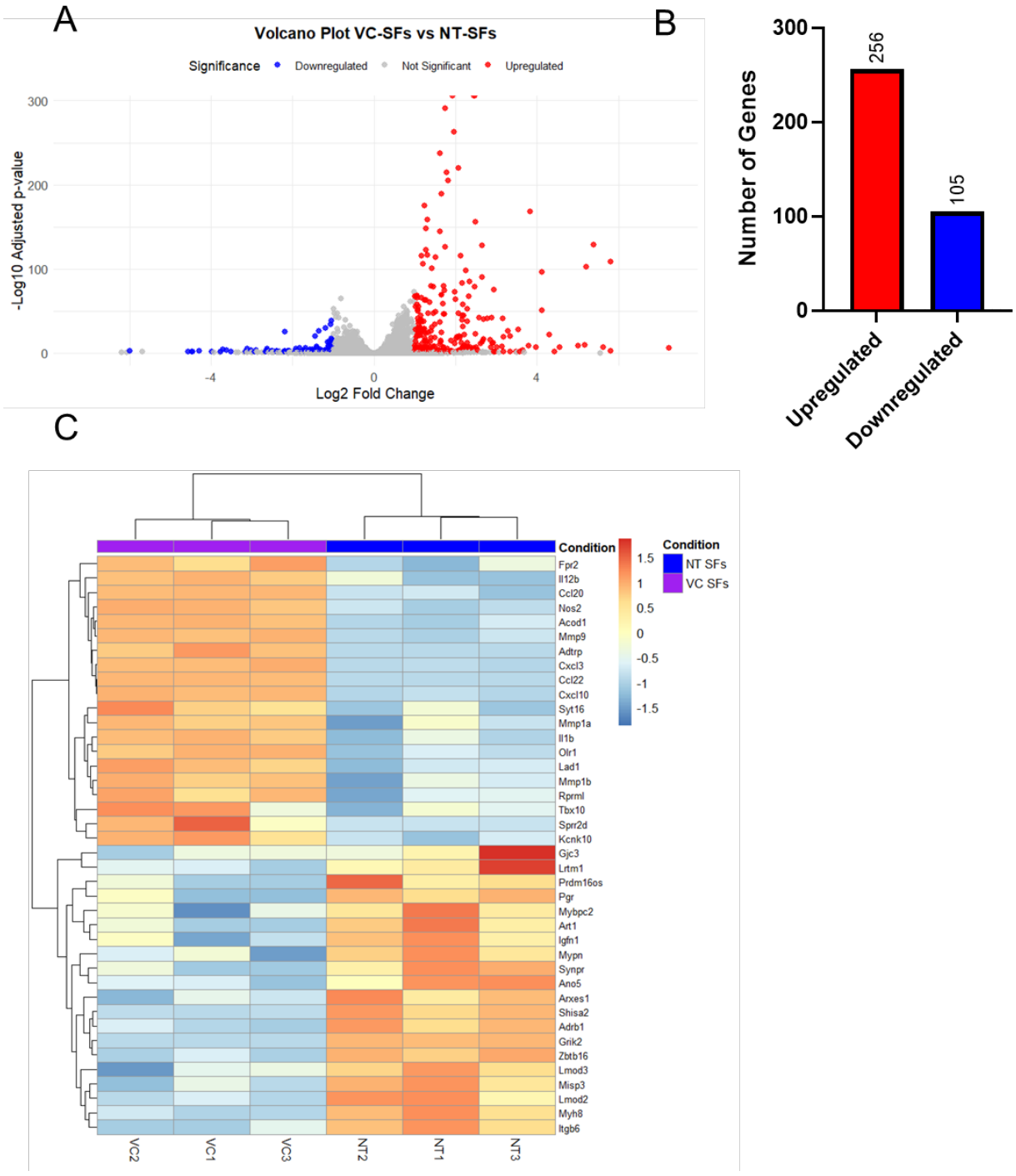

Figure 4-12 VC-treated naïve synovial fibroblasts demonstrate distinct inflammatory transcriptomics profiles.

Naïve SFs from C57b/6 mice stimulated with VC sialidase to evaluate gene expression. Differential gene expression was analysed using DESeq2, with significance defined as $|\log_2 FC| > 1$ and padj < 0.05.

A) Volcano Plot: Displays differentially expressed genes (DEGs) in VC-stimulated (VC-SFs) vs. nontreated naïve SFs (NT-SFs). Upregulated (red) and downregulated (blue) genes met the significance threshold, while non-significant genes are not met the significance shown in grey.
B) Bar Graph: Shows the number of significantly up- and downregulated genes, revealing a distinct distribution.
C) Heatmap: Highlights the top 20 DEGs, with red indicating high and blue low expression. Clustering groups samples by similarity, annotated by sample location and condition. Gene expression values are $\log_2$-transformed and Z-score normalised (row-scaled).

Lectenz-treated SFs (L-SFs), which underwent maximal cleavage of α2-3-linked sialic acids as confirmed by ELLA assays, exhibited robust transcriptional reprogramming indicative of a pro-inflammatory phenotype. The volcano plot and bar graph highlight a large number of significantly upregulated genes (Figure 4-13A-B), while the accompanying heatmap shows elevated expression of inflammatory mediators such as Il1b, Il12b, Ifnb1, Cxcl10, Csf3, and Nos2, many of which are hallmark signatures of activated SFs in RA (Figure 4-13C). Importantly, IL-6 production was also significantly increased in L-SFs at the protein level (see Figure 4-7), aligning with the transcriptomic upregulation of multiple upstream inflammatory drivers. This strongly supports the idea that selective loss of α2-3-linked sialylation is sufficient to induce SF activation, likely by disrupting inhibitory glycan-mediated interactions. Taken together, these findings suggest that α2-3 desialylation above certain levels, independent of α2-6 loss, is a potent trigger of inflammatory gene expression, mimicking the transcriptional shift seen in RA synovium and positioning α2-3-inked sialic acid as a critical regulator of SF homeostasis.

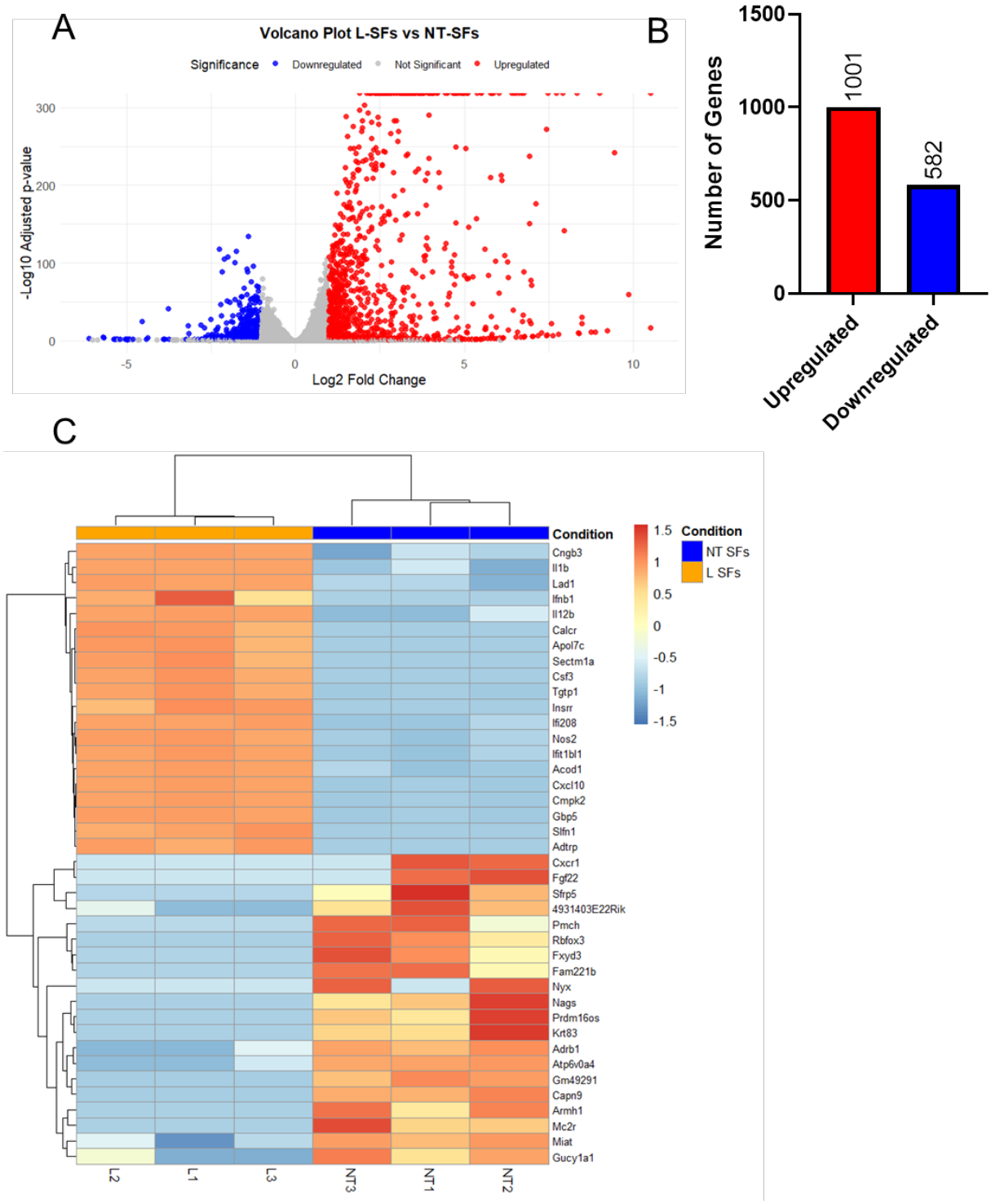

Figure 4-13 L-treated naïve synovial fibroblasts demonstrate distinct inflammatory transcriptomics profiles.

Naïve SFs from C57b/6 mice stimulated with Lectenz sialidase to evaluate gene expression. Differential gene expression was analysed using DESeq2, with significance defined as $|\log_2 FC| > 1$ and padj < 0.05.

A) Volcano Plot: Displays differentially expressed genes (DEGs) in Lectenz-stimulated (L-SFs) vs. nontreated naïve SFs (NT-SFs). Upregulated (red) and downregulated (blue) genes met the significance threshold, while non-significant genes are not met the significance shown in grey.
B) Bar Graph: Shows the number of significantly up- and downregulated genes, revealing a distinct distribution.
C) Heatmap: Highlights the top 20 DEGs, with red indicating high and blue low expression. Clustering groups samples by similarity, annotated by sample location and condition. Gene expression values are $\log_2$-transformed and Z-score normalised (row-scaled).

The KEGG pathway enrichment analysis highlights distinct inflammatory responses triggered by different sialidase treatments in SFs (Figure 4-14A). Pathways commonly enriched in CP-, VC-, and L-treated SFs include viral protein interaction with cytokine and cytokine receptor, rheumatoid arthritis, TNF signalling, and cytokine-cytokine receptor interaction, reflecting a shared inflammatory signature driven by desialylation. CP treatment, which cleaves both α2-3 and α2-6 sialic acids, and VC treatment, which predominantly targets α2-3 sialic acids, also led to enrichment of the IL-17 signaling and lipid and atherosclerosis pathways suggesting that partial or combined sialic acid removal is sufficient to activate broader pro-inflammatory and metabolic networks. In contrast, Lectenz, which selectively and maximally cleaves α2-3 sialic acids, uniquely enriched the NF-κB signalling and herpes simplex virus 1 infection pathways, indicating a more focused antiviral and NF-κB-driven activation. Together, these data suggest that the specificity and extent of α2-3 versus α2-6 sialic acid removal differentially shape the inflammatory landscape of SFs, with L eliciting the broader immune activation with the enrichment in more inflammatory and autoimmune-related KEGG pathways.

The GO enrichment analysis for biological processes reveals that desialylation of SFs using CP, VC, and L sialidases induces robust activation of innate immune-related pathways, whereas AU treatment shows no significant enrichment. Specifically, CP-treated SFs show selective enrichment in terms related to chemokine signalling, type II interferon response, cytokine-mediated signalling, and leukocyte migration, indicating early inflammatory activation likely triggered by broad glycan cleavage. L-treated SFs, which remove α2-3 sialic acids most efficiently, display the strongest enrichment across multiple innate immune responses, including defence response to virus, positive regulation of immune activation, and activation of innate immunity suggesting that α2-3-linked sialic acids may act as suppressive glycans restraining these pathways under homeostatic conditions. VC- and L-treated SFs both exhibit strong enrichment for overlapping GO terms such as defence response to virus, positive regulation of immune responses, and regulation of innate immunity, further supporting the conclusion that α2-3 desialylation is a dominant trigger of immune-related gene expression in SFs. In contrast, AU-treated SFs, which exhibited less α2-3 linked sialic acid cleavage, lack any significant biological process enrichment, reinforcing the notion that desialylation above a certain threshold is necessary to elicit meaningful transcriptional immune activation. Overall, the GO enrichment results align with prior transcriptional and cytokine data, highlighting a progressive immune activation hierarchy with AU < CP < VC < L, corresponding to their increasing a2-3 linked desialylation efficiency and glycan target breadth. This data underscores that α2-3 desialylation is sufficient to elicit a robust innate immune gene program above certain thresholds, while dual α2-3/α2-6 cleavage by CP leads to a more complex and diversified activation profile (Figure 4-14B).

Sialidase treatment of SFs led to distinct enrichment of molecular function GO terms, particularly in conditions involving CP, VC, and L enzymes, while AU-treated SFs showed no significant enrichment (Figure 4-14C). Notably, cytokine activity was commonly enriched across all effective desialylation conditions, indicating a shared proinflammatory functional profile. CP- and VC-treated SFs exhibited enrichment in CXCR chemokine receptor binding and G protein-coupled receptor binding, aligning with its dual α2-3 and α2-6 sialic acid cleavage profile. Meanwhile, both VC- and L-treated SFs, which primarily target α2-3 linkages, showed overlapping enrichment in cytokine activity and cytokine receptor binding, suggesting that even selective α2-3 desialylation can sufficiently prime SFs for

inflammatory signalling. Collectively, these results indicate that glycan remodelling via sialidase exposure significantly modulates the receptor-ligand signalling landscape of SFs, reinforcing a shift toward an immunoactive phenotype.

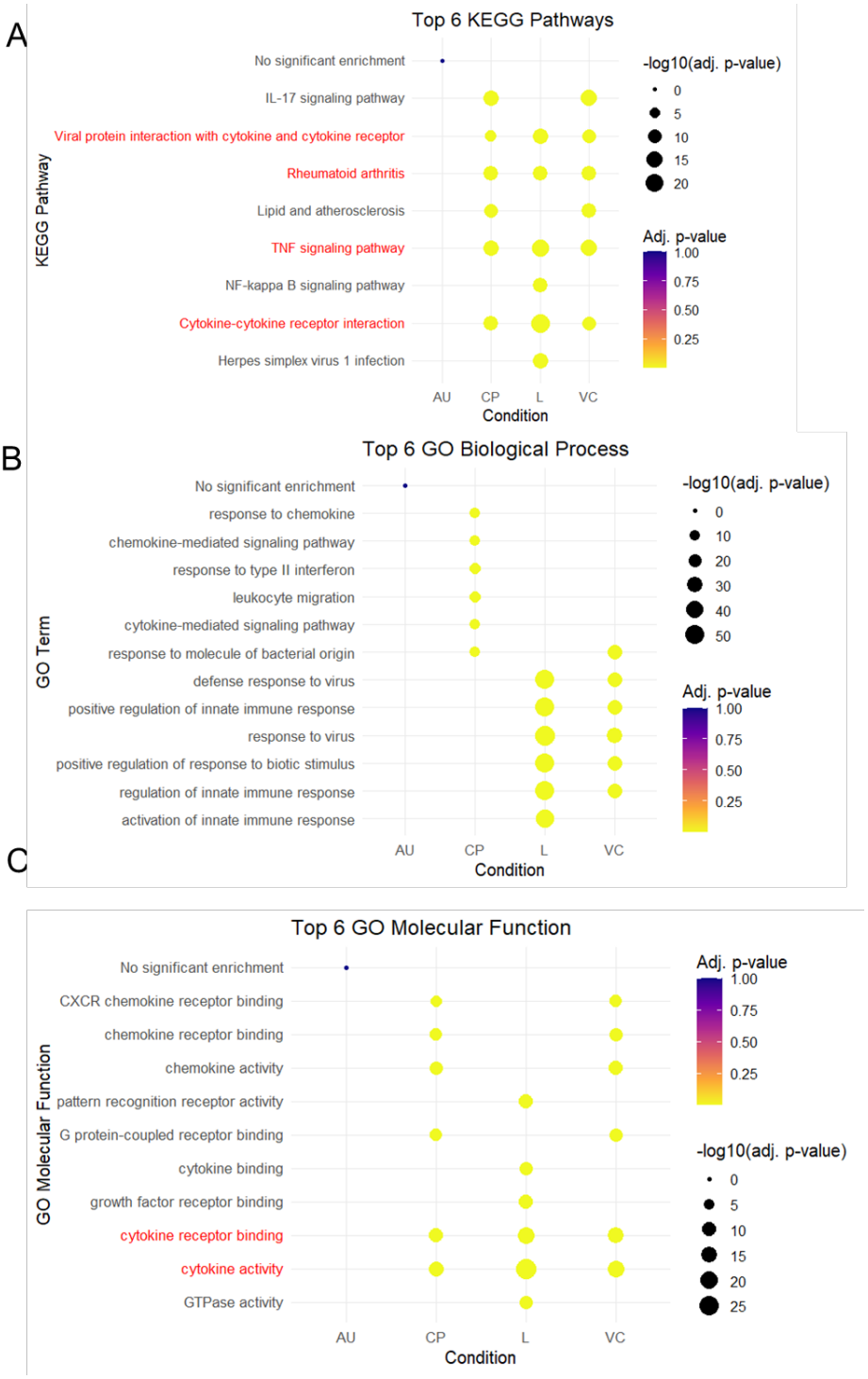

Figure 4-14 Comparative functional enrichment analysis of differentially expressed genes in sialidase-treated synovial fibroblasts.

A) KEGG pathway enrichment analysis showing the top 6 significantly enriched pathways per condition (AU, CP, L, VC). CP-, L-, and VC-treated SFs exhibited strong enrichment

for immune-related pathways including TNF signalling, cytokine-cytokine receptor interaction, rheumatoid arthritis, and IL-17 signalling, while AU-treated SFs showed no significant enrichment. NF-κB signalling and herpes simplex virus 1 infection pathways were uniquely enriched in L-treated SFs.
B) GO Biological Process enrichment revealed that CP-treated SFs exhibited enriched terms related to chemokine signalling and bacterial response, whereas L- and VC-treated SFs were enriched for innate immune activation and viral defence responses. Only CP and VC shared response to molecule of bacterial origin as a common term.
C) GO Molecular Function analysis showed significant enrichment in cytokine and chemokine-related activities in CP-, L-, and VC-treated SFs. All three conditions shared enrichment for cytokine binding and cytokine receptor binding. CP- and VC-SFs displayed CXCR chemokine receptor and G-protein coupled receptor binding enrichment. AU-treated SFs showed no significant enrichment in any category.
Analysis conducted based on differential gene expression data with significance defined as $|\log_2 FC| > 1$ and padj < 0.05. Each dot represents a pathway enriched in the respective condition. Dot size corresponds to the strength of pathway enrichment, represented as the negative logarithm of the adjusted p-value (-log10(adj. p-value)), where larger dots indicate higher statistical significance. Common pathways indicated with red colour.

To compare how different sialidase treatments change differential gene expression, we analysed common and specific transcriptional responses in naïve SFs. The Venn diagram shows substantial overlap among upregulated genes across CP, VC, and L treatments (Figure 4-15). Sialidase-mediated desialylation induces a shared inflammatory transcriptional core in synovial fibroblasts through the increased expression of inflammatory mediators, yet a smaller subset of genes that are specifically upregulated by individual sialidase treatments. These genes exhibit strong induction in one condition but remain unchanged or weakly expressed in others. The common genes include pro-inflammatory cytokines and chemokines such as Il1b, Cxcl3, Cxcl3, Cxcl10, Ccl20, and Ccl22, together with matrix-remodeling enzymes Mmp9. The induction of Nos2 further indicates a shift toward a highly activated, inflammatory fibroblast phenotype. In contrast to the large shared core, the treatment-specific bubble plot reveals a smaller but biologically informative set of genes selectively induced by individual sialidases. Notably, these include interferon- and stress-associated genes such as Slfn1, Csf3, Ifnb1, and Ltf, which are prominently upregulated in specific conditions but absent from others.

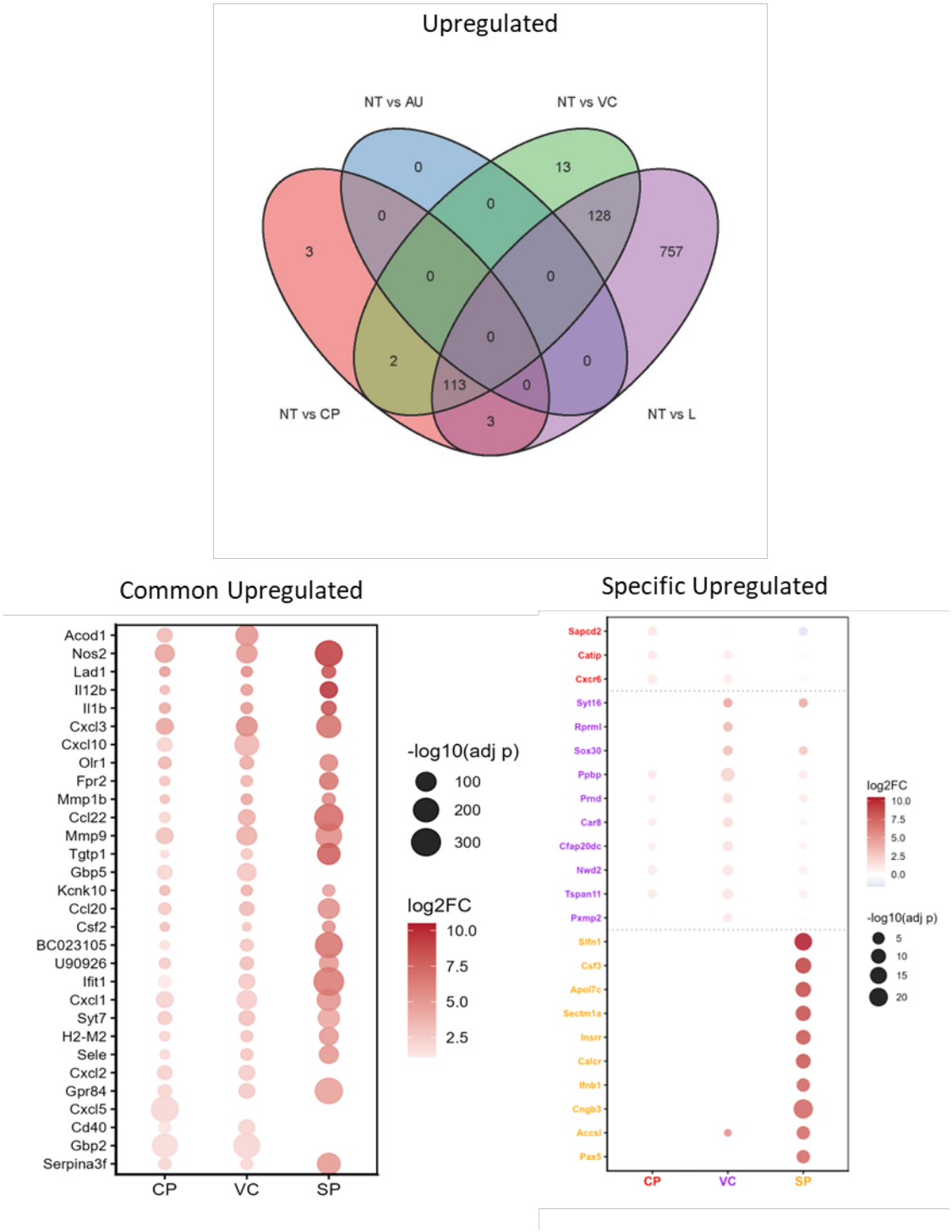

Figure 4-15 Shared and treatment-specific transcriptional responses to sialidase treatments

Venn diagram and bubble plots illustrating shared and treatment-specific upregulated genes in synovial fibroblasts following sialidase treatment. Bubble color indicates log2 fold change and bubble size reflects −log10(adjusted p value).

To understand SFs derived signals instructing macrophage polarisation across treatments, we checked some of the well now mediators involved in M1 or M2-like

macrophage polarisation. SFs upregulated multiple pro-inflammatory mediators associated with classical macrophage activation, including S100a8, Il1b, Il6, Ptgs2, and chemokines such as Cxcl1, Cxcl2, Cxcl9, and Cxcl10. This effect was most pronounced following L sialidase treatment, which induced the highest magnitude and significance of M1-associated signals, notably S100a8, Il1b, and Ccl2. In contrast, SF-derived factors linked to alternative (M2) macrophage polarization were comparatively limited. While expression of immunoregulatory mediators such as Lgals9, Il10, Ccl17, and Ccl22 was detectable, these signals were fewer in number and generally of lower magnitude than M1-associated factors, with modest induction observed primarily under L treatment. Collectively, these data indicate that SF desialylation drives a dominant pro-inflammatory secretory phenotype that favors macrophage M1 polarisation over M2 differentiation.

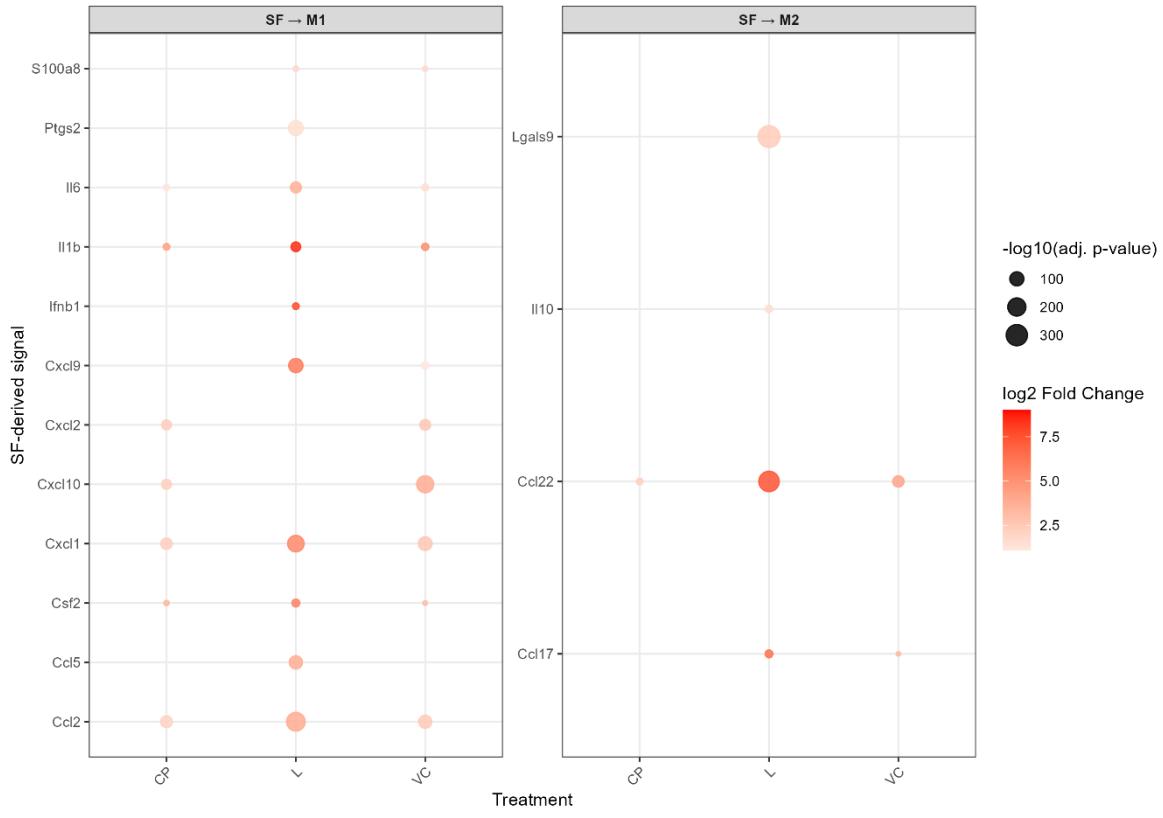

Figure 4-16 Synovial Fibroblasts Derived Signals Instructing Macrophage Polarisation

Bubble plots show differentially expressed SF-derived ligands associated with macrophage M1 (left panel) or M2 (right panel) polarisation after treatment with CP, L, or VC sialidases, compared with non-treated controls. The y-axis lists SF-derived genes, and the x-axis indicates treatment conditions. Bubble colour intensity represents the log2 fold

change in gene expression (red = higher induction), while bubble size corresponds to −log10 adjusted p-value, reflecting statistical significance. M1-associated signals include pro-inflammatory mediators such as S100a8, Il1b, Il6, Cxcl1/2/9/10, and Ccl2, whereas M2-associated signals are characterized by factors linked to immunoregulation and resolution, including Lgals9, Il10, Ccl17, and Ccl22.

4.3 Discussion

The present chapter demonstrates that enzymatic remodelling of the sialylation landscape on SFs profoundly alters their inflammatory potential, transcriptional profile, and functional behaviour. By systematically comparing the effects of distinct recombinant sialidases with known linkage specificities, we uncover a strong relationship between α2-3 sialic acid removal and pro-inflammatory activation in SFs, providing new mechanistic insight into the glyco-immune regulation of joint inflammation.

Our lectin-based profiling and immunofluorescence analyses revealed that CP sialidase efficiently cleaves both α2-6 and α2-3 sialic acid linkages, while VC and Lectenz enzymes exhibit higher selectivity and potency toward α2-3-linked residues. AU showed only modest desialylation capacity, particularly for α2-3 linkages, and served as an important comparator to establish threshold-dependent effects. These observations confirm that individual sialidases exert distinct and predictable effects on surface glycan structures, and that removal of α2-3-linked sialic acids, in particular, plays a dominant role in modulating cellular responses. Considering the combined analysis of enzyme-linked lectin assays (ELLA) and immunofluorescence imaging demonstrates that recombinant sialidase treatments induce distinct and selective desialylation patterns in naïve SFs, affecting α2-3- and α2-6-linked sialic acid residues differently depending on the enzyme used. ELLA results show a significant reduction in SNA and MAL binding in CP-treated cells, indicating efficient cleavage of α2-6 and α2-3 linked sialic acids, which is visually supported by the diminished red fluorescence intensity in SNA and MAL-stained CP-treated cells under the microscope. In contrast, VC and L-treated cells maintain higher SNA signal, reflecting weaker α2-6 activity. For α2-3-linked sialic acids, MAL binding is significantly reduced in VC- and L-treated cells, as shown by ELLA, and corroborated by immunofluorescence images where VC and L groups exhibit markedly reduced red staining intensity compared to non-treated controls. Furthermore, PNA binding, which detects exposed Galβ1-3GalNAc residues after

sialic acid removal, is significantly increased in all treatment groups, confirming the enzymatic desialylation removes sialic acids. Importantly, AAL binding, used as a control for detecting core fucosylation, remains unchanged across all groups in both ELLA and microscopy, confirming that sialidase treatments selectively target terminal sialic acids without affecting underlying glycan core structures. This integrated dataset robustly confirms that CP sialidase preferentially removes α2-6 and α2-3 sialic acids, VC and L more efficiently target α2-3 linkages, and the observed changes in glycan architecture are enzyme-specific, reproducible, and visually validated across independent methodological platforms.

One of the most striking findings is that desialylation induced IL-6 secretion compared to unstimulated SFs. This was most prominent in VC- and L-treated SFs, which exhibited the strongest α2-3 cleavage, indicating that these terminal glycans may function as suppressive modulators of inflammatory cytokine release. CP treatment, with its dual α2-3/α2-6 activity, also induced IL-6, but to a lesser extent, while AU-treated SFs showed no change, reinforcing the existence of a desialylation threshold required to trigger inflammatory activation. Notably, this basal inflammatory response mirrored that seen with exogenous stimulation by proinflammatory cytokines such as TNF, IL-1β, and IL-17, suggesting that loss of terminal sialylation could act as a cell-intrinsic danger signal, mimicking pathogen-associated or cytokine-driven cues in the joint environment.

Transcriptomic profiling further highlighted the distinct and graded effects of sialidase treatment on SF gene expression. PCA and heatmap analyses revealed that L- and VC-treated SFs underwent the most profound transcriptional reprogramming, with L-SFs forming a clearly distinct cluster. These treatments led to marked upregulation of inflammatory and chemotactic genes, including Nos2, Il1b, Ccl20, Cxcl10, and Csf3, mirroring key signatures of RA SFs. Importantly, Nos2 induction, suggests that desialylation contributes to nitric oxide-mediated inflammation and tissue damage in the joint. Previous reports demonstrated the presence of iNOS, the enzyme product of the Nos2 gene, in RA SFs and macrophages (McInnes et al., 1996; Sakurai et al., 1995). Considering the fact that desialylation highly upregulates Nos2 gene expression, desialylated SFs may rapidly adopt a phenotype reminiscent of the SFs found in the arthritic joint, mediated by the nitric oxide production that is particularly affected by TNF-α production (McInnes et al., 1996). On the other hand, GM-CSF release by SFs has

been demonstrated to impact monocyte survival, but only after stimulation by proinflammatory cytokines (Darrieutort-Laffite et al., 2014). The observed upregulation of Csf2 in desialylated SFs, along with increased IL-6 levels (Figure 4-7), indicates that desialylation may enhance SF-macrophage interactions by shaping a proinflammatory cytokine milieu. The strong transcriptional activation between desialylated SFs and activated RA-SFs underscore the disease relevance of this glycan remodelling. In contrast, AU-treated SFs, which exhibited less desialylation, clustered closely with nontreated controls and showed no differentially expressed genes, further supporting that incomplete glycan removal fails to cross the activation threshold.

The KEGG pathway enrichment analysis provided key insights into how distinct sialidase treatments differentially reprogram SF inflammatory signalling, depending on the type and extent of sialic acid removal. Several core inflammatory pathways including TNF signalling, cytokine-cytokine receptor interaction, and rheumatoid arthritis were consistently enriched in CP-, VC-, and L-treated SFs, suggesting that desialylation, particularly of α2-3-linked sialic acids, broadly enhances pro-inflammatory transcriptional circuits. This shared signature likely reflects the central role of sialic acid capping in suppressing cytokine receptor clustering or limiting glycan-dependent immune activation. In our previous paper, we used CP sialidase to desialylate naïve DBA mouse SFs and further applied a bulk RNA-Seq. The activated KEGG pathways were similar to those we found on the C57B/6 mouse CP-SFs validated the previous experimental findings (Wang et al., 2022).

Interestingly, CP- and VC-treated SFs also enriched additional pathways such as IL-17 signaling and lipid and atherosclerosis pathways, which were not significantly enriched in L-treated SFs. This suggests that although all three enzymes elicit inflammation, the breadth of the downstream response may vary based on cleavage specificity. CP's dual α2-3 and α2-6 cleavage likely perturbs a broader array of glycan-mediated interactions, leading to a wider transcriptional impact. VC, despite targeting primarily α2-3 linkages, may have achieved a threshold of desialylation sufficient to impact additional metabolic or inflammatory networks, particularly through enhanced receptor accessibility or galectin-mediated signaling.

Notably, Lectenz, which most effectively and selectively cleaves α2-3-linked sialic acids, showed unique enrichment of NF-κB signaling and herpes simplex virus 1 infection pathways. This suggests a more focused antiviral and innate immune activation signature in response to high-efficiency α2-3 desialylation. Given that α2-3 sialic acids are key ligands for inhibitory Siglecs, their complete removal may specifically release Siglec-mediated suppression of NF-κB-driven inflammatory cascades. These findings collectively underscore that not only the type but also the degree of desialylation shapes distinct signaling outcomes, with L-treated SFs exhibiting the most potent and focused immune activation, while CP- and VC-treated cells display broader, but somewhat more diffuse, pathway engagement.

The GO enrichment analysis provides compelling evidence that enzymatic desialylation of SFs is a critical determinant of their innate immune activation potential. Treatments with CP, VC, and Lectenz sialidases each demonstrating varying degrees and linkage specific desialylation elicited robust enrichment of biological processes associated with early and innate immune responses. In contrast, AU-treated SFs, which displayed less cleavage of α2-3 sialic acids in lectin-based assays, showed no significant enrichment across GO terms, reinforcing the idea that a minimal threshold of desialylation is required to reprogram cellular function.

Specifically, CP-treated SFs uniquely exhibited significant enrichment in pathways such as type II interferon response, chemokine signalling, leukocyte migration, and cytokine-mediated signalling. These suggest an early inflammatory alert status possibly triggered by broad loss of terminal sialic acid capping, possibly occur due to the loss of α2-6 sialic acids.

Lectenz-treated SFs, which underwent the most complete and selective removal of α2-3-linked sialic acids, displayed the strongest enrichment across antiviral defence, positive regulation of immune activation, and innate immunity. This points to a critical regulatory role for α2-3 sialylation in maintaining SF immune responses. The observed activation of viral defence pathways in the absence of infection further suggests that α2-3 desialylation may be interpreted by SFs as a danger-associated molecular pattern (DAMP), capable of mimicking pathogen exposure.

Both VC- and L-treated SFs, which shared efficient α2-3 cleavage activity, converged on several overlapping GO biological processes including defense response to virus and regulation of innate immunity, indicating that α2-3 desialylation is not only sufficient, but perhaps the dominant trigger for immune-related gene activation in SFs. In contrast, the lack of any meaningful GO term enrichment in AU-treated SFs despite enzyme exposure underscores that less α2-3 linked sialic acid cleavage is insufficient to rewire the immune transcriptional landscape. These findings define a hierarchy of immune activation (AU < CP < VC < L), which mirrors the increasing efficiency of α2-3 desialylation observed across enzymes.

From a molecular function perspective, sialidase treatment significantly altered the functional potential of SFs, particularly in terms of ligand-receptor signaling. All effective desialylation treatments (CP, VC, L) showed enrichment in cytokine activity, a hallmark of an inflammatory phenotype. Furthermore, CP- and VC-treated SFs were enriched in CXCR chemokine receptor binding and G protein-coupled receptor binding, reflecting the upregulation of a chemotactic and signalling-competent transcriptional state. VC- and L-treated SFs, with selective α2-3 cleavage, also displayed shared enrichment in cytokine receptor binding, suggesting that targeted removal of α2-3 sialic acids is sufficient to prime SFs for enhanced responsiveness to inflammatory cues.

Collectively, the GO enrichment data support the concept that α2-3-linked sialic acids function as suppressive glycans, maintaining SFs in a homeostatic state. Their enzymatic removal triggers a transcriptional and functional shift toward a pro-inflammatory, immunocompetent state. This shift includes both intrinsic cytokine production and enhanced receptor-mediated signalling, which may contribute to pathological SF activation seen in diseases like RA. Importantly, the lack of response in AU-treated SFs provides a negative control, validating the specificity and threshold-dependent nature of glycan-mediated immune regulation.

Functionally, as reflected by the enhanced migratory potential of SFs exposed to conditioned media from desialylated cells, VC- and L-treated SFs, in particular, produced soluble factors that increased the wound-healing capacity of naïve SFs, likely via IL-6 and other inflammatory mediators. This paracrine effect recapitulates

a feed-forward loop observed in RA, where activated SFs propagate inflammation and invasion across tissue planes.

The integration of shared and specific gene signatures suggests that desialylation releases a conserved inflammatory transcriptional core in synovial fibroblasts, while enzyme-specific glycan editing selectively amplifies distinct immune-modulatory gene programs.

Together, these findings establish a mechanistic link between surface glycan remodelling, and the induction of a pro-inflammatory, tissue-invasive SF phenotype particularly affected by α2-3 sialic acid cleavage. While α2-6 cleavage by CP contributed to some gene expression changes, our data suggest that α2-3 desialylation alone is sufficient to reprogram SFs into an RA-like state, likely by disrupting inhibitory Siglec interactions or unmasking pro-inflammatory glycotopes. The use of AAL staining and unaffected fucosylation across all conditions further confirms that these effects are specific to sialic acid removal, not global glycan degradation.

In summary, targeted desialylation of SFs reveals a critical role for α2-3 sialylation in maintaining their anti-inflammatory homeostatic state. Enzymatic removal of sialic acid especially beyond a certain threshold initiates a robust inflammatory transcriptional program and functional activation reminiscent of rheumatoid arthritis. These findings position terminal sialic acids as promising therapeutic targets in chronic inflammatory disease.

To further elucidate how glycan remodelling via sialidase treatment of SFs may impact inflammatory processes, we next investigated the potential effects of conditioned media derived from differently treated SFs on macrophage polarisation. Specifically, we aimed to determine whether these conditioned media could preferentially drive macrophages toward either a pro-inflammatory M1 or an anti-inflammatory M2 phenotype. Given that distinct patterns of sialic acid cleavage could modulate the secretome of SFs, assessing macrophage polarisation in response to these conditioned media would clarify the immunological consequences of targeted desialylation and provide mechanistic insights into glycan-mediated immune regulation in rheumatoid arthritis. These questions will be explored in detail in the subsequent chapter, where we

systematically characterise the effect of SF-conditioned media on macrophage polarisation towards M1 or M2 phenotypes.

5. Chapter 5 Reprogramming Macrophage Polarisation Through Glycan Remodelling: Transcriptomic and Functional Insights into Sialidase-Treated Synovial Fibroblast-Macrophage Crosstalk in Rheumatoid Arthritis

5.1 Introduction

The preceding chapter demonstrated that targeted desialylation of SFs using distinct sialidase enzymes leads to pronounced transcriptomic shifts, notably within pathways associated with innate immunity and inflammation. Among these, treatments that removed α2-3-linked sialic acids, particularly those using VC and L sialidases, elicited the most robust activation of pro-inflammatory mediators. These findings suggest that surface sialylation plays a critical suppressive role in maintaining fibroblast homeostasis, and that its removal may act as a trigger for immune activation.

Given the central role of macrophages in orchestrating synovial inflammation and tissue remodelling in RA, it is crucial to understand how altered fibroblast glycosylation affects intercellular communication with innate immune cells. In this chapter, we investigate whether desialylated SFs modulate macrophage polarisation by conditioning the local inflammatory environment. Using BMDMs as responders, we exposed them to conditioned media from SFs treated with individual sialidases and profiled macrophage responses via transcriptomic and pathway-level analyses.

To benchmark the polarisation states induced by these treatments, we first established transcriptional profiles of classical (M1) and alternative (M2) macrophages stimulated with IFN-γ/LPS or IL-4, respectively. We then compared BMDMs cultured with sialidase-SF conditioned media to these canonical states using PCA, differential gene expression, heatmaps, and GSVA scores. The aim was to delineate whether specific glycan alterations on SFs can drive pro- or anti-inflammatory macrophage phenotypes, providing mechanistic insight into how fibroblast glycosylation may tune innate immune responses in RA.

To complement transcriptomic findings, we also evaluated protein-level expression of key macrophage markers indicative of polarisation and functional states. These included co-stimulatory molecules (PD-L1, CD40, CD80, CD86), tissue-remodelling and anti-inflammatory markers (CD206, MERTK, TREM2), and lymphatic-associated proteins (LYVE1). This multimodal analysis enabled us to map how fibroblast-derived cues shaped by glycan remodelling alter both the transcriptional programs and surface protein expression profiles of macrophages.

The following sections explore these intercellular dynamics in detail, highlighting how different modes of desialylation differentially imprint macrophage phenotypes potentially shifting the inflammatory landscape of the RA synovium.

5.2 Results

5.2.1 Transcriptomic Profiling Reveals Glycan-Dependent Reprogramming of Macrophage Polarisation by SF-Conditioned Media

To validate the polarisation of BMDMs, we performed a standardised gating strategy following surface marker staining. Bone marrow cells were differentiated in vitro using M-CSF for seven days, after which polarisation was induced by either IFN-γ and LPS for M1-like activation or IL-4 for M2-like activation, both for 24 hours. Flow cytometric gating involved initial identification of single, viable cells, followed by selection of $CD11b^{+}F4/80^{+}$ macrophages. Within this population, M1 polarisation was confirmed by increased expression of CD80, while M2 polarisation was characterised by elevated CD206 expression. Histograms demonstrated distinct expression profiles between groups, indicating successful and reproducible polarisation into M1- and M2-like phenotypes. These validated macrophage states served as transcriptional and phenotypic benchmarks for comparison with BMDMs exposed to SF-conditioned media in subsequent experiments (Figure 5-1).

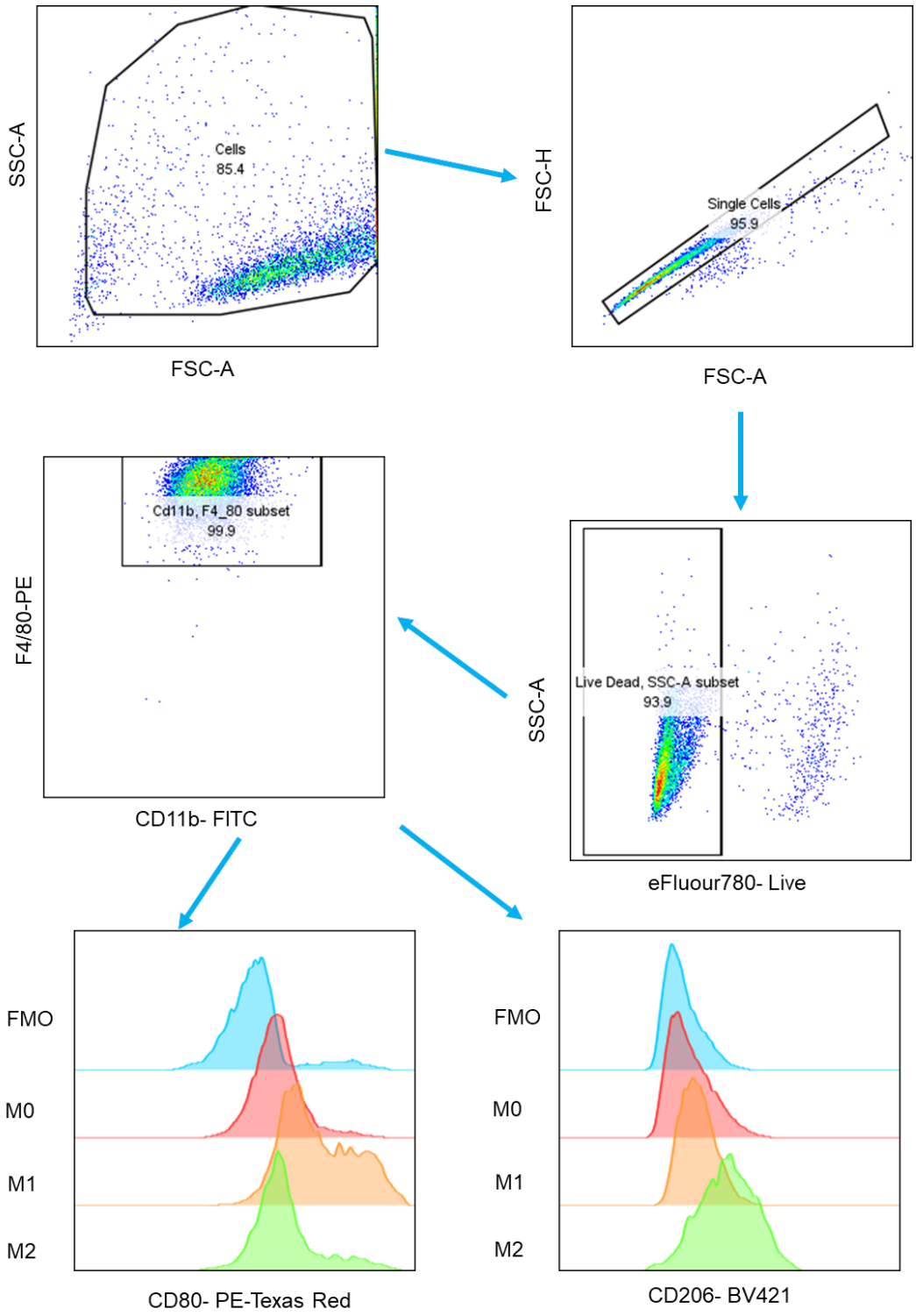

Figure 5-1 Gating strategy for Bone Marrow Derived Macrophages Polarisation.

Bone marrow cells cultured with 20ng/ml MCSF 7 days either polarised into to M1-like phenotype using 10ng/ml IFN-γ and 10ng/ml LPS or into M2-like phenotype with 10ng/ml IL-4 for 1 day. CD11b and F4/80 (M0), CD80 (M1) and CD206 (M2) markers used to detect appropriate states of BMDMs.

To evaluate how glycan remodelling of SFs influences macrophage polarisation, we cultured BMDMs with conditioned media collected from SFs treated with specific sialidases. These included CP, L, VC, and AU. To ensure that observed effects stemmed from fibroblast-secreted factors rather than residual enzyme activity, SFs were thoroughly washed after sialidase treatments, and conditioned media was collected 24 hours later for macrophage exposure. Following 7-day M-CSF-mediated differentiation, BMDMs were exposed to these conditioned media for 24 hours. As reference controls, M1 macrophages were generated using IFN-γ and LPS, while M2 macrophages were polarised using IL-4. Macrophages treated with supernatant from untreated SFs (NT) served as control. This experimental design enabled a systematic comparison of how distinct desialylation patterns in SFs reprogram macrophage responses (Figure 5-2).

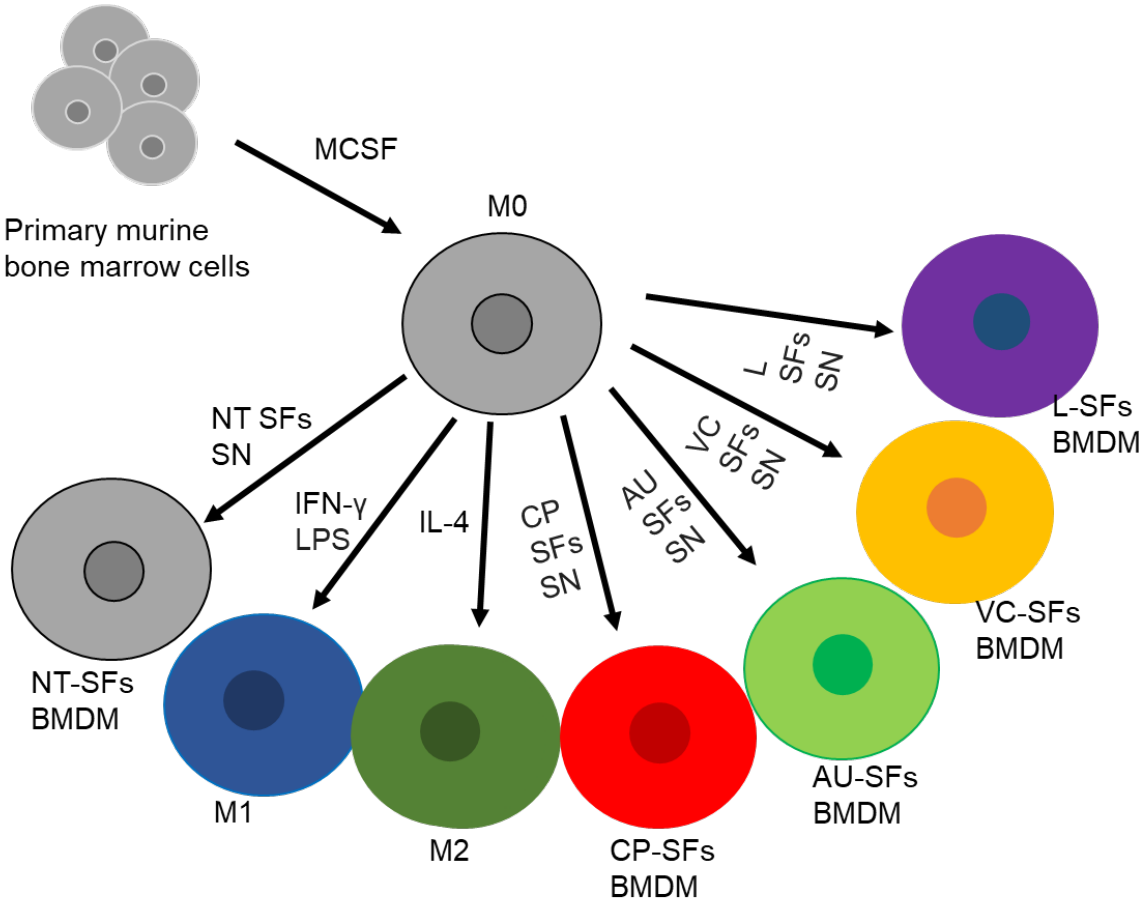

Figure 5-2 Experimental design for macrophage polarisation using sialidase-treated SF-conditioned media.

Bone marrow-derived macrophages (BMDMs) were differentiated from murine bone marrow cells in the presence of M-CSF for 7 days. Following differentiation, macrophages

were polarised for 24 hours into classical M1-like macrophages using IFN-γ and LPS, or into alternative M2-like macrophages using IL-4 (positive controls). In parallel, BMDMs were cultured with conditioned supernatants (SN) from SFs that had been pretreated with different sialidases: CP, AU, VC, or L, to assess the effect of glycan remodeling on macrophage polarisation. Untreated SF-conditioned media (NT) served as control. Each condition was subsequently analysed for transcriptomic and protein-level changes to evaluate polarisation outcomes.

This heatmap of DEGs in all conditions illustrates the diverse gene expression profiles induced in BMDMs by various conditioned media from sialidase treated SFs and by distinct macrophage polarisation states (Figure 5-3). Overall, samples exhibit strong clustering by their respective treatment groups, demonstrating that each condition elicits a unique transcriptional response. The most striking patterns are observed in the M1 and M2 macrophage polarisation states, which display highly distinct and often opposing up-regulation and down-regulation of large gene sets, indicative of their well-defined and antagonistic pro-inflammatory and anti-inflammatory phenotypes, respectively. In contrast to these strong polarisations, the CP-BMDM samples are distinctly positioned at the far right end of the heatmap, indicating a unique transcriptional signature separate from other treatments. Interestingly, the nontreated samples and those treated with AU-SF BMDMs appear to overlap significantly in their gene expression profiles, suggesting that the AU-conditioned media may not induce substantial changes compared to baseline, or that their effects are highly similar. Furthermore, BMDMs stimulated with conditioned media from L and VC-SFs cluster together, showing a specific impact on macrophage gene expression that is distinct from both the NT/AU group and the CP group. The clear clustering of genes into co-regulated blocks further highlights the coordinated transcriptional machinery at play, underscoring that different fibroblast treatments modulate the macrophage phenotype in distinct ways, with M1 and M2 polarisation representing the most potent drivers of gene expression alteration.

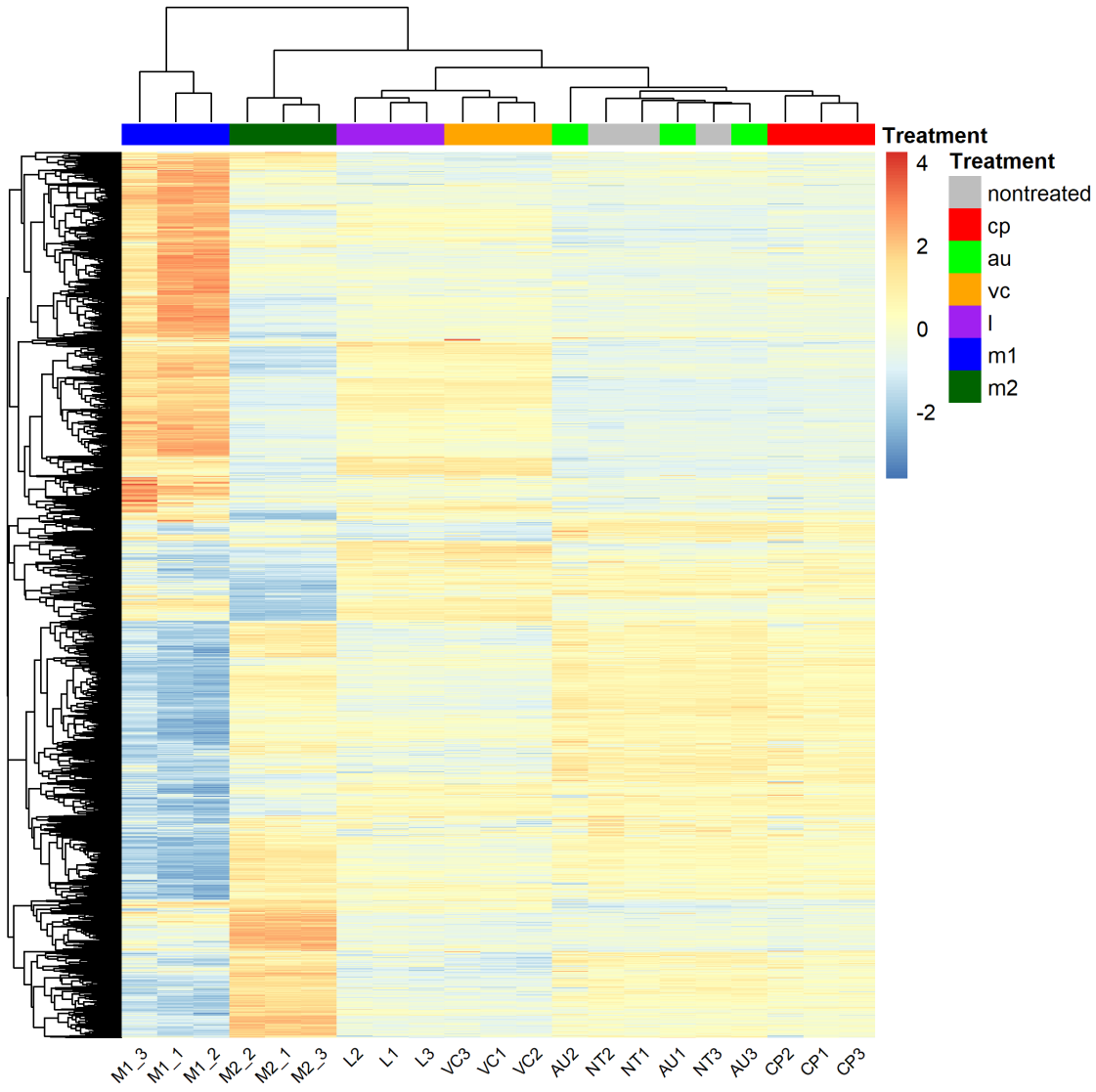

Figure 5-3 Differential Gene Expression Heatmap of BMDMs Cocultured with Sialidase Treated Synovial Fibroblasts Conditioned Media.

This heatmap provides a comprehensive visual summary of gene expression variations in BMDMs across different experimental conditions, representing the scaled expression levels (Z-scores) of differentially expressed genes where red denotes higher and blue indicates lower relative expression. The columns represent individual samples, organised by a top dendrogram that clusters samples with similar gene expression profiles, while the rows represent genes, clustered by their co-expression patterns. A crucial annotation bar at the top, coloured according to the provided legend, distinguishes the Treatment condition for each sample: nontreated (grey), cp (red), au (green), vc (orange), l (purple), m1 (blue), and and m2 (dark green).

PCA was performed to evaluate the global transcriptional variance across macrophage samples exposed to conditioned media from SFs treated with various

sialidases. In the first PCA plot, which includes reference populations (M1, M2, and non-polarised macrophages), BMDMs treated with L- and VC-sialidase-conditioned media (L1-3, VC1-3) clustered separately from untreated (NT1-3), AU-treated, and CP-treated groups along the PC1 axis, indicating a distinct transcriptional profile. Notably, L- and VC-treated groups were positioned closer to the M1 reference cluster, suggesting a shift toward a pro-inflammatory macrophage phenotype. Conversely, M2-polarised macrophages clustered on the opposite side of the PC1 axis, confirming separation of polarisation states (Figure 5-4A).

In the second PCA plot, which excludes M1 and M2 reference samples to enhance resolution among the experimental conditions, distinct clustering of L- and VC-treated macrophages persisted, reinforcing the observation that α2-3 sialidase treatments exert a strong and consistent influence on macrophage gene expression. NT-, AU-, and CP-treated groups clustered closely together, indicating relatively subtle transcriptomic changes. These results suggest that desialylation of SFs, particularly the removal of α2-3-linked sialic acids, reprograms macrophage phenotypes at the transcriptional level, with a tendency toward M1-like polarisation (Figure 5-4B).

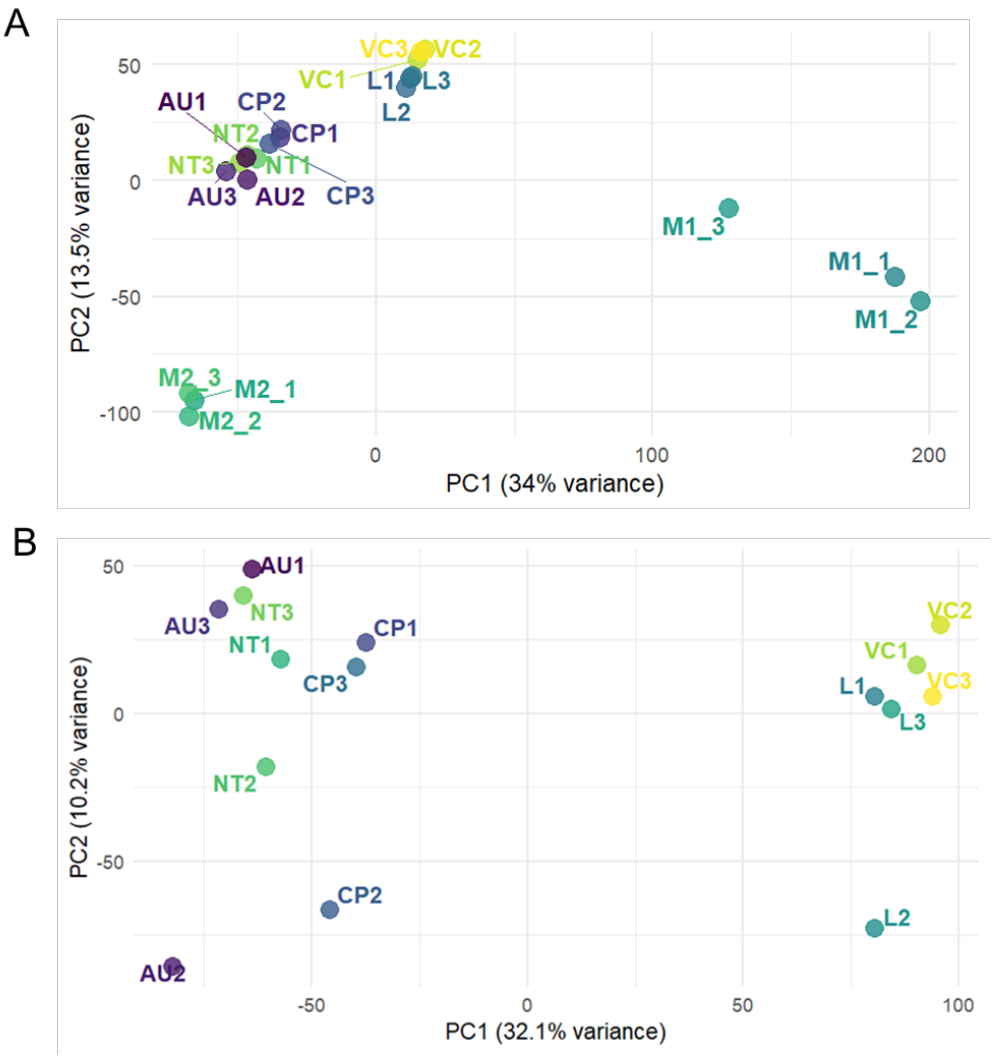

Figure 5-4 Principal Component Analysis (PCA) Bone Marrow Derived Macrophages (BMDMs) cocultured with desialylated SFs supernatants.

RNA-Seq was used to analysed gene expression in BMDMs cocultured with desialylated SFs supernatants. A) PCA plot shows the distribution of all samples based on gene expression profiles, x-axis shows the first principal component (PC1) accounting for 34.0% of the variance, y-axis represents the second principal component (PC2) accounting for 13.5%. B) PCA plot shows the distribution of samples except M1 and M2 macrophages based on gene expression profiles, x-axis shows the first principal component (PC1) accounting for 32.1% of the variance, y-axis represents the second principal component (PC2) accounting for 10.2%. Each dot represents individual BMDMs with different conditions, with colours distinguishing between groups. Each triplicates (1-3) represents a distinct treatment groups: CP-BMDMs, AU-BMDMs, VC-BMDMs, and L-

BMDMs. NT-BMDMs represent control macrophages with no sialidase treatments (buffer only).

To establish a transcriptional reference for classical (M1) macrophage activation, BMDMs were stimulated with IFN-γ and LPS and compared to NT macrophages. The volcano plot shows a substantial number of significantly differentially expressed genes, with a strong skew toward upregulation in the M1 condition (Figure 5-5A-B). Key upregulated genes included pro-inflammatory and interferon response markers such as Ifnb1, Gbp4, Slamf1, Adora2a, Cxcl10, Il1b, Serpina3f, and Nos2. Conversely, several genes associated with tissue remodelling, or alternative activation including Tmem204, Hoxa4, and Rasgrp3 were significantly downregulated in M1 macrophages (Figure 5-5C).

The heatmap further supports these findings, revealing clear segregation between NT and M1 groups, with consistent upregulation of immune activation genes in the M1 cluster. These transcriptional signatures confirm successful induction of M1 polarisation and establish a reference framework for comparing macrophage responses to SF-conditioned media in downstream experiments.

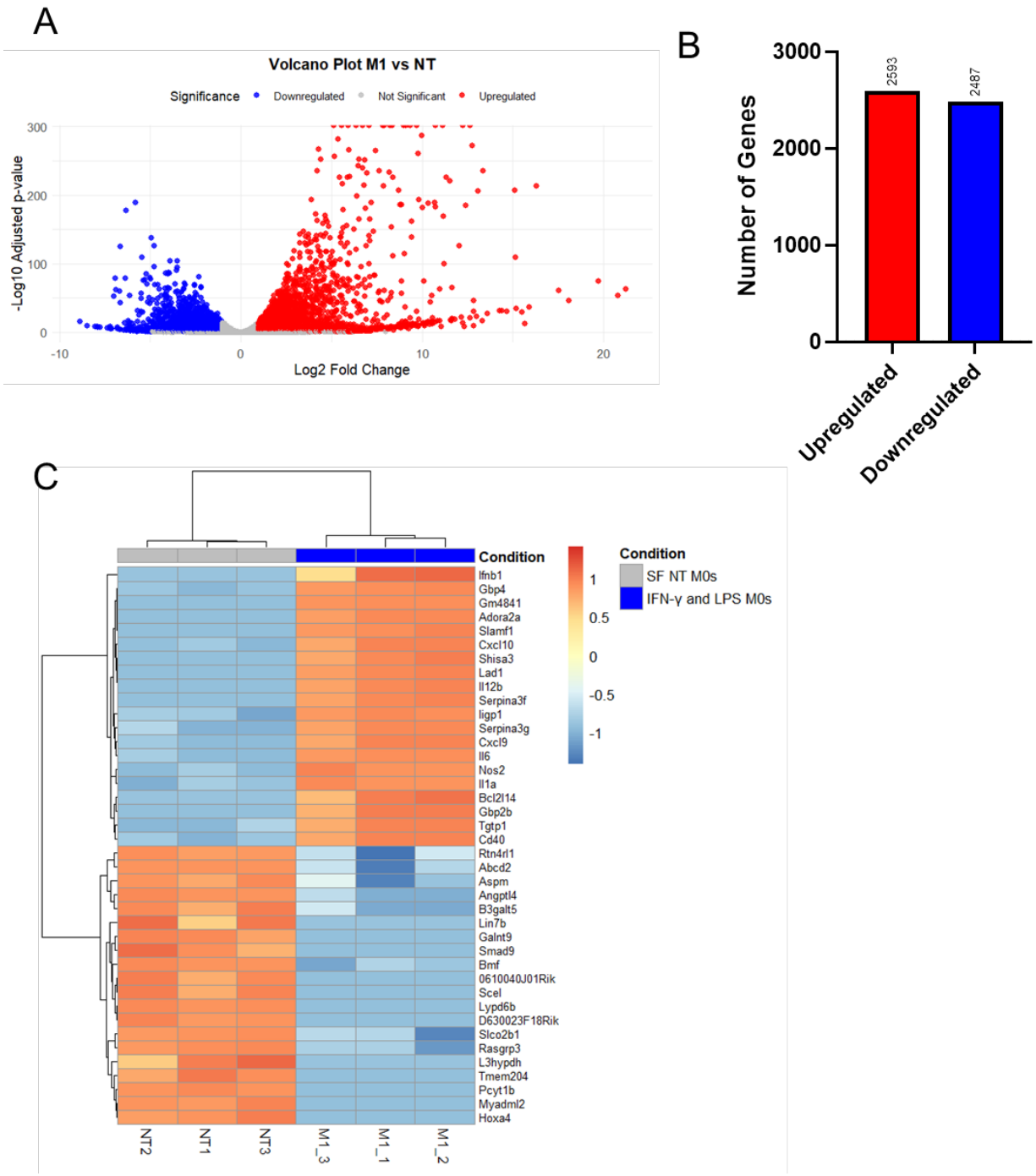

Figure 5-5 Bone Marrow Derived Macrophages Stimulated with IFN-γ and LPS shows M1-like Polarisation Profiles.

BMDMs stimulated with IFN-γ and LPS demonstrated a M1 like phenotype where differential gene expression was analysed using DESeq2, with significance defined as $|\log_2 FC| > 1$ and padj < 0.05.

A) Volcano Plot: Displays differentially expressed genes (DEGs) in M1-like vs. SF-NT BMDMs control. Upregulated (red) and downregulated (blue) genes met the significance

threshold, while non-significant genes are not met the significance shown in grey.
B) Bar Graph: Shows the number of significantly up- and downregulated genes, revealing a similar distribution.
C) Heatmap: Highlights the top 20 DEGs, with red indicating high and blue low expression. Clustering groups samples by similarity, annotated by sample location and condition. Gene expression values are $\log_2$-transformed, and Z-score normalised (row-scaled).

To define the transcriptional profile of alternatively activated (M2) macrophages, BMDMs were stimulated with IL-4 and compared to NT macrophages. The volcano plot demonstrates substantial transcriptional reprogramming, with a wide distribution of significantly upregulated and downregulated genes (Figure 5-6A-B). Among the most prominently upregulated genes in the M2 condition were Serpina3g, Retnla, Il34, Pla2g4a, Serpina3f, and Adipoq, which are the genes commonly associated with tissue repair, anti-inflammatory responses, and alternative macrophage activation. In contrast, several genes highly expressed in NT macrophages, including Tal2, Has1, and Ccr1, were downregulated in IL-4 stimulated macrophages (Figure 5-6C).

The corresponding heatmap clearly distinguishes M2-polarised macrophages from NT controls, with M2 samples clustering together and showing consistent upregulation of M2-associated transcripts. These results confirm the effective induction of an M2 phenotype at the transcriptomic level and provide a reliable reference for downstream comparisons with macrophages exposed to SF-conditioned media.

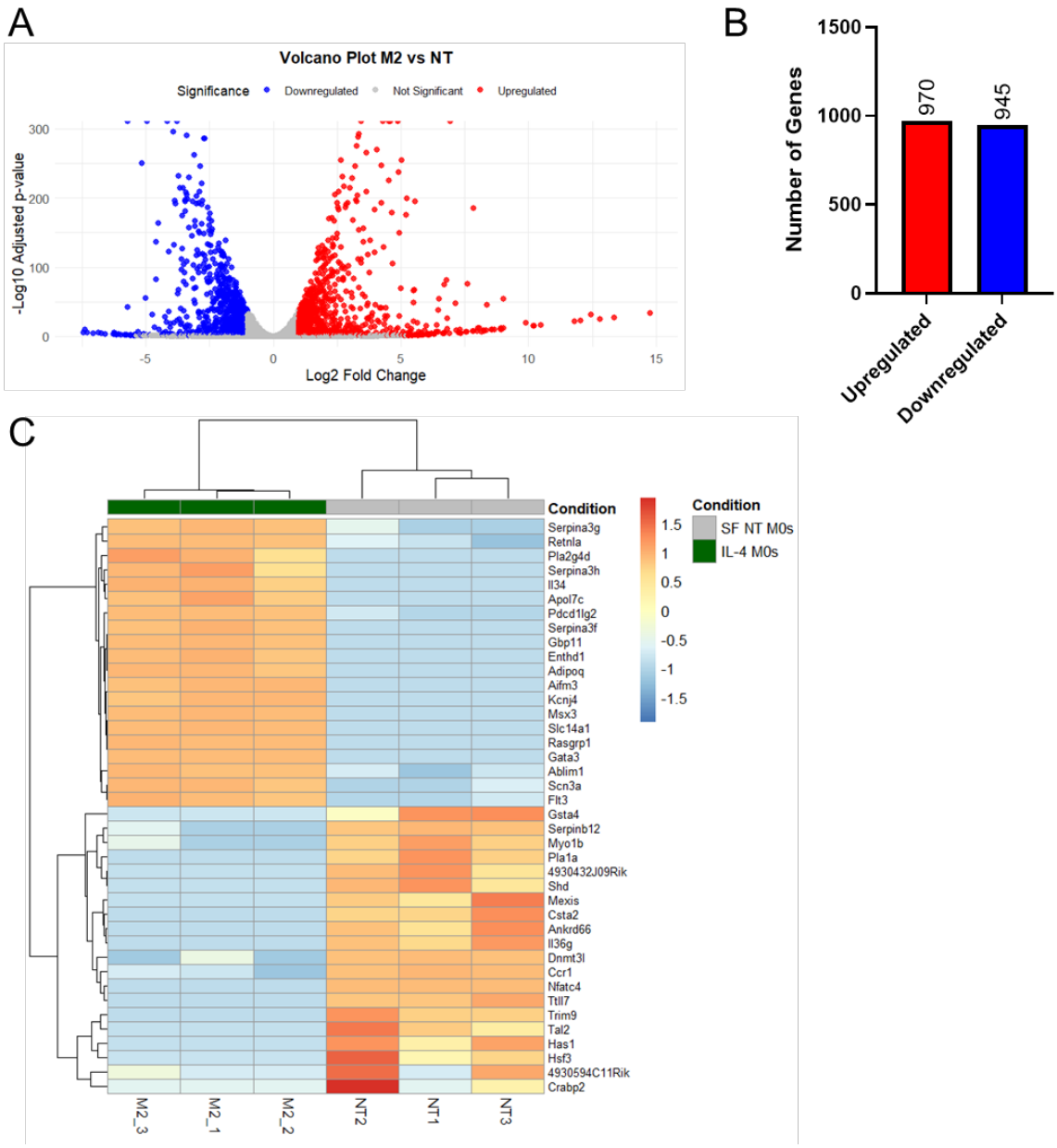

Figure 5-6 Bone Marrow Derived Macrophages Stimulated with IL-4 shows M2-like Polarisation Profiles.

BMDMs stimulated with IL-4 demonstrated a M2 like phenotype where differential gene expression was analysed using DESeq2, with significance defined as $|\log_2 FC| > 1$ and padj < 0.05.

A) Volcano Plot: Displays differentially expressed genes in M2-like vs. SF-NT BMDMs control. Upregulated (red) and downregulated (blue) genes met the significance threshold, while non-significant genes are not met the significance shown in grey.

B) Bar Graph: Shows the number of significantly up- and downregulated genes, revealing

a similar distribution.
C) Heatmap: Highlights the top 20 DEGs, with red indicating high and blue low expression. Clustering groups samples by similarity, annotated by sample location and condition. Gene expression values are $\log_2$-transformed, and Z-score normalised (row-scaled).

To assess how broad desialylation of SFs influences macrophage activation, BMDMs were exposed to conditioned media from SFs treated with CP sialidase. CP is a broad-spectrum sialidase that cleaves both α2-3 and α2-6-linked sialic acids, resulting in extensive glycan remodeling on the fibroblast surface.

Transcriptomic profiling revealed a modest yet distinct transcriptional response in CP-SF BMDMs. The volcano plot shows a mild skew toward gene upregulation, and although fewer genes reached significance compared to classical M1 or M2 polarisation (Figure 5-7A-B). Further analysis on the heatmap exhibited several key inflammatory mediators such as Il1b, Ccl7, Cxcl3, Grb10, Ccl6, and Socs2 were upregulated. The induction of Arg1, a hallmark of alternatively activated macrophages with known regulatory and tissue-repair functions, alongside chemokines and feedback inhibitors of inflammation, indicates a mixed or hybrid macrophage phenotype (Figure 5-7C). This intermediate activation pattern, which does not fully align with canonical M1 or M2 profiles. These results suggest that the dual cleavage of α2-3 and α2-6 sialic acids on SFs by CP treatment results in a partially polarised macrophage state, characterised by both pro-inflammatory signalling and induction of immunoregulatory mechanisms.

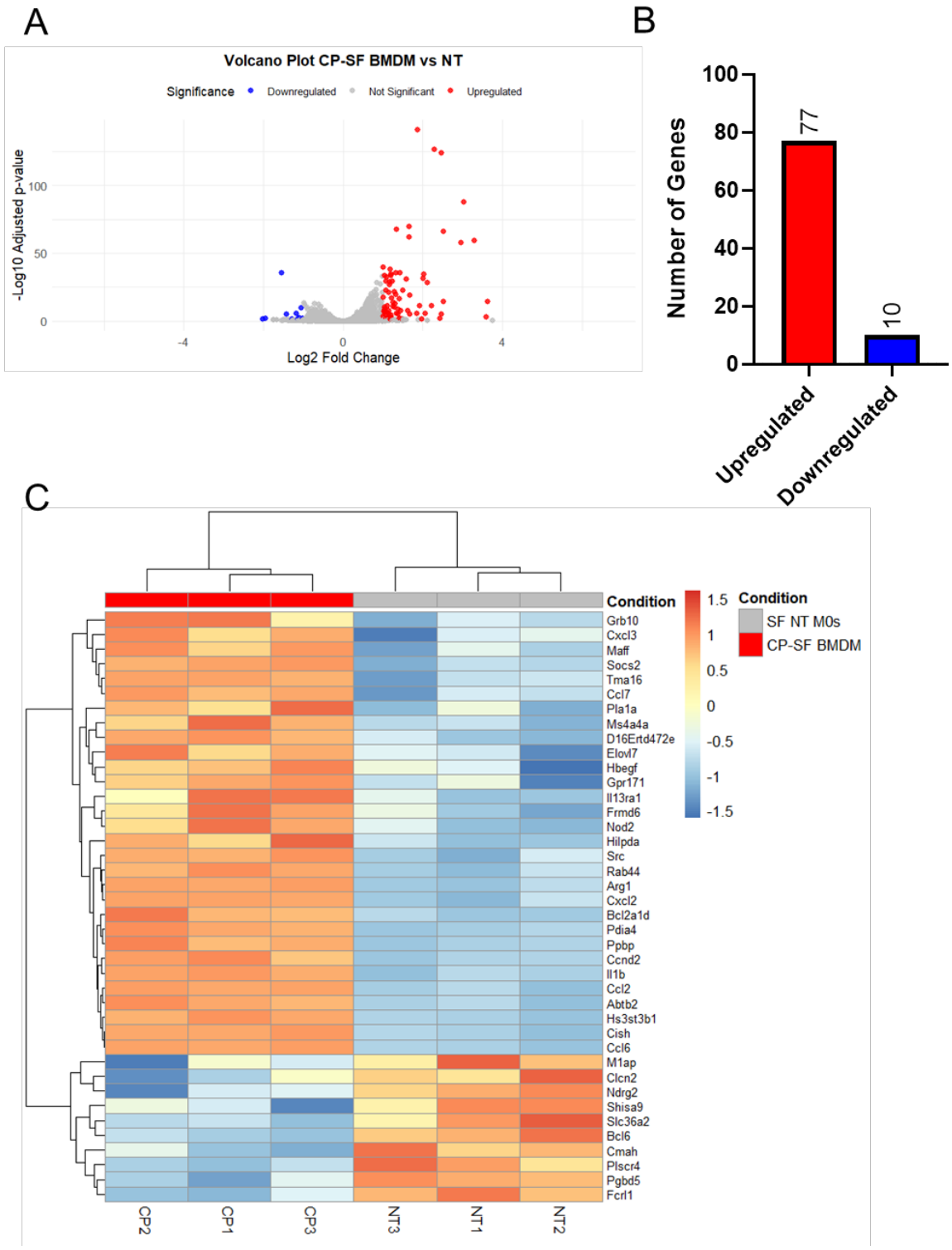

Figure 5-7 Bone Marrow Derived Macrophages Cocultured with CP-treated SF Supernatants Show Changes in Transcriptomic Profiles.

Differential gene expression was analysed using DESeq2, with significance defined as $|\log_2 FC| > 1$ and padj < 0.05.

A) Volcano Plot: Displays differentially expressed genes (DEGs) in CP-SF BMDM vs. SF-NT BMDMs (control. Upregulated (red) and downregulated (blue) genes met the

significance threshold, while non-significant genes are not met the significance shown in grey.
B) Bar Graph: Shows the number of significantly up- and downregulated genes, revealing a distinct distribution.
C) Heatmap: Highlights the top DEGs, with red indicating high and blue low expression. Clustering groups samples by similarity, annotated by sample location and condition. Gene expression values are log_2-transformed, and Z-score normalised (row-scaled).

To assess the impact of α2-3 desialylation on synovial fibroblast-macrophage communication, BMDMs were treated with conditioned media from AU sialidase-treated SFs (AU-SF BMDM). Unlike VC or L sialidases, AU has least activity toward α2-3 linked sialic acids, with cleavage efficiency remaining below the threshold required to elicit a robust glycoimmune response in naïve SFs. This was reflected in the transcriptional response of BMDMs, which showed only a subtle shift in gene expression. The volcano plot indicates very few significantly differentially expressed genes, with low log2 fold changes (Figure 5-8A-B).

The heatmap further supports this muted response with the genes involved in interferon signalling and chemokine production, such as Ifit1, Ifit2, Oasl2, and Cxcl2, showed significantly downregulation in AU-SF treated macrophages compared to NT controls. However, a few genes such as Il1a and Cxcl2 exhibited significant upregulation in AU-SF BMDMs (Figure 5-8C). These findings suggest that α2-3 sialic acid removal below a functional threshold is insufficient to reprogram the SF secretome in a way that activates macrophages. Thus, the AU-SF BMDM condition reinforces the importance of α2-3 linked sialic acids as key immunosuppressive structures and demonstrates that their partial cleavage on SFs under certain thresholds does not provoke macrophage polarisation.

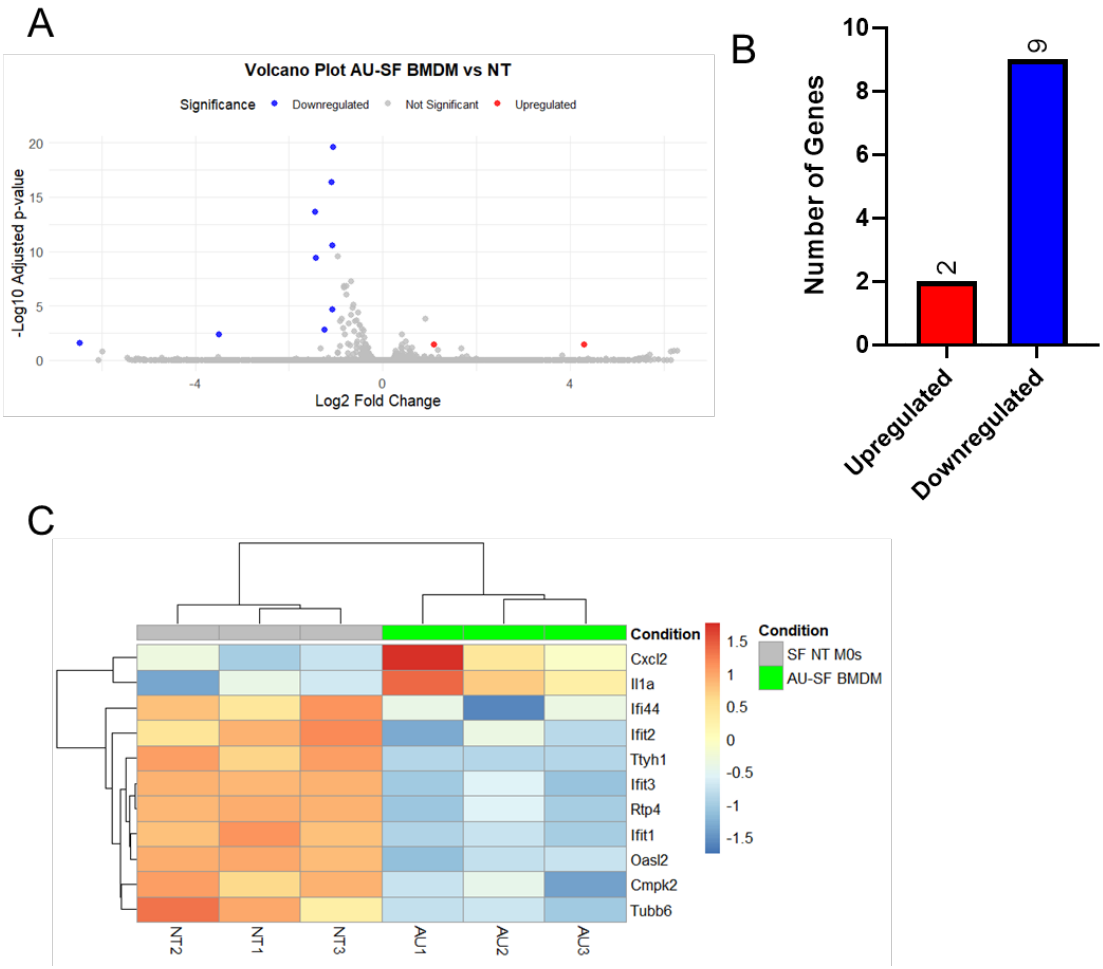

Figure 5-8 Bone Marrow Derived Macrophages Cocultured with AU-treated SF Supernatants Show Minimal Changes in Transcriptomic Profiles.

Differential gene expression was analysed using DESeq2, with significance defined as $|\log_2 FC| > 1$ and padj < 0.05.

A) Volcano Plot: Displays differentially expressed genes in AU-SF BMDM vs. SF-NT BMDMs control. Upregulated (red) and downregulated (blue) genes met the significance threshold, while non-significant genes are not met the significance shown in grey.
B) Bar Graph: Shows the number of significantly up- and downregulated genes, revealing a distinct distribution.
C) Heatmap: Highlights the top DEGs, with red indicating high and blue low expression. Clustering groups samples by similarity, annotated by sample location and condition. Gene expression values are $\log_2$-transformed, and Z-score normalised (row-scaled).

To determine the specific immunomodulatory effects of α2-3 sialic acid removal on macrophage activation, BMDMs were treated with conditioned media from VC-treated SFs (VC-SF BMDM), which cleaves α2-3-linked sialic acids with high

efficiency. Transcriptomic analysis revealed a robust inflammatory response. The volcano plot shows a large number of significantly upregulated genes, many with high fold changes, indicating strong activation of pro-inflammatory and interferon-regulated pathways (Figure 5-9A-B). The accompanying heatmap highlights the induction of key inflammatory genes such as Il6, Il1bos, Il1a, Nos2, Saa3, Ligp1, and Rsad2, which are strongly associated with type I interferon signalling, NF-κB activation, and macrophage effector responses (Figure 5-9C).

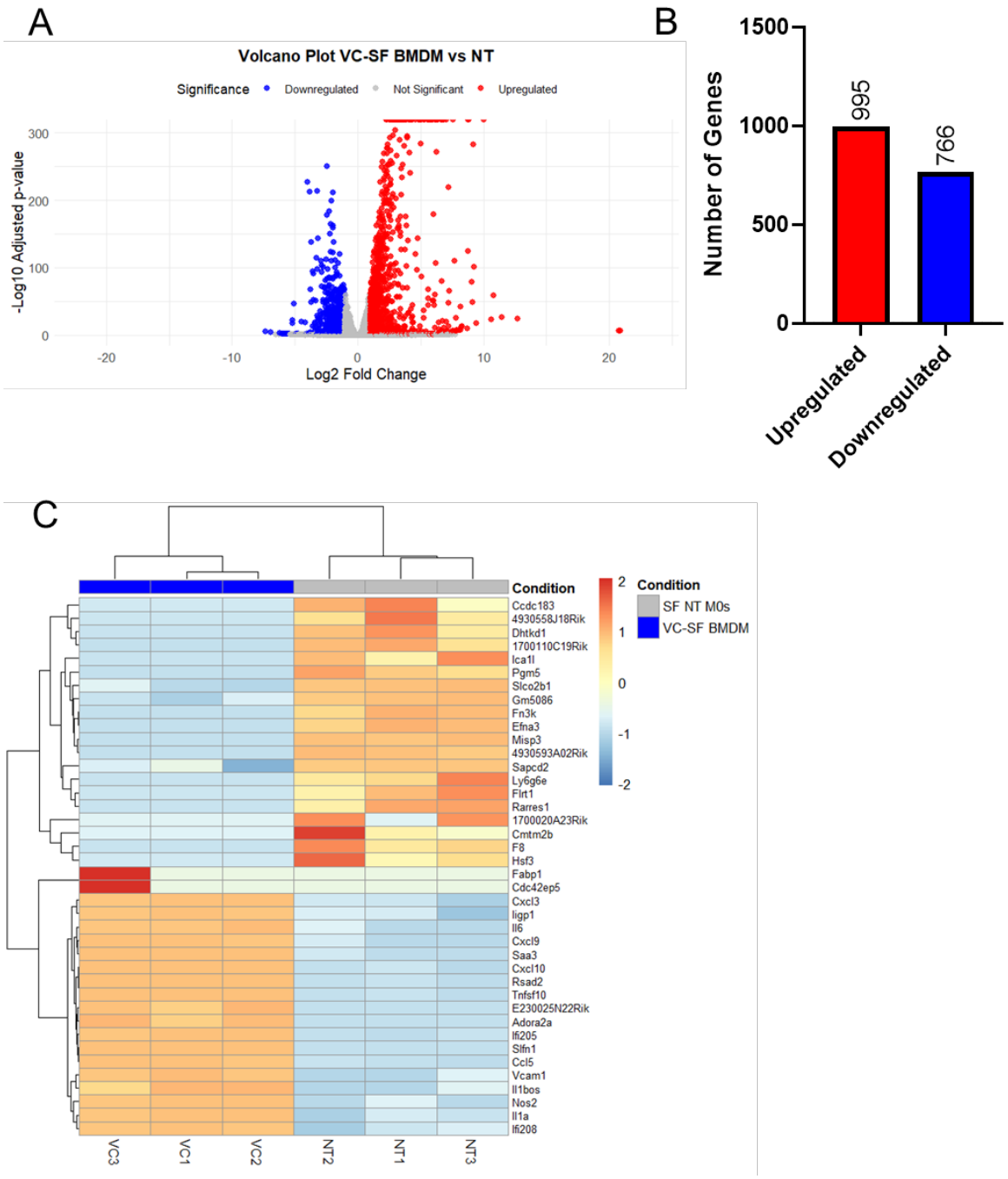

Figure 5-9 Bone Marrow Derived Macrophages Cocultured with VC-treated SF Supernatants Show Changes in Transcriptomic Profiles.

Differential gene expression was analysed using DESeq2, with significance defined as $|\log_2 FC| > 1$ and padj < 0.05.

A) Volcano Plot: Displays differentially expressed genes in VC-SF BMDM vs. SF-NT BMDMs control. Upregulated (red) and downregulated (blue) genes met the significance threshold, while non-significant genes are not met the significance shown in grey.
B) Bar Graph: Shows the number of significantly up- and downregulated genes, revealing a distinct distribution.
C) Heatmap: Highlights the top DEGs, with red indicating high and blue low expression. Clustering groups samples by similarity, annotated by sample location and condition. Gene expression values are $\log_2$-transformed, and Z-score normalised (row-scaled).

When compared to CP-SF BMDMs, the VC-SF condition elicited a far more potent activation profile. Although CP sialidase removes both α2-3 and α2-6 linkages, the transcriptional response in CP-SF BMDMs was notably weaker, with only modest upregulation of inflammatory mediators. This suggests that dual desialylation may have a dampening or balancing effect, possibly due to the removal of α2-6 linked sialic acids that normally constrain excessive inflammatory signalling.

In contrast, AU-SF BMDM, which reflects sialylation patterns with α2-3 cleavage below the activation threshold, failed to induce a meaningful macrophage response. Only a handful of genes showed minimal changes, reinforcing the interpretation that α2-3 linked sialic acids are the dominant suppressive glycans modulating fibroblast and macrophage signalling. Together, these findings demonstrate that selective α2-3 desialylation triggers a highly inflammatory macrophage phenotype, while either least cleavage by AU-sialidase or broad desialylation by CP sialidase leads to a muted or hybrid response.

Treatment of BMDMs with conditioned media from L-treated SFs (L-SF BMDM), which exhibit maximal cleavage of α2-3-linked sialic acids, resulted in a robust transcriptional activation of inflammatory programs. The volcano plot revealed widespread upregulation of genes, with several showing high fold changes and strong statistical significance (Figure 5-10A-B). The heatmap demonstrates this pronounced response, marked by induction of pro-inflammatory mediators such as Il6, Cxcl9, Cxcl10, Tnfsf10, and Nos2, alongside elevated expression of interferon-stimulated genes including Ligp1, Rsad2, Ifi213, and Gbp4 (Figure 5-10C).

Importantly, the strong upregulation of Gbp4, a canonical target of IFN-γ signaling, highlights activation of type II interferon pathways and polarisation toward an M1-like inflammatory state. These transcriptional changes suggest that extensive α2-3 desialylation on SFs removes key glycan-based suppressive signals, unleashing a potent macrophage activating response.

Compared to other sialidase treatments, L-SF BMDMs elicited the most pronounced pro-inflammatory gene expression, underscoring the dominant immunomodulatory role of α2-3 sialic acids in maintaining fibroblast-mediated immune suppression under homeostatic conditions.

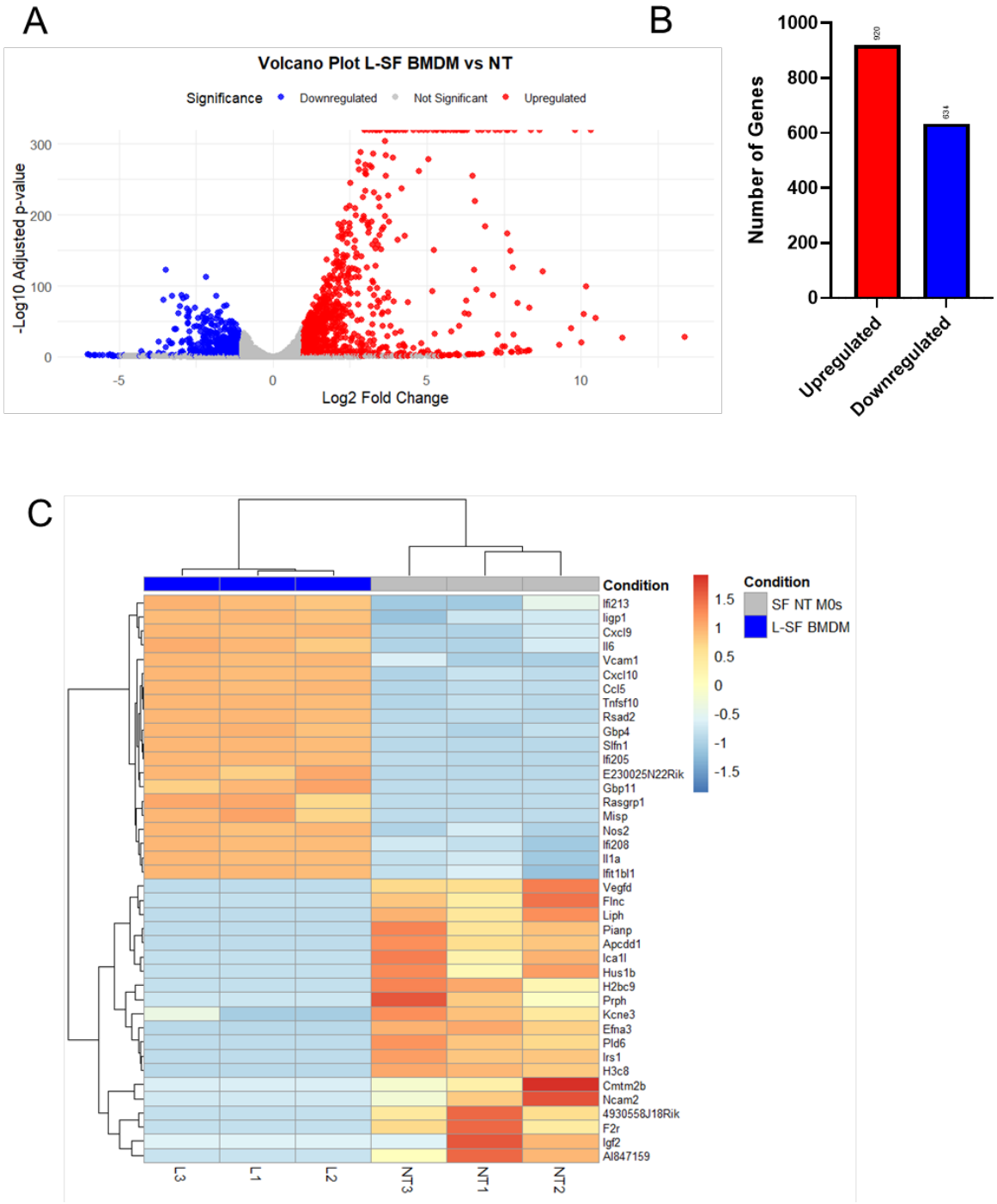

Figure 5-10 Bone Marrow Derived Macrophages Cocultured with L-treated SF supernatants Show Changes in Transcriptomic Profiles.

Differential gene expression was analysed using DESeq2, with significance defined as $|\log_2 FC| > 1$ and padj < 0.05.

A) Volcano Plot: Displays differentially expressed genes in L-SF BMDM vs. SF-NT BMDMs control. Upregulated (red) and downregulated (blue) genes met the significance threshold, while non-significant genes are not met the significance shown in grey.

B) Bar Graph: Shows the number of significantly up- and downregulated genes, revealing a distinct distribution.

C) Heatmap: Highlights the top DEGs, with red indicating high and blue low expression. Clustering groups samples by similarity, annotated by sample location and condition. Gene expression values are log_2-transformed, and Z-score normalised (row-scaled).

KEGG pathway enrichment analysis revealed that BMDMs exhibit distinct transcriptional responses when cocultured with conditioned media from sialidase-treated SFs (Figure 5-11A). BMDMs exposed to CP-conditioned media showed significant enrichment of multiple pro-inflammatory and immune-related pathways, including IL-17 signalling, TNF signalling, NF-κB signalling, NOD-like receptor signalling, cytokine-cytokine receptor interaction, and chemokine signalling, as well as disease-associated pathways such as rheumatoid arthritis, bladder cancer, and prolactin signalling. In contrast, VC-conditioned BMDMs displayed selective enrichment in the cell cycle and measles pathways, suggesting a more focused and potentially antiviral or proliferative response. Lectenz-conditioned BMDMs (L) specifically enriched the Kaposi sarcoma-associated herpesvirus infection pathway.

Beyond these distinct signatures, VC-, CP-, and L-conditioned BMDMs all shared enrichment of TNF-α and NF-κB signaling pathways with M1-polarised macrophages, indicating convergence toward classical inflammatory activation. Only CP-conditioned BMDMs shared the chemokine signalling pathway with M2-polarised macrophages, suggesting that CP-induced factors may also partially engage alternative activation programs. Additionally, VC- and L-conditioned BMDMs showed enrichment in a set of shared antiviral and inflammatory pathways, including influenza A, herpes simplex virus 1, Epstein-Barr virus infection, NOD-like receptor signalling, and TNF-α signalling, further supporting their pro-inflammatory and antiviral transcriptional states. Both CP and L conditions led to enrichment of the rheumatoid arthritis pathway, reinforcing the disease relevance of these desialylation-driven effects. Together, these findings highlight how SF-derived signals, shaped by sialic acid content, can differentially instruct macrophage activation and inflammatory pathway engagement. In contrast to the other conditions, BMDMs cocultured with conditioned media from AU-treated SFs showed no significant enrichment in KEGG pathways. This suggests that AU-mediated desialylation of SFs does not induce a secretory profile capable of triggering major transcriptional changes in macrophages under these experimental conditions. The absence of pathway enrichment highlights the

specificity of sialidase effects on SF-macrophage communication and underscores that desialylation under certain thresholds are not sufficient to reprogram macrophage responses.

GO Biological Process enrichment analysis revealed that BMDMs exhibit distinct immune activation profiles depending on the sialidase treatment applied to SFs, reflecting differential paracrine signalling (Figure 5-11B). BMDMs cocultured with AU-conditioned media showed enrichment in antiviral defence-related pathways, including defence response to virus, response to virus, response to interferon-alpha, antiviral innate immune response, and cellular response to molecules of bacterial origin. These results suggest that even though AU treatment had minimal impact in other analyses, it can still prime SFs to secrete factors capable of engaging antiviral and innate immune mechanisms in macrophages.

In contrast, CP-conditioned media led to enrichment in chemotactic and cellular migration pathways, including neutrophil chemotaxis, granulocyte migration, leukocyte chemotaxis, and cell chemotaxis, along with cellular response to bacterial origin. This implies that CP-treated SFs produce signals that promote macrophage activation linked to immune cell recruitment and migration, reflecting a pro-inflammatory, antibacterial-like response. VC- and L-conditioned BMDMs shared a highly similar enrichment profile, marked by significant activation of response to interferon-beta, defence response to virus, response to virus, activation of innate immune response, positive regulation of innate immune response, and regulation of innate immune response. These pathways suggest that desialylation by VC and L induces a strong interferon-mediated antiviral program in BMDMs, comparable to that seen with classical immune stimulation.

Interestingly, the cytokine-mediated signalling pathway was significantly enriched in CP-, VC-, and L-conditioned BMDMs, as well as in M1 macrophages, indicating that these conditions converge on cytokine-driven inflammatory programming.

Meanwhile, M2 macrophages showed a distinct and less inflammatory enrichment pattern, characterised by regulation of angiogenesis, small GTPase-mediated signal transduction, taxis, and chemotaxis which are hallmarks of tissue remodelling and wound-healing responses.

GO Molecular Function enrichment analysis revealed condition-specific activation of signalling and receptor pathways in BMDMs exposed to conditioned media from desialylated SFs, highlighting how distinct glycan alterations in SFs can shape macrophage receptor engagement and effector functions.

BMDMs cocultured with AU-conditioned media showed enrichment in a diverse set of molecular functions, including phosphotransferase activity, nucleoside monophosphate and diphosphate kinase activities, and nucleobase-containing compound kinase activity, suggesting alterations in nucleotide metabolism and signalling. Additionally, AU-conditioned BMDMs also enriched intercellular chloride channel activity, CXCR chemokine receptor binding, chemokine activity, and G protein-coupled receptor (GPCR) binding, indicating engagement of chemokine signalling and ion channel regulation.

CP-conditioned BMDMs were enriched for chemokine activity, chemokine receptor binding, kinase receptor activity, as well as heparin and glycosaminoglycan binding. These results suggest CP treatment leads to a microenvironment that promotes macrophage responses linked to cytokine signalling, extracellular matrix interaction, and immune cell recruitment. VC- and L-conditioned BMDMs demonstrated similar molecular signatures, showing enrichment in CXCR chemokine receptor binding, chemokine activity, and GPCR binding, consistent with activation of chemokine-driven immune responses. Importantly, cytokine activity was significantly enriched across AU-, CP-, VC-, and L-conditioned BMDMs, as well as in M1-polarised macrophages, underscoring a shared activation of inflammatory signalling pathways in these pro-inflammatory contexts. In contrast, M2 macrophages exhibited enrichment in functions related to cellular regulation and homeostasis, including diacylglycerol binding, histone methyltransferase binding, histone acetyltransferase binding, and sodium ion binding, reflecting epigenetic remodelling and ionic regulation typically associated with resolution and tissue repair (Figure 5-11C).

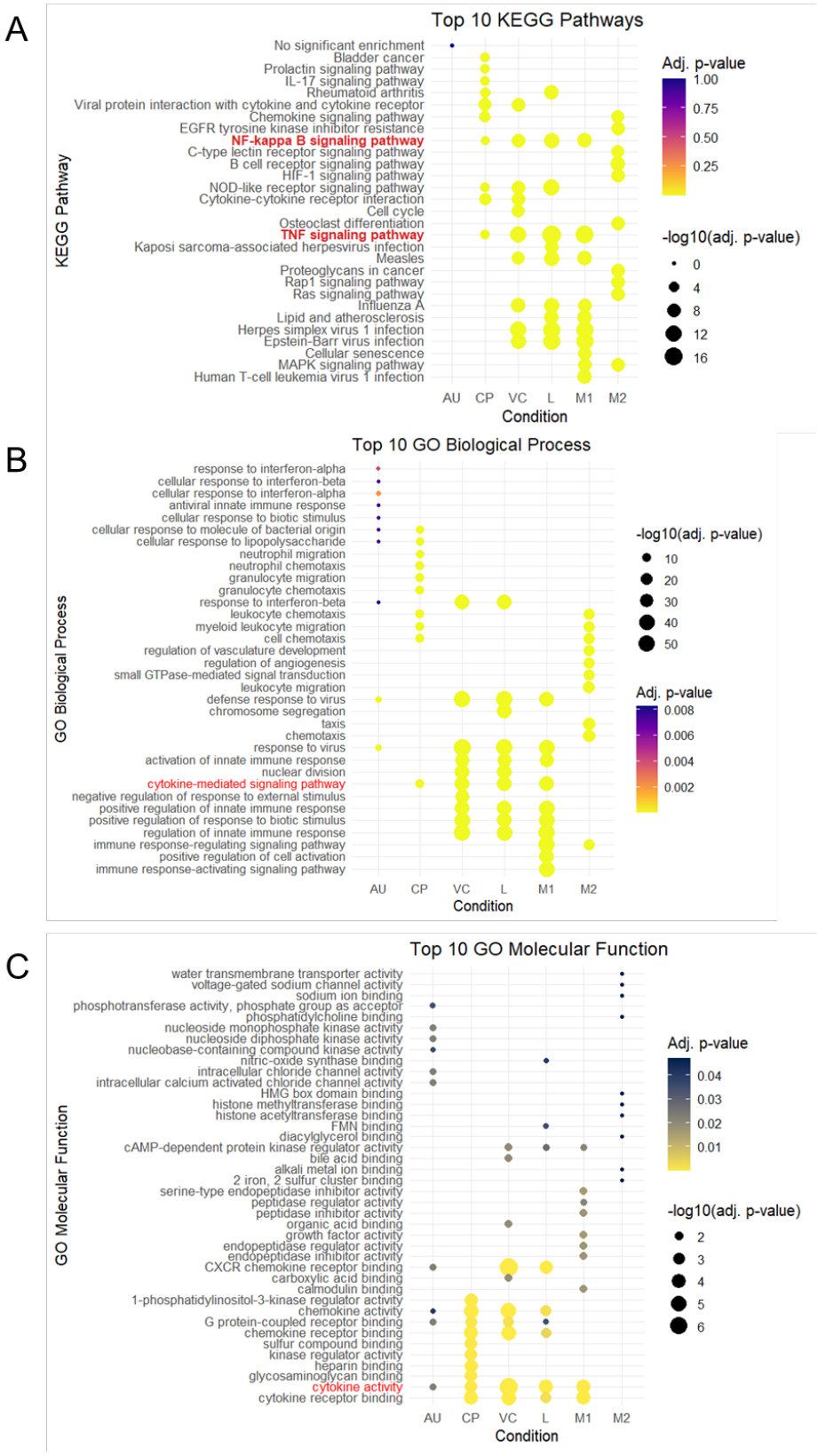

Figure 5-11 Comparative functional enrichment analysis of differentially expressed genes in BMDMs cocultured with different sialidase treated synovial fibroblasts conditioned media.

A) KEGG pathway enrichment analysis , B) GO Biological Process enrichment analysis, and C) GO Molecular Function enrichment of BMDMs cocultured with conditioned media from sialidase-treated SFs.

Dot size represents the strength of enrichment ($-\log_{10}$ adjusted p-value), and colour indicates statistical significance.

Gene Set Variation Analysis (GSVA) is a computational method that assesses the enrichment of gene sets at the individual sample level, transforming gene expression data into a pathway activity profile for each sample. This is particularly advantageous as it allows for the investigation of small, yet biologically significant, changes in pathway activity without the need for pre-defined experimental groups, making it ideal for exploring heterogeneity within a dataset and identifying distinct molecular phenotypes. Here, GSVA was applied to investigate the polarisation state of BMDMs subsequent to their co-culture with conditioned media derived from sialidase-treated SFs. The central aim was to understand whether these BMDMs would adopt an M1-like (pro-inflammatory) or M2-like (anti-inflammatory, tissue-remodelling) macrophage polarisation profile in response to the varied conditioned media, particularly in comparison to a non-treated baseline. The functional state of synovial fibroblasts is known to be significantly altered by inflammation and glycosylation changes, including sialylation, which can, in turn, influence immune cell responses.

Examination of the M1 Signature GSVA Scores revealed striking, statistically significant differences across the various treatment groups (ANOVA p-value = 3.8e-11). As expected, non-treated BMDMs (SF NT M0s), serving as a crucial baseline, displayed very low, near-zero M1 GSVA scores, indicating a largely unpolarised or minimally pro-inflammatory phenotype in their basal state. The positive control, BMDMs exposed to strong M1-polarising conditions, showed a robustly high positive M1 GSVA score (approximately 0.6), confirming the M1 gene set's accurate capture of pro-inflammatory characteristics. Conversely, M2-polarised BMDMs, the negative control for M1, exhibited a notably low, negative M1 GSVA score (below -0.4), underscoring a suppression of M1 characteristics. When considering the effects of sialidase-treated SF conditioned media, BMDMs treated with conditioned media from CP-SFs exhibited negative M1 GSVA scores (around -0.3), lower than the M1 BMDMs. In contrast, the VC-SF BMDM and L-SF BMDM groups displayed substantially high positive M1 GSVA scores (around 0.5), indicating a strong induction of M1-like polarisation in BMDMs. These results suggest that while a2-3 desialylation in SFs above certain threshold promoting a

distinctly pro-inflammatory M1 phenotype, dual sialylation of SFs through CP sialidase, may differently alter BMDMs behaviour (Figure 5-12A).

When M2 Signature GSVA Scores was investigated, which also demonstrated significant differences (ANOVA p-value = 0.0097) among different BMDM groups. Non-treated BMDMs presented with a negative M2 GSVA score (around -0.2), reflecting a relatively less M2-like polarisation at baseline. The M1-polarised control BMDMs, as expected, maintained a negative M2 GSVA score (around -0.2). As the positive control for M2, BMDMs treated with M2-polarising conditions showed a distinctly high positive M2 GSVA score (around 0.45). When we investigated the experimental groups, the CP-SF BMDM group revealed a modest positive M2 GSVA score (around 0.1), suggesting a slight shift of M2-like polarisation relative to the non-treated control. However, the AU-SF BMDM and VC-SF BMDM groups both exhibited negative M2 GSVA scores (around -0.3), indicating a reduction in M2 polarisation when compared to the non-treated baseline. The L-SF BMDM group showed a more heterogeneous response in M2 scores, with a median near zero, implying a less consistent or strong shift in M2 polarisation. This trends, on the other hand, when compared to NT-SF BMDMs, did not reach statistical significance (Figure 5-12B).

In summary, GSVA results provided critical understanding of how conditioned media from sialidase-treated SFs leads to macrophage polarisation, demonstrating clearly distinct effects compared to the non-treated control. While CP sialidase treatments appear to promote BMDMs away from a pro-inflammatory M1 state, the conditioned media from VC- and L-treated SFs conversely induce a robust M1 pro-inflammatory phenotype. This complex interplay, particularly the ability of different sialidase modifications to demonstrate divergent macrophage responses, underscores the multifaceted immunomodulatory roles of sialidases in the cellular crosstalk between SFs and macrophages, may hold significant implications for understanding inflammatory processes in conditions such as RA.

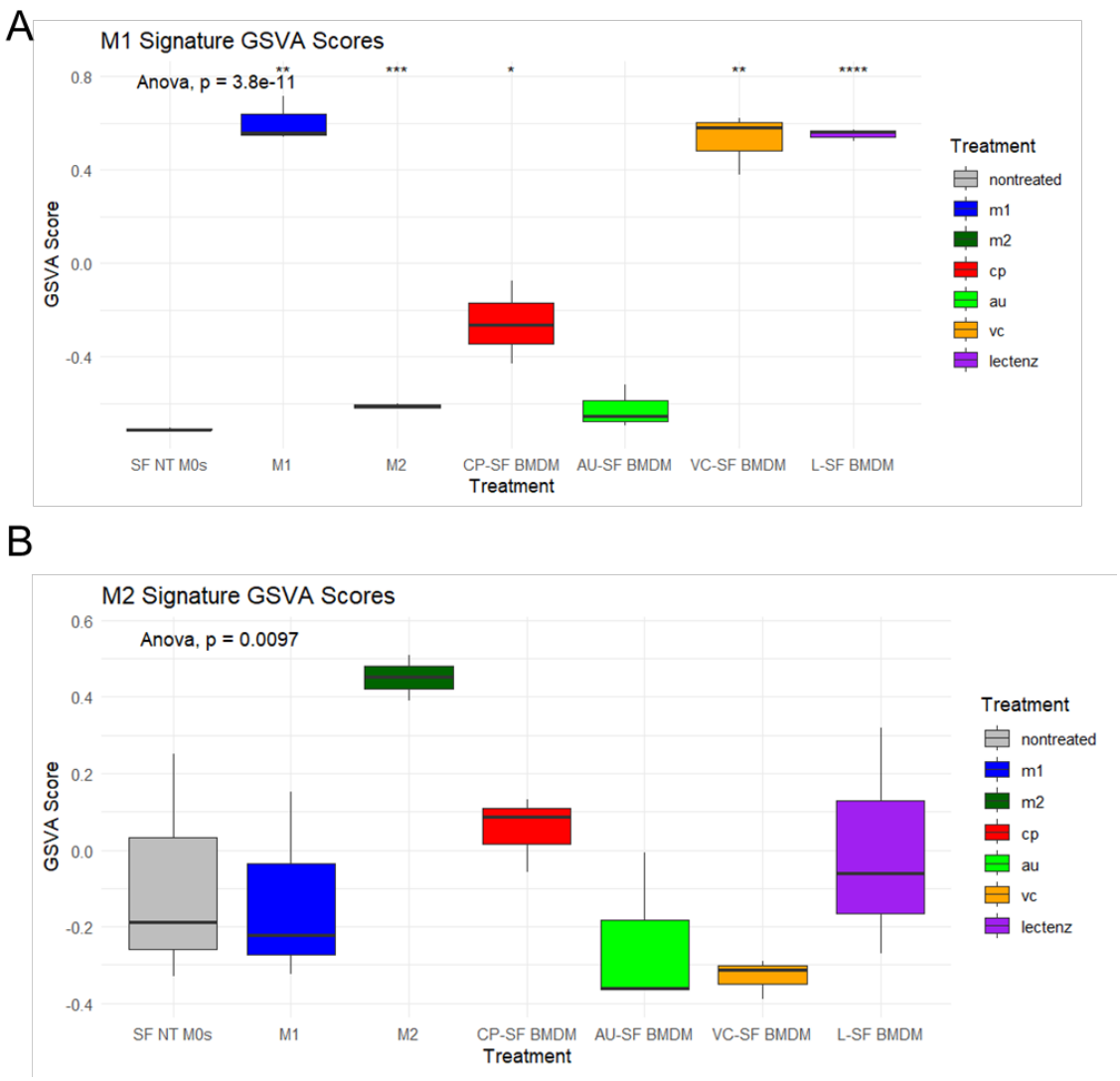

Figure 5-12 GSVA Scores Across Treatment Groups Demonstrate M1-like Phenotypes in BMDMs Cocultured with Desialylated SFs Supernatants.

Boxplot showing gene set variation analysis (GSVA) scores for the (A) M1 and (B) M2 macrophage signatures across different treatment conditions. Each box represents the distribution of GSVA scores for three biological replicates per treatment. The treatments include synovial fibroblast-conditioned media groups (CP-SF BMDM, AU-SF BMDM, VC-SF BMDM, L-SF BMDM), in vitro polarised M1 and M2 macrophages, and untreated buffer only exposed macrophages (SF NT M0s).

Statistical comparisons were performed using one-way ANOVA, followed by pairwise t-tests against the "SF NT M0s" reference group. Asterisks denote significance levels: $p < 0.05$ (*), $p < 0.01$ (**), $p < 0.001$ (***), $p < 0.0001$ (****).

Color coding: grey (SF NT M0s), blue (M1), dark green (M2), red (CP-SF BMDM), green (AU-SF BMDM), orange (VC-SF BMDM), and purple (L-SF BMDM).

After evaluating M1 and M2 macrophage signatures with GSVA, we next investigated the significantly differentially expressed genes responsible for the polarisation hits that we observed in BMDMs co-cultured with various SF conditioned media, as visualised by a heatmap (Figure 5-13).

The heatmap illustrates the expression patterns of M1 marker genes across the different treatment groups. As expected, BMDMs stimulated with IFN-γ and LPS (M1 positive control) showed robustly high expression of key M1 markers such as Nfkb1, Cd40, Cd80, Il1b, Ccl5, Stat1, Cxcl10, Tnf, Ptgs2, Il6, Cxcl9, Nfkb2, and Nos2. Conversely, BMDMs stimulated with IL-4 (M2 positive control) and non-treated BMDMs (SF NT M0s) consistently exhibited low expression of these M1 markers, confirming their non-M1 or suppressed M1 state.

Conditioned media from sialidase-treated SFs differentially impacted M1 polarisation. BMDMs co-cultured with conditioned media from CP-SFs and AU-SFs consistently displayed marked downregulation of most M1 markers compared to non-treated BMDMs. This suggests that these specific sialidase treatments on SFs lead to suppression of M1-like polarisation in BMDMs, fostering a less pro-inflammatory environment. In contrast, BMDMs exposed to conditioned media from VC-SFs and L-SFs exhibited prominent upregulation of numerous M1 markers, closely resembling the expression profile of the M1 positive control. This indicates a potent induction of M1-like pro-inflammatory polarisation by these specific sialidase treatments (Figure 5-13A).

The heatmap of M2 macrophage marker genes provided complementary insights into polarisation. M2 positive control samples (IL-4 stimulated BMDMs) demonstrated high expression of established M2 markers such as Egr2, Ccl17, Pparg, and Arg1. In contrast, M1 positive controls and non-treated BMDMs showed notably low expression of these M2 markers. M2 positive control samples demonstrated high expression of established M2 markers such as Egr2, Ccl17, Pparg, and Arg1. Notably, Timp1 and Il1rn, while potentially relevant in M2 contexts, showed low expression in these M2 positive control samples. Regarding the effects of conditioned media, BMDMs co-cultured with CP-SFs showed generally moderate to high expression of several M2 markers including Egr2, Ccl17, Pparg, and Arg1, suggesting a shift towards an M2-like profile compared to non-treated BMDMs. Expression of Timp1 and Il1rn remained low or moderate.

Conversely, AU-SF conditioned media led to consistently low expression of M2 markers across the board, including Egr2, Ccl17, Pparg, and Arg1, clearly implying a suppression of M2 polarisation compared to M2 controls. VC-SF conditioned media resulted in similar expression of M2 markers. The L-SF BMDM group displayed a mixed pattern of M2 marker expression; while Egr2 and Ccl17 remained relatively low, genes like Pparg, and Arg1 showed more moderate levels, suggesting a less consistent or pronounced M2 shift compared to other treated groups (Figure 5-13B).

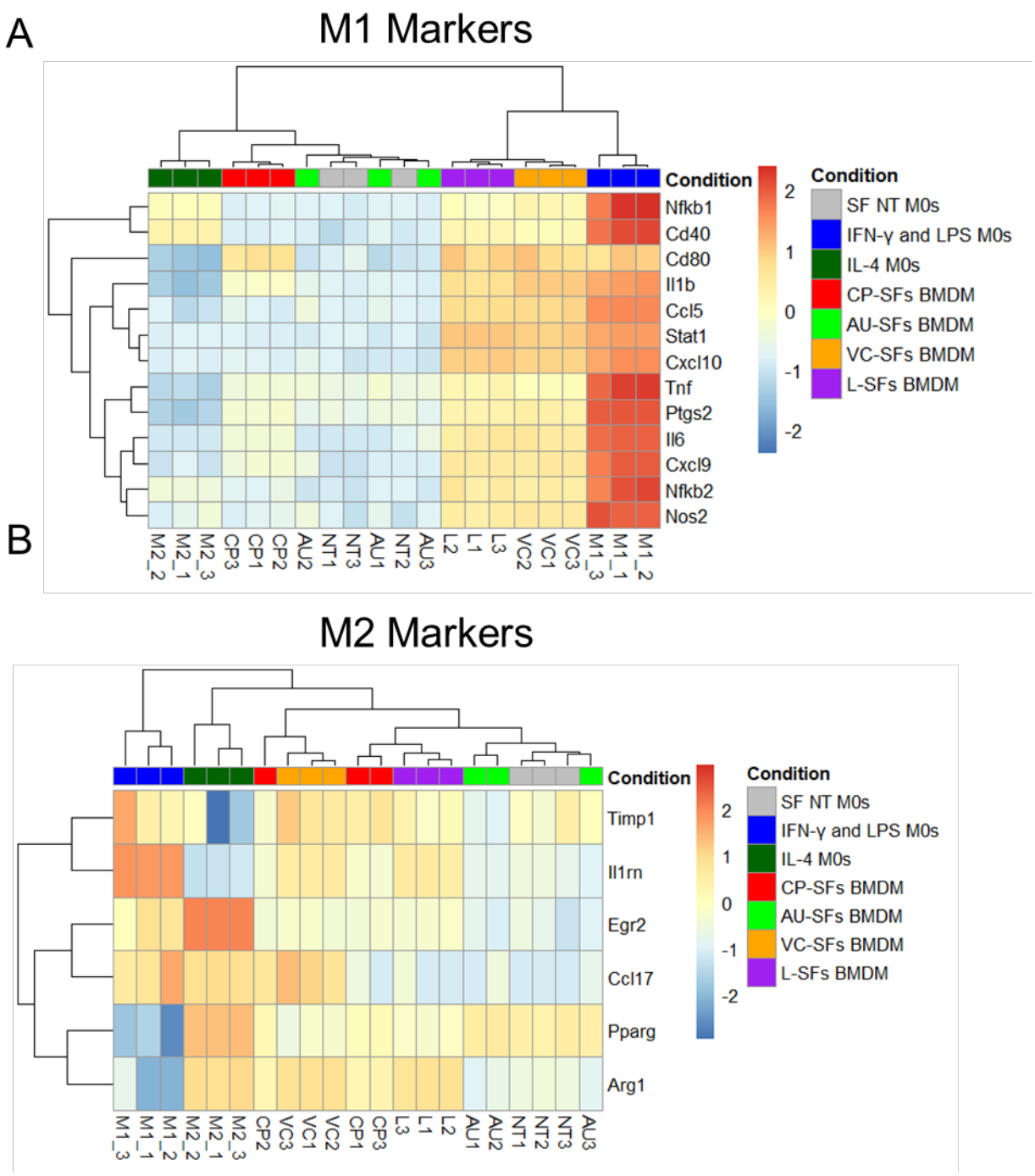

Figure 5-13 Heatmap showing the scaled expression of M1 and M2 macrophage marker genes across different treatment conditions and macrophage populations.

Differentially expressed genes (DEGs) were selected based on an adjusted p-value (padj) < 0.05 and an absolute log2 fold change > 1 from bulk RNA-seq data across all treatment conditions analysed with DESeq2. Marker genes representative of M1 and M2 macrophage polarisation were chosen from this DEG set. Normalised and log-transformed RNA-seq counts were used to generate the heatmaps, with rows scaled by gene expression (z-score). Samples include synovial fibroblasts (SF) under no treatment (SF NT M0s), classical M1-like macrophages stimulated with IFN-γ and LPS (IFN-γ and LPS M0s), alternatively activated M2-like macrophages stimulated with IL-4 (IL-4 M0s), and

bone marrow-derived macrophages (BMDMs) co-cultured with various SF conditioned media from different sialidase treatments (CP-SFs, AU-SFs, VC-SFs, L-SFs). Hierarchical clustering was applied to both genes and samples to reveal expression patterns and similarities. The colour scale represents z-score normalised expression values, where red indicates higher expression and blue indicates lower expression.

5.2.2 Time-Dependent Changes in Macrophage Phenotype Induced by Desialylated vs Untreated SF Secretomes

To evaluate the impact of desialylated SF supernatants on macrophage phenotype, BMDMs were cultured for 24hours or 36 hours with conditioned media collected from SFs treated with different sialidases. Following coculture, flow cytometry was performed to assess key macrophage surface markers within the $CD11b^{+}F4/80^{+}$ gated population. A robust gating strategy ensured high-purity selection of live, single-cell macrophages. Markers analysed included PDL-1, VSIG4, CD80, CD40, LYVE-1, CD206, CD86, MERTK, and TREM2, chosen to reflect activation status, antigen presentation capacity, and tissue-residency or immunoregulatory properties. Histograms shown in the figure represent fluorescence-minus-one (FMO) controls for each marker, which were used to establish gating thresholds for determining true positive expression in experimental samples. These FMOs define the background signal and are essential for setting accurate gates in low-expressing or dim populations. Therefore, while no experimental histograms are shown in this panel, the FMOs provide a crucial reference for subsequent quantification of marker expression in cocultured conditions (Figure 5-14).

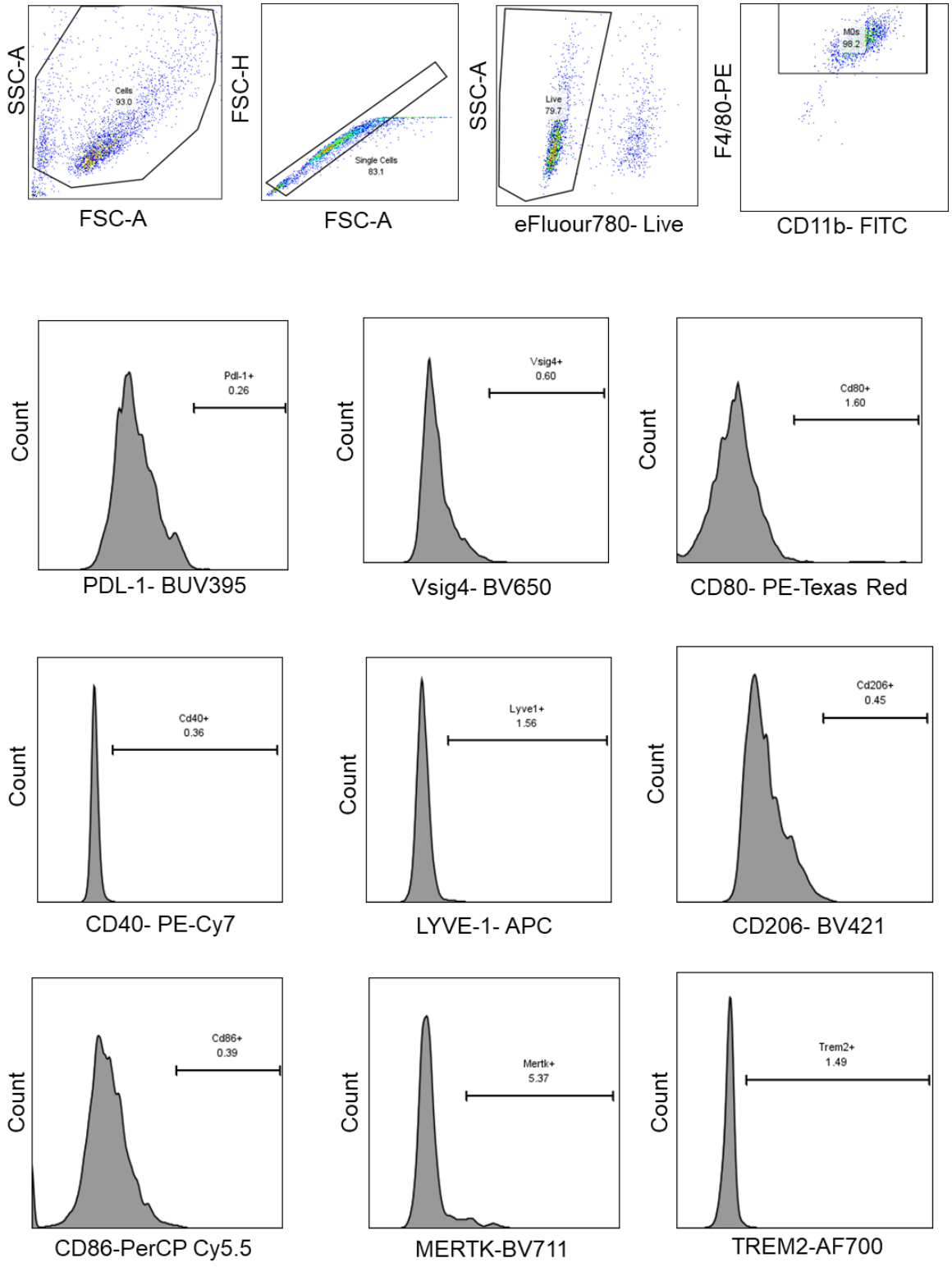

Figure 5-14 Gating strategy for Understanding Impact of Desialylated SF Supernatants on Resting State Bone Marrow Derived Macrophage Polarisation.

BMDMs were cultured with conditioned media collected from synovial fibroblasts (SFs) treated with various sialidases to assess important macrophage markers play important role in health vs arthritis. PDL-1, VSIG4, CD80, CD40, LYVE-1, CD206, CD86, MERTK,

and TREM2 expressions within CD11b and F4/80positive populations were evaluated after 36h coculture. For those corresponding markers FMOs were shown in histograms.

To investigate how desialylation of SFs influences the immunomodulatory state of macrophages, we examined PD-L1 expression in BMDMs after 24 and 36 hours of coculture with conditioned media from untreated or sialidase-treated SFs. Flow cytometry analysis revealed a significant upregulation of PD-L1 in response to SF supernatant conditioned media (Figure 5-15).

At 24 hours, BMDMs exposed to supernatants from CP-treated, VC-treated and L-treated SFs showed significantly elevated PD-L1 expression compared to the untreated control, as seen in both the histogram overlays and quantitative bar graphs. The most pronounced increase was observed in the L-treated condition, suggesting an early pro-resolving or tolerogenic shift driven by desialylated signals. By 36 hour, the difference only between untreated and L- treated groups remained significant, indicating a sustained induction of PD-L1. These data demonstrate that desialylated SF-conditioned media induces a robust and time-dependent upregulation of PD-L1 on BMDMs, supporting the hypothesis that altered sialylation on stromal cells can shape macrophage immunoregulatory function over time (Figure 5-15A-B).

The provided bar graphs illustrate the impact of various sialidases on the percentage of PD-L1 positive BMDMs after 24 and 36 hours of co-culture. At 24hours, compared to the non-treated, VC-SF and L-SF BMDMs showed statistically more percent positive PDL-1 population in comparison to non-treated controls. By 36 hours, the L-SF BMDM group once more shows the significantly highest average percentage of PD-L1 positive cells, approximately 30-35%, with individual data points ranging up to 50%, indicating its continued, albeit slightly attenuated compared to 24h, ability to upregulate PD-L1 expression on BMDMs (Figure 5-15C).

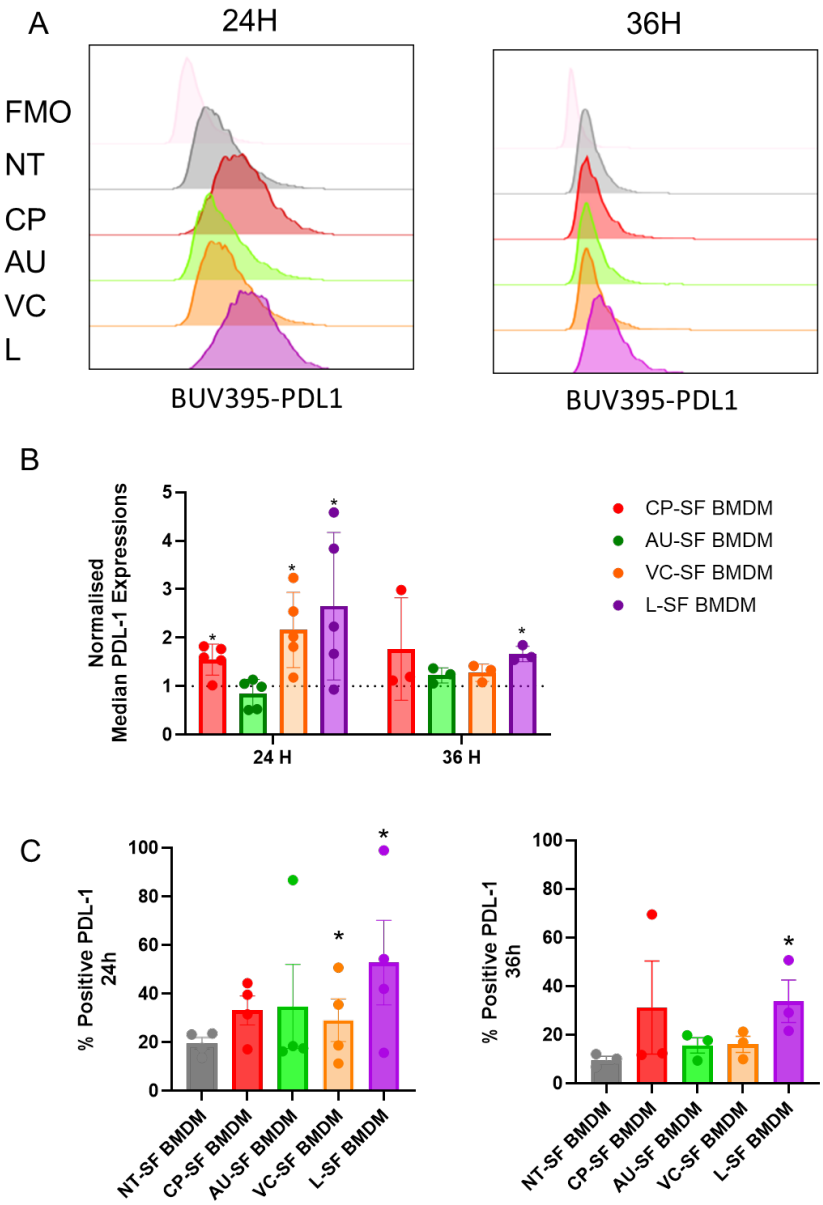

Figure 5-15 PD-L1 expression on macrophages is influenced by conditioned media from sialidase-treated synovial fibroblasts.

A) Representative flow cytometry histograms showing PDL-1 surface expression on bone marrow-derived macrophages (BMDMs) cultured with conditioned media from synovial fibroblasts (SFs) treated with control (grey), CP-SF BMDM (red), AU-SF BMDM (green), VC-SF BMDM (orange), or L-SF BMDM (purple) at 24h or 36h.
B) Quantification of median PDL-1 expression in BMDMs after exposure to conditioned media from sialidase treated SFs normalised to nontreated. MFIs provided with median ± SD. Statistical analysis was performed using one sample t-tests on normalised data. P values are indicated where significant.
C) Percentage of PDL-1^{+} macrophages demonstrated at 24h or 36h. Percent positive cells

expressed as mean ± SEM. Statistical analysis was performed using Kruskal Wallis tests. P values are indicated where significant.
Each independent dots represents independent biological replicates.

The expression of MerTK in BMDMs was analysed at 24- and 36-hours following treatment with conditioned media from various sialidases, as depicted in the provided histograms and quantitative bar charts (Figure 5-16). At the 24-hour time point, none of the treatments induced significant changes in MerTK expression compared to untreated control BMDMs. By 36 hours, treatment with CP-SF conditioned media significantly reduced MerTK expression compared to the control ($p<0.05$), as evidenced by a clear leftward shift in the histogram and a statistically significant decrease in MFI, suggesting that the ability to perform their critical efferocytic and anti-inflammatory functions by MerTK is reduced in CP-SF BMDMs. In contrast, treatment with AU-SF, VC-SF, and Lectenz-SF conditioned media did not induce changes in MerTK expression.

At the 24-hour time point, an analysis of the percentage of MerTK-positive BMDMs revealed that none of the sialidase conditioned media treatments significantly altered the proportion of cells expressing MerTK compared to the non-treated control. By 36 hours, control BMDMs maintained a high percentage of MerTK-positive cells, approximately 80-85%. Treatment with CP-SF conditioned media resulted in a clear reduction in the percentage of MerTK-positive cells, which significantly decreased to roughly 40-45%. In contrast, BMDMs treated with AU-SF, VC-SF, and Lectenz-SF conditioned media maintained a high percentage of MerTK-positive cells, similar to the control group, consistently ranging between approximately 80% and 90%. The substantial decrease observed with CP-SF is significant and suggests a significant impact on the proportion of MerTK-expressing cells at this later time point, also aligns with the reduced MFI data observed by 36 hour time point (Figure 5-16C).

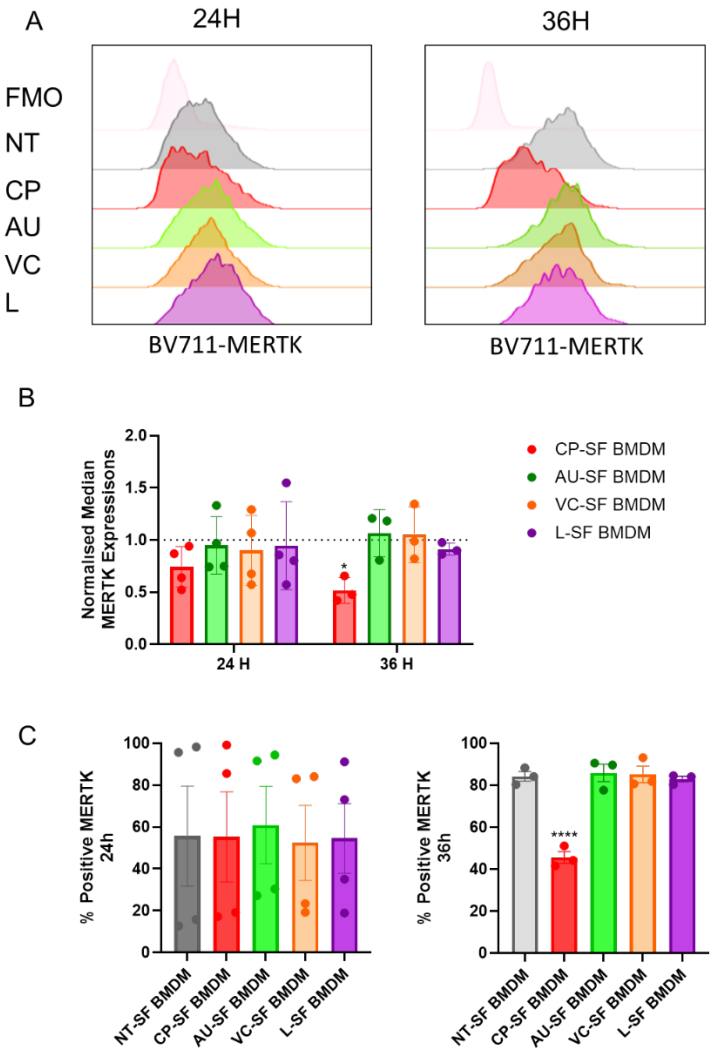

Figure 5-16 MERTK expression on macrophages is influenced by conditioned media from sialidase-treated synovial fibroblasts.

A) Representative flow cytometry histograms showing MERTK surface expression on bone marrow-derived macrophages (BMDMs) cultured with conditioned media from synovial fibroblasts (SFs) treated with control (grey), CP-SF BMDM (red), AU-SF BMDM (green), VC-SF BMDM (orange), or L-SF BMDM (purple) at 24h or 36h.
B) Quantification of median MERTK expression in BMDMs after exposure to conditioned media from sialidase treated SFs normalised to nontreated. MFIs provided with median ± SD. Statistical analysis was performed using one sample t-tests on normalised data. P values are indicated where significant.
C) Percentage of MERTK^{+} macrophages demonstrated at 24h or 36h. Percent positive cells expressed as mean ± SEM. Statistical analysis was performed using Kruskal Wallis tests for 24h data, and one way ANOVA for 36h data. P values are indicated where significant.
Each independent dots represents independent biological replicates.

We evaluated CD40 co-stimulatory molecule expressions in BMDMs at 24- and 36-hours following treatment with conditioned media from various sialidases (Figure 5-17). At 24 hours, none of the treatments induced significant changes in CD40 expressions. By 36 hours, these changes still did not reach a statistical significance, indicating that Cd40 expressions remained same in all treatment groups (Figure 5-17A-B).

At 24 hours, the percentage of CD40 positive BMDMs is relatively low in the NT-SF BMDM control group, typically ranging from 20-30%, with other treatment groups showing modest increases, particularly for L-SF BMDM. However, by 36 hours, there is a dramatic increase in CD40 expression across all groups, with nearly 100% of BMDMs becoming CD40 positive, suggesting a robust time-dependent upregulation of CD40 in these cells. Combining these results with the MFI one indicate that while almost all BMDMs express CD40 by 36 hours, CD40 protein expressions on the cells remained similar (Figure 5-17C).

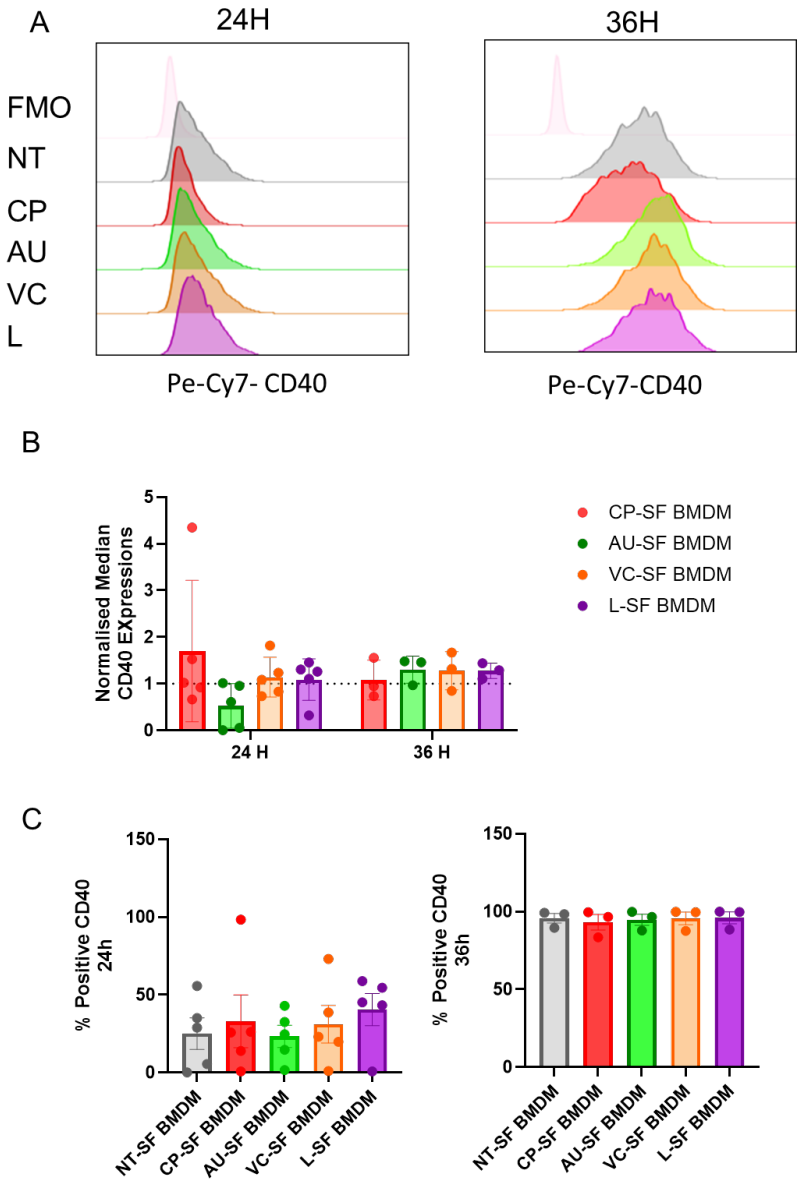

Figure 5-17 CD40 expression on macrophages is evaluated by flow cytometry.

A) Representative flow cytometry histograms showing CD40 surface expression on bone marrow-derived macrophages (BMDMs) cultured with conditioned media from synovial fibroblasts (SFs) treated with control (grey), CP-SF BMDM (red), AU-SF BMDM (green), VC-SF BMDM (orange), or L-SF BMDM (purple) at 24h or 36h.
B) Quantification of median CD40 expression in BMDMs after exposure to conditioned media from sialidase treated SFs normalised to nontreated. MFIs provided with median ± SD. Statistical analysis was performed using either one sample t-tests or one sample Wilcoxon rank tests on normalised data depending on the distribution of samples. P values are indicated where significant.
C) Percentage of $CD40^{+}$ macrophages demonstrated at 24h or 36h. Percent positive cells expressed as mean ± SEM. Statistical analysis was performed using one way ANOVA

tests for 24h data Kruskal Wallis tests for 36h data. P values are indicated where significant.
Each independent dots represents independent biological replicates.

To evaluate whether desialylated SFs secretomes modulate macrophage activation via CD80 upregulation, we measured both the frequency of $CD80^{+}$ cells and MFI in BMDMs after 24 and 36 hours of coculture. At 24 hours, none of the treatments resulted in significant changes in CD80 expressions. By 36-hour time point, only L-SF conditioned media demonstrated a statistically significant increase in CD80 expression on BMDMs, highlighting its potent and sustained effect on this crucial co-stimulatory molecule (Figure 5-18A-B).

The bar graphs illustrating % positive CD80 expression on BMDMs at 24 and 36 hours reveal a dynamic response to various SF conditioned media. At 24 hours, co-culture with all SF conditioned media generally led to an increase in the percentage of CD80 positive BMDMs compared to the non-treated control, albeit it did not reach statistical significance. By 36 hours, a more pronounced and widespread increase of % positive CD80 was observed across all conditions, including the non-treated control, the number of percent CD80 positive cells remained similar in all treatment groups (Figure 5-18C).

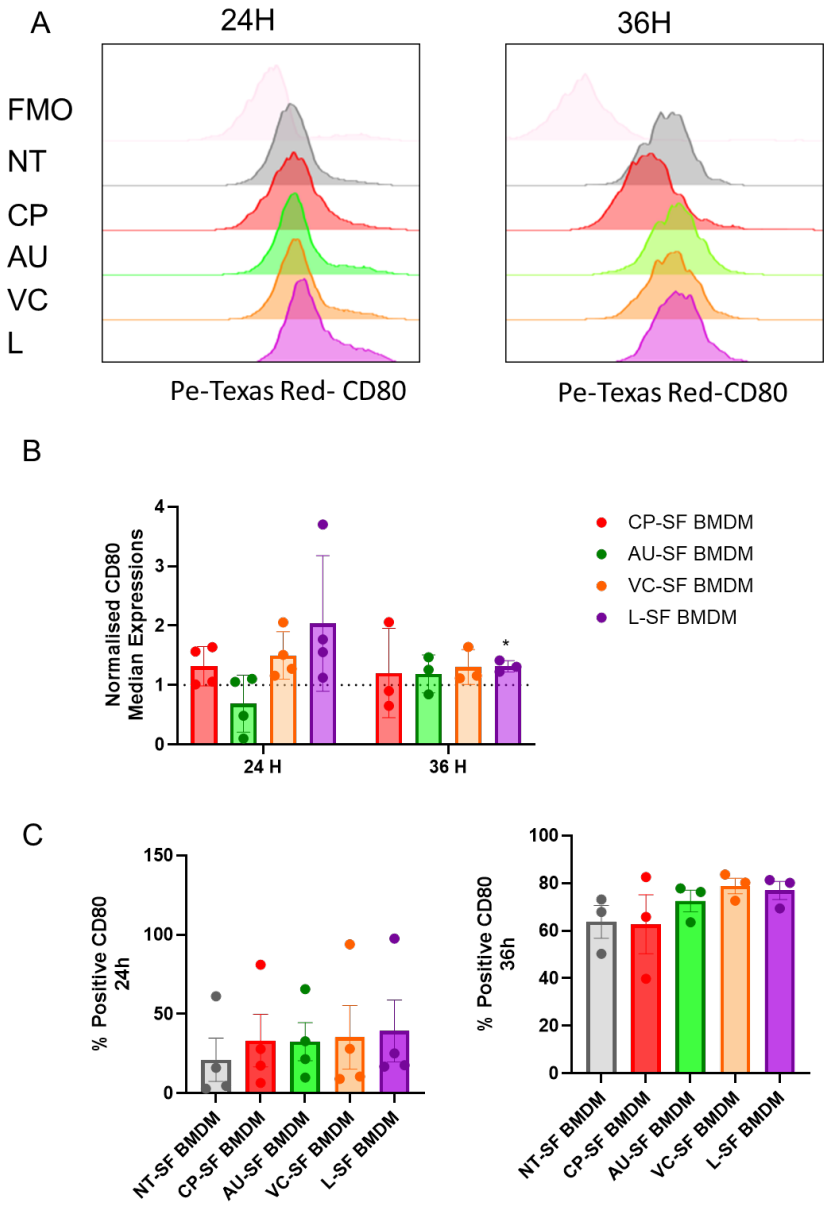

Figure 5-18 CD80 expression on macrophages is evaluated by flow cytometry.

A) Representative flow cytometry histograms showing CD80 surface expression on bone marrow-derived macrophages (BMDMs) cultured with conditioned media from synovial fibroblasts (SFs) treated with control (grey), CP-SF BMDM (red), AU-SF BMDM (green), VC-SF BMDM (orange), or L-SF BMDM (purple) at 24h or 36h.

B) Quantification of median CD80 expression in BMDMs after exposure to conditioned media from sialidase treated SFs normalised to nontreated. MFIs provided with median ± SD. Statistical analysis was performed using one sample t-tests on normalised data. P values are indicated where significant.

C) Percentage of $CD80^{+}$ macrophages demonstrated at 24h or 36h. Percent positive cells expressed as mean ± SEM.

Each independent dots represents independent biological replicates.

To evaluate whether desialylated SFs secretomes modulate macrophage activation via CD86 upregulation, we measured both the frequency of $CD86^+$ cells and MFI in BMDMs after 24 and 36 hours of coculture (Figure 5-19). At the 24-hour time point, the percentage of CD86 positive BMDMs remain low across all conditions. There is also no statistical difference in the normalised CD86 MFI values compared to NT control (Figure 5-19A-B). By the 36-hour time point, overall percentages of positive cells remain remarkably low compared to what might be expected for highly activated macrophages (Figure 5-19C). Only L-SF BMDMs demonstrated significantly higher CD86 MFI values compared to NT-SF BMDMs. However, considering the low frequency of $CD86^+$ cells among all tested conditions, it can be concluded that the secretome that comes from sialidase treated SFs do not have significant impact on the CD86 expressions on the BMDMs.

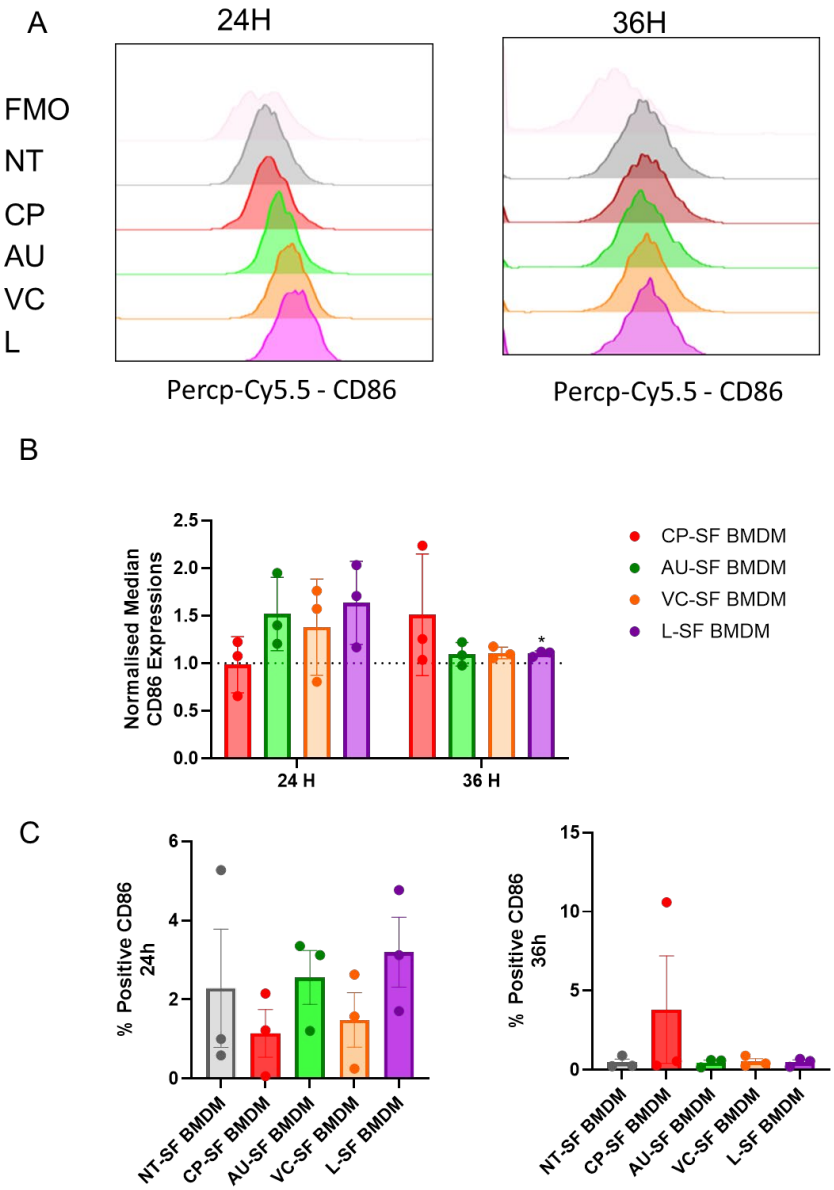

Figure 5-19 CD86 expression on macrophages is influenced by conditioned media from sialidase-treated synovial fibroblasts.

A) Representative flow cytometry histograms showing CD86 surface expression on bone marrow-derived macrophages (BMDMs) cultured with conditioned media from synovial fibroblasts (SFs) treated with control (grey), CP-SF BMDM (red), AU-SF BMDM (green), VC-SF BMDM (orange), or L-SF BMDM (purple) at 24h or 36h.
B) Quantification of median CD86 expression in BMDMs after exposure to conditioned media from sialidase treated SFs normalised to nontreated. MFIs provided with median ± SD. Statistical analysis was performed using one sample t-tests on normalised data. P values are indicated where significant.
C) Percentage of $CD86^{+}$ macrophages demonstrated at 24h or 36h. Percent positive cells

expressed as mean ± SEM. Statistical analysis was performed using ANOVA for 24h data and Kruskal Wallis for 36h data. P values are indicated where significant.
Each independent dots represents independent biological replicates.

To assess whether desialylated SF secretomes influence anti-inflammatory macrophage polarisation, we analysed CD206 surface expression, quantified by MFI, in BMDMs after 24h and 36h coculture. At 24 hours, CD206 MFI values were similar across all groups, including untreated SF supernatant and sialidase-treated conditions. As shown by the histogram and bar chart, the differences between conditions were minimal, indicating that CD206 surface expression is not significantly affected by desialylated inputs at this early timepoint. At 36 hours, Except CP-SF BMDMs, CD206 levels remained consistent across all other treatment groups, however CP-SF BMDMs group showed a trend toward slightly lower MFI compared to others. Still, this decrease did not reach statistical significance, and the overall expression pattern remained stable (Figure 5-20A-B). Taken together, these data suggest that CD206 expression is not dynamically regulated by the sialylation status of SF-derived factors, and macrophage exposure to desialylated supernatants does not substantially alter this M2-associated marker at either 24 or 36 hours.

We also quantified the frequency of $CD206^+$ macrophages following 24h and 36h coculture with SF-conditioned media. At 24 hours, the proportion of $CD206^+$ BMDMs was comparable across all conditions. The untreated group showed approximately 20-22% $CD206^+$ cells, and this frequency was largely unchanged in other groups. At 36 hours, the percentage of $CD206^+$ macrophages increased across all groups, reaching ~40-50%. CP-SF BMDMs showed numerically less $CD206^+$ frequencies than untreated controls, but this did not reach significance. (Figure 5-20C).

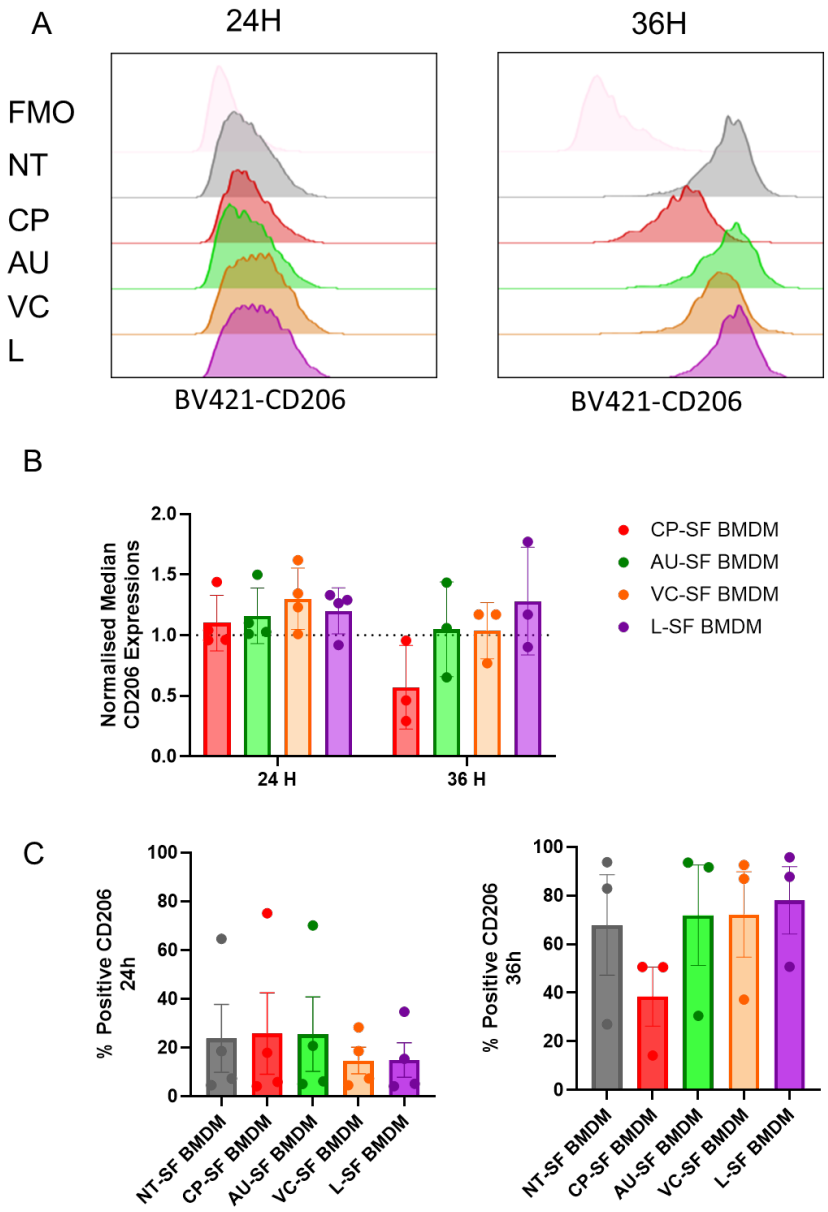

Figure 5-20 CD206 expression on macrophages is evaluated by flow cytometry.

A) Representative flow cytometry histograms showing CD206 surface expression on bone marrow-derived macrophages (BMDMs) cultured with conditioned media from synovial fibroblasts (SFs) treated with control (grey), CP-SF BMDM (red), AU-SF BMDM (green), VC-SF BMDM (orange), or L-SF BMDM (purple) at 24h or 36h.

B) Quantification of median CD206 expression in BMDMs after exposure to conditioned media from sialidase treated SFs normalised to nontreated. MFIs provided with median ± SD. Statistical analysis was performed using either one sample t-tests or one sample Wilcoxon rank tests on normalised data depending on the distribution of samples. P values are indicated where significant.

C) Percentage of $CD206^{+}$ macrophages demonstrated at 24h or 36h. Percent positive

cells expressed as mean ± SEM. Statistical analysis was performed using ANOVA for 24h data and Kruskal Wallis for 36h data. P values are indicated where significant.
Each independent dots represents independent biological replicates.

To assess the impact of sialidase-treated SFs on the expression of the regulatory macrophage marker VSIG4, we measured its MFI in BMDMs after 24h and 36h of coculture. At 24h, differences among different treatment groups did not reach statistical significance. By 36h, still, no statistically significant changes were detected. Overall, while variations in VSIG4 expression were observed across treatment groups and time points, these did not achieve significance, suggesting that desialylation of does not have effect on macrophage VSIG4 expression within the observed timeframe (Figure 5-21A-B).

To determine whether sialidase treatment of SFs influences the proportion of regulatory macrophages, we assessed the percentage of VSIG4$^+$ BMDMs after 24h and 36h of coculture. At 24h, all coculture conditions exhibited low percentages of VSIG4$^+$ BMDMs (generally below 5%), with no significant differences between NT and sialidase-treated groups. By 36h, no statistically significant changes were detected across treatment groups. These data suggest that while individual variation exists, sialidase treatment of SFs does not consistently alter the proportion of VSIG4$^+$ macrophages within 36 hours of coculture (Figure 5-21C).

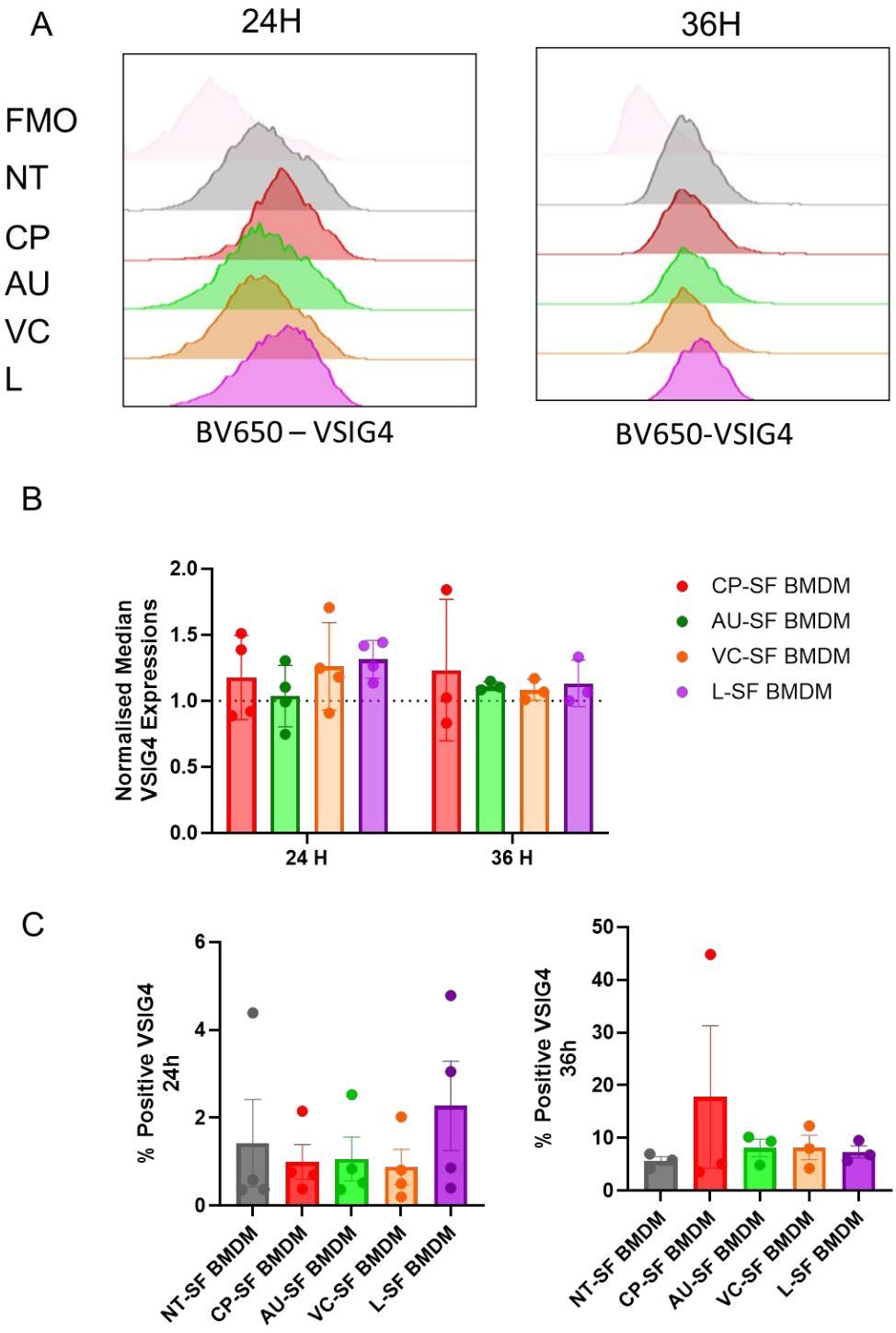

Figure 5-21 VSIG4 expression on macrophages is evaluated by flow cytometry.

A) Representative flow cytometry histograms showing CD206 surface expression on bone marrow-derived macrophages (BMDMs) cultured with conditioned media from synovial fibroblasts (SFs) treated with control (grey), CP-SF BMDM (red), AU-SF BMDM (green), VC-SF BMDM (orange), or L-SF BMDM (purple) at 24h or 36h.

B) Quantification of median VSIG4 expression in BMDMs after exposure to conditioned media from sialidase treated SFs normalised to nontreated. MFIs provided with median ± SD. Statistical analysis was performed using either one sample t-tests or one sample

Wilcoxon rank tests on normalised data depending on the distribution of samples. P values are indicated where significant.
C) Percentage of $CD206^+$ macrophages demonstrated at 24h or 36h. Percent positive cells expressed as mean ± SEM. Statistical analysis was performed using Kruskal Wallis for 24h data and ANOVA for 36h data. P values are indicated where significant.
Each independent dots represents independent biological replicates.

To assess the impact of co-culturing with sialidase-treated SFs on BMDMs phenotype, the expression of TREM2 and LYVE-1 was evaluated by flow cytometry. As shown in Figure 5-22, representative histograms for AF700-conjugated TREM2 (top panels, A) and APC-conjugated LYVE-1 (bottom panels, B) demonstrate that BMDMs did not exhibit detectable expression of either marker at 24 hours or by 36 hours. The fluorescence minus one (FMO) controls, which establish the baseline autofluorescence and non-specific binding, were consistently aligned with the experimental samples across all conditions, indicating an absence of specific TREM2 or LYVE-1 signal. Furthermore, no discernible shifts in median fluorescent intensity (MFI) peaks were observed for either TREM2 or LYVE-1, confirming that co-culture with sialidase-treated SFs under the tested conditions did not induce or alter the expression of these markers on BMDMs.

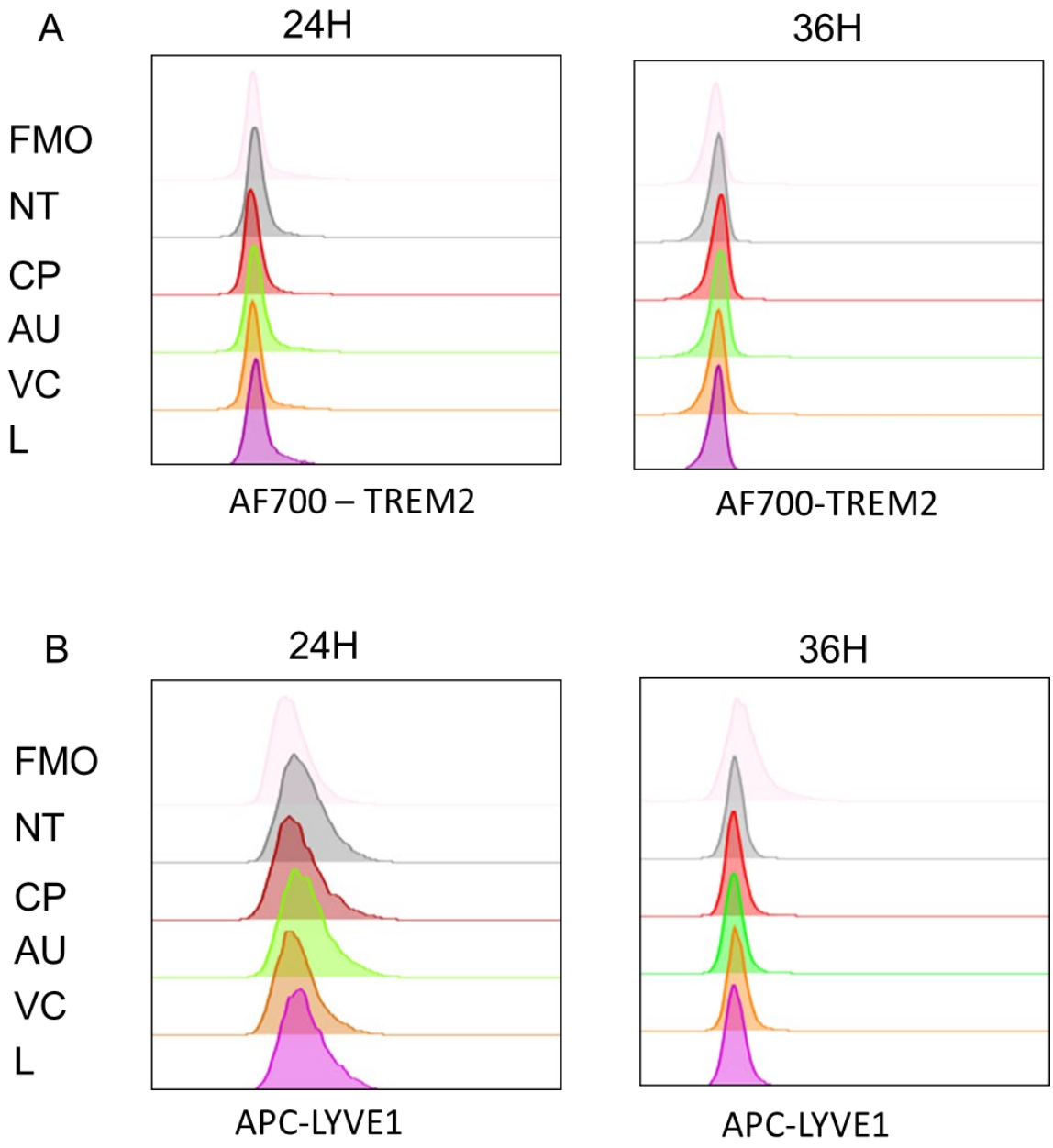

Figure 5-22 Histograms of TREM2 and LYVE-1 Median Fluorescent Intensities (MFI) on BMDMs Co-cultured with Sialidase-Treated SFs.

Representative flow cytometry histograms depicting the MFI for AF700-conjugated TREM2 (top panels) and APC-conjugated LYVE-1 (bottom panels) on BMDMs at 24h or 36h. BMDMs were co-cultured with SFs that had been pre-treated with sialidase. Each panel represents distinct time points. The similar peaks within each histogram illustrate the expression levels of TREM2 and LYVE-1, with no shifts in peak position indicating no alterations in MFI compared to FMOs. The various coloured lines within each histogram represent different experimental groups of sialidase treatment.

5.3 Discussion

This chapter extends our understanding of how sialylation patterns in SFs influence the inflammatory landscape of the synovial microenvironment, particularly through their paracrine interactions with macrophages. Building on prior findings that desialylation reprograms SF secretory and transcriptional profiles, we investigated how conditioned media derived from sialidase-treated SFs affect macrophage polarisation. The results reveal that the extent and type of sialic acid removal from SFs markedly influence macrophage phenotype at both transcriptomic and protein levels.

We observed that conditioned media from SFs treated with L and VC sialidases of which effectively remove α2-3-linked sialic acids induced a robust shift in bone marrow-derived macrophages (BMDMs) toward a classical M1-like state. This was evidenced by increased expression of pro-inflammatory cytokines and chemokines, including Il1b, Ccl6, Cxcl10, and Nos2, alongside elevated GSVA M1 signature scores. Notably, L-SF macrophages also upregulated Cd80, CD86 and Pdl1, markers commonly associated with inflammatory antigen-presenting cells. Pathway analysis further confirmed enrichment of TNF, NF-κB, and type I interferon signaling pathways that are key to macrophage-mediated inflammation. Importantly, these responses were not observed in BMDMs cultured with conditioned media from AU-treated SFs, which demonstrated less α2-3 cleavage efficiency. This highlights the critical and threshold-dependent role of α2-3 sialylation in dictating fibroblast-macrophage communication.

In contrast, the response to CP sialidase, which removes both α2-3 and α2-6 linkages, was notably distinct. While CP-treated conditioned media induced some inflammatory gene expression (Il1b, Ccl6), it also triggered upregulation of Arg1, a gene associated with alternative (M2-like) activation and tissue repair. This dual profile was reflected in GSVA scores, where both M1 and M2 signatures were modestly enriched. These findings suggest that broad desialylation may not necessarily enhance inflammation but instead yield a more balanced or transitional macrophage state, possibly as a result of competing signals in the conditioned media or partial regulatory feedback. This could be particularly relevant in chronic

disease contexts like RA, where plasticity between inflammatory and resolving macrophage phenotypes is common.

Interestingly, AU-treated SFs despite being exposed to a bacterial neuraminidase did not elicit significant changes in macrophage transcriptome or phenotype. Given that AU sialidase cleaves α2-3 linkages less than other sialidases under our experimental conditions, this reinforces the idea that partial glycan remodelling fails to reach the immunological threshold required to induce downstream effects in macrophages. This finding is critical, as it demonstrates that not all enzymatic treatments produce equivalent biological consequences.

At the protein level, the expression of M1-associated markers such as PDL1 increased significantly in BMDMs cultured with VC- and L- conditioned media. Taken together, our findings support a model in which α2-3 sialic acids on the SF surface function as immunosuppressive glycans that restrain the fibroblast inflammatory secretome. Their selective removal through VC or L sialidase potentiates a paracrine program that licenses macrophage pro-inflammatory activation. In contrast, broader desialylation (CP) or less cleavage (AU) either attenuates or fails to provoke such responses. These observations underscore the specificity of glycan-immune interactions and suggest that α2-3-linked sialic acids serve as self-associated molecular patterns (SAMPs), the removal of which mimics tissue injury or pathogen-derived signals, thereby triggering macrophage reprogramming (A. Varki, 2011).

The translational relevance of these findings is significant. Aberrant sialylation has been increasingly recognised in RA pathogenesis, particularly in the context of serum glycoproteins and cell surface receptors. Our data suggest that local alterations in SF sialylation may be equally important in shaping macrophage behaviour, contributing to the chronic inflammation and immune dysregulation characteristic of RA. Moreover, therapeutic strategies aimed at preserving α2-3 sialylation or blocking the downstream macrophage response may hold promise in modulating disease activity.

In summary, this chapter reveals that SF-derived glycans play a critical role in shaping the inflammatory microenvironment via control of macrophage polarisation. Specifically, removal of α2-3 sialic acids reprograms SFs to secrete

factors that strongly polarise macrophages toward a pro-inflammatory M1-like phenotype. In contrast, full desialylation or less cleavage generates distinct or muted responses. These insights highlight the potential of targeting glycosylation as a means to modulate stromal-immune cross-talk in RA and related autoimmune disorders.

To build on these findings and explore their relevance in human disease, we next turn to human single-cell RNA-sequencing datasets to examine how sialylation-related pathways differ across distinct synovial fibroblast subpopulations. Specifically, we will assess the expression of sialyltransferases in lining and sublining fibroblasts which are two transcriptionally and functionally distinct SF subsets implicated in RA pathogenesis. This will allow us to determine whether these key glycosylation enzymes exhibit compartment-specific regulation in inflamed human joints. In parallel, we will investigate the expression of Siglecs and Galectins in human tissue-resident synovial macrophages. These sialic acid-binding proteins play critical roles in mediating glycan-immune communication, and their regulation may further illuminate how altered stromal glycosylation shapes innate immune responses in rheumatoid arthritis.

6. Chapter 6 Investigation of Sialyltransferase, Siglec, and Galectin Expression Patterns in Human Active, Remission, and Early Rheumatoid Arthritis: Implications for Disease Pathogenesis

6.1 Introduction

The previous chapter demonstrated that altering the sialylation pattern of SFs profoundly influences their paracrine interactions with macrophages. Specifically, selective removal of α2-3-linked sialic acids from SFs using VC and L sialidases reprogrammed the fibroblast secretome, leading to a pronounced inflammatory activation of BMDMs. This was reflected by upregulation of M1-associated genes and surface markers, as well as enrichment of pro-inflammatory signalling pathways. In contrast, broader or less efficient desialylation via CP or AU sialidases led to more variable or minimal macrophage responses. These findings highlight α2-3 sialylation as a key modulator of stromal-immune cross-talk in the synovial microenvironment and establish a functional link between fibroblast glycan remodelling and innate immune activation.

In Chapter 3, we highlighted the integrated role of inflammation and glycosylation in shaping the pathogenic behaviour of SFs in RA. As shown, TNF-induced transcriptional reprogramming is accompanied by marked changes in glycosylation-related pathways particularly in galactosylation and sialylation which likely contribute to the enhanced immune-stimulatory potential of RA SFs. Furthermore, selective desialylation of SFs not only altered their inflammatory profile but also modulated their paracrine influence on macrophages, reinforcing the concept that glycan remodeling plays a critical role in stromal-immune crosstalk. To explore the in vivo relevance of these findings, we next turn to human single-cell RNA-sequencing datasets spanning early, active, and remission stages of RA. We will specifically examine the expression of sialyltransferases in lining and sublining fibroblast subsets, two anatomically and functionally distinct SF populations implicated in joint damage and inflammation. In parallel, we will assess the expression of Siglecs and Galectins in tissue-resident synovial macrophages. As key sialic acid-binding receptors and lectins, these molecules are central to regulating immune homeostasis, tolerance, and activation. By

mapping their expression and correlating them with fibroblast-derived sialylation signatures, we aim to elucidate potential glycan-lectin interaction networks that govern the balance between inflammation and resolution in the RA joint microenvironment.

In RA, fibroblast-like synovial cells (FLS) can be divided into two primary categories based on their distinct anatomical locations and functional characteristics: the lining FLS and the sublining FLS. Lining FLS are located within the synovial lining, which interfaces directly with the joint cavity. These cells significantly contribute to the pathogenesis of RA through their proliferative capabilities and cytokine production, such as IL-6 and TNF-α (Bottini & Firestein, 2013; F. Zhang et al., 2023). This layer of FLS is typically hyperplastic and contributes to the formation of a destructive pannus, which invades cartilage and bone, leading to joint erosion. Molecular studies suggest that lining FLS exhibit a distinct gene expression profile, with markers such as PDPN, CDH11 and CD55/PRG4 being commonly upregulated, indicating their heightened inflammatory state and pathogenic potential in RA (Køster et al., 2021; Qian et al., 2024). In contrast, sublining FLS reside in the sublining layer beneath the synovial lining and exhibit a different functional profile. Recent studies have identified various subpopulations of sublining FLS, which express distinct markers and display differential cytokine production profiles compared to lining FLS. For instance, sublining FLS often express THY1 and human leukocyte antigen-DRA (HLA-DRA), which suggest their involvement in pro-inflammatory responses and recruitment of other immune cells into the synovium (Køster et al., 2021; Qian et al., 2024). Tissue-resident macrophages in RA represent a specialised population of immune cells that play critical roles in both the pathogenesis of the disease and the maintenance of joint homeostasis. These macrophages originate from distinct embryonic precursors and remain in the tissues, where they develop unique characteristics and functional abilities relevant to the inflammatory environment of RA. Primarily, tissue-resident macrophages are essential for maintaining tissue integrity and regulating inflammatory responses. They reside predominantly within the synovial tissue and can be classified based on their phenotypic profiles and functional roles in health and disease (Davies et al., 2013; Misharin et al., 2014). In RA, tissue-resident macrophages promote local inflammation through enhanced secretion of cytokines and chemokines, such as TNF-α and IL-6, which can

perpetuate the inflammatory cycle and contribute to synovial hyperplasia (Q.-Q. Huang et al., 2021; Soler Palacios et al., 2015).

As mentioned previously, sialyltransferases, a family of enzymes that catalyse the addition of sialic acid residues to glycoproteins and glycolipids, play a central role in shaping the glycan landscape of SFs in both healthy and diseased states. In the inflammatory environment of RA, altered expression of sialyltransferases can lead to profound changes in sialylation patterns on the SF surface. These modifications may influence cell-cell and cell-matrix interactions by modulating how SFs are recognised by sialic acid-binding receptors, particularly Siglecs (sialic acid-binding immunoglobulin-type lectins) on immune cells and galectins, a class of β-galactoside-binding lectins involved in immunoregulation. For instance, enhanced α2,3- or α2,6-linked sialylation may inhibit galectin binding by masking terminal galactose residues, thereby disrupting galectin-mediated immune suppression or cell adhesion. Conversely, when sialic acid is reduced on the cell surface either through enzymatic removal or downregulation of sialyltransferases it exposes the underlying galactose residues that are normally masked by terminal sialylation. This unmasking significantly enhances the binding capacity of galectins, a family of β-galactoside-binding lectins such as Galectin-1, -3, and -9. In this context, galectin interactions become more important, influencing various cellular processes depending on the galectin involved. For instance, increased Galectin-3 binding can promote synovial fibroblast adhesion, migration, and pro-inflammatory signaling (Filer et al., 2009; Forsman et al., 2011; Hu et al., 2017). In the inflamed synovial microenvironment of RA, reduced sialylation may therefore shift the balance of galectin-mediated signaling, amplifying either inflammatory or immunomodulatory responses. This highlights the importance of sialylation as a regulatory gatekeeper that controls the accessibility of galectin ligands and, in turn, modulates intercellular communication within the joint. Simultaneously, these sialylated structures could engage inhibitory Siglecs on macrophages and dendritic cells, dampening inflammatory responses or, conversely, promote immune evasion if the interactions skew toward tolerance. Particularly soluble Siglec-9 levels in RA patients' serum and synovial fluids were associated with disease severity (X. Wang et al., 2017). Thus, sialyltransferase-driven remodelling of the SF glycome may critically influence crosstalk with the immune system, creating a potential axis of regulation in RA pathogenesis through Siglec and galectin engagement. The following section will investigate how genes involved in

sialic acid metabolism and sialic acid capping change in early arthritis, active and remission human RA samples, and then we will analyse siglec and galectin expressions in human tissue-resident macrophages in different disease states using a single cell dataset obtained from Mariola Kurowska-Stolarska group.

Single-cell RNA sequencing (scRNA-seq) has revolutionised our understanding of cellular heterogeneity by enabling transcriptomic profiling at single-cell resolution. Unlike bulk RNA-seq, which averages gene expression across entire populations of cells, scRNA-seq allows for the identification of rare cell types, dynamic cellular states, and lineage relationships within complex tissues. This high-resolution approach is particularly valuable in studying heterogeneous and inflamed environments such as the RA synovium, where diverse immune and stromal populations interact to drive chronic inflammation and tissue remodelling. By resolving the transcriptomes of thousands of individual cells, scRNA-seq provides a powerful tool to dissect the cellular composition, uncover disease-relevant subsets, and map intercellular communication networks with unprecedented precision (Figueiredo, 2024; Saliba et al., 2014).

6.2 Results

6.2.1 Cell-Type Specific Expression of Sialyltransferases, Siglecs, and Galectins in Human Synovial Tissues Reveals Different Signatures Across Disease States

To understand cellular changes in gene expressions in the human RA synovia, we used a dataset from Alivernini et al work (Alivernini et al., 2020). Initial dataset comprised of patients with early undifferentiated arthritis (UPA), active and remission RA. ScRNA-Seq of human RA synovial tissue revealed a heterogeneous cellular landscape, as visualised by UMAP dimensionality reduction. Distinct clusters were previously annotated based on transcriptomic profiles, identifying a wide range of stromal, endothelial, and immune populations. Stromal compartments included Lining FLS, Sublining FLS, Myofibroblasts, and a subset of Proliferating FLS, each forming discrete clusters. Vascular and lymphatic endothelial cells were also resolved as separate populations. Immune cell diversity was extensive, encompassing CD4 and CD8/NKT T cells, B cells, Plasma cells, Mast cells, Macrophages, cDCs, pDCs, and a distinct population of Proliferating Leukocytes. Platelets formed a minor yet discernible cluster (Figure 6-1).

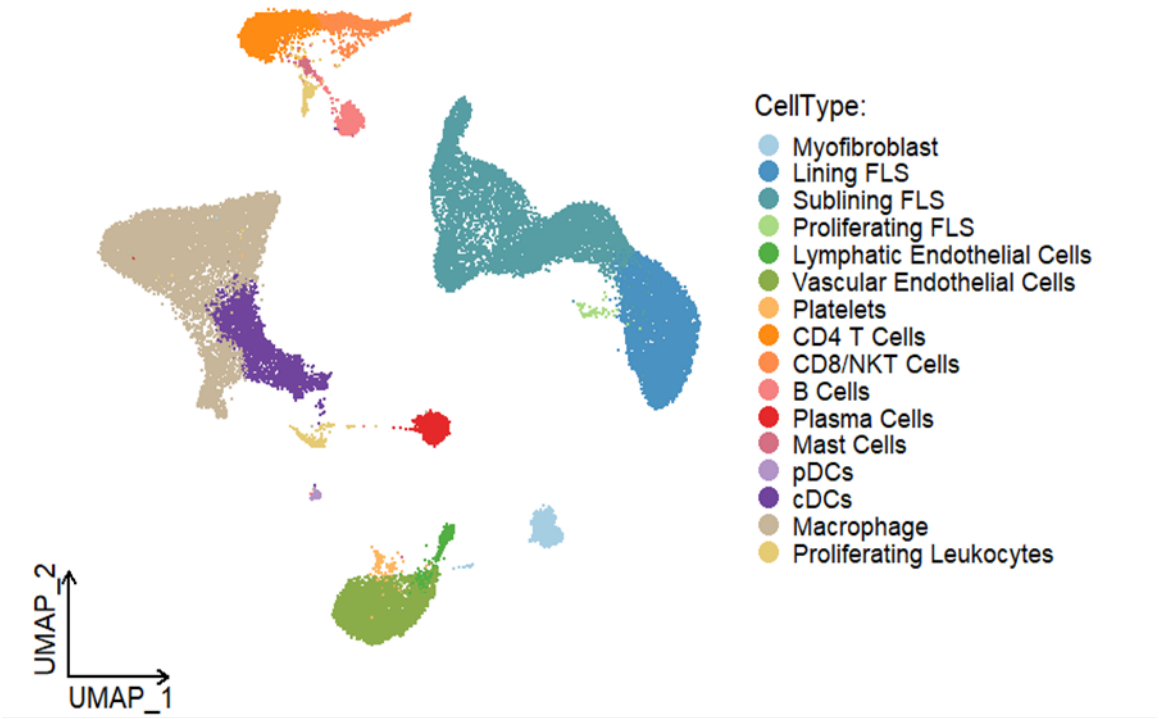

Figure 6-1 UMAP visualisation of single-cell RNA sequencing data from rheumatoid arthritis (RA) synovial tissue.

16 distinct clusters corresponding to various cell types identified as indicated. Each cluster is colour-coded to represent its specific cell type, as annotated based on the expression of canonical marker genes. The UMAP (Uniform Manifold Approximation and Projection) plot highlights the cellular heterogeneity within the RA microenvironment, indicating potential pathways involved in disease pathogenesis.

Cell-type-specific frequency analysis revealed changes in the composition of fibroblast and macrophage populations across disease states. From the stacked plot, fibroblasts and macrophages cell types together account for roughly 65% of all cells in Active, 55% in Remission, and 77% in UPA and the remainder are other cell types. In Active, proportions are approximately: Sublining FLS ~23%, Macrophage ~27%, Lining FLS ~15–16%, and Proliferating FLS <1%. In Remission, they are Sublining FLS ~22%, Macrophage ~21–22%, Lining FLS ~11–12%. In UPA, they rise to Sublining FLS ~29%, Macrophage ~30%, Lining FLS ~18–19%, and Proliferating FLS ~1%. Overall, UPA shows the highest combined share of Sublining FLS and Macrophage, Remission has the lowest Lining FLS, and Proliferating FLS remain rare in all groups. It is also important to note that cell type abundance did not significantly differ between Active-UPA,

Active-Remission, and Remission-UPA groups, indicating that similar number of cells appeared across different disease states (Figure 6-2).

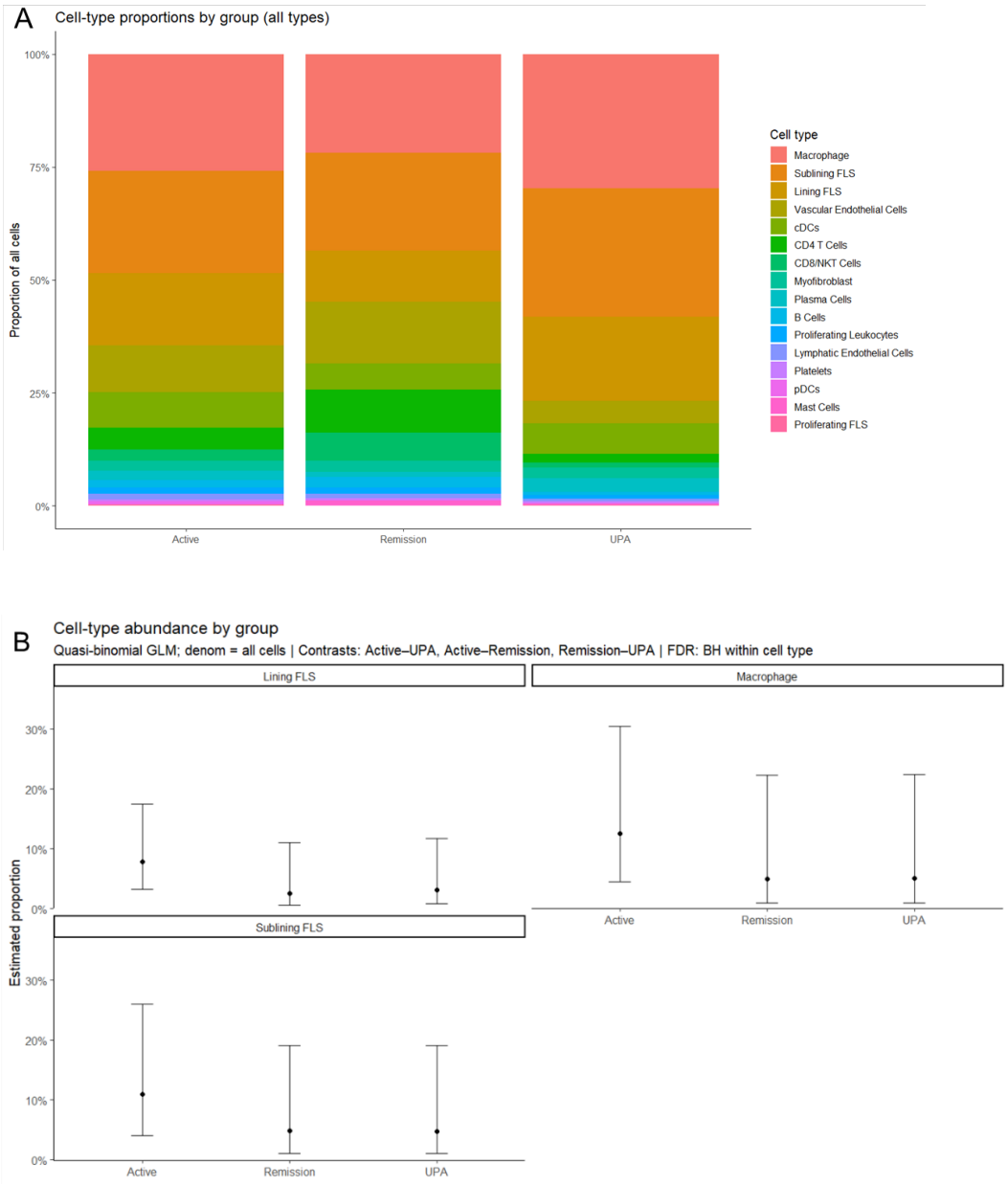

Figure 6-2 Statistics describing percentage of cells counts in all cell types among different RA groups.

Bar plots indicated (A) percentage and (B) statistics in corresponding cell types between UPA (n=2), active (n=4) and remission (n=3) RA samples where each cell type is represented with different colour codes. As Proliferating FLS was no cells in remission, it was excluded from further analysis. In Figure B, estimated proportions (mean ± 95% CI) of Lining FLS, Sublining FLS, and Macrophage cells in UPA, Active, and Remission were shown. For each sample, the proportion of a cell type was calculated as (number of cells of that type) ÷ (total number of cells in that sample) (i.e., the fraction of all cells that are that type). These per-sample proportions were modelled with a quasi-binomial GLM to

avoid per-cell pseudoreplication and account for overdispersion. Points show estimated marginal means on the response scale; error bars show 95% CIs. Pairwise contrasts (Active–UPA, Active–Remission, Remission–UPA) were Benjamini–Hochberg adjusted; asterisks denote significance ($p < 0.05$, $p < 0.01$, $p < 0.001$). Non-significant comparisons are not annotated. Proliferating FLS were excluded from the analysis.

In RA, lining FLS actively participating in and driving the pathological processes that lead to chronic inflammation and irreversible joint damage. In order to understand how expression of genes involved in sialic acid biosynthesis and sialic acid capping changes, we generated a dot plot of sialic acid related genes. Figure 6-3A illustrates the expression patterns of various sialic acid biosynthesis and sialyltransferase genes in Lining FLS cells across different disease states. Overall, gene expression levels and the percentage of expressing cells vary considerably among the different sialyltransferase genes and across the conditions. For instance, in the Lining FLS Remission group, genes like ST3GAL1, ST3GAL4, and ST3GAL5 show relatively high average expression and a notable percentage of expressing cells. In contrast, genes such as ST3GALNAC3 and ST8SIA6 exhibit low expression and a smaller percentage of expressing cells across all conditions. Comparing the conditions, there are some notable differences. For example, ST6GALNAC6 generally shows high average expression across all three conditions with a significant percentage of expressing cells. Similarly, NANS also appears to be highly expressed across all groups. Some genes, like ST3GAL4, show higher average expression in the Remission group compared to Active or UPA. These patterns highlight distinct expression profiles of sialyltransferase genes that may be associated with different states of Lining FLS cells. The differential gene expression analysis, presented as two bar plots, compares the expression of various genes related to the sialic acid biosynthesis and capping in Active RA samples against UPA and Remission conditions. In brief, we run MAST analysis to observe genes related to the sialic acid biosynthesis and capping are whether significantly differentially expressed or not (adjp<0.05). In the Active vs UPA comparison, only ST6GALNAC5 exhibited a statistically significant change, showing a substantial downregulation in the Active group relative to UPA with highest log2 fold change (Figure 6-3B). All other genes in this comparison, despite some showing positive or negative trends in expression, did not reach statistical significance. Similarly, in the Active vs Remission comparison, while several genes displayed either increased expression in the active group (e.g., ST8SIA6,

ST3GAL2) or increased expression in the remission group (e.g., ST6GALNAC5, ST6GALNAC2), none of these observed differences were found to be statistically significant (Figure 6-3C). This comparison suggests that, apart from the notable decrease in ST6GALNAC5 expression in the Active state compared to UPA, the majority of the analysed genes do not demonstrate statistically significant differential expression across these specific disease conditions or classifications.

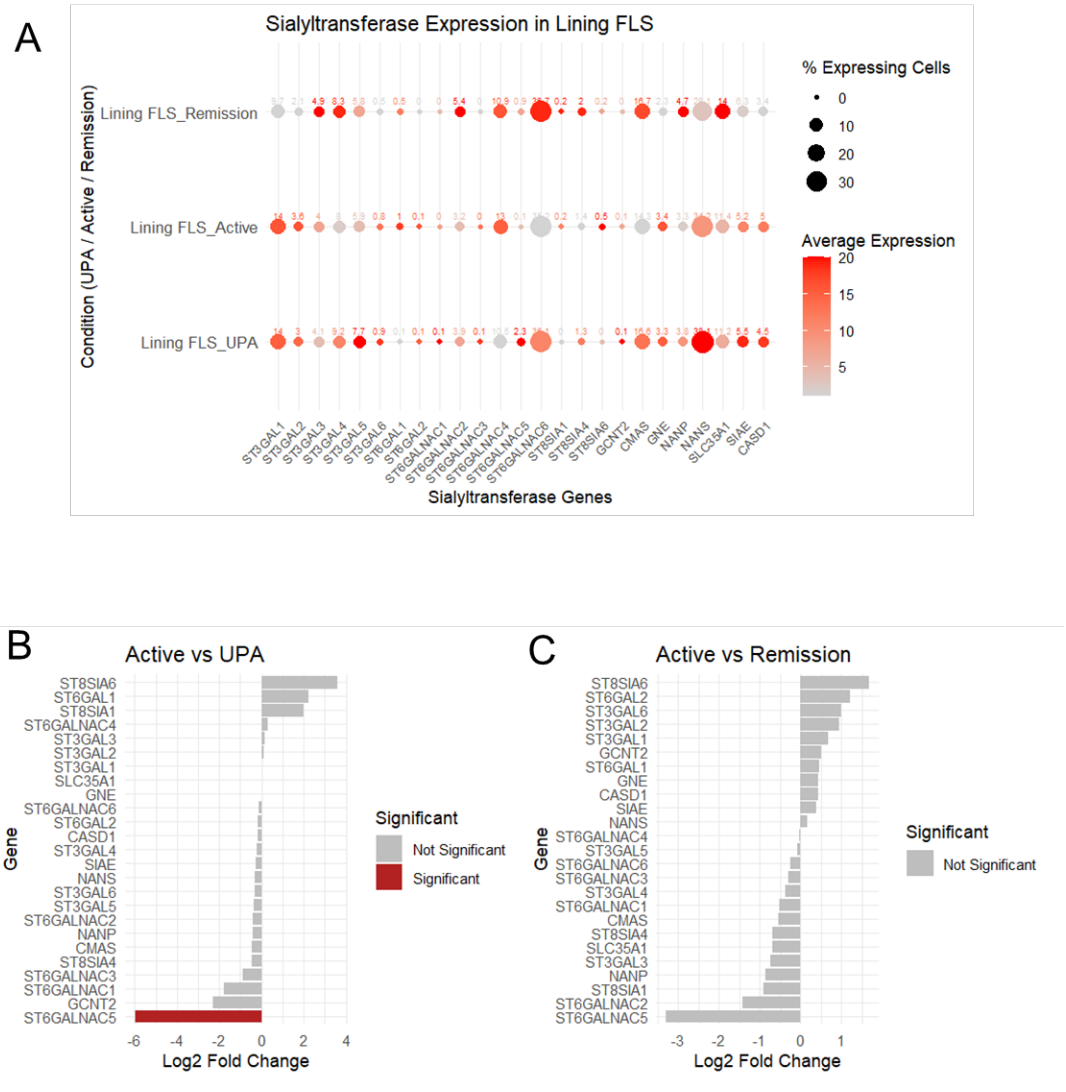

Figure 6-3 Expression patterns and differential regulation of genes related to sialic acid biosynthesis and capping in Lining Fibroblast-like Synoviocytes (FLS) across UPA, Active RA, and Remission groups.

DotPlot showing overall expression patterns (A) in Lining FLS. Dot size indicates the percentage of cells expressing each gene, and dot color reflects average scaled gene expression (light grey = low, dark red = high). Differential expression analysis of sialyltransferase genes in (B) Active vs. UPA and (C) Active vs. Remission comparisons. Bar plots represent log2 fold changes (log2FC) of selected sialyltransferase genes analysed by MAST. Genes showing significant differential expression (adjusted p-value <

0.05) are highlighted in red, while non-significant changes are shown in grey. Negative fold changes indicate downregulation in the Active group relative to UPA or Remission, whereas positive values indicate upregulation.

Sublining FLS drives the inflammatory milieu, supporting immune cell survival and local activation, contributing to chronic inflammation in RA. We next investigated how genes involved in sialic acid biosynthesis and sialic acid capping altered in sublining FLS. This dot plot in Figure 6-4A plot visualises the expression of various genes related to sialic acid biosynthesis and capping in Sublining FLS cells across different disease states. Overall, there is considerable variability in gene expression and the proportion of expressing cells among the different sialyltransferase genes and across the conditions. Notably, certain genes consistently exhibit higher average expression and a larger percentage of expressing cells across all conditions. For instance, ST3GAL1 shows high average expression and a substantial percentage of expressing cells. Similarly, ST6GALNAC6, ST3GAL4, NANS and CMAS also appears to be highly expressed across all groups. Upon comparing the conditions, some interesting patterns emerge. For example, ST6GALNAC4 shows a prominent average expression and percentage of expressing cells, particularly in the Remission and Active groups, although its expression in the UPA group is lower. Conversely, genes like ST6GALNAC5 and ST6GALNAC6 generally show very low average expression and a small percentage of expressing cells across all three conditions. Some genes like ST6GALNAC1 and ST6GALNAC2 maintain consistently low expression and low percentages of expressing cells across all conditions. These observations highlight specific expression profiles for sialyltransferase genes that may contribute to the distinct characteristics of Sublining FLS in different disease states. We also compared the differential expression of various genes in active RA samples against UPA and Remission conditions in sublining FLS. In the Active vs UPA plot (Figure 6-4B), most genes show minor, non-significant differential expression. While some genes like ST8SIA6 and ST6GALNAC1 exhibit a positive Log2 Fold Change, suggesting higher expression in the active group, and others like ST6GALNAC3 show a negative Log2 Fold Change, none of these differences are statistically significant. Conversely, the Active vs Remission plot (Figure 6-4C) reveals three genes with statistically significant differential expression. ST3GAL1, ST3GAL2 and ST3GAL4 are significantly upregulated in the active RA condition compared to remission, both showing positive Log2 Fold Changes. ST3GAL1 has

a Log2 Fold Change of 1, ST3GAL2 has a Log2 Fold Change of approximately 2, and ST3GAL4 approximately 1, suggesting a notable increase in their expression in the active state. Other genes in this comparison, such as ST6GALNAC5 and ST6GAL2, also show a positive Log2 Fold Change but do not reach statistical significance. Similarly, several genes like ST6GALNAC3 and ST8SIA4 show negative Log2 Fold Changes, implying higher expression in remission but these differences are not statistically significant. In summary, while there is broad non-significant variability in gene expression when comparing active vs UPA in Sublining FLS, the active state in Sublining FLS is characterised by a statistically significant upregulation of α2-3 linked sialic acids when compared to the remission state. Analysis of sialyltransferase gene expression in lining and sublining FLSs revealed only modest transcriptional differences across UPA, Active, and Remission states. In both subsets, overall expression of these enzymes was relatively low to moderate, with ST6GAL1, ST3GALs, and ST6GALNAC family members being the most consistently detected. Differential expression analysis showed that lining FLSs remained largely transcriptionally stable, with only ST6GALNAC5 significantly reduced in Active versus UPA, whereas sublining FLSs displayed small but consistent increases in several sialyltransferases, in ST3GAL family members, in Active compared to Remission. These subtle differences are expected, as sialyltransferases are generally stable housekeeping enzymes, and glycosylation remodelling in disease is often driven by post-transcriptional regulation, substrate availability, or enzyme compartmentalization rather than large shifts in mRNA levels. However, the limited but detectable changes in sublining FLSs may reflect their immunomodulatory role, whereas lining FLSs, specialized for matrix invasion, show less plasticity in this pathway.

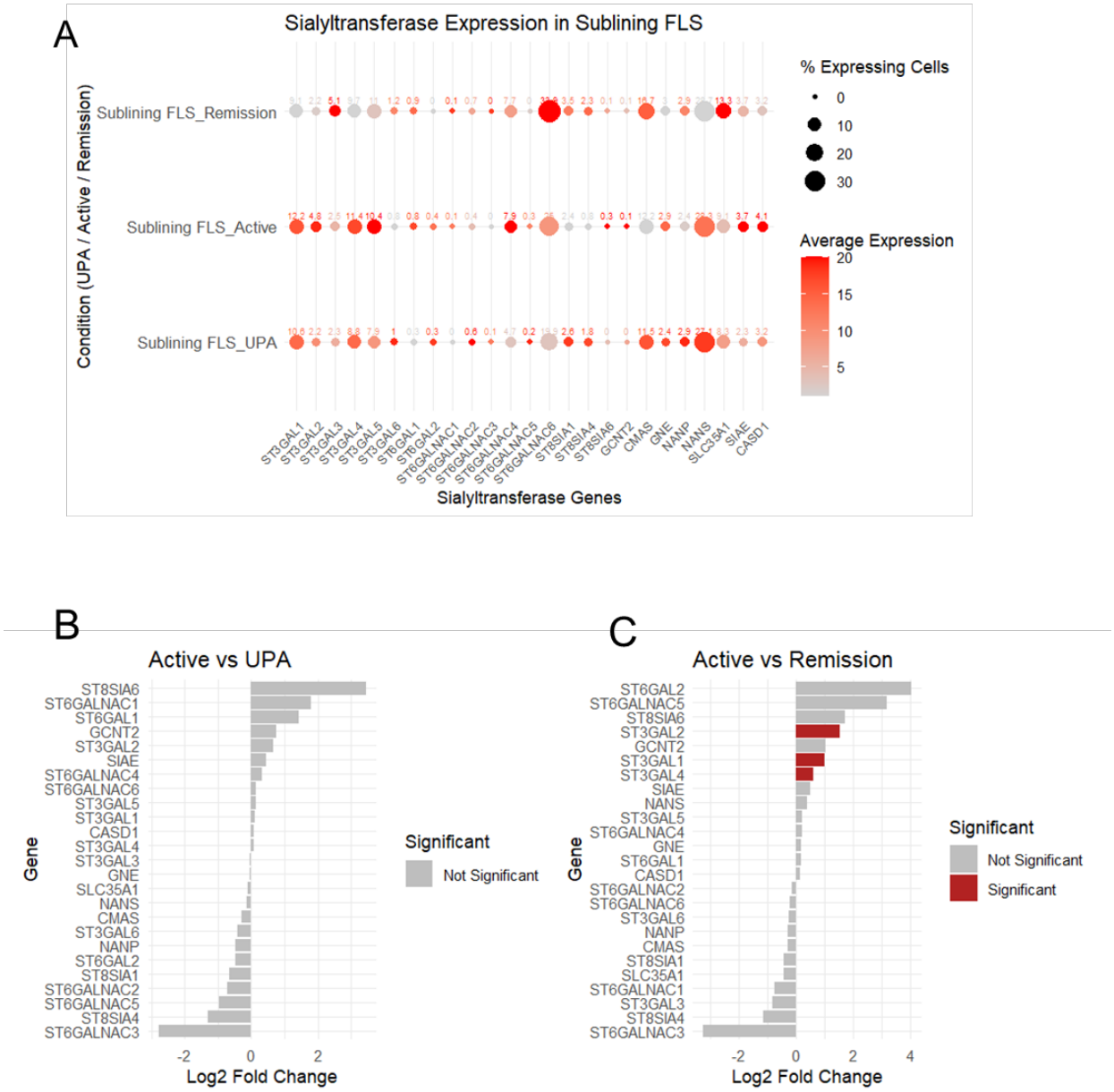

Figure 6-4 Expression patterns and differential regulation of genes related to sialic acid biosynthesis and capping in Sublining Fibroblast-like Synoviocytes (FLS) across UPA, Active RA, and Remission groups.

DotPlot showing overall expression patterns (A) in Sublining FLS. Dot size indicates the percentage of cells expressing each gene, and dot color reflects average scaled gene expression (light grey = low, dark red = high). Differential expression analysis of sialyltransferase genes in (B) Active vs. UPA and (C) Active vs. Remission comparisons. Bar plots represent log2 fold changes (log2FC) of selected sialyltransferase genes analysed by MAST. Genes showing significant differential expression (adjusted p-value < 0.05) are highlighted in red, while non-significant changes are shown in grey. Negative fold changes indicate downregulation in the Active group relative to UPA or Remission, whereas positive values indicate upregulation.

Tissue-resident macrophages play a central role in the immunopathology and resolution of RA. Unlike monocyte-derived inflammatory macrophages, tissue-resident macrophages are embedded within the synovial niche and contribute to immune homeostasis, tissue repair, and the orchestration of local inflammatory responses. Recent studies have highlighted that these cells are not only phenotypically distinct but also display a unique expression pattern of glycan-binding receptors, particularly Siglecs and Galectins (Mendez-Huergo et al., 2019; Paclik et al., 2011). These receptors enable macrophages to sense changes in the glycosylation patterns of surrounding cells and extracellular matrix components, where synovial fibroblasts undergo profound glycan remodeling during inflammation. Dysregulation of Siglec or Galectin pathways may impair the ability of tissue-resident macrophages to dampen inflammation, thereby contributing to the persistence of RA. To understand how siglec and galectin expressions changed in RA macrophages, we generated a dot plot for to visualise their average expressions. Figure 6-5A suggests that while certain Siglec genes such as CD22 and CD33 show consistent moderate expression across all groups, Galectin genes, particularly LGALS1, LGALS3, LGALS8, and LGALS9, demonstrate highly variable and often exceptionally high expression levels that are group-specific, potentially important for different macrophage activation or disease states. The significantly high average expression values for LGALS1 in active, LGALS9 in remission, and LGALS3 in UPA requires further investigation as they suggest these genes could be key players in defining the characteristics of each macrophage group in different disease states. Next, we investigated how siglec and galectin expressions differ between different disease states. SIGLEC10, and LGALS2 show the highest positive log2 fold changes, suggesting significantly higher expression in Active macrophages compared to UPA macrophages. In addition, LGALS1, LGALS8 and LGALS9 showed significant upregulation in Active vs UPA samples. Conversely, LGALS3, SIGLEC9, and SIGLEC14 exhibit negative log2 fold changes, with LGALS3 being significant, indicating higher expression in UPA macrophages (Figure 6-5B). In active vs remission comparison, LGALS2, LGALS12, LGALS3, and SIGLEC11 show positive log2 fold changes, with LGALS3 being the only significant gene in this group, indicating its higher expression in Active macrophages. Conversely, a substantial number of genes, including SIGLEC12, SIGLEC8, SIGLEC5, SIGLEC6, LGALS4, SIGLEC14, SIGLEC10, SIGLEC7, SIGLEC9, SIGLEC15, CD33, LGALS9, and LGALS8 exhibit negative log2 fold changes. Among these, while LGALS3 showed significantly

higher expression in active RA, CD33 demonstrated to express significantly higher in remission RA patient groups (Figure 6-5C).

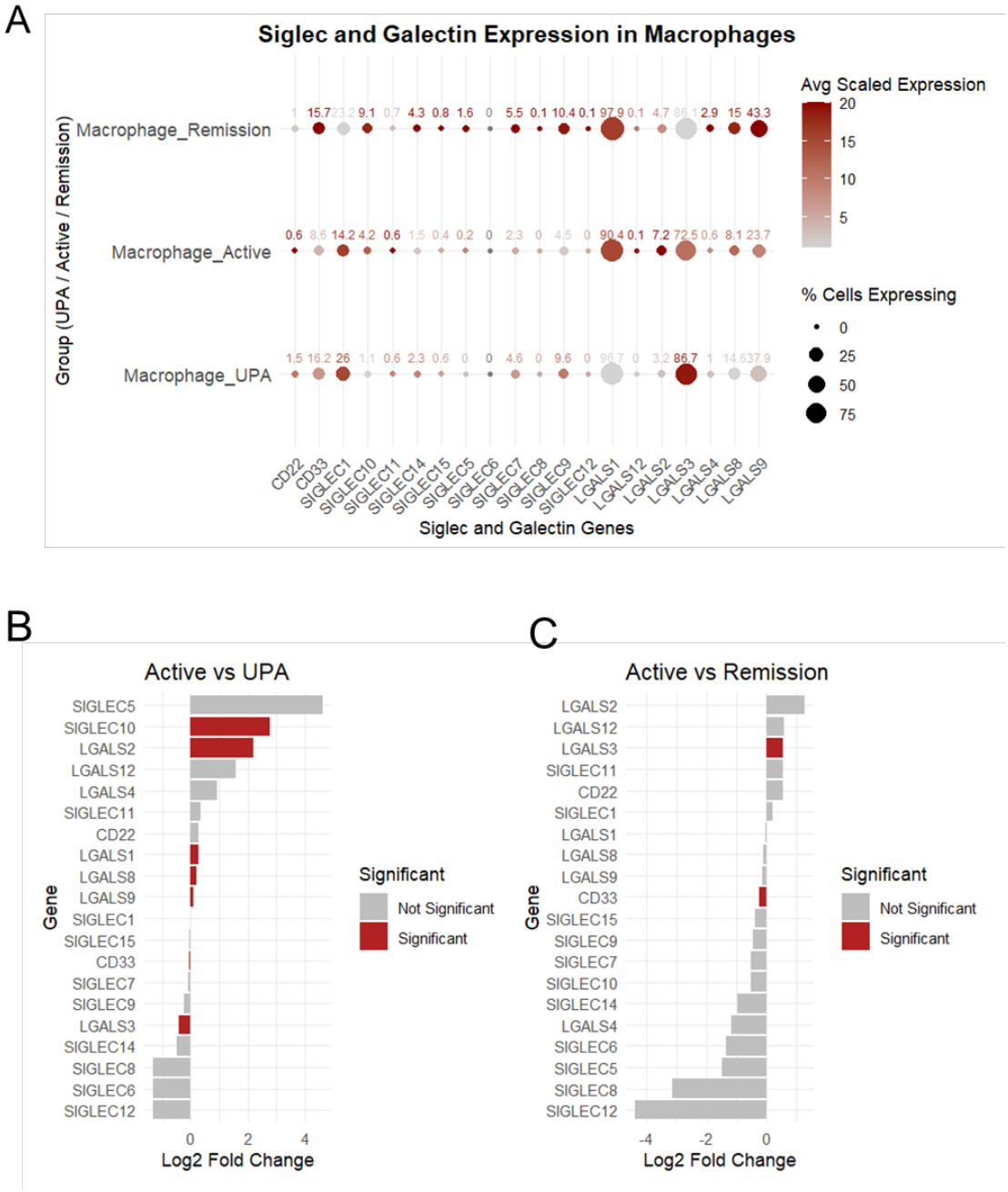

Figure 6-5 Expression patterns and differential regulation of siglec and galectin genes in Macrophages across UPA, Active RA, and Remission groups.

DotPlot showing overall expression patterns (A) in Macrophages. Dot size indicates the percentage of cells expressing each gene, and dot color reflects average scaled gene expression (light grey = low, dark red = high). Differential expression analysis of siglec and galectin genes in (B) Active vs. UPA and (C) Active vs. Remission comparisons. Bar plots represent log2 fold changes (log2FC) of selected sialyltransferase genes analysed by MAST. Genes showing significant differential expression (adjusted p-value < 0.05) are

highlighted in red, while non-significant changes are shown in grey. Negative fold changes indicate downregulation in the Active group relative to UPA or Remission, whereas positive values indicate upregulation.

6.3 Discussion

In this study, by profiling synovial tissue from patients across different disease states including early undifferentiated arthritis, active RA, and remission, we identified distinct transcriptional signatures within key cellular compartments, particularly FLS and tissue-resident macrophages. These changes highlight the central roles of both stromal and myeloid lineages in driving inflammation and tissue remodelling in RA. Lining FLS, known for their direct contribution to cartilage invasion and matrix degradation, displayed altered expression patterns in Active vs UPA state. Interestingly, ST6GALNAC5 was the only gene significantly downregulated in active RA compared to UPA, suggesting potential role in reduced α2-6 linked sialylation in active disease state. Sublining FLS, which contribute more importantly to the inflammatory milieu, displayed a different sialylation signature. Notably, genes involved in α2-3 sialic acid linked sialylation such as ST3GAL1, ST3GAL2, and ST3GAL4 were significantly upregulated in active RA compared to remission. This suggests a disease-specific shift in glycan capping that may influence interactions with glycan-binding proteins such as Siglecs and Galectins. The selective upregulation of α2-3 sialyltransferases in sublining FLS during active disease points to a potential mechanism for enhancing fibroblast-immune cell interactions via sialic acid dependent recognition pathways.

Lining and sublining SFs displayed clearly distinct glycosylation programs during active RA that mirror their spatial niches and functional roles. In lining SFs, transcriptomic data show downregulation of ST6GALNAC5, predicting reduced α2-6 sialylation of core-1 O-glycans and increased availability of the T antigen (Galβ1-3GalNAc). In contrast, sublining SFs in active disease exhibit coordinated upregulation of ST3GAL1, ST3GAL2, and ST3GAL4, establishing a strong α2-3 sialylation bias across multiple glycan substrates, including core-1 O-glycans and terminal LacNAc structures on both N- and O-glycans. Compared with the LacNAc-exposed, invasion-permissive state of lining SFs, this α2-3-dominant program in sublining SFs predicts a more extensively sialylated surface, likely tuned to immune lectin engagement and cytokine-responsive signaling within the immunoregulatory synovial niche.

Our study also highlights the critical role of tissue-resident macrophages and their glyco-immune sensing machinery in RA. Macrophages from different disease states expressed distinct expressions of Siglec and Galectin genes, implicating these molecules in the regulation of inflammation and tissue homeostasis. Notably, LGALS3 was consistently higher in active vs remission disease states, aligning with its known pro-inflammatory role and potential as a therapeutic target (Mendez-Huergo et al., 2019). CD33, a member of the inhibitory Siglec family, was more highly expressed in remission, potentially acting as a checkpoint molecule to temper inflammation. The divergent expression of Siglec10, Galectin-1, Galectin-2, Galectin-8 and Galectin-9 in active disease further supports the idea that glycan-binding receptors contribute to shaping macrophage activation states in a disease-specific manner.

Recent research provided important evidence about the interactions between CD33 (Siglec-3) and ST3GAL4 by recognising α2-3/6 linkages on the N-glycan surfaces (Büll et al., 2021). In the context of RA, our data reveal a striking observation in this potential regulatory axis: sublining FLS in the active disease state exhibit significantly elevated ST3GAL4 expression, while CD33 expression in macrophages is simultaneouslty reduced compared to remission. This suggests that although FLS may be increasing the presentation of sialylated ligands potentially as a compensatory or regulatory mechanism, macrophages may be less responsive due to reduced CD33 expression. The loss of this glycan-lectin interaction could impair inhibitory signaling in macrophages, promoting a sustained inflammatory state. Thus, the ST3GAL4 increase vs CD33 decrease patterns may reflect a breakdown in glycoimmune homeostasis, contributing to the persistence of synovial inflammation in active RA.

The interaction between galectins and sialylated glycans is critical in mediating various cellular processes, including cell adhesion, immune responses, and apoptosis. Galectins, a family of carbohydrate-binding proteins, recognise and bind to specific glycan structures that are decorated with sialic acids, significantly influencing their biological functions. Research has shown that different types of sialic acid linkages markedly affect galectin binding. For instance, galectin-1 has a preferential binding affinity for non-sialylated and α2,3-sialylated glycans, while its interaction with α2,6-sialylated structures is reduced (Stowell et al., 2008; Zhuo & Bellis, 2011). In our data, we see significant increase in Galectin-1 expressions in

active disease state. Considering the increase in the α2-3 sialylation in sublining FLS in active disease state, Galectin-1 in macrophages may be interacting with increased sialylated epitopes. In other words, simultaneously, sublining FLS in active RA may show increased expression of α2-3 sialyltransferases specifically ST3GAL1, ST3GAL2, and ST3GAL4 resulting in enhanced α2,3-linked sialylation on their surface glycoproteins. This coordinated shift may suggest a biologically relevant interaction where Galectin-1 produced by macrophages may have an increased binding capacity to sublining FLS in active disease due to the enhanced presentation of α2,3-sialylated glycans. This interaction could mediate cell-cell adhesion, immune cell retention, or apoptotic signalling, potentially contributing to the persistence of synovial inflammation or failed resolution. Rather than acting solely as an anti-inflammatory mediator, Galectin-1 in this context might participate in establishing a glycan-dependent pro-inflammatory niche, where stromal and myeloid cells are engaged in sustained crosstalk through sialylated glycan-Galectin-1 interactions. However, it is important to note that single-cell RNA sequencing does not capture all gene transcripts equally, especially those with low or transient expression. This is evident in our data, where several Siglec genes despite their known roles in immune modulation were expressed at low levels or undetected in tissue-resident macrophages. Such technical limitations underscore the need for complementary approaches such as analysing cells in protein levels to fully characterise the regulatory landscape of glycan-lectin interactions in RA. It should also be noted that single-cell RNA-seq analyses are limited by relatively low sample sizes and the sparse, gene-focused nature of the technology, which can underestimate the complexity of glycome remodeling and miss regulatory changes occurring at the protein or structural glycan level.

Together, our findings reveal a dynamic and disease-specific glycoimmune landscape within the RA synovium, shaped by coordinated changes in both glycosyltransferase expression in fibroblast subsets and lectin receptor expression in tissue-resident macrophages. The upregulation of α2-3 sialyltransferases in sublining FLS and the simultaneous modulation of Galectin and Siglec expression in macrophages suggest that sialylated glycan-lectin interactions are central to the persistence and regulation of synovial inflammation. Notably, the expression of ST3GAL4 and CD33 highlights a potential breakdown in inhibitory glycan recognition, which may contribute to unchecked macrophage activation in active RA. Moreover, the increased expression of Galectin-1, alongside enhanced α2-3

sialylation in FLS, points to a potentially pro-inflammatory role for Galectin-1 in reinforcing stromal-myeloid crosstalk. While single-cell RNA sequencing has provided crucial insights, the limited detection of several key Siglecs underscores the need for integrative analyses at the protein level to fully unravel the functional impact of these interactions. Ultimately, understanding how altered glycosylation shapes immune cell communication may offer novel therapeutic avenues to restore tissue homeostasis and resolve chronic inflammation in RA.

7. Chapter 7 General Discussion

This thesis aimed to understand how sialic acid modulates synovial fibroblasts inflammatory responses. We took a combined approach, analysing publicly available datasets from human RA, and experiments using murine cells as a model. We aimed to study effects on the synovial fibroblasts themselves, but also on the crosstalk between fibroblasts and macrophages. This should provide a broader perspective. The work was built on previous research done in the lab, although data regarding the human disease was more limited. Our bioinformatic work includes chapter 3, integrating bulk RNA sequencing of SFs from RA versus healthy synovium with and without TNF-α, and chapter 6, focusing on single cell transcriptomics across disease states from undifferentiated arthritis to active rheumatoid arthritis to remission. Together these data show that glycosylation, especially sialylation, acts as an organising layer of stromal myeloid communication in rheumatoid arthritis. Beyond confirming canonical inflammatory activation such as NF-κB, JAK-STAT, and TNF signalling, we find that cytokine exposure reprograms the synovial fibroblast glycome at several levels. These include transcription of glycosyltransferases for example the ST3GAL family, and the sialic acid pathway covering biosynthesis activation and transport GNE, NANS, NANP to CMAS to SLC35A1. Single cell data then place these changes into spatially and functionally distinct fibroblast subsets lining versus sublining and link them to tuning of lectin receptors on tissue resident macrophages including Siglecs and Galectins. These results combined support a model in which TNF-α and microenvironmental cues build a glyco-code that biases cell-cell recognition receptor clustering and signalling thresholds. This helps explaining inflammatory persistence and variable treatment responses. For context on fibroblast subset biology and single cell atlases in RA see Mizoguchi and colleagues, Croft and colleagues, and atlas work from Zhang and colleagues (Croft et al., 2019; Mizoguchi et al., 2018; F. Zhang et al., 2019).

In Chapter 4 and 5, we explored how changes in the sialylation of fibroblasts could indirectly affect macrophages biology. Interestingly, not all changes in sialic acid expression were triggering inflammatory responses, and specific sialic acid-containing molecules seem to exert a variable degree of activation of the SF-

Macrophage communication. Conditioned media from SFs selectively desialylated at α2-3 (Lectenz, VC) potently reprograms bone marrow-derived macrophages towards an M1-like, state, marked by increased Il1b, Ccl6, Cxcl10 and Nos2, higher GSVA M1 scores, and upregulation of CD80/CD86/PD-L1, with pathway enrichment for TNF-α, NF-κB, and type I interferon signaling; in contrast, broad α2-3/α2-6 cleavage (induced by CP sialidase treatment) elicits a mixed phenotype with concurrent Il1b and Arg1 induction, while inefficient α2-3 removal (AU) is largely no affecting cell behaviour, despite cells still lost significant amount of sialic acid in other linkages. At the protein level, PD-L1 rises in VC/L conditions, and MerTK decreases in CP-SF BMDMs. Together, these data support a thresholded model in which α2-3 sialylation on SFs acts as a suppressive, SAMP-like glyco-checkpoint where its selective removal amplifies a pro-inflammatory SF secretome that drives macrophage polarisation, whereas broad or less cleavage yields blended or muted responses which is implicating preservation of α2-3 sialylation or blockade of downstream myeloid signalling as potential therapeutic strategies in RA. These data correlated with distinct activation of SFs from distinct sialidase treatment. Overall, we observed that not all the sialic acid found in SFs act in the same way or contains the same inflammatory or anti-inflammatory potential. This may also relate to the high degree of heterogeneity seen in the human datasets, where glycan biosynthetic pathways were studied. Whether such changes are induced by genetic or environmental factors is still unknown, but these results provide further evidence of the involvement of sialic acid in local inflammatory responses supported by stromal cells.

7.1 Speculations on TNF-α Driven Remodelling of the SF Glycome

Together, our data indicate that SFs in RA undergo a two-tiered reprogramming of their sialylation machinery. At baseline, RA SFs differ from healthy SFs by maintaining or enhancing sialic acid biosynthesis while selectively dysregulating glycan capping, characterized by reduced expression of specific α2-3 and α2-8 sialyltransferases and increased α2-6 sialylation. On the other hand, inflammatory stimulation with TNF induces a dynamic remodelling of sialylation, driving increased α2-3 sialyltransferase expression and sialic acid production while constraining alternative modification and transport pathways. This TNF-driven shift toward α2-3 dominant sialylation may fine-tune SF responsiveness within the inflamed synovium, reshaping lectin engagement and reinforcing pathogenic fibroblast functions. Collectively, these findings support the concept that RA-

associated sialylation changes are not static but are progressively reinforced and redirected by inflammatory cues, contributing to the persistence and amplification of synovial pathology.

In bulk synovial fibroblasts TNF-α does more than simply inducing cytokines and chemokines. It selectively reprograms glycosylation pathways with upregulation of α2-3 sialyltransferases, ST3GAL1, ST3GAL3 and ST3GAL4 and galactosyltransferases B3GALT1, B3GALT2 and B3GALT5 together with downregulation of ST6GALNAC6. Functionally these shifts are predicted to extend N-acetyllactosamine LacNAc chains and increase α2-3 capping while constraining α2-6 capping of O glycans, thereby remodelling the ligand landscape for glycan binding proteins (Dennis, Lau, et al., 2009; Nabi et al., 2015).

α2-3 capping on integrins and on CD44 can modulate adhesion and motility which offers a route by which TNF-α exposed SFs acquire more invasive and retentive behaviour in pannus. CD44 is highlighted here because its binding to hyaluronan depends on sialylation. Terminal sialic acids and especially α2-3 linkages reduce hyaluronan affinity, while desialylation increases binding, making CD44 a sensitive readout of linkage shifts. Studies demonstrate increased hyaluronan binding after neuraminidase treatment or after site specific removal of CD44 N-glycans (Faller & Guvench, 2014; Katoh et al., 1995). A TNF-α driven move away from α2-6 towards α2-3 together with more LacNAc from B3GALT upregulation would also be expected to enhance galectin binding to CD44 and related receptors which favours lattice formation and stabilises adhesive contacts. This follows the well-established principle that α2-6 sialylation acts as an off switch for galectin binding whereas α2-3 often preserves it (Stowell et al., 2008; Zhuo & Bellis, 2011). Finally, these transcript shifts occur on a background of TNF-α driven metabolic rewiring toward glycolysis which limits pools of CMP-Neu5Ac and UDP sugars. Changes in biosynthesis and transport transcripts may therefore be compensatory responses to these bottlenecks, a concept that aligns with work linking nutrient flux, hexosamine pathway intermediates, and cell-surface organisation (Dennis, Nabi, et al., 2009; Grigorian et al., 2009). Together these points position TNF-α not only as a driver of inflammation but also as an architect of the synovial glycome. Of note prior work in arthritis models reports that TNF-α reduces ST6GAL1 dependent α2-6 sialylation in SFs which fits the trend we observe (Y. Wang et al., 2021).

7.2 Glycosylation Signatures of Distinct SF Subsets

Single cell profiling can help to understand how glycosylation changes in fibroblast types and disease state aligns with function. Lining fibroblasts (cartilage adjacent, leading tissue damage) and sublining fibroblasts (immunoregulatory niche) carry distinct glyco-codes, probably shaped by their micro niches and tasks. In lining fibroblasts, downregulation of ST6GALNAC5 in active disease implies reduced α2-6 capping on core 1 O- glycans, leaving the T antigen Gal β1-3 GalNAc more available for further extension such as poly LacNAc or for α2-3 capping by ST3GAL1. Functionally, this likely increases LacNAc exposure, which improves galectin ligands, changes mucin type glycoprotein conformation, and lowers the sialic acid brake on receptors that mediate matrix engagement and invasion such as CD44 and integrins. The predicted result could involve more protease activity, integrin activation, and firm adhesion at the cartilage interface during invasive phases. In sublining fibroblasts during active rheumatoid arthritis, upregulation of the sialyltransferases ST3GAL1, ST3GAL2, and ST3GAL4 creates a strong α2-3 sialylation bias. ST3GAL1 mainly targets core-1 O-glycans, ST3GAL4 caps terminal LacNAc structures on N- and O-glycans, and ST3GAL2 acts in more specific glycolipid or protein contexts. Together, this remodeling increases α2-3 sialylation across multiple glycan classes, altering how fibroblast glycans are recognised by lectins such as Siglecs and Galectins, and thereby promoting pro-inflammatory cell-cell interactions within the synovium. This shift increases the density of α2-3 sialylated LacNAc which tends to preserve galectin binding because α2-6 is the structurally stronger inhibitor. When there is α2-6 sialic acid, it sits right on that C6 hydroxymethyl position, sterically and electrostatically blocking interactions with the carbohydrate binding domain in galectins and the galactose residue. By contrast, α2-3 sialic acid decorates the C3 position and usually leaves the C6 face accessible, so most galectins can still bind or bind internal LacNAc repeats. This is why α2-6 capping is widely described as a stronger off-switch for galectin binding (Zhuo & Bellis, 2011). The resulting surfaces finally favour multivalent galectin lattices that stabilise cytokine and adhesion receptors on fibroblasts and, may tune cell-cell and cell-endothelium interactions consistent with increased migratory behaviour of SFs (Nabi et al., 2015; Stowell et al., 2008). Because different Siglecs and Galectins have linkage and context dependent preferences, an α2-3 skewed surface on sublining fibroblasts is well placed to modulate tissue resident macrophages by biasing contact duration, receptor

clustering, and downstream transcriptional states. This compartmental view of lining versus sublining function agrees with prior work that functionally separated fibroblast subsets that drive damage versus those that drive inflammation (Croft et al., 2019). These subset specific glycomes are likely reinforced by micro niche variables. Hypoxia through HIF-1 α pushes glycolysis and the hexosamine pathway which changes UDP-GlcNAc and UDP-Gal availability (Paneque et al., 2023; Shirato et al., 2010). TNF-α and IL-1β gradients may regulate glycosyltransferases and nucleotide sugar transporters such as the SLC35 family. Extracellular matrix stiffness and mechanical stress through YAP-TAZ and Golgi positioning alter Golgi trafficking and enzyme compartmentalisation and together these factors set effective flux through branching MGAT enzymes and capping ST3GAL and ST6GALNAC steps involved in glycosylation (Z. Zhang et al., 2025). The result is a compartmentalised glycosylation with lining fibroblasts tuned for matrix invasion and sublining fibroblasts tuned for immune orchestration.

These mechanistic links and hypothesis are supported by the literature and our data, but further experiments are required to validate them. Modern technologies such as spatial and multi omic approaches could provide an excellent alternative to confirm these functional cell-cell interactions. Although glycans are not commonly included in spatial analysis, combination of these techniques with lectin histochemistry, for example SNA and MAL II for α2-6 and α2-3, PHA L and PHA E for branching, could integrate glycans in current spatial omics methods, increasing the value of the biological information extracted from these expensive experiments.

Furthermore, future experiments could take advantage of Siglec Fc and Galectin Fc binding, mass spectrometry glycomics and glycopeptidomics, to develop the field of spatial glycomics and its integration with other omics to locate glycan linkages, branching, and lectin engagement by subset and disease state. These techniques would be limited to available glycan-recognising molecules, which somehow limits the scope. Broader spatial glycomics are limited by the available tools, as only N-glycans can be identified by MS-based approaches, and technological advances are needed to fully integrate glycans in general overarching spatial omics.

7.3 Potential Role of Siglec Signalling in Stromal Inflammation

Integrating stromal changes with macrophage receptor profiles points towards a disease state mismatch that could lead to the loss of inhibitory glycan Siglec signalling, and potentially exacerbation of autoimmune responses. In active disease, sublining fibroblasts increase ST3GAL4 and therefore α2-3 capped ligands, while macrophages reduce expression of Siglec 3 (CD33) relative to remission. If stromal cells increase sialylation and immune cells reduce the corresponding inhibitory receptor, the net effect could be a loss of inhibitory tone. This would be a failed glyco-checkpoint that can lock macrophages in pro inflammatory states despite stromal attempts to restore homeostasis. Siglec 3 recognises both α2-3 and α2-6 sialylated ligands although linkage preferences are context-dependent (Büll et al., 2016; Crocker & Varki, 2001). An environment with more α2-3 and constrained α2-6 likely changes the repertoire and affinity of ligands seen by macrophages. Cell-based glycan array studies support these hypothesis and show that Siglecs differ in their linkage preferences and that Siglec 3 can engage both α2-3 and α2-6 contexts (Büll et al., 2016; Kukan et al., 2024). This can offer therapeutic alternatives, since clinical interventions aimed to reengage inhibitory Siglec pathways could restore tissue homeostasis by rewiring SF-Macrophages communication. Examples can be multivalent sialylated compounds or nanoparticles or engineered α2-6 ligands. For instance, sialic acid mimetrics with improved binding affinity and selectivity towards Siglecs have currently been developing to target diseases involving sialic acid-siglec axis (Büll et al., 2016).

Galectin-1 provides a second context dependent axis. Although often described as immunosuppressive, Galectin-1 is elevated in macrophages during active disease alongside increased α2-3 sialylation on sublining fibroblasts. Because α2-6 capping blocks galectin binding more strongly than α2-3, a shift toward α2-3 capping on LacNAc bearing glycoproteins together with moderate N-glycan branching should increase Galectin-1 avidity and promote multivalent bridging. In this glycan context, Galectin-1 may stabilise stromal myeloid contacts, retain immune cells within inflamed niches, and bias survival and apoptosis decisions in ways that fail to resolve inflammation. Blocking Galectin-1 or disfavouring its binding geometry by altering linkage therefore becomes an attractive way to disrupt retentive stromal-myeloid circuits. Evidence that α2-6 sialylation specifically

suppresses galectin binding underlines the rationale for interventions that increase α2-6 presentation at selected sites (Zhuo & Bellis, 2011).

7.4 Multi-Layered Glycoimmune Regulation in RA

These findings support a three-layer model of glycoimmune regulation. Layer 1 is the cytokine and metabolic layer. TNF-α and other mediators reprogram the sialic acid pathway, terminal transferases, and branching enzymes under constraints set by nucleotide sugar availability and Golgi transport which defines the feasible glycome. Layer 2 is the subset and niche layer. Lining and sublining fibroblasts occupy distinct biophysical and cytokine microenvironments that imprint divergent glyco signatures aligned with their core functions with lining favouring matrix engagement and sublining prioritizing immune orchestration. Layer 3 is receptor tuning in myeloid cells. Macrophages adjust inhibitory Siglecs and context dependent Galectins which sets response thresholds to stromal ligands. In active disease this balance shifts toward reduced Siglec mediated inhibition and enhanced Galectin mediated retention.

Because this study is based on a transcriptomic approach, it is important to acknowledge certain limitations from the outset. Transcript levels alone do not uniquely determine the realised glycome, as factors such as enzyme localization, Golgi pH, nucleotide sugar transport efficiency, and substrate competition also play critical roles. Moreover, single-cell RNA sequencing can under-detect low-abundance Siglecs. Finally, extended two-dimensional culture systems tend to erode disease-relevant phenotypes, which highlights the need for more physiologically relevant models such as three-dimensional scaffolds, organoids, synovial explants, or cartilage-on-chip systems. Further validations should combine lectin flow cytometry for α2-3 versus α2-6 signatures on prospectively purified lining and sublining fibroblasts with mass spectrometry glycomics and site specific glycopeptidomics of key receptors such as CD44, PDPN, ICAM-1 and integrins. Binding assays using Siglec Fc and Galectin-1 Fc should be performed with and without TNF-α while CRISPR or siRNA manipulation of ST3GAL4 and ST6GAL1 can test causality for predicted binding shifts and downstream signalling. Functional cocultures of fibroblasts and macrophages under Galectin-1 blockade or CD33 agonism should assess cytokine profiles. Spatial multi omics including transcript protein comapping and multiplexed lectin imaging together with MALDI mass spectrometry imaging of glycans will be essential to anchor

mechanisms in RA tissues. Finally small prospective cohorts that relate baseline α2-3 to α2-6 balance and synovial macrophage CD33 levels to anti-TNF outcomes would establish clinical utility, while ex vivo synovial explant studies can test combinations of anti-TNF with Galectin-1 blockade or CD33 agonism.

Overall, the data support a glycoimmune axis in which TNF-α driven and subset specific glycosylation changes in SFs intersect with altered lectin receptor landscapes in macrophages to create a retentive pro-inflammatory circuit characterised by loss of inhibitory Siglec engagement and reinforcement by Galectin-1. This framework elevates glycosylation to a primary regulator of synovial chronicity identifies druggable glycol-checkpoints with translational promise and motivates biomarker development that could refine RA subtyping and guide therapy selection.

7.5 α2-3 desialylation as a key activator of synovial fibroblasts and macrophages

Desialylation may serve as a molecular switch, converting a tolerogenic synovial niche into a self-sustaining inflammatory environment by modulating SF-macrophage interactions. When α2-3 desialylation is below certain thresholds, the effect on inflammation is minimal because partial removal of these sialic acids doesn't sufficiently expose underlying glycans to trigger robust immune responses. At low levels of desialylation, the remaining α2-3-linked sialic acids are still adequate to maintain normal interactions with inhibitory receptors like Siglecs, or to mask pro-inflammatory glycan epitopes recognised by activating lectins, including certain Galectins. In other words, limited removal doesn't cross the threshold needed to significantly alter immune receptor engagement or downstream signalling. Hence, macrophages or other immune cells perceive the partially desialylated surface as essentially unchanged (similar to untreated conditions), resulting in minimal or no activation of inflammation. Only when desialylation surpasses a critical threshold does significant glycan remodelling occur, enhancing exposure of pro-inflammatory glycan epitopes and thus tipping the balance toward inflammation and immune cell activation.

While investigating siglecs and galectins in the SFs and BMDMs, we have found that L desialylated SFs, VC-BMDMs and L-BMDMs, increased galectin-9 and siglec-1 expressions (Figure 7-1). The interaction between Siglec-1 and Galectin-9

in the context of desialylation is an area of growing interest, particularly in how these glycan-binding proteins influence immune responses and cell interactions during various physiological and pathological processes. Siglec-1, a member of the Siglecs, is primarily expressed on dendritic cells and macrophages. Siglec-1 is unique among Siglecs because it lacks inhibitory motifs and is the only member of the family that drives pro-inflammatory actions, particularly through macrophage activation and antigen presentation. This receptor is implicated in mediating the effects of sialylated glycoproteins and glycolipids. It has a high affinity for sialic acid, which can affect how cells recognise and respond to desialylated entities. It should be noted that desialylation may not directly induce Siglec-1 expression, which is largely regulated at the transcriptional level by type I interferons. Instead, selective removal of sialic acids remodels the glycan landscape, unmasking or enriching ligands that are preferentially recognised by Siglec-1. This shift enhances the functional engagement of Siglec-1 positive macrophages with surrounding cells, thereby amplifying pro-inflammatory interactions without altering receptor expression itself. Siglec-1 preferentially recognises accessible α2-3-linked sialylated glycans (Gonzalez-Gil & Schnaar, 2021), and not all sialic acids contribute equally to binding. In inflamed tissues, selective removal of certain sialic acids such as α2-6 linkages that normally cap N-glycans, can unmask underlying glycan backbones or expose α2-3 sialylated motifs on O-glycans and glycolipids that are high-affinity Siglec-1 ligands. Thus, rather than abolishing recognition, partial desialylation reshapes the glycan landscape by removing steric hindrance and enriching the presentation of preferred epitopes. In this way, inflammatory remodeling of the glycome can increase the availability of Siglec-1 ligands, thereby strengthen macrophage-cell interactions and promoting pro-inflammatory signaling. Desialylation may also enhance the expression of Siglec-1 and Galectin-9 through a combination of immune disinhibition and cytokine-driven feedback. In the healthy synovium, sialylated glycoproteins on SFs engage inhibitory Siglecs on macrophages, maintaining immune quiescence. Upon desialylation, the loss of α2-3 sialic acids disrupts these inhibitory interactions, leading to activation of NF-κB and STAT pathways in macrophages. As a result, exposed LacNAc-rich glycans promote binding and clustering by Galectin-3 and Galectin-9, amplifying pro-inflammatory signalling. This activated state triggers the secretion of IFN-β, TNF-α, and IL-6, which in turn induce Siglec-1 and Galectin-9 expression as part of the type I interferon response. The result is a self-reinforcing loop in which desialylation not only unmasks pro-inflammatory ligands but also drives

upregulation of Siglec-1 and Galectin-9, further enhancing macrophage activation and synovial inflammation. Indeed, the top upregulated genes we observed in L-BMDMs were predominantly interferon-stimulated genes (ISGs), including Ligp1, Rsad2, Ifi213, and Gbp4. This transcriptional profile strongly suggests that desialylation triggers a type I interferon response in macrophages. The loss of sialic acid likely disrupts inhibitory Siglec signalling, leading to immune disinhibition and activation of downstream pathways such as NF-κB and IRF3. These pathways are known to drive the expression of ISGs, many of which are involved in antiviral defence, antigen processing, and amplification of inflammatory signalling. Notably, the upregulation of Siglec-1 (CD169) and Galectin-9 may be part of this interferon-driven program, further supporting a model in which desialylation promotes a shift toward an IFN-enriched, pro-inflammatory macrophage phenotype (Figure 7-1). This experimental proposal does not mean necessarily that what happens *in vivo*, but murine transcriptional data allows us to correlate changes and responses.

7.6 α2-3 Desialylation Primes SF Secretomes to Drive M1-like Macrophage Polarisation

Our results support a working model in which α2-3 sialylation on SFs functions as an immunosuppressive glyco-checkpoint that restrains a pro-inflammatory secretome. Selective removal of α2-3 residues with VC or L bypasses this checkpoint, amplifying IL-6/chemokine output and type I interferon–skewed programs in SFs and, in turn, licensing a paracrine push that drives macrophages toward a classical, APC-competent M1-like state (elevated Nos2, Il1b, Cxcl10; increased CD80/CD86/PD-L1). In contrast, broader desialylation with CP, which removes both α2-3 and α2-6 linkages, elicits a mixed macrophage phenotype with concurrent induction of Il1b and Arg1, while less α2-3 cleavage with AU fails to cross the activation threshold and leaves macrophages largely unchanged. Taken together, these patterns argue that α2-3 capping is the dominant sialylation feature governing SF and macrophage inflammatory crosstalk.

Two non-exclusive mechanisms could underlie the α2-3 dependence. First, a Siglec-centric loss-of-brake model where α2-3-capped SF ligands may tonically engage inhibitory Siglecs on myeloid cells, and their removal lowers the threshold for NF-κB and type I IFN activation in macrophages exposed to SF-conditioned media. Second, a galectin/lattice gain-of-signal model where α2-3 loss unmasks LacNAc motifs and remodels galectin lattices on SFs, stabilising or clustering

cytokine receptors, thereby boosting SF signaling and producing a more inflammatory secretome that secondarily imprints macrophages. Conceptually, α2-3 sialic acids may act as self-associated molecular patterns (SAMPs); their removal mimics tissue damage or microbial cues and converts homeostatic SF signals into danger signals that reprogram nearby macrophages (A. Varki, 2011).

The mixed CP phenotype likely reflects the broader surface re-wiring that accompanies dual α2-3/α2-6 cleavage. One possibility is that CP-treated SFs co-secrete resolving or tissue-repair mediators sufficient to raise Arg1 without fully extinguishing M1-associated genes, producing a transitional macrophage state akin to that observed in chronic inflammation. An alternative or complementary explanation is receptor desensitization where extensive glycan loss may destabilise specific SF receptors or their lattices, capping the maximal inflammatory output relative to the α2-3-focused perturbation produced by VC/L.

These hypotheses yield several testable predictions. Enzymatic re-capping of α2-3 on SFs (e.g., ST3GAL add-back in the presence of CMP-Neu5Ac) before conditioned media collection should blunt the M1-skewing capacity of VC/L-conditioned media. Conversely, blocking inhibitory Siglecs or galectins on macrophages should restore M1 skew even when SFs are partially re-sialylated, while Siglec agonism should dampen the VC/L-conditioned media effect. If galectin organisation is causal, galectin-3 inhibition during SF desialylation should reduce IL-6/CXCL10 in the conditioned media and attenuate macrophage polarisation.

The disease relevance of this axis is compelling. As mentioned in the general introduction, endogenous neuraminidases (e.g., NEU1/NEU3) and microbial neuraminidases present in inflamed joints could reproduce the α2-3 loss modeled ex vivo, creating a self-sustaining SF-macrophage inflammatory loop characteristic of rheumatoid arthritis. This loop may intersect with current therapies which preserving α2-3 sialylation or dampening downstream myeloid responses might complement IL-6R or GM-CSF blockade and JAK inhibition. Notably, PD-L1 induction on M1-skewed macrophages could restrain T-cell activation while sustaining myeloid-driven inflammation, offering a potential explanation for heterogeneous clinical responses and suggesting combinatorial strategies that rebalance stromal-myeloid-lymphoid interactions.

Therapeutically, multiple intervention points emerge. Strategies that preserve or restore α2-3 sialylation (neuraminidase inhibition, sialomimetic scaffolds, or boosting ST3GAL activity) could re-establish the stromal glyco-checkpoint. On the myeloid side, Siglec agonists might reinstate inhibitory tone, whereas selective galectin inhibitors could disrupt pathogenic receptor lattices on SFs and blunt the pro-inflammatory secretome. Careful dosing will be essential to avoid over-correction, given the affect of CP-like transitional states we observe when the glycan landscape is broadly perturbed.

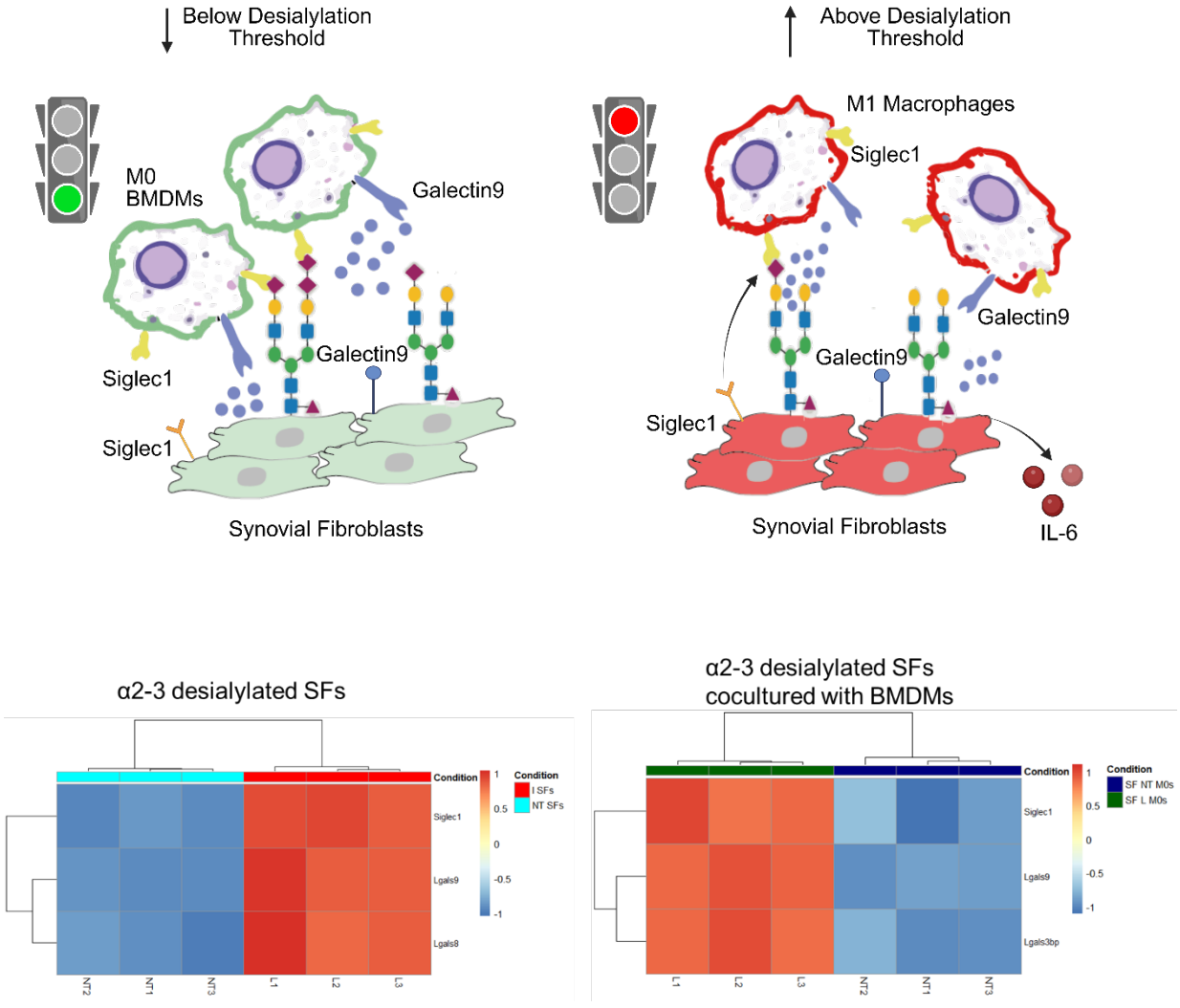

Figure 7-1 Proposed model for SFs and BMDMs crosstalk.

Synovial fibroblasts α2-3 desialylation above certain thresholds activates macrophages into M1 like phenotype with increased expressions in Siglec1 and Galectin 9. Differential gene expression was analysed using DESeq2, with significance defined as $|\log_2 FC| > 1$ and padj < 0.05.

8. REFERENCES

Abbasifard, M., Imani, D., & Bagheri-Hosseinabadi, Z. (2020). PTPN22 gene polymorphism and susceptibility to rheumatoid arthritis (RA): updated systematic review and meta-analysis. *The Journal of Gene Medicine*, *22*(9), e3204.

Adams, O. J., Stanczak, M. A., von Gunten, S., & Läubli, H. (2018). Targeting sialic acid–Siglec interactions to reverse immune suppression in cancer. *Glycobiology*, *28*(9), 640–647.

Al-Ani, N., Gorial, F., Yasiry, D., Al Derwibee, F., Abbas Humadi, Y., Sunna, N., & AlJabban, A. (2021). Clinical outcomes in Iraqi patients with rheumatoid arthritis following earlier or later treatment with etanercept. *Open Access Rheumatology: Research and Reviews*, 57–62.

Alex, A. M., Kunkel, G., Sayles, H., Flautero Arcos, J. D., Mikuls, T. R., & Kerr, G. S. (2020). Exposure to ambient air pollution and autoantibody status in rheumatoid arthritis. *Clinical Rheumatology*, *39*(3), 761–768.

Alivernini, S., MacDonald, L., Elmesmari, A., Finlay, S., Tolusso, B., Gigante, M. R., Petricca, L., Di Mario, C., Bui, L., & Perniola, S. (2020). Distinct synovial tissue macrophage subsets regulate inflammation and remission in rheumatoid arthritis. *Nature Medicine*, *26*(8), 1295–1306.

Allendorf, D. H., Franssen, E. H., & Brown, G. C. (2020). Lipopolysaccharide activates microglia via neuraminidase 1 desialylation of toll-like receptor 4. *Journal of Neurochemistry*, *155*(4), 403–416.

Anders, H.-J., & Ryu, M. (2011). Renal microenvironments and macrophage phenotypes determine progression or resolution of renal inflammation and fibrosis. *Kidney International*, *80*(9), 915–925.

Angiolilli, C., Kabala, P. A., Grabiec, A. M., Van Baarsen, I. M., Ferguson, B. S., García, S., Fernandez, B. M., McKinsey, T. A., Tak, P. P., & Fossati, G. (2017). Histone deacetylase 3 regulates the inflammatory gene expression programme of rheumatoid arthritis fibroblast-like synoviocytes. *Annals of the Rheumatic Diseases*, *76*(1), 277–285.

Armaka, M., Gkretsi, V., Kontoyiannis, D., & Kollias, G. (2009). *A standardized protocol for the isolation and culture of normal and arthritogenic murine synovial fibroblasts*.

Axford, J. S. (1999). Glycosylation and rheumatic disease. *Biochimica et Biophysica Acta (BBA)-Molecular Basis of Disease*, *1455*(2–3), 219–229.

Bartok, B., & Firestein, G. S. (2010). Fibroblast-like synoviocytes: key effector cells in rheumatoid arthritis. *Immunological Reviews*, *233*(1), 233–255.

Bonelli, M., Dalwigk, K., Platzer, A., Olmos Calvo, I., Hayer, S., Niederreiter, B., Holinka, J., Sevelda, F., Pap, T., & Steiner, G. (2019). IRF1 is critical for the

TNF-driven interferon response in rheumatoid fibroblast-like synoviocytes: JAKinibs suppress the interferon response in RA-FLSs. *Experimental & Molecular Medicine*, *51*(7), 1–11.

Bordron, A., Morel, M., Bagacean, C., Dueymes, M., Pochard, P., Harduin-Lepers, A., Jamin, C., & Pers, J.-O. (2021). Hyposialylation must be considered to develop future therapies in autoimmune diseases. *International Journal of Molecular Sciences*, *22*(7), 3402.

Bottini, N., & Firestein, G. S. (2013). Duality of fibroblast-like synoviocytes in RA: passive responders and imprinted aggressors. *Nature Reviews Rheumatology*, *9*(1), 24–33.

Boyette, L. B., Macedo, C., Hadi, K., Elinoff, B. D., Walters, J. T., Ramaswami, B., Chalasani, G., Taboas, J. M., Lakkis, F. G., & Metes, D. M. (2017). Phenotype, function, and differentiation potential of human monocyte subsets. *PloS One*, *12*(4), e0176460.

Brentano, F., Schorr, O., Gay, R. E., Gay, S., & Kyburz, D. (2005). RNA released from necrotic synovial fluid cells activates rheumatoid arthritis synovial fibroblasts via Toll-like receptor 3. *Arthritis & Rheumatism*, *52*(9), 2656–2665.

Bucala, R., Ritchlin, C., Winchester, R., & Cerami, A. (1991). Constitutive production of inflammatory and mitogenic cytokines by rheumatoid synovial fibroblasts. *The Journal of Experimental Medicine*, *173*(3), 569–574.

Büll, C., Heise, T., Adema, G. J., & Boltje, T. J. (2016). Sialic acid mimetics to target the sialic acid–Siglec axis. *Trends in Biochemical Sciences*, *41*(6), 519–531.

Büll, C., Nason, R., Sun, L., Van Coillie, J., Madriz Sørensen, D., Moons, S. J., Yang, Z., Arbitman, S., Fernandes, S. M., & Furukawa, S. (2021). Probing the binding specificities of human Siglecs by cell-based glycan arrays. *Proceedings of the National Academy of Sciences*, *118*(17), e2026102118.

Chang, K., Yang, S. M., Kim, S. H., Han, K. H., Park, S. J., & Shin, J. Il. (2014). Smoking and rheumatoid arthritis. *International Journal of Molecular Sciences*, *15*(12), 22279–22295.

Chang, K.-H., Hsu, C.-C., Muo, C.-H., Hsu, C. Y., Liu, H.-C., Kao, C.-H., Chen, C.-Y., Chang, M.-Y., & Hsu, Y.-C. (2016). Air pollution exposure increases the risk of rheumatoid arthritis: a longitudinal and nationwide study. *Environment International*, *94*, 495–499.

Chang, L.-Y., Mir, A.-M., Thisse, C., Guérardel, Y., Delannoy, P., Thisse, B., & Harduin-Lepers, A. (2009). Molecular cloning and characterization of the expression pattern of the zebrafish α 2, 8-sialyltransferases (ST8Sia) in the developing nervous system. *Glycoconjugate Journal*, *26*(3), 263–275.

Chang, X., Xia, Y., Pan, J., Meng, Q., Zhao, Y., & Yan, X. (2013). PADI2 is significantly associated with rheumatoid arthritis. *PLoS One*, *8*(12), e81259.

Chen, X., & Varki, A. (2010). Advances in the biology and chemistry of sialic acids. *ACS Chemical Biology*, *5*(2), 163–176.

Chen, Y., Wang, B., Chen, Y., Wu, Q., Lai, W.-F., Wei, L., Nandakumar, K. S., & Liu, D. (2022). HAPLN1 affects cell viability and promotes the pro-inflammatory phenotype of fibroblast-like synoviocytes. *Frontiers in Immunology*, *13*, 888612.

Cheng, L., Wang, Y., Wu, R., Ding, T., Xue, H., Gao, C., Li, X., & Wang, C. (2021). New insights from single-cell sequencing data: synovial fibroblasts and synovial macrophages in rheumatoid arthritis. *Frontiers in Immunology*, *12*, 709178.

Choi, Y. J., Lee, W.-S., Lee, E.-G., Sung, M.-S., & Yoo, W.-H. (2014). Sulforaphane inhibits IL-1β-induced proliferation of rheumatoid arthritis synovial fibroblasts and the production of MMPs, COX-2, and PGE2. *Inflammation*, *37*(5), 1496–1503.

Christensen, S., & Egebjerg, J. (2005). Cloning, expression and characterization of a sialidase gene from Arthrobacter ureafaciens. *Biotechnology and Applied Biochemistry*, *41*(3), 225–231.

Ciaffi, J., Vanni, E., Mancarella, L., Brusi, V., Lisi, L., Pignatti, F., Naldi, S., Assirelli, E., Neri, S., & Reta, M. (2023). Post-acute COVID-19 joint pain and new onset of rheumatic musculoskeletal diseases: a systematic review. *Diagnostics*, *13*(11), 1850.

Crocker, P. R., & Varki, A. (2001). Siglecs, sialic acids and innate immunity. *Trends in Immunology*, *22*(6), 337–342.

Croft, A. P., Campos, J., Jansen, K., Turner, J. D., Marshall, J., Attar, M., Savary, L., Wehmeyer, C., Naylor, A. J., & Kemble, S. (2019). Distinct fibroblast subsets drive inflammation and damage in arthritis. *Nature*, *570*(7760), 246–251.

Cros, J., Cagnard, N., Woollard, K., Patey, N., Zhang, S.-Y., Senechal, B., Puel, A., Biswas, S. K., Moshous, D., & Picard, C. (2010). Human CD14dim monocytes patrol and sense nucleic acids and viruses via TLR7 and TLR8 receptors. *Immunity*, *33*(3), 375–386.

Culemann, S., Grüneboom, A., Nicolás-Ávila, J. Á., Weidner, D., Lämmle, K. F., Rothe, T., Quintana, J. A., Kirchner, P., Krljanac, B., & Eberhardt, M. (2019). Locally renewing resident synovial macrophages provide a protective barrier for the joint. *Nature*, *572*(7771), 670–675.

Cvjetićanin, S., Terzić, M., & Nikolić, D. (2019). Association of rheumatoid arthritis according to the degree of genetic homozygosity and gender: Pilot study. *Genetika*, *51*(3), 1139–1149.

Darrieutort-Laffite, C., Boutet, M.-A., Chatelais, M., Brion, R., Blanchard, F., Heymann, D., & Le Goff, B. (2014). IL-1β and TNFα Promote Monocyte Viability through the Induction of GM-CSF Expression by Rheumatoid Arthritis Synovial Fibroblasts. *Mediators of Inflammation*, *2014*(1), 241840.

Davies, L. C., Jenkins, S. J., Allen, J. E., & Taylor, P. R. (2013). Tissue-resident macrophages. *Nature Immunology*, *14*(10), 986–995.

de Andres, M. C., Perez-Pampin, E., Calaza, M., Santaclara, F. J., Ortea, I., Gomez-Reino, J. J., & Gonzalez, A. (2015). Assessment of global DNA methylation in peripheral blood cell subpopulations of early rheumatoid arthritis before and after methotrexate. *Arthritis Research & Therapy*, *17*(1), 233.

Dědová, T., Braicu, E. I., Sehouli, J., & Blanchard, V. (2019). Sialic acid linkage analysis refines the diagnosis of ovarian cancer. *Frontiers in Oncology*, *9*, 261.

Dennis, J. W., Lau, K. S., Demetriou, M., & Nabi, I. R. (2009). Adaptive regulation at the cell surface by N-glycosylation. *Traffic*, *10*(11), 1569–1578.

Dennis, J. W., Nabi, I. R., & Demetriou, M. (2009). Metabolism, cell surface organization, and disease. *Cell*, *139*(7), 1229–1241.

Dobie, C., & Skropeta, D. (2021). Insights into the role of sialylation in cancer progression and metastasis. *British Journal of Cancer*, *124*(1), 76–90.

Dobre, M., Salvi, A., Pelisenco, I. A., Vasilescu, F., De Petro, G., Herlea, V., & Milanesi, E. (2021). Crosstalk between DNA methylation and gene mutations in colorectal cancer. *Frontiers in Oncology*, *11*, 697409.

dos Anjos Cassado, A. (2017). F4/80 as a major macrophage marker: the case of the peritoneum and spleen. *Macrophages: Origin, Functions and Biointervention*, 161–179.

England, B. R., Thiele, G. M., Anderson, D. R., & Mikuls, T. R. (2018). Increased cardiovascular risk in rheumatoid arthritis: mechanisms and implications. *Bmj*, *361*.

Eun, Y., Jeon, K. H., Han, K., Kim, D., Kim, H., Lee, J., Lee, D.-Y., Yoo, J. E., & Shin, D. W. (2020). Menopausal factors and risk of seropositive rheumatoid arthritis in postmenopausal women: a nationwide cohort study of 1.36 million women. *Scientific Reports*, *10*(1), 20793.

Faller, C. E., & Guvench, O. (2014). Terminal sialic acids on CD44 N-glycans can block hyaluronan binding by forming competing intramolecular contacts with arginine sidechains. *Proteins: Structure, Function, and Bioinformatics*, *82*(11), 3079–3089.

Fang, Q., Zhou, C., & Nandakumar, K. S. (2020). Molecular and cellular pathways contributing to joint damage in rheumatoid arthritis. *Mediators of Inflammation*, *2020*(1), 3830212.

Ferrante, C. J., Pinhal-Enfield, G., Elson, G., Cronstein, B. N., Hasko, G., Outram, S., & Leibovich, S. J. (2013). The adenosine-dependent angiogenic switch of macrophages to an M2-like phenotype is independent of interleukin-4 receptor alpha (IL-4Rα) signaling. *Inflammation*, *36*(4), 921–931.

Figueiredo, M. L. (2024). Applications of single-cell RNA sequencing in rheumatoid arthritis. *Frontiers in Immunology*, *15*, 1491318.

Filer, A., Bik, M., Parsonage, G. N., Fitton, J., Trebilcock, E., Howlett, K., Cook, M., Raza, K., Simmons, D. L., & Thomas, A. M. C. (2009). Galectin 3 induces a

distinctive pattern of cytokine and chemokine production in rheumatoid synovial fibroblasts via selective signaling pathways. *Arthritis & Rheumatism: Official Journal of the American College of Rheumatology*, *60*(6), 1604–1614.

Firestein, G. S., & McInnes, I. B. (2017). Immunopathogenesis of rheumatoid arthritis. *Immunity*, *46*(2), 183–196.

Forsman, H., Islander, U., Andréasson, E., Andersson, A., Önnheim, K., Karlström, A., Sävman, K., Magnusson, M., Brown, K. L., & Karlsson, A. (2011). Galectin 3 aggravates joint inflammation and destruction in antigen-induced arthritis. *Arthritis & Rheumatism*, *63*(2), 445–454.

Frank-Bertoncelj, M., Trenkmann, M., Klein, K., Karouzakis, E., Rehrauer, H., Bratus, A., Kolling, C., Armaka, M., Filer, A., & Michel, B. A. (2017). Epigenetically-driven anatomical diversity of synovial fibroblasts guides joint-specific fibroblast functions. *Nature Communications*, *8*(1), 1–14.

Fukushima, K., Takahashi, T., Ueyama, H., Takaguchi, M., Ito, S., Oishi, K., Minami, A., Ishitsubo, E., Tokiwa, H., & Takimoto, T. (2015). Amino acid substitutions contributing to α2, 6-sialic acid linkage binding specificity of human parainfluenza virus type 3 hemagglutinin–neuraminidase. *FEBS Letters*, *589*(11), 1278–1282.

Gao, C., Hanes, M. S., Byrd-Leotis, L. A., Wei, M., Jia, N., Kardish, R. J., McKitrick, T. R., Steinhauer, D. A., & Cummings, R. D. (2019). Unique binding specificities of proteins toward isomeric asparagine-linked glycans. *Cell Chemical Biology*, *26*(4), 535–547.

Ge, X., Frank-Bertoncelj, M., Klein, K., McGovern, A., Kuret, T., Houtman, M., Burja, B., Micheroli, R., Shi, C., & Marks, M. (2021). Functional genomics atlas of synovial fibroblasts defining rheumatoid arthritis heritability. *Genome Biology*, *22*(1), 1–39.

Godha, Y., Kumar, S., & Wanjari, A. (2023). Role of Gut Microbiota in the Development and Management of Rheumatoid Arthritis: A Narrative Review. *Cureus*, *15*(11).

Gonzalez-Gil, A., & Schnaar, R. L. (2021). Siglec ligands. *Cells*, *10*(5), 1260.

Grigorian, A., Torossian, S., & Demetriou, M. (2009). T-cell growth, cell surface organization, and the galectin–glycoprotein lattice. *Immunological Reviews*, *230*(1), 232–246.

Groth, T., Diehl, A. D., Gunawan, R., & Neelamegham, S. (2022). GlycoEnzOnto: a GlycoEnzyme pathway and molecular function ontology. *Bioinformatics*, *38*(24), 5413–5420.

Gul, R., Nazir, I., Amirzada, M. I., Jahan, F., Naseer, F., & Baig, T. A. (2024). Aging and Synovial Joint Function: Changes in Structure and Implications for Mobility. In *Advancements in Synovial Joint Science-Structure, Function, and Beyond*. IntechOpen.

Guo, Q., Wang, Y., Xu, D., Nossent, J., Pavlos, N. J., & Xu, J. (2018). Rheumatoid arthritis: pathological mechanisms and modern pharmacologic therapies. *Bone Research*, *6*(1), 15.

Hafkenscheid, L., Bondt, A., Scherer, H. U., Huizinga, T. W. J., Wuhrer, M., Toes, R. E. M., & Rombouts, Y. (2017). Structural analysis of variable domain glycosylation of anti-citrullinated protein antibodies in rheumatoid arthritis reveals the presence of highly sialylated glycans. *Molecular & Cellular Proteomics*, *16*(2), 278–287.

Hafkenscheid, L., de Moel, E., Smolik, I., Tanner, S., Meng, X., Jansen, B. C., Bondt, A., Wuhrer, M., Huizinga, T. W. J., & Toes, R. E. M. (2019). N-linked glycans in the variable domain of IgG anti–citrullinated protein antibodies predict the development of rheumatoid arthritis. *Arthritis & Rheumatology*, *71*(10), 1626–1633.

Hamshere, M. L., Segurado, R., Moskvina, V., Nikolov, I., Glaser, B., & Holmans, P. A. (2007). Large-scale linkage analysis of 1302 affected relative pairs with rheumatoid arthritis. *BMC Proceedings*, *1*, 1–5.

Harduin-Lepers, A., Krzewinski-Recchi, M.-A., Colomb, F., Foulquier, F., Groux-Degroote, S., & Delannoy, P. (2012). Sialyltransferases functions in cancers. *Frontiers in Bioscience-Elite*, *4*(1), 499–515.

Harduin-Lepers, A., Vallejo-Ruiz, V., Krzewinski-Recchi, M.-A., Samyn-Petit, B., Julien, S., & Delannoy, P. (2001). The human sialyltransferase family. *Biochimie*, *83*(8), 727–737.

Hazlewood, G. S., Barnabe, C., Tomlinson, G., Marshall, D., Devoe, D. J. A., & Bombardier, C. (2016). Methotrexate monotherapy and methotrexate combination therapy with traditional and biologic disease modifying anti-rheumatic drugs for rheumatoid arthritis: a network meta-analysis. *Cochrane Database of Systematic Reviews*, *8*.

Hitchon, C. A., & El-Gabalawy, H. S. (2011). The synovium in rheumatoid arthritis. *The Open Rheumatology Journal*, *5*, 107.

Honma, K., Mishima, E., & Sharma, A. (2011). Role of Tannerella forsythia NanH sialidase in epithelial cell attachment. *Infection and Immunity*, *79*(1), 393–401.

Hou, W., Qiu, Y., Hashimoto, N., Ching, W.-K., & Aoki-Kinoshita, K. F. (2016). A systematic framework to derive N-glycan biosynthesis process and the automated construction of glycosylation networks. *BMC Bioinformatics*, *17*, 465–472.

Hu, Y., Yéléhé-Okouma, M., Ea, H.-K., Jouzeau, J.-Y., & Reboul, P. (2017). Galectin-3: A key player in arthritis. *Joint Bone Spine*, *84*(1), 15–20.

Huang, Q.-Q., Doyle, R., Chen, S.-Y., Sheng, Q., Misharin, A. V, Mao, Q., Winter, D. R., & Pope, R. M. (2021). Critical role of synovial tissue–resident macrophage niche in joint homeostasis and suppression of chronic inflammation. *Science Advances*, *7*(2), eabd0515.

Huang, Y.-F., Aoki, K., Akase, S., Ishihara, M., Liu, Y.-S., Yang, G., Kizuka, Y., Mizumoto, S., Tiemeyer, M., & Gao, X.-D. (2021). Global mapping of glycosylation pathways in human-derived cells. *Developmental Cell*, *56*(8), 1195–1209.

Huber, L. C., Brock, M., Hemmatazad, H., Giger, O. T., Moritz, F., Trenkmann, M., Distler, J. H. W., Gay, R. E., Kolling, C., & Moch, H. (2007). Histone deacetylase/acetylase activity in total synovial tissue derived from rheumatoid arthritis and osteoarthritis patients. *Arthritis & Rheumatism*, *56*(4), 1087–1093.

Huber, L. C., Distler, O., Tarner, I., Gay, R. E., Gay, S., & Pap, T. (2006). Synovial fibroblasts: key players in rheumatoid arthritis. *Rheumatology*, *45*(6), 669–675.

Hugonnet, M., Singh, P., Haas, Q., & von Gunten, S. (2021). The distinct roles of sialyltransferases in cancer biology and onco-immunology. *Frontiers in Immunology*, *12*, 799861.

Imperiali, B., & O'Connor, S. E. (1999). Effect of N-linked glycosylation on glycopeptide and glycoprotein structure. *Current Opinion in Chemical Biology*, *3*(6), 643–649.

Ingersoll, M. A., Platt, A. M., Potteaux, S., & Randolph, G. J. (2011). Monocyte trafficking in acute and chronic inflammation. *Trends in Immunology*, *32*(10), 470–477.

Isozaki, T., Ruth, J. H., Amin, M. A., Campbell, P. L., Tsou, P.-S., Ha, C. M., Haines III, G. K., Edhayan, G., & Koch, A. E. (2014). Fucosyltransferase 1 mediates angiogenesis, cell adhesion and rheumatoid arthritis synovial tissue fibroblast proliferation. *Arthritis Research & Therapy*, *16*(1), R28.

Jablonski, K. A., Amici, S. A., Webb, L. M., Ruiz-Rosado, J. de D., Popovich, P. G., Partida-Sanchez, S., & Guerau-de-Arellano, M. (2015). Novel markers to delineate murine M1 and M2 macrophages. *PloS One*, *10*(12), e0145342.

Jeganathan, S., Fiorino, C., Naik, U., Sun, H. S., & Harrison, R. E. (2014). Modulation of osteoclastogenesis with macrophage M1-and M2-inducing stimuli. *PloS One*, *9*(8), e104498.

Kaisar, M. H., Bhuiyan, M. S., Akter, A., Saleem, D., Iyer, A. S., Dash, P., Hakim, A., Chowdhury, F., Khan, A. I., & Calderwood, S. B. (2021). Vibrio cholerae sialidase-specific immune responses are associated with protection against cholera. *Msphere*, *6*(2), 10–1128.

Kapellos, T. S., Bonaguro, L., Gemünd, I., Reusch, N., Saglam, A., Hinkley, E. R., & Schultze, J. L. (2019). Human monocyte subsets and phenotypes in major chronic inflammatory diseases. *Frontiers in Immunology*, *10*, 2035.

Karouzakis, E., Raza, K., Kolling, C., Buckley, C. D., Gay, S., Filer, A., & Ospelt, C. (2018). Analysis of early changes in DNA methylation in synovial fibroblasts of RA patients before diagnosis. *Scientific Reports*, *8*(1), 7370.

Katoh, S., Zheng, Z., Oritani, K., Shimozato, T., & Kincade, P. W. (1995). Glycosylation of CD44 negatively regulates its recognition of hyaluronan. *The Journal of Experimental Medicine*, *182*(2), 419–429.

Kawecki, C., Bocquet, O., Schmelzer, C. E. H., Heinz, A., Ihling, C., Wahart, A., Romier, B., Bennasroune, A., Blaise, S., & Terryn, C. (2019). Identification of CD36 as a new interaction partner of membrane NEU1: potential implication

in the pro-atherogenic effects of the elastin receptor complex. *Cellular and Molecular Life Sciences*, *76*(4), 791–807.

Kerschbaumer, A., Sepriano, A., Smolen, J. S., van der Heijde, D., Dougados, M., van Vollenhoven, R., McInnes, I. B., Bijlsma, J. W. J., Burmester, G. R., & de Wit, M. (2020). Efficacy of pharmacological treatment in rheumatoid arthritis: a systematic literature research informing the 2019 update of the EULAR recommendations for management of rheumatoid arthritis. *Annals of the Rheumatic Diseases*, *79*(6), 744–759.

Khan, A., Dobre, O., Wang, Y., Sartyoungkul, T., Salmeron-Sanchez, M., Harnett, M. H., & Pineda, M. A. (2022). Inflammatory Synovial Fibroblast Culture in 3D Systems: A Comparative Transcriptomic and Functional Study. *BioRxiv*, 2012–2022.

Knab, K., Chambers, D., & Krönke, G. (2022). Synovial macrophage and fibroblast heterogeneity in joint homeostasis and inflammation. *Frontiers in Medicine*, *9*, 862161.

Komano, Y., Nanki, T., Hayashida, K., Taniguchi, K., & Miyasaka, N. (2006). Identification of a human peripheral blood monocyte subset that differentiates into osteoclasts. *Arthritis Research & Therapy*, *8*(5), R152.

Køster, D., Egedal, J. H., Lomholt, S., Hvid, M., Jakobsen, M. R., Müller-Ladner, U., Eibel, H., Deleuran, B., Kragstrup, T. W., & Neumann, E. (2021). Phenotypic and functional characterization of synovial fluid-derived fibroblast-like synoviocytes in rheumatoid arthritis. *Scientific Reports*, *11*(1), 22168.

Kouka, T., Akase, S., Sogabe, I., Jin, C., Karlsson, N. G., & Aoki-Kinoshita, K. F. (2022). Computational modeling of O-linked glycan biosynthesis in CHO cells. *Molecules*, *27*(6), 1766.

Krychtiuk, K. A., Kastl, S. P., Pfaffenberger, S., Lenz, M., Hofbauer, S. L., Wonnerth, A., Koller, L., Katsaros, K. M., Pongratz, T., & Goliasch, G. (2015). Association of small dense LDL serum levels and circulating monocyte subsets in stable coronary artery disease. *PloS One*, *10*(4), e0123367.

Kudaeva, F. M., Speechley, M. R., & Pope, J. E. (2019). A systematic review of viral exposures as a risk for rheumatoid arthritis. *Seminars in Arthritis and Rheumatism*, *48*(4), 587–596.

Kudelka, M. R., Ju, T., Heimburg-Molinaro, J., & Cummings, R. D. (2015). Simple sugars to complex disease—mucin-type O-glycans in cancer. *Advances in Cancer Research*, *126*, 53–135.

Kukan, E. N., Fabiano, G. L., & Cobb, B. A. (2024). Siglecs as modulators of macrophage phenotype and function. *Seminars in Immunology*, *73*, 101887.

Kuninaka, Y., Ishida, Y., Ishigami, A., Nosaka, M., Matsuki, J., Yasuda, H., Kofuna, A., Kimura, A., Furukawa, F., & Kondo, T. (2022). Macrophage polarity and wound age determination. *Scientific Reports*, *12*(1), 20327.

Kuo, D., Ding, J., Cohn, I. S., Zhang, F., Wei, K., Rao, D. A., Rozo, C., Sokhi, U. K., Shanaj, S., & Oliver, D. J. (2019). HBEGF+ macrophages in rheumatoid

arthritis induce fibroblast invasiveness. *Science Translational Medicine*, *11*(491), eaau8587.

Kurnia, R. S., Tarigan, S., Nugroho, C. M. H., Silaen, O. S. M., Natalia, L., Ibrahim, F., & Sudarmono, P. P. (2022). Potency of bacterial sialidase Clostridium perfringens as antiviral of Newcastle disease infections using embryonated chicken egg in ovo model. *Veterinary World*, *15*(8), 1896.

Kurowska-Stolarska, M., & Alivernini, S. (2022). Synovial tissue macrophages in joint homeostasis, rheumatoid arthritis and disease remission. *Nature Reviews Rheumatology*, *18*(7), 384–397.

Lauzier, A., Charbonneau, M., Harper, K., Jilaveanu-Pelmus, M., & Dubois, C. M. (2011). Formation of invadopodia-like structures by synovial cells promotes cartilage breakdown in collagen-induced arthritis: Involvement of the protein tyrosine kinase Src. *Arthritis & Rheumatism*, *63*(6), 1591–1602.

Lee, K. Y. (2019). M1 and M2 polarization of macrophages: a mini-review. *Med Biol Sci Eng*, *2*(1), 1–5.

Lefèvre, S., Knedla, A., Tennie, C., Kampmann, A., Wunrau, C., Dinser, R., Korb, A., Schnäker, E.-M., Tarner, I. H., & Robbins, P. D. (2009). Synovial fibroblasts spread rheumatoid arthritis to unaffected joints. *Nature Medicine*, *15*(12), 1414–1420.

Lefevre, S., Meier, F. M. P., Neumann, E., & Muller-Ladner, U. (2015). Role of synovial fibroblasts in rheumatoid arthritis. *Current Pharmaceutical Design*, *21*(2), 130–141.

Li, J., & McClane, B. A. (2014). The sialidases of Clostridium perfringens type D strain CN3718 differ in their properties and sensitivities to inhibitors. *Applied and Environmental Microbiology*, *80*(5), 1701–1709.

Li, R., Wu, X., Peng, S., Shen, J., Cheng, Y., & Chu, Q. (2023). CCR2 antagonist represses fibroblast-like synoviocyte-mediated inflammation in patients with rheumatoid arthritis. *International Immunopharmacology*, *122*, 110570.

Li, S., Yu, Y., Yue, Y., Zhang, Z., & Su, K. (2013). Microbial infection and rheumatoid arthritis. *Journal of Clinical & Cellular Immunology*, *4*(6), 174.

Li, Y., & Chen, X. (2012). Sialic acid metabolism and sialyltransferases: natural functions and applications. *Applied Microbiology and Biotechnology*, *94*, 887–905.

Li, Y., Wang, Z., Ma, X., Shao, B., Gao, X., Zhang, B., Xu, G., & Wei, Y. (2014). Low-dose cisplatin administration to septic mice improves bacterial clearance and programs peritoneal macrophage polarization to M1 phenotype. *Pathogens and Disease*, *72*(2), 111–123.

Lillehoj, E. P., Hyun, S. W., Liu, A., Guang, W., Verceles, A. C., Luzina, I. G., Atamas, S. P., Kim, K. C., & Goldblum, S. E. (2015). NEU1 sialidase regulates membrane-tethered mucin (MUC1) ectodomain adhesiveness for Pseudomonas aeruginosa and decoy receptor release. *Journal of Biological Chemistry*, *290*(30), 18316–18331.

Lin, Y.-H., Wang, Y.-H., Peng, Y.-J., Liu, F.-C., Lin, G.-J., Huang, S.-H., Sytwu, H.-K., & Cheng, C.-P. (2020). Interleukin 26 skews macrophage polarization towards M1 phenotype by activating cJUN and the NF-κB pathway. *Cells*, *9*(4), 938.

Liu, N., Zhu, M., Linhai, Y., Song, Y., Gui, X., Tan, G., Li, J., Liu, Y., Deng, Z., & Chen, X. (2018). Increasing HER2 α2, 6 sialylation facilitates gastric cancer progression and resistance via the Akt and ERK pathways. *Oncology Reports*, *40*(5), 2997–3005.

Long, L., Yu, P., Liu, Y., Wang, S., Li, R., Shi, J., Zhang, X., Li, Y., Sun, X., & Zhou, B. (2013). Upregulated microRNA-155 expression in peripheral blood mononuclear cells and fibroblast-like synoviocytes in rheumatoid arthritis. *Journal of Immunology Research*, *2013*(1), 296139.

Ma, X., & Xu, S. (2013). TNF inhibitor therapy for rheumatoid arthritis. *Biomedical Reports*, *1*(2), 177–184.

Mahajan, V. S., & Pillai, S. (2016). Sialic acids and autoimmune disease. *Immunological Reviews*, *269*(1), 145–161.

Malhotra, R., Wormald, M. R., Rudd, P. M., Fischer, P. B., Dwek, R. A., & Sim, R. B. (1995). Glycosylation changes of IgG associated with rheumatooid arthritis can activate complement via the mannose-binding protein. *Nature Medicine*, *1*(3), 237–243.

Manwar Hussain, M. R., Hassan, M., Shaik, N. A., & Iqbal, Z. (2012). The role of Galactose in human health and disease. *Central European Journal of Medicine*, *7*, 409–419.

Matsuda, K., Shiba, N., & Hiraoka, K. (2023). New insights into the role of synovial fibroblasts leading to joint destruction in rheumatoid arthritis. *International Journal of Molecular Sciences*, *24*(6), 5173.

Matsuo, Y., Mizoguchi, F., Saito, T., Kawahata, K., Ueha, S., Matsushima, K., Inagaki, Y., Miyasaka, N., & Kohsaka, H. (2016). Local fibroblast proliferation but not influx is responsible for synovial hyperplasia in a murine model of rheumatoid arthritis. *Biochemical and Biophysical Research Communications*, *470*(3), 504–509.

McInnes, I. B., Leung, B. P., Field, M., Wei, X. Q., Huang, F.-P., Sturrock, R. D., Kinninmonth, A., Weidner, J., Mumford, R., & Liew, F. Y. (1996). Production of nitric oxide in the synovial membrane of rheumatoid and osteoarthritis patients. *The Journal of Experimental Medicine*, *184*(4), 1519–1524.

Mendez-Huergo, S. P., Hockl, P. F., Stupirski, J. C., Maller, S. M., Morosi, L. G., Pinto, N. A., Berón, A. M., Musuruana, J. L., Nasswetter, G. G., & Cavallasca, J. A. (2019). Clinical relevance of galectin-1 and galectin-3 in rheumatoid arthritis patients: differential regulation and correlation with disease activity. *Frontiers in Immunology*, *9*, 3057.

Mia, S., Warnecke, A., Zhang, X., Malmström, V., & Harris, R. A. (2014). An optimized protocol for human M2 macrophages using M-CSF and IL-4/IL-

10/TGF-β yields a dominant immunosuppressive phenotype. *Scandinavian Journal of Immunology*, *79*(5), 305–314.

Micheroli, R., Elhai, M., Edalat, S., Frank-Bertoncelj, M., Bürki, K., Ciurea, A., MacDonald, L., Kurowska-Stolarska, M., Lewis, M. J., & Goldmann, K. (2022). Role of synovial fibroblast subsets across synovial pathotypes in rheumatoid arthritis: a deconvolution analysis. *RMD Open*, *8*(1).

Misharin, A. V, Cuda, C. M., Saber, R., Turner, J. D., Gierut, A. K., Haines, G. K., Berdnikovs, S., Filer, A., Clark, A. R., & Buckley, C. D. (2014). Nonclassical Ly6C− monocytes drive the development of inflammatory arthritis in mice. *Cell Reports*, *9*(2), 591–604.

Mizoguchi, F., Slowikowski, K., Wei, K., Marshall, J. L., Rao, D. A., Chang, S. K., Nguyen, H. N., Noss, E. H., Turner, J. D., & Earp, B. E. (2018). Functionally distinct disease-associated fibroblast subsets in rheumatoid arthritis. *Nature Communications*, *9*(1), 1–11.

Moremen, K. W., Tiemeyer, M., & Nairn, A. V. (2012). Vertebrate protein glycosylation: diversity, synthesis and function. *Nature Reviews Molecular Cell Biology*, *13*(7), 448–462.

Müller-Ladner, U., Ospelt, C., Gay, S., Distler, O., & Pap, T. (2007). Cells of the synovium in rheumatoid arthritis. Synovial fibroblasts. *Arthritis Research & Therapy*, *9*(6), 223.

Nabi, I. R., Shankar, J., & Dennis, J. W. (2015). The galectin lattice at a glance. *Journal of Cell Science*, *128*(13), 2213–2219.

Nakano, K., Boyle, D. L., & Firestein, G. S. (2013). Regulation of DNA methylation in rheumatoid arthritis synoviocytes. *The Journal of Immunology*, *190*(3), 1297–1303.

Németh, T., Nagy, G., & Pap, T. (2022). Synovial fibroblasts as potential drug targets in rheumatoid arthritis, where do we stand and where shall we go? *Annals of the Rheumatic Diseases*, *81*(8), 1055–1064.

Noss, E. H., & Brenner, M. B. (2008). The role and therapeutic implications of fibroblast-like synoviocytes in inflammation and cartilage erosion in rheumatoid arthritis. *Immunological Reviews*, *223*(1), 252–270.

Ohmi, Y., Ise, W., Harazono, A., Takakura, D., Fukuyama, H., Baba, Y., Narazaki, M., Shoda, H., Takahashi, N., & Ohkawa, Y. (2016). Sialylation converts arthritogenic IgG into inhibitors of collagen-induced arthritis. *Nature Communications*, *7*(1), 11205.

Okada, T., Tsukano, H., Endo, M., Tabata, M., Miyata, K., Kadomatsu, T., Miyashita, K., Semba, K., Nakamura, E., & Tsukano, M. (2010). Synoviocyte-derived angiopoietin-like protein 2 contributes to synovial chronic inflammation in rheumatoid arthritis. *The American Journal of Pathology*, *176*(5), 2309–2319.

Orecchioni, M., Ghosheh, Y., Pramod, A. B., & Ley, K. (2019). Macrophage polarization: different gene signatures in M1 (LPS+) vs. classically and M2

(LPS–) vs. alternatively activated macrophages. *Frontiers in Immunology*, *10*, 1084.

Ou, L., He, X., Liu, N., Song, Y., Li, J., Gao, L., Huang, X., Deng, Z., Wang, X., & Lin, S. (2020). Sialylation of FGFR1 by ST6Gal-I overexpression contributes to ovarian cancer cell migration and chemoresistance. *Molecular Medicine Reports*, *21*(3), 1449–1460.

Paclik, D., Werner, L., Guckelberger, O., Wiedenmann, B., & Sturm, A. (2011). Galectins distinctively regulate central monocyte and macrophage function. *Cellular Immunology*, *271*(1), 97–103.

Paneque, A., Fortus, H., Zheng, J., Werlen, G., & Jacinto, E. (2023). The hexosamine biosynthesis pathway: regulation and function. *Genes*, *14*(4), 933.

Pap, T., Müller-Ladner, U., Gay, R. E., & Gay, S. (2000). Fibroblast biology: role of synovial fibroblasts in the pathogenesis of rheumatoid arthritis. *Arthritis Research & Therapy*, *2*, 1–7.

Paton, B., Suarez, M., Herrero, P., & Canela, N. (2021). Glycosylation biomarkers associated with age-related diseases and current methods for glycan analysis. *International Journal of Molecular Sciences*, *22*(11), 5788.

Pearson, M. J., Bik, M. A., Ospelt, C., Naylor, A. J., Wehmeyer, C., Jones, S. W., Buckley, C. D., Gay, S., Filer, A., & Lord, J. M. (2018). Endogenous galectin-9 suppresses apoptosis in human rheumatoid arthritis synovial fibroblasts. *Scientific Reports*, *8*(1), 1–8.

Pietrobono, S., & Stecca, B. (2021). Aberrant sialylation in cancer: biomarker and potential target for therapeutic intervention? *Cancers*, *13*(9), 2014.

Pillai, S., Netravali, I. A., Cariappa, A., & Mattoo, H. (2012). Siglecs and immune regulation. *Annual Review of Immunology*, *30*, 357–392.

Pongracz, T., Verhoeven, A., Wuhrer, M., & de Haan, N. (2021). The structure and role of lactone intermediates in linkage-specific sialic acid derivatization reactions. *Glycoconjugate Journal*, *38*(2), 157–166.

Pongracz, T., Wuhrer, M., & de Haan, N. (2019). Expanding the reaction space of linkage-specific sialic acid derivatization. *Molecules*, *24*(19), 3617.

Qian, H., Deng, C., Chen, S., Zhang, X., He, Y., Lan, J., Wang, A., Shi, G., & Liu, Y. (2024). Targeting pathogenic fibroblast-like synoviocyte subsets in rheumatoid arthritis. *Arthritis Research & Therapy*, *26*(1), 103.

Qu, J., Zou, T., & Lin, Z. (2021). The roles of the ubiquitin–proteasome system in the endoplasmic reticulum stress pathway. *International Journal of Molecular Sciences*, *22*(4), 1526.

Reesink, H. L., Bonnevie, E. D., Liu, S., Shurer, C. R., Hollander, M. J., Bonassar, L. J., & Nixon, A. J. (2016). Galectin-3 binds to lubricin and reinforces the lubricating boundary layer of articular cartilage. *Scientific Reports*, *6*(1), 25463.

Reily, C., Stewart, T. J., Renfrow, M. B., & Novak, J. (2019). Glycosylation in health and disease. *Nature Reviews Nephrology*, *15*(6), 346–366.

Rong, M., Wang, C., Wu, Z., Zeng, W., Zheng, Z., Han, Q., Jia, J., Li, X., & Zhu, P. (2014). Platelets induce a proinflammatory phenotype in monocytes via the CD147 pathway in rheumatoid arthritis. *Arthritis Research & Therapy*, *16*(6), 478.

Rosa, I., Faussone-Pellegrini, M. S., Romano, E., Ibba-Manneschi, L., Matucci-Cerinic, M., & Manetti, M. (2021). Impairment in the telocyte/CD34+ stromal cell network in human rheumatoid arthritis synovium. *Journal of Cellular and Molecular Medicine*, *25*(4), 2274–2278.

Sakurai, H., Kohsaka, H., Liu, M.-F., Higashiyama, H., Hirata, Y., Kanno, K., Saito, I., & Miyasaka, N. (1995). Nitric oxide production and inducible nitric oxide synthase expression in inflammatory arthritides. *The Journal of Clinical Investigation*, *96*(5), 2357–2363.

Saliba, A.-E., Westermann, A. J., Gorski, S. A., & Vogel, J. (2014). Single-cell RNA-seq: advances and future challenges. *Nucleic Acids Research*, *42*(14), 8845–8860.

Santos-Moreno, P., Rodríguez-Vargas, G.-S., Martínez, S., Ibatá, L., & Rojas-Villarraga, A. (2022). Metabolic abnormalities, cardiovascular disease, and metabolic syndrome in adult rheumatoid arthritis patients: current perspectives and clinical implications. *Open Access Rheumatology: Research and Reviews*, 255–267.

Sata, T., Roth, J., Zuber, C., Stamm, B., & Heitz, P. U. (1991). Expression of alpha 2, 6-linked sialic acid residues in neoplastic but not in normal human colonic mucosa. A lectin-gold cytochemical study with Sambucus nigra and Maackia amurensis lectins. *The American Journal of Pathology*, *139*(6), 1435.

Scherer, H. U., van der Woude, D., Ioan-Facsinay, A., el Bannoudi, H., Trouw, L. A., Wang, J., Häupl, T., Burmester, G., Deelder, A. M., & Huizinga, T. W. J. (2010). Glycan profiling of anti–citrullinated protein antibodies isolated from human serum and synovial fluid. *Arthritis & Rheumatism*, *62*(6), 1620–1629.

Schwegmann-Weßels, C., & Herrler, G. (2006). Sialic acids as receptor determinants for coronaviruses. *Glycoconjugate Journal*, *23*(1), 51–58.

Scott, B. B., Weisbrot, L. M., Greenwood, J. D., Bogoch, E. R., Paige, C. J., & Keystone, E. C. (1997). Rheumatoid arthritis synovial fibroblast and U937 macrophage/monocyte cell line interaction in cartilage degradation. *Arthritis & Rheumatism: Official Journal of the American College of Rheumatology*, *40*(3), 490–498.

Seta, N., & Kuwana, M. (2007). Human circulating monocytes as multipotential progenitors. *The Keio Journal of Medicine*, *56*(2), 41–47.

Shirato, K., Nakajima, K., Korekane, H., Takamatsu, S., Gao, C., Angata, T., Ohtsubo, K., & Taniguchi, N. (2010). Hypoxic regulation of glycosylation via the N-acetylglucosamine cycle. *Journal of Clinical Biochemistry and Nutrition*, *48*(1), 20–25.

Singh, S., & Singh, S. (2020). JAK-STAT inhibitors: Immersing therapeutic approach for management of rheumatoid arthritis. *International Immunopharmacology*, *86*, 106731.

Slouma, M., Mhemli, T., Abbes, M., Triki, W., Dhahri, R., Metoui, L., Gharsallah, I., & Louzir, B. (2022). Rheumatoid arthritis occurring after coronavirus disease 2019 (COVID-19) infection: Case based review. *The Egyptian Rheumatologist*, *44*(3), 275–278.

Smith, M. D. (2011). The normal synovium. *The Open Rheumatology Journal*, *5*, 100.

Soler Palacios, B., Estrada-Capetillo, L., Izquierdo, E., Criado, G., Nieto, C., Municio, C., González-Alvaro, I., Sánchez-Mateos, P., Pablos, J. L., & Corbí, A. L. (2015). Macrophages from the synovium of active rheumatoid arthritis exhibit an activin A-dependent pro-inflammatory profile. *The Journal of Pathology*, *235*(3), 515–526.

Stowell, S. R., Arthur, C. M., Mehta, P., Slanina, K. A., Blixt, O., Leffler, H., Smith, D. F., & Cummings, R. D. (2008). Galectin-1,-2, and-3 exhibit differential recognition of sialylated glycans and blood group antigens. *Journal of Biological Chemistry*, *283*(15), 10109–10123.

Suarez-Arnedo, A., Figueroa, F. T., Clavijo, C., Arbeláez, P., Cruz, J. C., & Muñoz-Camargo, C. (2020). An image J plugin for the high throughput image analysis of in vitro scratch wound healing assays. *PloS One*, *15*(7), e0232565.

Suila, H., Hirvonen, T., Kotovuori, A., Ritamo, I., Kerkelä, E., Anderson, H., Natunen, S., Tuimala, J., Laitinen, S., & Nystedt, J. (2014). Human umbilical cord blood-derived mesenchymal stromal cells display a novel interaction between P-selectin and galectin-1. *Scandinavian Journal of Immunology*, *80*(1), 12–21.

Thomas, G., Tacke, R., Hedrick, C. C., & Hanna, R. N. (2015). Nonclassical patrolling monocyte function in the vasculature. *Arteriosclerosis, Thrombosis, and Vascular Biology*, *35*(6), 1306–1316.

Troncoso, M. F., Elola, M. T., Blidner, A. G., Sarrias, L., Espelt, M. V, & Rabinovich, G. A. (2023). The universe of galectin-binding partners and their functions in health and disease. *Journal of Biological Chemistry*, *299*(12), 105400.

Ulgen, E., Ozisik, O., & Sezerman, O. U. (2019). pathfindR: an R package for comprehensive identification of enriched pathways in omics data through active subnetworks. *Frontiers in Genetics*, *10*, 858.

Valencia, X., Higgins, J. M. G., Kiener, H. P., Lee, D. M., Podrebarac, T. A., Dascher, C. C., Watts, G. F. M., Mizoguchi, E., Simmons, B., & Patel, D. D. (2004). Cadherin-11 provides specific cellular adhesion between fibroblast-like synoviocytes. *The Journal of Experimental Medicine*, *200*(12), 1673–1679.

van Delft, M. A. M., & Huizinga, T. W. J. (2020). An overview of autoantibodies in rheumatoid arthritis. In *Journal of Autoimmunity* (Vol. 110). https://doi.org/10.1016/j.jaut.2019.102392

Van Steenbergen, H. W., Da Silva, J. A. P., Huizinga, T. W. J., & van der Helm-van Mil, A. H. M. (2018). Preventing progression from arthralgia to arthritis: targeting the right patients. *Nature Reviews Rheumatology*, *14*(1), 32–41.

Varki, A. (2008). Sialic acids in human health and disease. *Trends in Molecular Medicine*, *14*(8), 351–360.

Varki, A. (2011). Letter to the glyco-forum: since there are PAMPs and DAMPs, there must be SAMPs? Glycan “self-associated molecular patterns” dampen innate immunity, but pathogens can mimic them. *Glycobiology*, *21*(9), 1121–1124.

Varki, A., & Angata, T. (2006). Siglecs—the major subfamily of I-type lectins. *Glycobiology*, *16*(1), 1R-27R.

Varki, A., & Schauer, R. (2009). Sialic acids. *Essentials of Glycobiology. 2nd Edition*.

Varki, N. M., & Varki, A. (2007). Diversity in cell surface sialic acid presentations: implications for biology and disease. *Laboratory Investigation*, *87*(9), 851–857.

Viniegra, A., Goldberg, H., Çil, Ç., Fine, N., Sheikh, Z., Galli, M., Freire, M., Wang, Y., Van Dyke, T. E., Glogauer, M., & Sima, C. (2018). Resolving Macrophages Counter Osteolysis by Anabolic Actions on Bone Cells. *Journal of Dental Research*, 0022034518777973. https://doi.org/10.1177/0022034518777973

Wang, L., Liu, Y., Wu, L., & Sun, X.-L. (2016). Sialyltransferase inhibition and recent advances. *Biochimica et Biophysica Acta (BBA)-Proteins and Proteomics*, *1864*(1), 143–153.

Wang, L., Zhang, S., Wu, H., Rong, X., & Guo, J. (2019). M2b macrophage polarization and its roles in diseases. *Journal of Leukocyte Biology*, *106*(2), 345–358.

Wang, X., Liu, D., Ning, Y., Liu, J., Wang, X., Tu, R., Shen, H., Chen, Q., & Xiong, Y. (2017). Siglec-9 is upregulated in rheumatoid arthritis and suppresses collagen-induced arthritis through reciprocal regulation of Th17-/Treg-cell differentiation. *Scandinavian Journal of Immunology*, *85*(6), 433–440.

Wang, Y., Khan, A., Antonopoulos, A., Bouché, L., Buckley, C. D., Filer, A., Raza, K., Li, K.-P., Tolusso, B., & Gremese, E. (2021). Loss of α2-6 sialylation promotes the transformation of synovial fibroblasts into a pro-inflammatory phenotype in arthritis. *Nature Communications*, *12*(1), 1–18.

Wang, Y., Pan, P., Khan, A., Çil, Ç., & Pineda, M. A. (2022). Synovial fibroblast sialylation regulates cell migration and activation of inflammatory pathways in arthritogenesis. *Frontiers in Immunology*, *13*, 847581.

Wang, Z., Geng, Z., Shao, W., Liu, E., Zhang, J., Tang, J., Wang, P., Sun, X., Xiao, L., & Xu, W. (2020). Cancer-derived sialylated IgG promotes tumor immune escape by binding to Siglecs on effector T cells. *Cellular & Molecular Immunology*, *17*(11), 1148–1162.

Wei, K., Korsunsky, I., Marshall, J. L., Gao, A., Watts, G. F. M., Major, T., Croft, A. P., Watts, J., Blazar, P. E., & Lange, J. K. (2020). Notch signalling drives synovial fibroblast identity and arthritis pathology. *Nature*, *582*(7811), 259–264.

Wei, M., & Wang, P. G. (2019). Desialylation in physiological and pathological processes: New target for diagnostic and therapeutic development. *Progress in Molecular Biology and Translational Science*, *162*, 25–57.

Wilkinson, H., & Saldova, R. (2020). Current methods for the characterization of O-glycans. *Journal of Proteome Research*, *19*(10), 3890–3905.

Witoszyńska-Sobkowiak, J., Sikorska, D., Niklas, K., Żychowska, I., Rutkowski, R., & Samborski, W. (2024). The kynurenine pathway in patients with rheumatoid arthritis during tumor necrosis factor α inhibitors treatment. *Reumatologia*, *62*(4), 220.

Woods, J. M., Klosowska, K., Spoden, D. J., Stumbo, N. G., Paige, D. J., Scatizzi, J. C., Volin, M. V, Rao, M. S., & Perlman, H. (2006). A cell-cycle independent role for p21 in regulating synovial fibroblast migration in rheumatoid arthritis. *Arthritis Research & Therapy*, *8*(4), R113.

Wu, T., Hu, E., Xu, S., Chen, M., Guo, P., Dai, Z., Feng, T., Zhou, L., Tang, W., & Zhan, L. I. (2021). clusterProfiler 4.0: A universal enrichment tool for interpreting omics data. *The Innovation*, *2*(3).

Xu, D., Cui, Z., Liu, W., Tao, R., Tao, T., Shen, A., & Wang, Y. (2011). Tumor necrosis factor-α up-regulates the expression of β1, 4-galactosyltransferase-I in human fibroblast-like synoviocytes. *Inflammation*, *34*(6), 531–538.

Xue, M., McKelvey, K., Shen, K., Minhas, N., March, L., Park, S.-Y., & Jackson, C. J. (2014). Endogenous MMP-9 and not MMP-2 promotes rheumatoid synovial fibroblast survival, inflammation and cartilage degradation. *Rheumatology*, *53*(12), 2270–2279.

Yang, J., Zhang, L., Yu, C., Yang, X.-F., & Wang, H. (2014). Monocyte and macrophage differentiation: circulation inflammatory monocyte as biomarker for inflammatory diseases. *Biomarker Research*, *2*(1), 1.

Yang, S., & Yang, Y. (2015). Downregulation of microRNA-221 decreases migration and invasion in fibroblast-like synoviocytes in rheumatoid arthritis. *Molecular Medicine Reports*, *12*(2), 2395–2401.

Yoon, B. R., Yoo, S.-J., Choi, Y. H., Chung, Y.-H., Kim, J., Yoo, I. S., Kang, S. W., & Lee, W.-W. (2014). Functional phenotype of synovial monocytes modulating inflammatory T-cell responses in rheumatoid arthritis (RA). *PloS One*, *9*(10), e109775.

Yu, H., Li, M., Wen, X., Yang, J., Liang, X., Li, X., Bao, X., Shu, J., Ren, X., & Chen, W. (2022). Elevation of α-1, 3 fucosylation promotes the binding ability of TNFR1 to TNF-α and contributes to osteoarthritic cartilage destruction and apoptosis. *Arthritis Research & Therapy*, *24*(1), 93.

Zeilinger, S., Kühnel, B., Klopp, N., Baurecht, H., Kleinschmidt, A., Gieger, C., Weidinger, S., Lattka, E., Adamski, J., & Peters, A. (2013). Tobacco smoking

leads to extensive genome-wide changes in DNA methylation. *PloS One*, *8*(5), e63812.

Zhang, F., Jonsson, A. H., Nathan, A., Millard, N., Curtis, M., Xiao, Q., Gutierrez-Arcelus, M., Apruzzese, W., Watts, G. F. M., & Weisenfeld, D. (2023). Deconstruction of rheumatoid arthritis synovium defines inflammatory subtypes. *Nature*, *623*(7987), 616–624.

Zhang, F., Wei, K., Slowikowski, K., Fonseka, C. Y., Rao, D. A., Kelly, S., Goodman, S. M., Tabechian, D., Hughes, L. B., & Salomon-Escoto, K. (2019). Defining inflammatory cell states in rheumatoid arthritis joint synovial tissues by integrating single-cell transcriptomics and mass cytometry. *Nature Immunology*, *20*(7), 928–942.

Zhang, X., Nan, H., Guo, J., & Liu, J. (2021). NLRP12 reduces proliferation and inflammation of rheumatoid arthritis fibroblast-like synoviocytes by regulating the NF-κB and MAPK pathways. *European Cytokine Network*, *32*(2), 15–22.

Zhang, Y., He, X., Yin, D., & Zhang, Y. (2025). Redefinition of Synovial Fibroblasts in Rheumatoid Arthritis. *Aging and Disease*, *16*(4), 2.

Zhang, Z., He, P., Yang, L., Gong, J., Qin, R., & Wang, M. (2025). Posttranslational modifications of YAP/TAZ: molecular mechanisms and therapeutic opportunities. *Cellular & Molecular Biology Letters*, *30*(1), 83.

Zhao, S., Grieshaber-Bouyer, R., Rao, D. A., Kolb, P., Chen, H., Andreeva, I., Tretter, T., Lorenz, H., Watzl, C., & Wabnitz, G. (2022). Effect of jak inhibition on the induction of proinflammatory HLA–DR+ CD90+ rheumatoid arthritis synovial fibroblasts by interferon-γ. *Arthritis & Rheumatology*, *74*(3), 441–452.

Zheng, Y., Wei, K., Jiang, P., Zhao, J., Shan, Y., Shi, Y., Zhao, F., Chang, C., Li, Y., & Zhou, M. (2024). Macrophage polarization in rheumatoid arthritis: signaling pathways, metabolic reprogramming, and crosstalk with synovial fibroblasts. *Frontiers in Immunology*, *15*, 1394108.

Zhou, C., Gao, S., Yuan, X., Shu, Z., Li, S., Sun, X., Xiao, J., & Liu, H. (2021). Association between CTLA-4 gene polymorphism and risk of rheumatoid arthritis: a meta-analysis. *Aging (Albany NY)*, *13*(15), 19397.

Zhuo, Y., & Bellis, S. L. (2011). Emerging role of α2, 6-sialic acid as a negative regulator of galectin binding and function. *Journal of Biological Chemistry*, *286*(8), 5935–5941.

Zhuo, Y., Chammas, R., & Bellis, S. L. (2008). Sialylation of β1 integrins blocks cell adhesion to galectin-3 and protects cells against galectin-3-induced apoptosis. *Journal of Biological Chemistry*, *283*(32), 22177–22185.

Zieger, B., Boeckelmann, D., Anani, W., Falet, H., Zhu, J., Glonnegger, H., Full, H., Andresen, F., Erlacher, M., & Lausch, E. (2022). Novel GNE gene variants associated with severe congenital thrombocytopenia and platelet sialylation defect. *Thrombosis and Haemostasis*, *122*(07), 1139–1146.

Zimmermann, T., Kunisch, E., Pfeiffer, R., Hirth, A., Stahl, H.-D., Sack, U., Laube, A., Liesaus, E., Roth, A., & Palombo-Kinne, E. (2000). Isolation and characterization of rheumatoid arthritis synovial fibroblasts from primary

culture—primary culture cells markedly differ from fourth-passage cells. *Arthritis Research & Therapy*, *3*, 1–20.